DISS. ETH NO. 29807

UNRAVELING UNKNOWNS IN TROPICAL CYCLONE RISK ASSESSMENT

A thesis submitted to attain the degree of

DOCTOR OF SCIENCES
(Dr. sc. ETH Zurich)

presented by

SIMONA MEILER
MSc ETH Environmental Science, ETH Zurich
born on 13 September 1989

accepted on the recommendation of

Prof. Dr. David N. Bresch, examiner
Prof. Dr. Kerry Emanuel, co-examiner
Prof. Dr. Adam Sobel, co-examiner
Prof. Dr. Olivia Romppainen-Martius, co-examiner

2023

“Panta rhei.”

— Heraclitus

Abstract

The powerful impact of tropical cyclones disrupts societies in many coastal regions in the tropics and subtropics. For example, Hurricane Ian (2022) wreaked havoc in western Cuba with sustained winds over 200 $\mathrm{km\,h^{-1}}$, leaving the entire island without power and prompting the evacuation of over 38,000 residents. Continuing towards the US coast, the tropical cyclone intensified into a Category 4 storm on the Saffir-Simpson scale (1-5). Upon making landfall in Florida, Hurricane Ian claimed over 100 lives and left millions without electricity, becoming the state's costliest tropical cyclone with estimated insured losses between 50 to 65 billion USD. This recent hurricane illustrates the destructive nature of such events too well. Tropical cyclones not only cause immediate destruction but also have long-term impacts on developmental progress in affected areas and include broader economic disruption of global supply chains and markets. Climate change is projected to intensify tropical cyclone hazards while socio-economic development leads to an expansion of population and assets potentially in harm's way. Together, both factors exacerbate tropical cyclone risks, making accurate and reliable risk assessments imperative for effective planning, risk reduction, and response strategies. However, uncertainties in current risk assessment models and approaches complicate reliable tropical cyclone risk assessment.

In this thesis, I aim to identify and systematically quantify crucial uncertainties in global tropical cyclone risk assessments. Three specific aims underpin this overarching objective. Firstly, I analyze how the choice among different available global tropical cyclone track sets influences calculations of expected present-day impact. Based on this, I provide guidance on the relative advantages and disadvantages of each track set depending on the application. Secondly, I quantify the drivers and uncertainties of future global tropical cyclone risks, attributing these uncertainties to variations in model input factors. Lastly, I synthesize uncertainty and sensitivity analyses across multiple hazard models and evaluate these by uncertainty types in order to provide perspectives on the implications and reducibility of uncertainties. Explored over four chapters, these aims collectively enhance the reliability and value of tropical cyclone risk assessments for risk analysis, research, and decision-making.

Present-day tropical cyclone risk assessment relies on synthetic models, as sparse historical observations limit the reliability of these assessments. Although validated and applied in diverse contexts, these synthetic tropical cyclone models have not been directly compared as input hazard datasets in catastrophe models for tropical cyclone risk and loss estimation. In response, this thesis introduces the first intercomparison of four global-scale synthetic tropical cyclone datasets, evaluating their performance through various risk metrics. To achieve this, I use the open-source CLIMADA (CLIMate ADAptation) platform, integrating hazard, exposure, and vulnerability data to estimate risks. Adopting a multi-model perspective, I simulate risk as the direct economic damage of tropical cyclones

on the built environment. Through this comparison, it is evident that selecting an appropriate hazard set is crucial, particularly when examining tail events, analyzing basins with limited historical event sets, or focusing on small areas. In these cases, modelled losses vary by more than an order of magnitude across the different synthetic hazard sets.

Future tropical cyclone risk assessment requires additional model input layers representing future climate and socio-economic systems, each introducing its own set of uncertainties. While previous studies have explored changes in the physical properties of tropical cyclones or future tropical cyclone exposure, none have conducted a systematic uncertainty and sensitivity analysis throughout the entire risk model. To address this gap, I conduct such an analysis for future tropical cyclone risk estimates, incorporating a wide range of hazards from various climate models and emission scenarios, along with alternate representations of socio-economic development and variations in vulnerability. Furthermore, it is crucial to note that uncertainty and sensitivity analyses are intricately linked to the selected model setup. The interpretation and extrapolation of results thus warrants caution. Consequently, this thesis contrasts uncertainty and sensitivity analyses of future tropical cyclone risks across four hazard models to discern their influence on outcomes.

The results derived from analyzing drivers of future tropical cyclone risk highlight non-trivial interactions between climate change and socio-economic development, which are not the mere sum of their parts nor simple, a posteriori multiplication of hazard and exposure. Moreover, I find that socio-economic factors consistently drive increased risk across all hazard models. In contrast, the results of the uncertainty and sensitivity analysis differ between hazard models. For example, results based on the MIT model are sensitive to the underlying global climate model. Interestingly, the climate sensitivity of these models serves as a powerful indicator of subsequent changes in tropical cyclone risk. Conversely, risk estimates derived from CHAZ, STORM, and climate-conditioned IBTrACS are primarily influenced by exposure scaling based on Shared Socio-economic Pathways.

This thesis advances the understanding and quantification of uncertainties in present-day and future global tropical cyclone risk assessments. It guides modelers in hazard set choice, thereby strengthening risk assessment reliability. The systematic assessment and quantification of uncertainty and sensitivity enhance both the transparency and depth of risk assessments. By synthesizing uncertainty and sensitivity analyses across multiple hazard models and discerning whether uncertainty originates from randomness in the system, our limited knowledge, or normative choices, it offers further guidance to navigate the implications and reducibility of uncertainties. This advancement aids model developers in focusing research efforts on significant model inputs for reducing output uncertainty. It also provides decision-makers with a more representative range of plausible future outcomes, presenting a more robust and valuable information basis. Together, the insights and approaches presented in this thesis advance global tropical cyclone risk assessments, yielding enhanced and actionable insights in the face of uncertainty.

Resumaziun

La starmentusa repercussiun entras stemprads tropics turmenta la societad en bleras regiuns a las costas da las tropas e subtropas. Il hurican Ian (2022) ha per exempel chaschunà devastaziuns en il vest da la Cuba cun bufs da vent da pli che 200 $\mathrm{km\,h^{-1}}$, uschia che l'entira insla è stada senza electricitad e varga 38,000 residents èn vegnids evacuads. Il ciclon tropic ha cuntinuà en direcziun da la costa dals Stadis Unids ed è s'intensivà ad in stemprà da la categoria 4 sin la scala Saffir-Simpson (1-5). Cun l'arrivada a Florida ha il hurican Ian chaschunà dapli che 100 victimas, privà milliuns da persunas da l'electricitad ed è cun 50 fin 65 milliardas USD donns assicurads il pli char ciclon tropic dal stadi.

Quest hurican recent illustrescha fitg bain la natira destructiva d'eveniments sco tals. Ciclons tropics n'han betg be per consequenza devastaziuns immediatas, ma era effects a lung term sin il svilup en las regiuns pertutgadas inclus vasts disturbis economics da chadainas da furniziun globalas e da martgads. I vegn prognostitgà che la midada dal clima vegn ad intensivar las ristgas da ciclons tropics, fertant ch'il svilup socio-economic maina ad ina expansiun da la populaziun e da las valurs da facultads potenzialmain en ristga. Omadus facturs rinforzan las ristgas da ciclons tropics, uschia che la stimaziun accurata e reliabla da ristgas è imperativa per ina planisaziun effectiva, per ina reducziun da ristgas e per strategias da reacziun. Ma ozendi cumplitgeschan intschertezzas da models e da metodas da stimaziun da ristgas ina stimaziun reliabla da las ristgas da ciclons tropics.

En questa lavur hai jau per finamira d'identifitgar e sistematicamain quantifitgar intschertezzas decisivas en la stimaziun da ristgas da ciclons tropics globala. Trais finamiras specificas assistan questa intenziun principala. Emprim, jau analisesch sco la schelta tranter differents sets da trajects globals disponibels da ciclons tropics influenzescha la calculaziun d'ozendi da consequenzas spetgadas. Sin questa basa offrel jau ina survista d'avantatgs e disavantatgs relativs da mintga set da trajects dependent da l'applicaziun. Sco segund, jau quantifitgesch ils stimuls e las intschertezzas da las ristgas futuras globalas da ciclons tropics, attribuind questas intschertezzas a variaziuns da facturs d'endataziun dals models. Ultim, jau sintetisesch analisas d'intschertezza e da sensitivitad per differents models da privels ed evaluesch questas tenor tips d'intschertezza per offrir ina perspectiva sin las implicaziuns e pussaivlas reducziuns da talas. Cun ina exploraziun sur quatter chapitels mainan questas finamiras communablamain ad ina meglieraziun da la reliabilitad e valur da stimaziun da ristgas da ciclons tropics per l'analisa da ristgas, la perscrutaziun e proceduras da decisiuns.

Las stimaziuns da ristgas da ciclons tropics d'ozendi sa fundan sin models sintetics perquai ch'observaziuns istoricas èn stgars e limiteschan la reliabilitad da questas stimaziuns. Era sche quels models èn validads ed applitgads en divers contexts n'èn quests models sintetics da ciclons tropics betg directamain vegnids cumparegliads sco sets d'input da datas da privels en models da catastrofas per la valitaziun da ristgas da ciclons tropics e da donns. Questa lavur porscha l'emprima cumparegliaziun

da quatter sets da datas da ciclons tropics sin nivel global, evaluond lur performanza cun l'agid da differentas mesiras da ristga. Per pudair realisar quai nizzegel jau la plattafurma open-source CLIMADA (CLIMate ADAptation), integrond datas davart privels, exposiziun e vulnerabilitad per valitar las ristgas. Cun ina perspectiva da plirs models simulesch jau las ristgas operaziunalisadas sco donns economics directs da ciclons tropics sin l'ambient cultivà. Tras questa cumparegliaziun vegn evident che la schelta d'in set da privels adequat è decisiva, en spezial per eveniments marginals, per l'analisa dad intschess cun pacs eveniments istorics ni cun in focus sin regiuns pitschnas. En quests cas varieschan ils donns modellads per dapli ch'ina dimensiun tranter ils differents sets da privels sintetics.

La stimaziun da ristgas da ciclons tropics en il futur basegna ulteriurs nivels d'input da model che represchentan il clima ed ils sistems socio-economics futurs, tge che agiunscha ulteriuras intschertezzas. Studis existents han explorà midadas da las caracteristicas fisicas da ciclons tropics ni l'exposiziun futura a ciclons tropics, ma nagins studis han realisà ina analisa sistematica da l'intschertezza e da la sensitivitad da l'entir model da ristga. Per adressar questa largia en la perscrutaziun realisesch jau uschè in'analisa per la stimaziun da la ristga da ciclons tropics en il futur, includend ina vasta dimensiun da privels da differents models da clima e scenaris d'emissiuns sco era represchentaziuns alternativas dal svilup socio-economic e variaziuns da lur vulnerabilitad. Igl è plinavant decisiv da resguardar che las analisas d'intschertezza e sensitivitad èn fermamain entretschadas cun la configuraziun dal model. L'interpretaziun ed extrapolaziun dals resultads pretenda uschia prudientscha. Per quai motiv cuntrastescha questa lavur las analisas d'intschertezza e sensitivitad da quatter models da privel per distinguer lur influenza sin ils resultads.

Ils resultads derivads da l'analisa da stimuls da ristgas da ciclons tropics el futur accentueschan las interacziuns nun-trivialas tranter la midada dal clima ed il svilup socio-economic, che n'èn ni be la summa da lur parts ni simplamain ina multiplicaziun a posteriori da lur privels ed exposiziun. Ultra da quai constatesch jau ch'ils facturs socio-economics stimuleschan consequentamain ristgas elevadas en tut ils models da privel. Sco cuntrast differenzieschan ils resultads da l'analisa d'intschertezza e sensitivitad tenor model da privel. Per exempel èn ils resultads sin fundament dal model MIT pli sensitivs al model climatic global. La sensitivitad sin il clima da quests models è in interessant e ferm indicatur da las consequenzas per la ristga da ciclons tropics. Da l'autra vart èn stimaziuns da ristgas derivadas da CHAZ, STORM e da IBTrACS cundiziunà sin il clima primarmain influenzadas da la scala d'exposiziun sin basa dals percurs socio-economics communabels.

Questa lavur avanza la chapientscha e quantificaziun dad intschertezzas en las stimaziuns da ristgas da ciclons tropics globalas dad ozendi e dal futur. Ella guida modellaturs tar la schelta da sets da privels e rinforza uschia la reliabilitad da la stimaziun da ristgas. Cun giuditgar e quantifitgar sistematicamain l'intschertezza e la sensitivitad vegnan uschè bain la transparenza sco era la profunditad da stimaziuns da ristgas megliuradas. Tras la sintetisaziun da las analisas d'intschertezza e da sensitivitad cun plirs models da privel e cun percepir sche l'intschertezza originescha en la casualitad dal sistem, da nossa savida limitada u da scheltas normativas, vegn purschì in mussavia per navigar las implicaziuns e reducibilitad dad intschertezzas. Quest avanzament gida a sviluppaders da models da focusar la perscrutaziun sin inputs significativs da models per reducir l'intschertezza da l'output. Ella porscha era ina survista pli represchentativa dals resultats

futurs plausibels ed ina basa pli robusta e valurusa d'infurmaziuns per purtadras da decisiuns. Las invistas e metodas preschentadas en questa lavur avanzan ensemen la stimaziun da ristgas da ciclons tropics globala, effectuond invistas megliuradas e la capabilitad d'agir en vista a l'intschertezza.

Acknowledgements

My gratitude goes to all those who made this thesis and the work leading to it possible. I am deeply grateful to my supervisors David Bresch and Kerry Emanuel, who gave me the opportunity to follow my curiosity and operate with large freedom over the course of this thesis and who opened many doors for me along the way. I thank David Bresch for his trust, generosity, and guidance in letting me define and pursue my own research projects, explore my research interests, and build my own network. I thank Kerry Emanuel for his kind supervision, invaluable contributions to scientific discussions, for enhancing the depth and relevance of my work, and for his incredibly fast replies to all my inquiries.

I am very thankful for the community of researchers whose insights have shaped my work. This thesis bears the imprint of many minds; from the early days of brainstorming to final edits, I was surrounded by a supportive and stimulating community. I thank Adam Sobel, Suzana Camargo, Chia-Ying Lee and Nadia Bloemendaal for their collaboration, discussions, and support. I especially thank Thomas Vogt for his invaluable and patient help with coding, generous support, and accurate contributions. And I thank Francesca Pianosi for helping me navigate the field of uncertainty and sensitivity analysis.

I thank my colleagues from the Weather and Climate Risks Group for welcoming me amidst the first pandemic lockdown and helping me enter a new field of research, code base, and work environment. Thank you all for sharing office space, coffee breaks, and fortunately, fewer and fewer hours on zoom. Alessio and Chahan, thank you for the regular exchanges and guidance; Chahan and Jamie thank you for proofreading parts of this thesis; Sarah, Sandro, and Urs thank you for easing administrative and technical challenges. A particular thank you goes to Evelyn and Sam for sharing this journey with friendship and support.

Finally, I am deeply grateful to my family and friends who supported me in countless ways over the past years. In spezial engraziament vala a Clau per la translaziun digl abstract. Thank you Mara, Ariana, Andrea, Martin, Stephi.

Contents

CHAPTER 1

Introduction

Tropical cyclones (TCs) represent one of the most devastating natural hazards, causing extensive loss of life, livelihoods, and infrastructure, particularly in coastal and island regions. For instance, Hurricane Katrina in 2005 resulted in over 1,800 fatalities and an estimated 125 billion USD in damage (Knabb et al., 2005), while Typhoon Haiyan in 2013 killed at least 6,300 people in the Philippines (NDRRMC, 2014). Most recently, Hurricane Idalia was included in the 2023 list of billion-dollar weather and climate disasters, as it caused losses exceeding 1 billion USD in the United States (NCEI, 2023). The situation is further aggravated by climate change, which is expected to intensify the frequency and severity of these extreme weather events, and by socio-economic development that often places more people and assets in high-risk coastal areas. Furthermore, tropical cyclone impacts extend far beyond immediate damage, setting back years of developmental progress and requiring billions of dollars for recovery and rebuilding efforts (Hsiang and Jina, 2014; Hallegatte et al., 2017; Berlemann and Wenzel, 2018; Hallegatte et al., 2017). In this context, the importance of reliable tropical cyclone risk assessment cannot be overstated; it is indispensable for various sectors all aimed at enhancing resilience against these catastrophic events.

Acting as the foundation of emergency planning, infrastructure design, insurance pricing, and policy formulation, risk assessments are tailored to meet the distinct and specific needs of each sector. For instance, emergency management services require short-term forecasts for evacuation planning (e.g., Merz et al., 2020), while urban planners need long-term risk assessments for infrastructure development (e.g., UNISDR, 2015). The insurance industry, on the other hand, necessitates a blend of short-term and long-term assessments, but with an added emphasis on quantifying financial risk. This raises the issue of fitness for purpose (Parker, 2010), as different sectors may require different types of model outputs and varying degrees of precision and spatiotemporal resolution. These diverse specifications pose challenges in developing universally applicable risk assessment tools. Indeed, a uniform modelling approach is unlikely to meet the diverse requirements of all stakeholders. Understanding this variability in needs is crucial for the development of tailored risk assessment tools and consequently for the evaluation thereof.

Furthermore, the demand for robust climate risk assessments, including for tropical cyclones, is emerging in new areas like the Task Force on Climate-related Financial Disclosures (TCFD) (TCFD, 2017) and Loss and Damage (UNFCCC, 2007) funding mechanisms discussed in COP27 (UNFCCC, 2023) while it is changing in traditional sectors like insurance. The TCFD, for instance, is particularly

interested in how extreme weather events could impact financial markets, shareholder value, and long-term business sustainability (TCFD, 2017). Therefore, their focus is often on high-resolution, probabilistic models that can provide detailed risk scenarios over multiple time horizons, which can be used for stress-testing financial resilience. Loss and Damage mechanisms are focused on assessing both the immediate and long-term economic and social impacts of climate-related disasters (UNFCCC, 2007; UNFCCC, 2023). These mechanisms require assessments that link to economic models to quantify the potential for irreversible loss, such as loss of livelihoods or permanent displacement. In contrast, traditional markets like the insurance sector are undergoing shifts as requirements for robust tropical cyclone risk assessments are evolving. Regulatory changes and climate-aware frameworks like the above-mentioned TCFD (TCFD, 2017) are pushing these sectors toward more advanced modelling and public risk disclosure. Furthermore, the insurance industry faces a notable challenge posed by the increasing destructive potential of tropical cyclones, which are leading to issues of uninsurability, where the risks are so high that they cannot be effectively covered under traditional insurance models (Gray, 2021; Flavelle, 2022; Smith, 2023). This impacts both the insurers and the insured, causing a shift towards more complex financial instruments like catastrophe bonds and greater reliance on public-private partnerships for disaster coverage (Kunreuther, 2000; Swiss Re, 2021, 2023; Jarzabkowski et al., 2023). This changing landscape adds complexity to existing operations and mandates a shift toward more adaptive and transparent practices.

The paucity of observations for tropical cyclones is a significant challenge in risk assessment. While satellites have greatly improved our ability to monitor these systems, reliable observational data has only been available for a few decades, providing a relatively short history for analysis (Knapp et al., 2010). In addition, the focus of risk assessment is primarily on landfalling tropical cyclones, which represent a subset of the storms that form over open oceans. Moreover, not all coastal regions that are potentially at risk have experienced a direct hit, creating a heterogeneous and incomplete picture of the true risk landscape (Weinkle et al., 2012). This data scarcity necessitates the use of numerical models to fill in the gaps. However, such tropical cyclone models vary considerably in structural design, from simplistic statistical models (Vickery et al., 2000) to complex, statistical-dynamical (Emanuel et al., 2006; Lee et al., 2018) or fully dynamical models (Roberts et al., 2020b). Regardless of their structural differences, all models are subject to inherent uncertainties. For instance, these can arise from approximations in physical processes, initial condition sensitivities, and the stochastic nature of weather systems. These uncertainties are not isolated; they interact and compound when integrated into comprehensive risk models, which hinge on the interplay of hazard, exposure and vulnerability. The *hazard* defines the physical attributes of tropical cyclones, including their intensity, frequency and geographical location. *Exposure* delineates the spatial mapping of potentially affected populations, assets, and ecosystems. Meanwhile, *vulnerability* quantifies their susceptibility to damage or harm. As these components are modeled and integrated, each layer introduces distinct uncertainties, further complicating the challenging task of producing reliable risk assessments.

This thesis investigates state-of-the-art tropical cyclone models and risk assessment approaches with an emphasis on the quantification of uncertainties and sensitivities. By adopting a multi-model perspective, it aims to deliver a nuanced understanding of both current and future global tropical

cyclone risks. The primary objective is to identify and systematically quantify the crucial sources of uncertainty in global tropical cyclone risk assessments. This endeavor guides the prioritization of future research and fosters the design of more robust and tailored risk assessments, responding to the growing need for dependable, actionable risk information and facilitating the development of sector-specific strategies. Such strategies are crucial to minimize the broader societal, economic, and environmental impacts of tropical cyclones in a changing climate.

1.1 Aims and focus of the thesis

This thesis seeks to answer the following overarching research question: What are the crucial sources of uncertainty in global tropical cyclone risk assessments, and how does the systematic assessment and quantification of these uncertainties enhance the value for risk analysis, research and decision-making?

More specifically, the aims of this thesis are to:

I Compare the most influential, academically available, present-day, global tropical cyclone track sets on the impact level and provide guidance on which hazard set to choose depending on the application.

II Systematically quantify the drivers and uncertainties of future global tropical cyclone risk changes, attributing these uncertainties to variations in model input factors.

III Synthesize uncertainty and sensitivity analysis of future global tropical cyclone risk changes across various hazard models and reflect on the implications for risk modeling.

The three aims are investigated in four chapters, which consist of three original scientific publications and an additional thesis chapter. Aim I is addressed in Chapter 2, Aim II in Chapters 3 and 4, and Aim III is covered in Chapter 5. The following sections briefly introduce the content of the chapters and my contributions to further publications that are relevant to the aims of the thesis.

1.1.1 Intercomparison of regional loss estimates from global synthetic tropical cyclone models (Chapter 2)

There is a growing need for consistent global tropical cyclone risk assessments, particularly to inform adaptation planning, risk reduction strategies, and physical risk disclosures. While synthetic tropical cyclone models help address the spatial and temporal constraints of historical data, no prior study has evaluated their performance and applicability in risk assessments. We thus present the first global model intercomparison of the most influential (academically available/non-commercial) synthetic tropical cyclone hazard sets as input for tropical cyclone risk modelling. We find that the choice of hazard set becomes more critical when studying tail events, basins with smaller historical event sets, and in small areas. In these cases, we discover modelled losses to vary by more than an order of magnitude across the different synthetic hazard sets. Furthermore, our study provides guidance for other researchers to determine the applicability of each hazard set depending on the research objective. Such insights are directly relevant for risk assessment efforts both in public (e.g.,

academia, policymakers, and non-governmental organizations) and private sectors (e.g., consultancy and (re)insurance companies).

1.1.2 Drivers, uncertainties and sensitivities of future tropical cyclone risks (Chapter 3 and 4)

Changes in the climate and socio-economic systems largely drive future tropical cyclone risks (e.g. Mendelsohn et al., 2012; Gettelman et al., 2018; Geiger et al., 2018). However, quantifying these future risks is particularly challenging because it requires dealing with the absence of robust verification data (Pianosi et al., 2016; Wagener et al., 2022) and large, possibly cascading uncertainties in the model input components and model structure (Kropf et al., 2022). In Chapters 3 and 4, we thus assess the drivers of future tropical cyclone risk and perform a systematic uncertainty and sensitivity analysis throughout the entire TC risk model. We conduct two individual studies using tropical cyclone hazard sets of two distinct tropical cyclone models in an otherwise unchanged setup. This effort results in two separate scientific publications presented as Chapters 3 and 4 in this thesis. Our results surpass the standard climate risk analyses, which often only provide a comparably basic uncertainty estimation but rarely include a thorough, systematic global sensitivity analysis. Specifically, we study tropical cyclone risk increases across various global climate models (GCMs), greenhouse gas emission scenarios, socio-economic development factors, wide ranges of vulnerability, and other risk model input variables. This allows us to explore a broad uncertainty distribution of model outputs and assess how these variations can be attributed to variations in input factors. The results of both chapters reveal that socio-economic development contributes more strongly to future tropical cyclone risk increases than climate change. However, there is divergence on which of the two is the more uncertain risk driver. Moreover, we demonstrate that it is crucial to include socio-economic development in future tropical cyclone risk assessments because, effectively, climate impacts manifest as non-trivial interactions between the two components. Besides, we find that the choice of GCM underlying the tropical cyclone hazard set is the input variable with the most significant impact on tropical cyclone risk change calculations for the study setup of Chapter 3. Most strikingly, the related climate sensitivity is a powerful indicator of the resulting tropical cyclone risk change. In Chapter 4, we identify the exposure scaling based on the Shared Socioeconomic Pathways (SSPs) as the input variable with the most significant impact on tropical cyclone risk change calculations. Finally, we assert that the value of climate risk assessments is substantially increased by quantitative estimates of uncertainty and sensitivity to model parameters, enabling better-informed decision-making and offering a richer context for future research efforts.

1.1.3 A cross-model exploration of uncertainty and sensitivity analysis for future tropical cyclone risk (Chapter 5)

Systematic and thorough uncertainty and sensitivity analysis are crucial for robust decision-making and model improvement. Nevertheless, it is important to approach the results of such analyses with caution as they are inherently dependent on the selected model setup. Chapter 5, therefore, explores how four distinct tropical cyclone hazard models as well as alternate representations of

socio-economic development influence future tropical cyclone risk and their associated uncertainties and sensitivities. Specifically, we perform an uncertainty and sensitivity analysis analogous to the setup of Chapters 3 and 4 for the four hazard sets that we compared in Chapter 2. Comparing the results of these four studies allows us to reflect on the structural nuances among tropical cyclone hazard models and discuss the level of development of the hazard component of our risk model in contrast to exposure and vulnerability. Furthermore, we discern findings that are generalizable beyond the single studies from those intrinsically linked to specific hazard model components and methodologies. We find that socio-economic factors consistently drive increased risk across all models, while the uncertainty in these risk drivers is hazard model-specific. For instance, the MIT model-based results are sensitive to the choice of global climate model, while estimates from CHAZ, STORM, and climate-conditioned, probablistic IBTrACS are mainly influenced by exposure scaling based on Shared Socio-economic Pathways. Finally, we relate our findings to different categories of uncertainty. This structured and holistic approach allows us to navigate the implications and reducibility of uncertainties, enabling better-informed decision-making and offering a richer context for future research efforts.

1.1.4 Additional contributions

In addition to the four publications included as Chapters 2, 3, 4, and 5 of this thesis, I also co-authored four further studies, one of which directly contributes to the research aims of this thesis. Specifically, the study addresses the topic of uncertainty in weather and climate risk modelling and how to systematically assess and quantify them (Kropf et al., 2022). We accordingly introduce a new feature in the CLIMADA risk modeling platform (Aznar-Siguan and Bresch, 2019) that enables uncertainty and sensitivity analysis. The new feature is illustrated and applied to a case study of tropical cyclone storm surge in Vietnam (Rana et al., 2022), showcasing how uncertainty and sensitivity analysis can inform risk assessments and adaptation options. Our findings underscore that the broader use of these analyses among climate-risk modelers can increase transparency, facilitate comparison of studies, and improve decision-making regarding climate adaptation. The uncertainty and sensitivity quantification module introduced with the study is a central element to my work presented in Chapters 3, 4, and 5. I was involved in ideation and study design and contributed to the writing and editing of the manuscript. More scientific background of uncertainty and sensitivity analysis beyond the study and details of the study with relevance to this thesis are provided in Section 1.2.3.

The other three studies I have been involved in are more broadly contributing to the field of extreme weather and climate risk science. Namely, the publication on increasing countries' financial resilience to tropical cyclones through risk pools (Ciullo et al., 2023), a framework for global-multi hazard risk assessment (Stalhandske et al., 2023) and a study on the relationship between the historical impacts of extreme weather events and climate change emotions (Cologna et al., 2023) all extend beyond the scope of this thesis and are not discussed further.

1.2 Scientific Background

This section provides background information relevant to this thesis, supplementing the scientific background presented in Chapters 2, 3, 4, and 5. This background section covers aspects of the physical characteristics of tropical cyclones, climate risk modelling and uncertainty and sensitivity analysis. In Section 1.2.1, I provide an overview of the physical aspects of tropical cyclones, the effects of climate change, and tropical cyclones as natural hazards. In Section 1.2.2, I describe key concepts of climate risk and features of weather and climate risk modelling, which form the backbone of this thesis. In Section 1.2.3, I briefly review the types and possible sources of uncertainties in tropical cyclone risk modelling and the concept of uncertainty and sensitivity analysis.

1.2.1 Tropical cyclones

Tropical cyclones, depending on where they form, also called *Hurricanes* (Eastern Pacific, North Atlantic), *Typhoons* (Western North Pacific), and *Cyclones* (South Pacific and Indian Ocean) (Lohmann et al., 2016), originate over tropical or subtropical waters in a complex interplay between atmospheric dynamics and thermodynamics (e.g., Emanuel, 1986; Montgomery and Smith, 2014, 2017). In short, warm ocean waters provide the energy source that fuels these storms, while the Earth's rotation imparts the spin required for their formation. In more detail, a tropical cyclone is a tropical storm system with a closed circulation around a low-pressure center, organized deep convection, and driven by latent heat fluxes released as air humidified over warm ocean waters rises and condenses (e.g., Emanuel, 1986; Montgomery and Smith, 2014, 2017). Tropical cyclones are characterized by a cloud-free eye at the center surrounded by the eyewall, where the most vigorous convection with a high level of thunderstorm activity occurs. Consequently, the eyewall contains the highest wind speeds and the most intense precipitation of the storm system (Lohmann et al., 2016). Wind speeds of up to $95\,\mathrm{m\,s^{-1}}$ and rainfall exceeding 1100 mm in 12 hours have been measured (WMO, 2023). Furthermore, upon making landfall, tropical cyclones may induce strong storm surges. With landfall, tropical cyclones also lose their primary energy source and decay quickly (Lohmann et al., 2016). A tropical cyclone can undergo extratropical transition, which implies both a poleward displacement of the cyclone and the conversion of the cyclone's primary energy source from the release of latent heat of condensation to baroclinic processes (Jones et al., 2003; Evans et al., 2017). The latter describes the temperature contrast between warm and cold air masses. It is important to note that cyclones can become extratropical and still retain winds of tropical cyclone force. In this thesis I focus on tropical cyclones only and do not investigate extratropical storms further.

Tropical cyclones represent one of the most powerful and destructive atmospheric phenomena on Earth, and particularly tropical and subtropical coastal regions are vulnerable to direct impacts of tropical cyclones. Understanding the fundamental physics driving these storms is essential to predicting their behavior and assessing associated risks.

Over recent decades, the effects of climate change have added an additional layer of complexity to the behavior of tropical cyclones. Such changes in TC activity due to climate change have been detected in historical records as summarized in a meta-study by Knutson et al. (2019). They

encompass the migration of the location of maximum intensity (Kossin et al., 2014; Altman et al., 2018; Sharmila and Walsh, 2018), changes in intensity (Elsner et al., 2008; Kossin et al., 2013), and possible shifts in frequency (Kang and Elsner, 2015). A reduction in propagation speeds since 1949 is disputed (Kossin, 2018; Lanzante, 2019; Moon et al., 2019), and changes in precipitation associated with individual TCs have been proposed (Emanuel, 2017; Risser and Wehner, 2017; Van Oldenborgh et al., 2017).

The future effects of climate change on tropical cyclones have further been simulated with coarse- to high-resolution climate models and are summarized in Knutson et al. (2020), complementing their first meta-study focused on observations. Tropical cyclone projections from high-resolution models converge globally in predicting heightened maximum surface wind speeds throughout a TC's lifecycle. Specifically, the intensity of TCs was found to increase by 5% globally (Knutson et al., 2020). These results are consistent with the potential intensity (PI) theory of (Emanuel, 1987), which projects an intensity increase in a climate warmed by the greenhouse effect. Besides, TC frequencies over all storm categories, from tropical storm to category 5 TC, are projected to decrease; however, with low confidence in such projections (Knutson et al., 2020). In contrast, the proportion and frequency of high-intensity TCs (category 4-5) are increasing in high-resolution models (Emanuel, 2013). Models with a horizontal resolution of 60 km or coarser yield a decrease in the most intense TCs because they represent such storms insufficiently (Murakami and Sugi, 2010; Murakami et al., 2015; Knutson et al., 2020). The frequency of very intense TCs is particularly important in the context of this thesis since category 4 and 5 TCs cause nearly half of the normalized economic losses of all TC damages but only account for 6% of all TC events (Pielke et al., 2008). A change in TC size is hard to detect since the physical understanding of this variable is still limited. Some studies (e.g., Kim et al., 2014; Yamada et al., 2017) project increasing TC sizes with climate change, while other studies report non-significant changes (Knutson et al., 2015; Gutmann et al., 2018; Knutson et al., 2020). Furthermore, effects of climate change on TCs include higher storm inundation levels due to sea level rise (e.g., Mcinnes et al., 2003; Lin et al., 2012; Little et al., 2015; McInnes et al., 2014; Garner et al., 2017) and an increased TC precipitation rate. While existing modeling studies agree on a projected increase in global average TC rainfall rates, there is less agreement on details like the exact value of this rate ($\sim 7\,\%\,^{\circ}\mathrm{C}^{-1}$) or spatial distribution at which rainfall increases (Knutson et al., 2013, 2015; Wright et al., 2015; Liu et al., 2018). Finally, a poleward expansion of the latitude of maximum TC intensity in the western North Pacific (Kossin et al., 2016) and diverging findings in changes of TC translational speed (Knutson et al., 2013; Kim et al., 2014; Gutmann et al., 2018) conclude the list of effects of climate change on tropical cyclones.

These recent discoveries from observations (Knutson et al., 2019) and model projections (Knutson et al., 2020) of future TC activity highlight the need for a better understanding of connections between climate change and tropical cyclone behavior to anticipate their impacts in a rapidly changing world.

Tropical cyclones emerge as potent hazards in the context of weather and climate risk assessment. Their potential to cause widespread damage, disrupt critical infrastructure, and induce humanitarian crises underscores the need for comprehensive risk analysis. Therefore, physical aspects of tropical cyclones are used as hazard information, together with exposure and vulnerability attributes in the weather and climate risk landscape (see Section 1.2.2). Depending on the application, different

data sources and approaches are used for TC hazard representation. For example, TC forecast tracks from the European Centre for Medium-Range Weather Forecasts Integrated Forecasting System (ECMWF-IFS) can be used for TC early warning systems and impact forecasts (ECMWF, 2022). While output from numerical weather predictions is suitable for studying TC hazards over timescales of days (up to 15 days ahead), we need other data sources for TC risk assessment over longer timescales.

In this thesis, I focus on annual to long-term TC risk assessment for the historical period since 1980 (Chapter 2) and the future period over the 21st century (Chapters 3, 4, and 5). The TC hazard variable is the lifetime maximum wind speed at each location, derived from a) a TC track set and b) a parametric wind model to yield a 2D wind field. Section 2.1 features an overview of tropical cyclone track sources used for risk assessment of the historical period. Sections 3.4.2, 4.2.1 i), and 5.2.2 provide details on TC track sets for future climate conditions, including all the intricacies related to global climate models and emission scenarios underlying these hazard sets. Besides, we use two different parametric wind models to compute the gridded 1-minute sustained winds at 10 meters above ground (Holland, 2008; Emanuel and Rotunno, 2011). These two parametric wind models are of comparable model structure and complexity. They both fit functions to the TC tracks and environmental parameters usually provided with the track set to characterize the radial profile of wind and pressure from the TC center. The models are computationally efficient and thus widely used, particularly for continental to global scale analyses. However, fast computation comes at the price of resolution. The resulting wind fields are smooth and empirical corrections are required to represent surface terrain effects. Other models, for instance, consider wind field variability related to variations in intensity, outer storm size, and latitude (Chavas and Lin, 2016) or include variable surface drag and terrain height (Done et al., 2020) for a more realistic representation of wind footprints - at the price of computational efficiency. We note that the assumption of wind as the sole driving physical force for TC impacts is imperfect. Damages from most TC events are caused by rainfall-induced freshwater floods, wind-driven storm surges, and direct impacts from TC winds together. However, state-of-the-art global scale TC risk assessments do not explicitly represent these sub-hazards due to computational limitations and consider wind as the primary driving force for damages. The effects of TC wind and water hazards are implicitly captured in this thesis as the vulnerability curves used to calculate risk and impact were calibrated with damage data reported for all TC sub-hazards combined (see Eberenz et al., 2021).

In the subsequent section, I delve deeper into the relevant concepts and methodologies for tropical cyclone risk assessment.

1.2.2 Climate risk modelling

Assessing tropical cyclone risk emerges as a pivotal endeavor within the broader context of climate risk management, particularly in an era characterized by the intensifying effects of climate change on human and natural systems. The Sendai Framework for Disaster Risk Reduction, a seminal global framework adopted at the Third UN World Conference on Disaster Risk Reduction in 2015, acknowledges the need to enhance resilience to all hazards, including tropical cyclones, by guiding nations toward comprehensive risk reduction strategies (UNISDR, 2015). Reducing risk is also recognized as a key aspect of sustainable development in the Sustainable Development Goals (SDGs)

(UN General Assembly, 2015) and the Paris Agreement on climate change (UNFCCC, 2015). As framed by the Intergovernmental Panel on Climate Change (IPCC, 2012), risk is understood as the product of hazard, exposure, and vulnerability - thereby highlighting the role of vulnerability and exposure in addition to hazards for changes in risks. This doctoral thesis is situated within the Sendai Framework's principles and adopts the IPCC's concept of climate risk as outlined in Box 1.1, along with associated definitions and ideas. This risk concept is drawn explicitly from the IPCC Special Report on Extremes (IPCC, 2012) and the Fifth Assessment Report (2014), while also incorporating insights from Zscheischler et al. (2018).

Box 1.1: Definitions of climate risk and related terms; adapted from Zscheischler et al. (2018).

Risk: "The *effect of uncertainty on objectives* (ISO, 2009, 2018; Lark, 2015). According to the IPCC (Oppenheimer et al., 2014), risk is the potential for consequences when something of value is at stake and the outcome is uncertain, recognizing the diversity of values. Risks arise from the interaction between hazard, vulnerability and exposure and can be described by the formula:

$$risk = (probability\ of\ events\ or\ trends)\ \times consequences \tag{1.1}$$

where consequences are a function of the intensity of hazard (event or trend), exposures, and vulnerability. Here, we use the term risk to refer to environmental and societal impacts from weather and/or climate events." (Zscheischler et al., 2018)

Exposure: "The presence of people, livelihoods, species or ecosystems, environmental functions, services, and resources, infrastructure, or economic, social, or cultural assets in places and settings that could be adversely affected" (IPCC, 2012; Oppenheimer et al., 2014; Zscheischler et al., 2018)

Vulnerability: "The propensity or predisposition to be adversely affected" (IPCC, 2012; Oppenheimer et al., 2014); "Vulnerability encompasses a variety of concepts and elements including sensitivity or susceptibility to harm and lack of capacity to cope and adapt." (Zscheischler et al., 2018)

Hazard: "The potential occurrence of a natural or human induced physical event or trend or physical impact that may cause loss of life, injury, or other health impacts, as well as damage and loss to property, infrastructure, livelihoods, service provision, ecosystems and environmental resources" (Oppenheimer et al., 2014). In this thesis, "the term hazard usually refers to climate-related physical events." (Zscheischler et al., 2018)

Weather and climate events: "Events at spatial and temporal scales varying from local weather to large-scale climate modes." (Zscheischler et al., 2018)

Impacts: "The effects of physical events on natural and human systems". (Zscheischler et al., 2018)

When calculating a measure of tropical risk following Equation 1.1, *consequences* are represented

by quantifiable impacts of a tropical cyclone event. In this thesis, these impacts are direct damages of tropical cyclones on physical assets reported in monetary values. The *probability of events* in Equation 1.1 can be derived from a statistically modeled distribution or estimated as a frequency probability based on how often similar events have happened in simulations or observations.

The breakdown of risk into the components hazard, exposure, and vulnerability (Box 1.1) offers a methodological path to disentangle the complexity of quantifying risk and has thus been widely adapted for climate risk assessments (Ward et al., 2020). A particular approach for climate risk assessment incorporating this logic is event-based modelling, which emanates from the catastrophe models the insurance industry uses. As used in the insurance industry, many existing catastrophe models have limitations that may restrict their applicability to climate risk assessments beyond the insurance industry. First, they are not open-source, and their scientific basis might not be fully documented in the peer-reviewed literature (Sobel and Tippett, 2018). Second, most catastrophe models developed in the insurance industry report impacts as (insured) financial losses and neglect other impacts like loss of life or livelihoods, or even losses in regions where insurance penetration is limited. Yet, in recent years, catastrophe models have found a more comprehensive range of applications, for example, in international development finance and disaster risk reduction considering a wider range of assets and, in some cases, risk transfer mechanisms (e.g., Cummins and Mahul, 2009; Joyette et al., 2015; Linnerooth-Bayer and Hochrainer-Stigler, 2015; Souvignet et al., 2016; Bresch, 2016; Ciullo et al., 2023; Steinmann et al., 2023). Third, the hazard component of many catastrophe models is based on a statistical analysis of historical events and incorporates little if any of the physics that relates extreme weather events to the large-scale climate (Sobel and Tippett, 2018). This limits the models' utility for assessing changing risks under climate change. Even if we were performing risk assessments for the present, the assumption of stationary statistics is flawed because climate change has already altered hazard characteristics (for TCs e.g., Knutson et al., 2019). However, evolving from the industry catastrophe models, other probabilistic climate risk models overcome these limitations and are built in a modular, open fashion for risk assessments across different temporal and spatial scales and various hazards, including multi-hazard perspectives. Examples of such event-based, open-source, peer-reviewed modeling platforms include CAPRA (Cardona et al., 2014), CLIMADA (Aznar-Siguan and Bresch, 2019; Bresch and Aznar-Siguan, 2021), HAZUS (Schneider and Schauer, 2006), and RISKSCAPE (Paulik et al., 2022).

In this thesis, I use the CLIMADA (CLIMate ADAptation) risk and impact modelling framework. CLIMADA is implemented in the high-level and general-purpose programming language Python and is developed and maintained as a community project. The source code is openly available under the terms of the GNU General Public License Version 3 (Aznar-Siguan and Bresch, 2019; Bresch and Aznar-Siguan, 2021). In CLIMADA, the risk formulation provided by Equation 1.1 is reformulated as:

$$risk = probability \times severity \tag{1.2}$$

with

$$\begin{aligned} severity &= F(hazard\ intensity,\ exposure,\ vulnerability) \\ &= exposure * f_{imp}(hazard\ intensity) \end{aligned} \tag{1.3}$$

In its simplest form, × in Equation 1.2 stands for a multiplication; more generally, it denotes the convolution of the respective distributions of probability and severity. As defined in Equation 1.3, *severity* can be understood as the interaction of hazard intensity, exposure and vulnerability (Aznar-Siguan and Bresch, 2019; Bresch and Aznar-Siguan, 2021). In detail, the hazard component is organized into sets of events, where each event is characterized by a spatial distribution of hazard intensity and time-related information like occurrence date, frequency, or probability. The exposure component depicts the spatial arrangement of population, assets, or ecosystems that could potentially be impacted by a hazard. The vulnerability component is described using impact functions f_{imp} parameterizing to what extent a certain kind of exposure might be influenced by a specific hazard. Note that impact functions are also called damage functions or vulnerability curves (Aznar-Siguan and Bresch, 2019). Furthermore, the CLIMADA framework may be embedded in the economics of climate adaptation (ECA) methodology to inform decision-makers about the impact on their economies, including cost/benefit perspectives on specific risk reduction measures (Bresch and Aznar-Siguan, 2021).

The default setup of CLIMADA used in this thesis is to simulate direct economic damage in the form of impact on the built environment from a given tropical cyclone hazard set on a continental to global scale. Throughout this thesis, I work with largely the same exposure and vulnerability setup and alter hazard representations. In Chapter 2, I compare different hazard sets for global, present-day impact assessment. In each of the Chapters 3 and 4, I use one of the hazard models compared in 2 in an uncertainty and sensitivity analysis for future, global tropical cyclone risk change. In Chapter 5, I repeat the uncertainty and sensitivity analysis of the previous chapters and revisit the idea of an intermodel comparison; this time for uncertainty and sensitivity of future TC risk assessment. The common thread across these studies is that I aim to translate these variations in hazard model choice into implications for risk assessment more broadly.

Note that while I express tropical cyclone risks as direct economic damage in this thesis, the same hazard sets could just as well be applied to model impacts on human lives and livelihoods, forests, power production, the agricultural sector, or indirect economic effects. Finally, throughout this thesis, I often use the two terms *risk* and *impact* interchangeably even though they are strictly speaking not the same (see Box 1.1). Generally, risk is concerned with the likelihood of an event happening and the potential negative outcomes, while impact deals with the actual effects and consequences that occur when the event or hazard takes place. In my work, I often call backward-looking assessments *impact* and forward-looking assessments *risk*. For instance, I refer to CLIMADA as *impact modelling platform* in Chapter 2 concerning the historical period and *risk modelling platform* in Chapters 3, 4, and 5 pertaining to future assessments. Hence, depending on the context, the interplay of hazard, exposure and vulnerability is termed *risk* or *impact* but should not be understood as mutually exclusive.

1.2.3 Uncertainty and sensitivity analysis

Providing reliable tropical cyclone risk assessment is particularly challenging due to severe uncertainties in the model input components and model structure (Kropf et al., 2022). Consequently, there is a growing consensus in the risk modelling community that a systematic and thorough treatment of uncertainties and sensitivities is indispensable for a transparent and robust risk assessment (e.g.,

Pianosi et al., 2016; Kropf et al., 2022; Dawkins et al., 2023; Meiler et al., 2023b). The first step towards this aim is to acknowledge different types of uncertainty and assess if these can be quantified and reduced. I briefly review these aspects in the following paragraphs. The next step is the actual quantification of uncertainties in the tropical cyclone risk model. An overview of such approaches is subject to the subsequent section.

Philosophers, policy analysts, and scientists have suggested various ways to characterize and categorize uncertainties. Here, I focus on the three types of aleatory, epistemic and normative uncertainty relevant to tropical cyclone risk assessment.

Aleatory uncertainty, also known as stochastic uncertainty, arises from inherent randomness or variability in the natural processes involved (Walker et al., 2003). In the context of tropical cyclones, this type of uncertainty includes the intrinsic variability in atmospheric conditions, ocean temperatures, and other factors that influence the formation and behavior of tropical cyclones. For example, the random variations in wind patterns or sea surface temperatures that can affect the track and intensity of a tropical cyclone are sources of aleatory uncertainty. Aleatory uncertainty can be quantified using statistical methods like Monte Carlo simulations to estimate the probability distribution of potential outcomes. However, it cannot be entirely reduced as it is an inherent characteristic of natural processes (Henrion and Morgan, 1990).

Epistemic uncertainty, also known as model uncertainty, stems from limitations in our knowledge and understanding of the modeled system (Walker et al., 2003). For tropical cyclone risk assessment, this includes uncertainties related to the accuracy of synthetic tropical cyclone models, the completeness and quality of historical data, and gaps in our understanding of how various environmental factors interact to influence tropical cyclones. Epistemic uncertainty can be quantified, for example, when using multiple climate models to project future tropical cyclone behavior. The spread of results from these models provides a measure of the level of epistemic uncertainty in the projections. Epistemic uncertainty can be reduced through improved models, data collection, and research (Walker et al., 2003; Curry and Webster, 2011; Bradley and Steele, 2015; Knutti, 2018). However, complete elimination is unlikely as natural systems can be inherently unpredictable and new research may reveal further complexities.

Normative uncertainty, also known as ethical or value-based uncertainty, arises from value judgments, ethical considerations, and subjective decision-making processes (Bradley and Drechsler, 2014; Bradley and Steele, 2015; Mayer et al., 2017). Examples of normative uncertainties in tropical cyclone risk modelling include the decision on the valuation unit (monetary valuation or valuation of human life) (Mayer et al., 2017), the choice of model type or the unit of risk metric (e.g., expected annual damage or tail risk assessment). Normative uncertainties are generally not quantifiable in the same way as aleatory and epistemic uncertainties. However, efforts can be made to reduce normative uncertainty by promoting transparency and inclusiveness in decision-making, engaging stakeholders with diverse perspectives, and considering ethical considerations in risk assessment (Hansson, 2016).

It is important to note that these types of uncertainties are not mutually exclusive, and often, multiple uncertainties coexist in risk assessment.

In the context of climate-related studies and assessments, it is furthermore helpful to distinguish

two types of epistemic uncertainty: scenario uncertainty and projection uncertainty. Scenario uncertainty refers to the uncertainty associated with the future pathways of greenhouse gas emissions originating from different potential trajectories of human activities, such as economic development, energy use, and population growth (Walker et al., 2003). For tropical cyclone risk assessments, scenario uncertainty may involve considering how tropical cyclone intensity and frequencies change for different emission scenarios and how various economic growth pathways alter the asset value potentially exposed to tropical cyclones. Therefore, using different emission scenarios to model hazard and exposure helps account for possible futures based on socioeconomic and policy choices. Scenario uncertainty is not directly quantifiable (as it depends on future human choices), but it can be represented using multiple scenarios that encompass a range of possible futures (Moss et al., 2010; Knutti, 2018).

In contrast, projection (or model) uncertainty describes the uncertainty inherent in the climate models themselves. Specifically, climate scientists refer to uncertainties in the model structure, the numerical approximation of the model equations, and the choice of parameter values as model uncertainty (e.g., Hawkins and Sutton, 2009). However, it is crucial to acknowledge that climate models, in essence, are not inherently uncertain. Instead, the uncertainty lies in the connection between these models and the actual climate system they are designed to represent. In other words, what is often termed *projection or model uncertainty* may be better described as *representational uncertainty* (Parker, 2010; Knutti, 2018). For tropical cyclone risk assessment, projection uncertainty might involve using tropical cyclone hazard sets downscaled from multiple climate models (Chapter 3), different parametric wind models for the hazard generation (Chapters 3, 4, and 5), or tropical cyclone event sets from multiple tropical cyclone hazard models (Chapters 2 and 5).

In summary, while some uncertainties in tropical cyclone risk assessment can be diminished, others cannot be entirely addressed. Normative uncertainty is inherently subjective, making it impossible to fully quantify or eliminate. Aleatory uncertainty arises from natural randomness and, as a fundamental aspect of the system, cannot be completely reduced, although it can often be described. Epistemic uncertainty can be partially reduced through continuous improvement in knowledge and models, but complete elimination is challenging due to the inherent complexities of tropical cyclones and the climate system.

In the following section, I focus on approaches and methods to quantify uncertainties in tropical cyclone (and other weather and climate) risk assessments. First, assessing tropical cyclone risk involves making several subjective decisions regarding the representation of hazards, exposure, and vulnerability. As a result, transparent and reliable climate risk assessments and subsequent adaptation decision-making must consider and explore the numerous uncertainties involved in the process.

Uncertainty in the tropical cyclone hazard component includes choosing an appropriate tropical cyclone hazard set for the application at hand. There are different types of tropical cyclone models, ranging from fully statistical (e.g., Vickery et al., 2000; Bloemendaal et al., 2020b) to fully dynamical (e.g., Roberts et al., 2020b) all with their strengths and weaknesses. I thus investigate how the choice of tropical cyclone model influences the modeled tropical cyclone impact in Chapter 2. Furthermore, hazard uncertainties comprise the choice for the parametric wind model used to compute a 2D wind

field from the tracks (see Chapters 3 and 4). These are two examples of epistemic uncertainties in the hazard component. In contrast, sources of natural variability, such as the inherent fluctuations of the El Niño-Southern Oscillation (ENSO), represent aleatory uncertainty. It is, therefore, important to include multiple realizations (i.e., ensembles) of the same model to represent this type of uncertainty. Moreover, when studying future tropical cyclone risks, modelers need to choose between tropical cyclone hazard sets originating from different climate models and climate model generations (CMIP5 vs. CMIP6) and different emission scenarios (see Chapters 3 and 4). Hence, these choices fall into the categories of projection or model uncertainty and scenario uncertainty, as described in the paragraphs above. Finally, because hazard models are *models* and thus imperfect representations of reality, they require steps of evaluation, calibration and interpretation, which are additional sources of uncertainty.

Uncertainty in the exposure is subject to choices of the exposure unit, for instance, exposed people, assets or ecosystems to tropical cyclones (normative uncertainty). It furthermore includes uncertainties in the methods to represent these exposed people, assets or ecosystems (epistemic uncertainties). Besides, the exposure is subject to representation and scenario uncertainty analogous to the hazard component. Various models describe different levels of future socio-economic development (representation uncertainty) for different pathways (scenario uncertainty) (Riahi et al., 2017). In Chapters 3 and 4, I investigate some of these epistemic uncertainties of the exposure component.

Lastly, the vulnerability component stands out for its inherent complexities and modelling challenges, often exacerbated by significant data limitations (Füssel, 2007; Hinkel, 2011). We describe vulnerability by impact functions, which are calibrated by regressing recorded impacts against information about hazard and exposure. However, impact data required to derive such relationships are very scarce and often must be aggregated across large regions and other discriminators such as social welfare to obtain enough data points for calibration; hence are subject to normative and epistemic uncertainty (Baldwin et al., 2023). Furthermore, other sources of epistemic uncertainty include different methods used to derive and fit impact functions, different (idealized) forms describing them, and consequently, different parameters, which need to be constrained in the calibration step (Wilson et al., 2022). For example, Eberenz et al. (2021) estimated the impact function parameter describing the hazard intensity at which 50 % of the assets are damaged (V_{half}) to be 188.4 $\mathrm{m\,s^{-1}}$ when fitted against the total damages of all storms in the Philippines in contrast to 85.7 $\mathrm{m\,s^{-1}}$ for fitting damages from each storm individually. Reasons for this significant uncertainty may include variations in vulnerability between urban and rural areas, lack of surface roughness modeling, unaccounted tropical cyclone sub-hazards (rainfall-driven flooding, storm surge, landslides), and limitations of the exposed asset value layer (Eberenz et al., 2021). Finally, knowledge and expertise to represent vulnerability of future socio-economic systems is largely missing. For lack of better options, I therefore default to assume no future vulnerability changes in this thesis.

This list of uncertainties in hazard, exposure and vulnerability is not exhaustive. But it illustrates which types and sources of uncertainties risk modellers may propagate through their risk modelling chain. Next, I describe how to quantify uncertainties and sensitivities in climate risk assessments.

Different methods for uncertainty and sensitivity analysis have been proposed in the scientific literature (e.g., Saltelli et al., 2008; Pianosi et al., 2016; Saltelli et al., 2019; Kropf et al., 2022).

Uncertainty and sensitivity analysis both involve running model simulations repeatedly against different values of the uncertain input factors (i.e., hazard, exposure, vulnerability) by Monte Carlo simulations, but they differ in their objectives. Uncertainty analysis deals with understanding the overall variability and uncertainty in model outputs due to the uncertainty in input parameters or data. Sensitivity analysis focuses on identifying and quantifying the relative importance of individual input parameters in influencing the variability or uncertainty in model outputs. In other words, uncertainty analysis focuses on *quantifying* uncertainty, while sensitivity analysis focuses on *apportioning* output uncertainty to the different sources input factors (e.g., Saltelli et al., 2008). Sensitivity analysis can be performed to consider the output variability against variations of input factors around a specific value (local sensitivity analysis) or variations within the entire variability space of the input factors (global sensitivity analysis) (Pianosi et al., 2016). Moreover, input factors can be varied individually, keeping all other input factors fixed or varying all the input factors simultaneously (Pianosi et al., 2016). Usually, in local sensitivity analysis, input factors are varied individually, and in global sensitivity analysis, all simultaneously. In this thesis, I conduct global sensitivity analysis to avoid shortcomings of local analyses, which fail to properly explore the space of the input factors as discussed by Saltelli et al. (2019).

CLIMADA and other probabilistic risk assessment frameworks are a great starting point for uncertainty and sensitivity analysis, as they are designed to be run repeatedly with minimal computational expense. Therefore, Kropf et al. (2022) integrated the *SALib – Sensitivity Analysis Library in Python package* (Herman and Usher, 2017) into the CLIMADA code environment via the UNcertainty and SEnsitity QUAntification (unsequa) module, enabling uncertainty and sensitivity quantification for all risk assessments conducted within the CLIMADA environment. The module follows similar steps as a generic uncertainty and sensitivity analysis (Pianosi et al., 2016).

In detail, it requires the specification of a probability distribution for each uncertain input factor (i.e., input data and parameters related to the hazard, exposure and vulnerability components). Then samples from these distributions are used to generate plausible alternative input combinations. The resulting output is computed for each input combination, yielding a probability distribution of results and providing the basis for the uncertainty analysis. The unsequa module then calculates sensitivity indices for each input factor. Sensitivity indices quantify the relative importance of each uncertain input factor with a number varying between 0 and 1. There are different methods to compute these sensitivity indices. The default method in the unsequa module is a variance-based approach. Variance-based methods rely on treating input factors as random variables, creating output distributions. The output's variance represents uncertainty, and an input factor's contribution to this variance indicates its sensitivity (Pianosi et al., 2016). Variance-based indices are defined as *first-order indices* (or main effects), which measure the direct contribution to the output variance from individual factors. They are often used to rank the input factors according to their relative contribution to the output variability (ranking) (Saltelli et al., 2008). *Total-order indices* (or total effects) measure the overall contribution from an input factor considering its direct effect and its interactions with all the other factors, which might amplify the individual effects. They are commonly used for screening, which aims at identifying the input factors - if any - with negligible influence on the output variability (Saltelli et al., 2008).

The most delicate step of an uncertainty and sensitivity analysis is the definition of input factor probability distributions. Often this information is not readily available, and consequently, it is not evident how to perturb the input components to represent their uncertainty meaningfully. In particular, it is challenging to define physically consistent statistical perturbations of geospatial data (Kropf et al., 2022). In this thesis, I have thus defined discrete sets of scientifically justified inputs instead of specifying probability distributions for the input factors more or less arbitrarily. For example, when representing the uncertainty in the hazard component, we sample from a list of tropical cyclone simulations informed by different climate models of the CMIP6 generation, each of which has been assessed as plausible by different climate modelling centres or inter-comparison projects. In doing so, we make no assumption about which input selections are more or less likely, but instead define the results in terms of the uncertainty and sensitivity across these discrete settings (Chapters 3.4.8, 4.2.2 & 5.2.4). This approach still relies on expert judgment in defining the discrete set of plausible inputs and is thus subject to normative uncertainty. Consequently, the results depend significantly on this definition of inputs, as is characteristic for uncertainty and sensitivity analysis (Pianosi et al., 2016; Kropf et al., 2022). Furthermore, it is impossible to define discrete input sets for all input factors. For instance, we vary the input parameter describing the impact functions across a continuous range because no scientifically justified alternative representations of impact functions exist that we could sample from. Instead, we inform these input parameter ranges from a measure of uncertainty reported in the study accompanying the set of calibrated impact functions we use (Eberenz et al., 2021). In sum, I aim to capture and quantify uncertainties in hazard, exposure, and vulnerability systematically while limiting the normative uncertainty I introduce by making model choices. Ultimately, the two main goals of the uncertainty and sensitivity analysis I perform in this thesis are to 1) enhance the information value of tropical cyclone risk assessments, producing transparent outputs and providing a comprehensive context to quantitative results for robust decision-making; and 2) inform future research efforts to reduce the uncertainty in tropical cyclone risk assessments further.

CHAPTER 2

Intercomparison of regional loss estimates from global synthetic tropical cyclone models

Tropical cyclones (TCs) cause devastating damage to life and property. Historical TC data is scarce, complicating adequate TC risk assessments. Synthetic TC models are specifically designed to overcome this scarcity. While these models have been evaluated on their ability to simulate TC activity, no study to date has focused on model performance and applicability in TC risk assessments. This study performs the intercomparison of four different global-scale synthetic TC datasets in the impact space, comparing impact return period curves, probability of rare events, and hazard intensity distribution over land. We find that the model choice influences the costliest events, particularly in basins with limited TC activity. Modelled direct economic damages in the North Indian Ocean, for instance, range from 40 *to* 246 *billion USD for the* 100*-yr event over the four hazard sets. We furthermore provide guidelines for the suitability of the different synthetic models for various research purposes.*

2.1 Introduction

The powerful impact of tropical cyclones (TCs) disrupts societies in many coastal regions in the tropics and subtropics. For example, the 2017 Hurricanes Harvey, Irma and Maria, caused total damages exceeding 260 billion USD (NOAA, 2021). The last, Maria, impacted several countries, including Dominica, Dominican Republic, Guadeloupe (FRA), Haiti, Martinique (FRA), Puerto Rico, United States of America, Virgin Island (US), and Virgin Island (UK). The losses in Dominica alone totaled to 1.5 billion USD - estimated at over 200% of its Gross Domestic Product (GDP) (IMF, 2021). It is therefore crucial to support risk mitigation efforts and increase societal resilience towards such events with reliable TC risk assessment. Such assessments, however, are complicated as reliable TC records are scarce. Additionally, only a small number of the TCs make landfall every year (Weinkle et al., 2012), and when they do, a relatively small stretch of coastline is affected (Pugh and Woodworth, 2014). The resulting impacts are higher in urban areas than rural or uninhabited regions, yielding a

This chapter is published as Meiler et al. (2022b)

heterogeneous picture of TC damage. Moreover, reliable, global-scale documentation of past TCs is only available since the 1980s, which means that there might not be a single event on record for many coastal locations in the observational dataset. This substantial lack of information on the potential magnitude and probability of TCs complicates risk assessment and risk management efforts.

A common practice to overcome this data scarcity is synthetic modelling, in which larger datasets of TC behavior (theoretically possible in given climate conditions) are created. Prominent methods are purely statistical techniques (Vickery et al., 2000; Bloemendaal et al., 2020b) and coupled statistical-dynamical models (Emanuel et al., 2006, 2008; Lee et al., 2018). The fully statistical methods use autoregressive formulas to simulate both the track and intensity of a TC (Bloemendaal et al., 2020b). The statistical-dynamical approaches use a dynamical model (beta-and-advection model (Marks, 1992)) for the track generation, and simulate intensity changes along the track using a dynamical model (Emanuel et al., 2006, 2008) or an autoregressive model using physics-based drivers (Lee et al., 2018). This dynamical downscaling of TC tracks from climate model output is not limited to current climate conditions but has also been used to model future TC characteristics (Bhatia et al., 2018; Emanuel et al., 2008; Emanuel, 2013; Knutson et al., 2015; Lee et al., 2018, 2020; Roberts et al., 2020a,b; Walsh et al., 2015, 2016). Note that TCs can also be partially resolved by high-resolution global climate models with a horizontal scale of 10 km to 25 km and may be studied without further downscaling (Camargo and Wing, 2016; Bacmeister et al., 2018; Gettelman et al., 2018). However, the convergence on intensity is not achieved until grid spacings are in the range of 1 km to 2 km (Davis, 2018) and the number of TCs generated in these simulations is not large enough to conduct risk assessment.

The synthetic modelling approaches described above provide us with insights on synthetic TC tracks and intensities, which often form the input hazard datasets in catastrophe models. Translating this hazard into risk also requires information on social and economic variables (IPCC, 2012). Catastrophe models integrate hazard, exposure, and vulnerability data to compute risk and quantify socio-economic impacts (Aznar-Siguan and Bresch, 2019). Risk from a catastrophe modelling perspective is often expressed in expected annual damages (EAD) or similar metrics and visualized using impact return period (RP) curves, showing the inverse of an exceedance probability and being evaluated at the spatial unit of interest (e.g. countries, cities or insurance portfolios). In this study, we use the open-source, peer-reviewed CLIMADA (CLIMate ADAptation) (Aznar-Siguan and Bresch, 2019) platform to simulate direct economic damage in the form of impact on the built environment from a given TC hazard set. Note that we only consider wind as the driving physical hazard for the resulting socio-economic impact.

Past comparisons of synthetic TC models have been limited to the hazard component (Sobel et al., 2019; Bloemendaal et al., 2020b; Jing et al., 2021) and have not evaluated differences in risk estimates. We hypothesize that the models which predict TC climatology may not cover the full range of important metrics and views in TC risk assessment and loss estimation. Hence, we overcome this research gap and evaluate how the choice of hazard models influences the estimation of losses rather than the estimation of TC climatology. In this study, the most influential (academically available/non-commercial) synthetic TC hazard models are compared in their function to serve as input for TC risk modelling. More specifically, we couple the following sources of tropical cyclone

tracks with CLIMADA to evaluate their performance on an impact and risk level: i) historical TCs from the International Best Track Archive for Climate Stewardship (IBTrACS) (Knapp et al., 2010); ii) probabilistic events obtained from historical TCs by a direct random-walk process (IBTrACS_p) (Kleppek et al., 2008); iii) synthetic tracks from a fully statistical model, the Synthetic Tropical cyclOne geneRation Model (STORM) (Bloemendaal et al., 2020b); and synthetic tracks from the coupled statistical-dynamical models iv) developed by Emanuel et al. (2006, 2008) (hereafter the MIT model) (Emanuel et al., 2006, 2008) and v) the Columbia HAZard model (CHAZ)(Lee et al., 2018). After assessing these models at an impact- and risk-level, we can use our results to link some of the intermodel differences to key TC model characteristics and provide guidelines for other researchers to determine the applicability of each dataset depending on the research objective. Such insights will support risk assessment efforts both in the public (e.g., academia, policymakers, and non-governmental organizations) and the private sectors (e.g., consultancy and (re)insurance companies).

2.2 Results

2.2.1 Comparison of tropical cyclone intensities

The impact model used in this study is driven by the TC's intensity expressed as maximum 1-minute sustained wind speed experienced at any land point. To support the interpretation of economic impacts, we first evaluate the distribution of the TC intensity over land across the five TC datasets. When solely looking at TC intensity as reported in the synthetic datasets, we find an average relative deviation from synthetic to historical frequencies across the categories of 28.4%. Next, to translate these TC intensities to impact, we couple the same parametric wind field model(Holland, 2008) to all five sources of TC tracks. Aside from TC intensity, parametric wind models also depend on the reported radius of maximum winds (RMW), which is often poorly documented outside of the North Atlantic (if at all). Therefore, our wind fields often rely on statistical estimates of the RMW. Still, the agreement of TC intensity in the synthetic datasets with the observational records does not change significantly if we use the estimate based on the wind fields (25.4%) instead of TC intensity values directly from the synthetic track datasets (see Supplementary Figure A.1).

Therefore, and because the hazard component of the CLIMADA impact model used in this study consists of the 2D wind field, we only contrast the intensities from the wind fields in the following paragraphs. Across all basins and datasets, the agreement with IBTrACS for weak (Cat. 1 or weaker) TCs is better than for major (Cat. 3-5) TCs. There are only very few exceptions, like CHAZ in Western Pacific where the agreement is comparable. Overall, the average relative deviation for major TCs (19.6%) is much higher than the average relative deviation for weak TCs (8.0%). The larger disagreement of intense TCs highlights the challenge for reliable TC risk assessments to generate TC datasets with a realistic representation of the major TCs (Cat. 3-5). This is of particular importance because the highest impacts are often driven by intense TCs (Emanuel, 2021).

More and larger differences between the different models emerge when comparing the results across the different basins. The region with highest intermodel differences and intra-model uncer-

tainties is the North Indian Ocean, where observational data is particularly sparse (average of 5 TCs per year (Liu et al., 2021)). In this region, the relative variability in each TC intensity bin (see Methods) is large for all TC categories and track sets, with the largest variability found for the MIT dataset, amounting to a factor 5 for the Cat. 5 TCs (Fig. 2.1). The STORM and CHAZ datasets stand out with notably more Cat. 3-5 events than in the other synthetic datasets, amounting to 27.58% (± 10.77%) and 24.25% (± 5.62%), respectively (compared to 10.13% (± 3.70%) and 12.39% (± 4.26%) in the other datasets).

The relative variability within each dataset is generally highest for the MIT tracks with regional standard deviations ranging from 0.16 to 0.62 (IBTrACS_p 0.04–0.21, STORM 0.15–0.39, CHAZ 0.11–0.27). Only for Cat. 5 TCs in the Southern Hemisphere, the STORM model shows a substantially larger relative variability than the other track sets, with a standard deviation of 0.39 (IBTrACS_p 0.04, MIT 0.16, CHAZ 0.11).

Overall, the Western Pacific is predominantly the region with the most intense TCs, consistently across all datasets: In case of IBTrACS, the average TC (including tropical storms) in the Western Pacific has a maximum wind speed of 41.5 m/s (North Atlantic/Western Pacific 34.2 m/s, North Indian Ocean 34.7 m/s, Southern Hemisphere 36.0 m/s). The only exception is the MIT dataset, where the average TC in the Southern Hemisphere has higher maximum wind speed (41.0 ± 1.0 m/s) than in the Western Pacific (39.6 ± 0.6 m/s) (Fig. 2.1).

2.2.2 Impact analysis

To move from TC hazard to impact and risk requires additional information on exposure of assets or populations and their specific vulnerability to the hazard (IPCC, 2012). However, the specific objective of the analysis determines what (hazard) input data is required for the impact calculation. If one is interested in estimating impacts from a historical event, the hazard component can be retrieved from observational data directly (i.e., IBTrACS). More specifically, synthetic datasets are unsuitable for such cases, as they do not contain actual historical events. For example, by coupling IBTrACS to CLIMADA, we find that damages from Hurricane Maria (2017) are estimated to be 77 billion USD. This estimate is in line with the reported damage of 90 billion USD at a 90% confidence range of 65 to 115 billion USD (Pasch et al., 2017). A comprehensive evaluation of how modelled losses in CLIMADA compare to reported losses can be found in Eberenz et al. (2021).

Another impact-related analysis consists of determining the probability of a certain impact in a location or region. This information is of particular importance for the implementation of adaptation measures, aimed at reducing impacts of TC events (Ha, 2018). Such measures often follow protection standards, which are given in terms of a probability of exceedance; the inverse being the RP (in years). However, adequately calculating such RPs and corresponding impacts requires hazard data with a temporal range exceeding the RP of interest. Observational data sets are therefore generally unfit for answering such questions, as their spatial and temporal distribution is sparse, particularly when assessing extreme events. Synthetic TC tracks, on the other hand, provide a wealth of information on a wide range of possible TC events in any region of interest, thereby overcoming the limitations imposed by the historical data. We can therefore use the different synthetic datasets to derive impact RP curves for each of the four study regions (Fig. 2.2). Note that RP curves are shaped by the

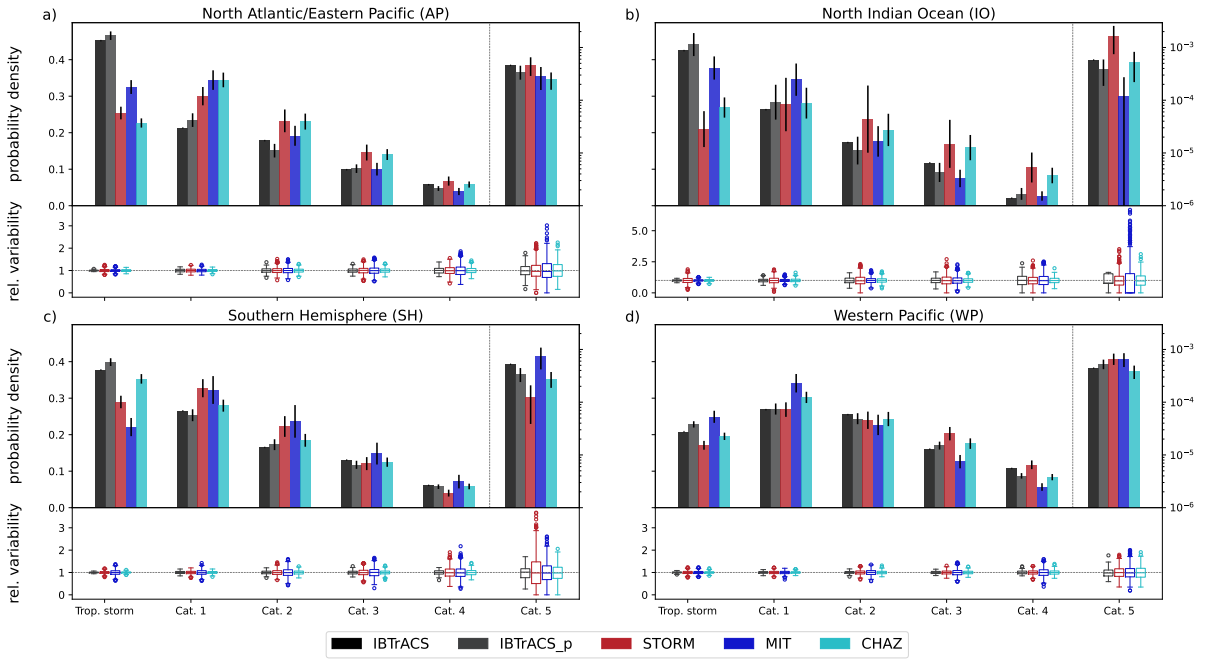

Figure 2.1: Regional distribution of tropical cyclone intensities for the five track sets. Panels a)-d) compare the relative frequency of tropical cyclones (TCs) belonging to each category of the Saffir-Simpson Hurricane Wind Scale across the five track sets (IBTrACS, IBTrACS_p, STORM, MIT, CHAZ), separately for the four regions a) North Atlantic/Eastern Pacific, b) North Indian Ocean, c) Southern Hemisphere, and d) Western Pacific. The mean and standard deviation (black error bars) over all the subsamples in each category (see Methods) of the frequencies are shown in the upper part of each plot while the lower part displays the relative variability in each intensity bin (as box plots with a line at the median, a box denoting the inter-quartile range (IQR) and whiskers extending 1.5-times IQR; points are outliers). Note that the frequencies of Cat. 5 TCs are shown on a secondary y-axis in log scale. The wind speeds of each TC event are taken from the modelled wind fields over land. The same plot with wind speeds taken directly from the track data is provided in Supplementary Figure A.1.

intensity and frequency of events. The latter is modelled differently across datasets, and, most notably, needs to be bias-corrected for the CHAZ hazard set (see Discussion and Methods). We also plot the RP curves of the historical IBTrACS for reference including records from the recent time period since 1980 because there is no globally consistent, reliable meteorological information on historical (high-impact) TCs that occurred in the pre-satellite era (Knapp et al., 2010; Schreck et al., 2014). Up until the 39-year RP, the historical impact RP curves are well within the range of the impact RP curves of the synthetic tracks. However, we refrain from suggesting the IBTrACS impact RP curves as a modelling benchmark for synthetic datasets since our impact model depends on unreliable storm size data (see Methods).

We observe that, generally, STORM tends to produce less low-impact events and more high-impact events than the other synthetic models. For high-frequency/low-impact events, CHAZ stands out as the dataset with the lowest RPs over all regions. This finding is not mirrored in the distribution of hazard intensities as shown in Figure 2.1, but it results from the interplay of hazard, exposure and vulnerability that feed into the impact calculation. In other words, part of the model differences in estimating impacts are driven by the underlying exposure rather than hazard alone (Fig. 2.1 and Supplementary Figure A.1). To demonstrate the sensitivity of our results to exposure, we plot the

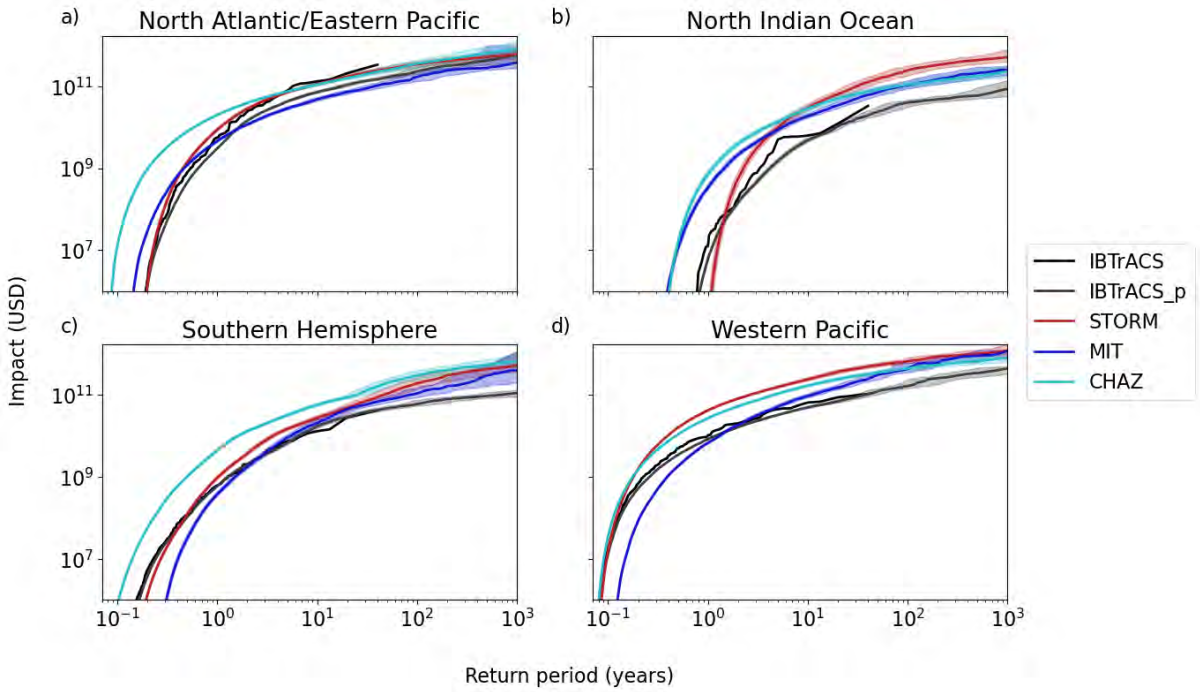

Figure 2.2: Impact return period curves for the five tropical cyclone track sets. Return periods up to 1000 years for the synthetic track sets (IBTrACS_p, STORM, MIT, CHAZ) and 39 years for the IBTrACS record (black solid curve) are shown in the four regions (a) North Atlantic/Eastern Pacific, b) North Indian Ocean, c) Southern Hemisphere, d) Western Pacific). We use a sub-sampling approach on the synthetic track sets to calculate the median (colored solid curves), the 90% confidence intervals of the impact distribution over 1000 years.

impact RP curves and values for EAD, 100-yr and 1000-yr events on a normalized exposure layer without the spatial heterogeneity of asset values on land in the Supplementary Tables A.3 and A.4.

At fixed RPs, estimated direct economic damages in the North Atlantic/Eastern Pacific (derived from the median impact RPs; solid line in Fig. 2.2) range from 169 to 359 billion USD for the 100-yr event over the four synthetic hazard sets (see Supplementary Table A.2). Comparable values were also computed for the 100-yr events in the Western Pacific, where only the IBTrACS_p diverge from the other synthetic track sets and are estimated to be at approximately one fourth to one third of the STORM and MIT and half the CHAZ damages. The estimated impacts in the Southern Hemisphere are below the 100 billion USD mark for IBTrACS_p and up to 295 billion USD for CHAZ. In the North Indian Ocean, the highest impacts for RPs of more than 1-in-100 years result from the STORM hazard set (246 billion USD), followed by CHAZ (109 billion USD) and MIT data (106 billion USD), and the least damage for the IBTrACS_p (40 billion USD). Generally, the 90% confidence interval (CI) around the 100-yr events ranges from approximately 30 % to 60 % of the median 100-yr loss estimate. This 90% CI can be viewed as a measure for uncertainty and it increases for almost all calculated 1000-yr events, meaning that the estimated impacts deviate more strongly with increasing RPs. The widest possible impact range on the 90% CI for events with RPs of 1000 years stem from the MIT hazard set in the North Atlantic/Eastern Pacific region (185%) and the STORM (143%) and MIT (231%) data in the Southern Hemisphere. In these cases, the CIs span a much larger impact range than for the other hazard sets (∼40 % to 100 %). The impact RP curves are also particularly beneficial to deduce the probability of certain high-impact events. For Hurricane Maria, we can infer

that a Maria-like event in the North Atlantic basin has a RP of approximately 12, 6, 24 and 6 years for the IBTrACS_p, MIT, STORM and CHAZ simulations respectively. We do note here that the RP is inherently dependent on the spatial scale at which the RP is computed (Bloemendaal et al., 2020a). While high-impact events such as Hurricane Maria may occur on average every few years in the North Atlantic basin (as shown through the RP estimations), the chances of such event occurring in a specific country or coastal region are lower, resulting in higher RPs.

Aside from estimating impacts for individual events and at certain RP levels, another commonly used metric is the Expected Annual Damage (EAD; in USD). Mathematically speaking this is the integrated value of impacts across all probabilities. The EAD provides a quantification of risk and is therefore commonly used as a proxy for risk-based insurance premiums (Unterberger et al., 2019) in catastrophe modelling. Comparing the EAD calculated from the different synthetic datasets and historical IBTrACS in the four regions, we find values all within one order of magnitude difference in the North Atlantic/Eastern Pacific region, amounting to 25.65 to 82.47 billion USD (see Supplementary Table A.1). In the other three regions, the intermodel differences are larger, exceeding one order of magnitude. Particularly, we note the high EADs for CHAZ compared to the other synthetic datasets. This difference is likely driven by CHAZ overestimating the impacts of frequent (low RP) events (Fig. 2.2). Moreover, in all regions, the MIT dataset exhibits the largest variance over subsamples (see Methods) around the mean EAD with a standard deviation of 5 % to 10 %, IBTrACS_p and CHAZ the smallest (3 % to 5 %).

2.2.3 Most expensive tropical cyclone events

Understanding the frequency of occurrence of the most expensive (costliest) and rare events is vital for the design and implementation of risk reduction strategies. The three costliest U.S. TC events on record all exceeded the 100 billion USD mark, being Hurricanes Katrina (2005), Harvey (2017), and Maria (2017) (NOAA National Centers for Environmental Information (NCEI), 2023). However, this sample size of historical observations is too small to adequately assess the probability of such rare events; synthetic models, on the other hand, are specifically designed to capture these rare TCs. The probability density of impacts exceeding 100 billion USD (referred to as tail risk in this study) shows that the shape over almost all models is comparable in most regions (Fig. 2.3). However, for the Indian Ocean and Southern Hemisphere we observe that IBTrACS_p is unsuitable for such analysis due to the low-intensity bias in this dataset. Additionally, we also note that in the North Indian Ocean, approximately 3% of all TC events in STORM exceed the 100 billion USD threshold, compared to 0.3-0.4% in MIT and CHAZ. This directly follows from STORM's overestimation of intense (Cat. 4-5) TCs in this basin (see Fig. 2.1), which are the predominant drivers of high impacts. For the other basins, we find a good agreement in tail risk distributions between STORM, MIT, and CHAZ.

The shape of the probability density also reflects some intermodel differences. The STORM and CHAZ simulations contain the highest absolute number of TCs (see Methods) and thus result in a smooth shape of the violinplots. In contrast, the MIT dataset exhibits some distortions at certain impact values and a slightly lower fraction of tail events. This follows from our subsampling routine during which we draw some of the events in the MIT dataset multiple times (see A). Despite this

difference in shape, we conclude that STORM, CHAZ, and the MIT model all contain a sufficiently large and distributed set of tail risk events to robustly and reliably assess the long-term TC risk.

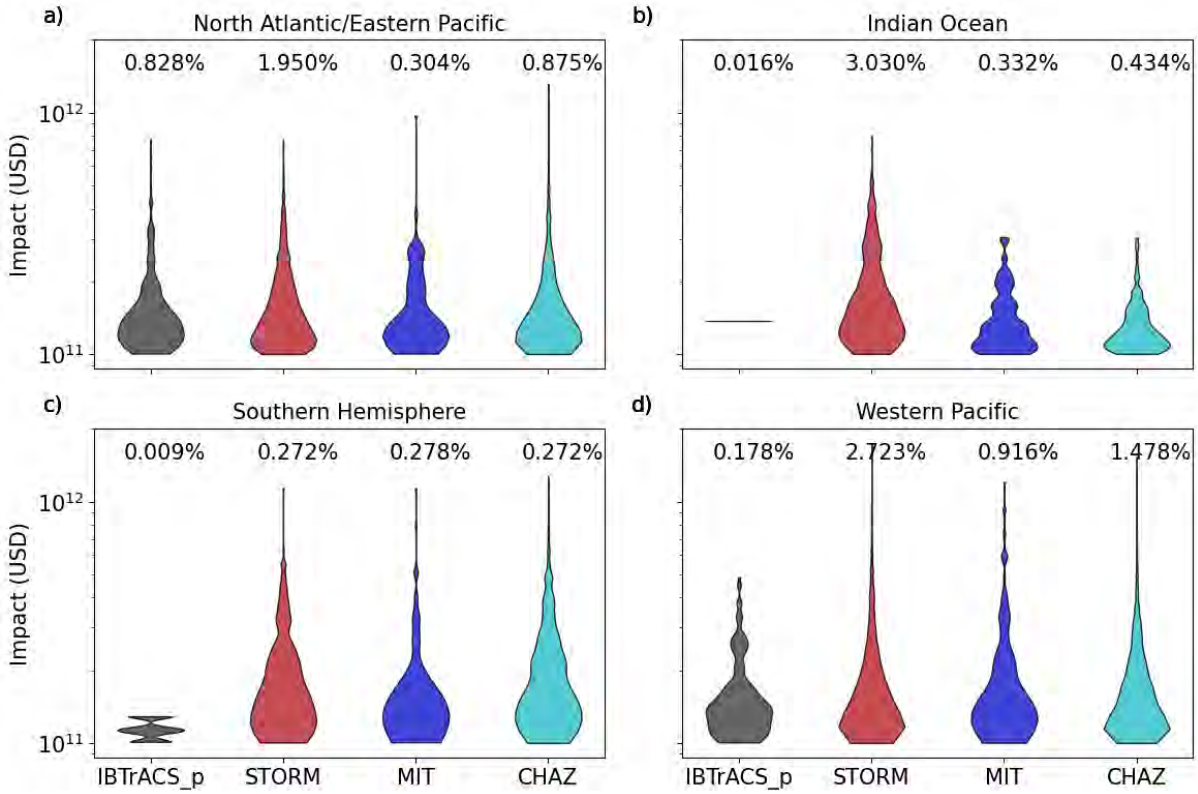

Figure 2.3: Tail risk assessment of the synthetic tropical cyclone datasets across regions. Probability density of impacts exceeding the 100 billion USD impact for the four synthetic datasets (IBTrACS_p, STORM, MIT, CHAZ) in our four study regions (a) North Atlantic/Eastern Pacific, b) North Indian Ocean, c) Southern Hemisphere, d) Western Pacific). Percentages printed above each probability density indicate the fraction of all impacts in the corresponding dataset above the 100 billion USD threshold. Note, the width of the violin plots indicates the probability density of tropical cyclones exceeding a given damage value (symmetric along the y-axis). Also, in the Southern Hemisphere, there is only one event in the IBTrACS_p dataset, which exceeds the 100 billion USD threshold, displayed as horizontal line in panel b).

2.2.4 Guidance on tropical cyclone track set application

Depending on their question and goals, users may be looking for different properties of TC datasets and models. The key qualitative properties of the five sources of TC tracks compared in this study are compiled in the Methods Section and model versions specified in the Data Availability Section. We link these TC model characteristics with the suitability for distinct applications to guide the TC track set choice, complementing the TC risk views across different datasets as presented in the previous results sections.

When studying historical TC events like damages from Hurricane Maria, only the historically recorded IBTrACS are fit for purpose. The compilation of observed TCs in the best track archive (Knapp et al., 2010) is the most complete global set of historical TCs available. These data can be used to study past hurricane seasons (Klotzbach et al., 2018) or to hindcast and evaluate early warning protocols such as those used by the Red Cross 510 (Red Cross 510, 2021). However, historical data

are also characterized by spatial and temporal data scarcity, making them unsuitable for analysis requiring large sample sizes.

Synthetic models are specifically designed to overcome the spatial and temporal limitation imposed by historical records, making them a good choice for robust risk assessment of TC impacts, both on larger scales (see previous results sections) as well as for small regions (Bloemendaal and Koks, 2022). Our analysis did reveal the importance of the synthetic model type or robust TC risk assessment. The different synthetic modelling approaches discussed here all exhibit different limitations and in this study we discover two distinct cases where the synthetic modelling type is clearly important. First, a notable finding from the impact RPs curves (Fig. 2.2) is that IBTrACS often did not lie within the 90% confidence range of IBTrACS_p. Prima facie, this may seem surprising because each track in IBTrACS_p is directly generated from a single IBTrACS record. IBTrACS_p contains each of the observed IBTrACS TCs together with 99 derived tracks. However, the explanation for the bad fit lays in the modelling approach of IBTrACS_p. In the design of this simple interpolation method, the TC track is perturbed using a random walk algorithm (Kleppek et al., 2008; Gettelman et al., 2018; Aznar-Siguan and Bresch, 2019). While this is a very efficient approach to generate a regular track density field and spatially extend the historical data, this method does not vary the TC intensity along the track, introducing a low-intensity bias in IBTrACS_p compared to IBTrACS. The second prominent case where robust TC risk assessment is limited by the TC track modelling approach is for the STORM dataset in the North Indian Ocean, predominantly in the Bay of Bengal (Bloemendaal et al., 2020a). The difference between STORM and the other models is presumably related to STORM's fully statistical nature combined with specific environmental conditions in this basin, resulting in too many high-intensity landfalling TCs (see Supplementary Discussion A for an extensive discussion on this). As such, we do not recommend usage of STORM here, but instead to use CHAZ or MIT for impact assessments in the North Indian Ocean.

Tail risk assessments particularly require a large sample set of reliable simulations of highly destructive TCs. As was discussed previously, three historical events exceeded the 100 billion USD impact threshold in the USA, a too small sample size to adequately calculate the RPs and distributions of such events. Generally speaking, all synthetic datasets have the required size for reliable TC tail risk assessment. However, our results revealed the influence of the model specifications on the distribution of these extreme events: the IBTrACS_p hazard sets capture a limited set of tail risk events in most regions due to the low-intensity bias (discussed previously), which hampers their suitability for tail risk assessment. In contrast, MIT, STORM and CHAZ hazard sets are all fit for the purpose of a tail risk assessment.

The availability of models and data is a crucial aspect for many applications, particularly when developing climate services to support risk reduction, adaptation or risk financing policies. This guarantees transparency, reproducibility and it facilitates the exchange of climate information as demanded by the Global Framework for Climate Services (Hewitt et al., 2012). The model and data availability of the four synthetic models can be found in the Data Availability statement and may be considered as another critical discriminator depending on the application and context in which TC risk assessment is performed.

2.3 Discussion

Our analysis shows that differences between hazard sets are most pronounced when analyzing rare TC events; being either extreme (high-impact) TCs or in regions rarely hit by TCs. In particular, we find the largest variability and highest uncertainty over different risk metrics for the North Indian Ocean. For this region, the maximum values of TC intensity over land (Fig. 2.1) show high relative variability over the entire range of intensities and the CIs of the impact RP curves (Fig. 2.2, Supplementary Figure A.2) are all relatively wide. One explanation for this very high variability is the low number of TCs that form in the North Indian Ocean (∼5 TCs per year (Liu et al., 2021)). That is because the North Indian Ocean is a small basin, which leaves limited space for TC formation in the first place. Furthermore, there are no TCs during the monsoon period, when the vertical wind shear is too high and prevents TC formation, thus reducing the months during which TCs typically form (Liu et al., 2021). Finally, not only the number of TCs but also the data quality of these records is substantially lower in the Indian Ocean than in the other regions. For example, in the Western Pacific there were reconaissance flights in the 1980s until 1987 and several countries produce best-track datasets for the region (China, US, Japan, Philippines (Knapp et al., 2013; Schreck et al., 2014); see Methods). Hence, this leaves the Indian Ocean with a very limited database to study TC risk but also to inform and calibrate synthetic TC models to and the resulting large uncertainty is not surprising. In contrast, regions with high TC activity like the WP (∼26 TCs per year (Liu et al., 2020)) are better constrained, which is reflected in the narrow CIs (Fig. 2.2) and the least relative variability of TC track and hazard intensities; except for the STORM Cat. 5 tracks (Fig. 2.1, Supplementary Figure A.1). Furthermore, the costliest events that constitute the tails of probability distributions are rare by definition. The increasing variability of these high intensity, low frequency events is mirrored in the increasing range of the 90% CI of 100-yr and 1000-yr events reported in Supplementary Table A.2. These infrequent events are the ones that have the potential to be the most destructive and it is therefore particularly crucial to tailor TC risk assessment towards a robust representation of tail risk.

In the context of how the different synthetic TC models work, the small sample size of the input dataset is not equally relevant across models. It presumably plays a minor role for MIT and CHAZ simulations as they use global atmospheric fields to seed TCs (see Methods). For STORM, however, this small sample size does have a substantial effect. It is apparent that there is a limit for capturing complex physics with statistical factors and regression coefficients. In cases when data is scarce (like in the North Indian Ocean), statistics need to be aggregated over larger areas, thereby omitting spatial heterogeneity within the basin. For a full discussion of these limitations, please refer to the Supplementary Discussion A.

To understand further intermodel differences in TC impacts we need to study the different components that drive the impact calculation. We find that a part of the intermodel differences in TC impacts arises from the inhomogeneously distributed asset values: The intermodel differences from the impact RP curves, EAD, 100-yr and 1000-yr events calculated for a normalized exposure layer omitting all spatial heterogeneity on land (Supplementary Figure A.2, Supplementary Tables A.3 and A.4) are in general lower than the ones reported in the results section, which are computed on a spatially explicit representation of asset exposure value (LitPop)(Eberenz et al., 2020). However,

we note that the inhomogeneously distributed assets may also cancel some of the variability in the hazard set out and not only increase it. Our results also show that the hazard component alone may yield an incomplete picture for TC risk. Specifically, from the comparison of TC track and hazard intensities (Supplementary Figure A.1, Fig. 2.1), we would expect impacts to be largest for the CHAZ and STORM datasets because these two hazard sets have the largest share of severe TCs (Cat. 3 and more). However, the impact RP curves (Fig. 2.2), impact values (Supplementary Table A.2), and results for the long-term risk (Fig. 2.3) do not support this hypothesis. Conversely, the MIT hazard sets do not stand out with particularly high intensities but yield similar results in impact as the other hazard set. We thus conclude that TC impacts are largely driven by the specific interplay of individual tracks with assets on land and that studying TC track and hazard intensities alone draws an incomplete picture of TC risk for coastal communities and economies.

The impact calculation is not only driven by uncertainties introduced from the exposure data but also linked to differences in the provided synthetic data. The first inconsistency arises from the various degrees of information that accompany each track set. The STORM data contains a comprehensive set of 13 physical variables (Bloemendaal et al., 2020b). The CHAZ model, however, outputs fewer variables, implying that we needed to calculate other relevant variables such as the radius of maximum winds and TC pressure through dependencies on the known variables. Lastly, the full MIT dataset consists of TC track information as well as 2D-wind fields. However, to consistently compare the different synthetic datasets here, we solely use the track datasets and couple them with the Holland (2008) parametric wind field model. This may result in potential differences in our impact estimates compared to using the MIT wind field directly. On a related note, we want to mention that the synthetic track models depend on IBTrACS to varying degrees. The MIT track model is completely independent of historical tracks, the downscaling of CHAZ too but its genesis frequency is fit to IBTrACS records. In contrast, the STORM model is largely based on IBTrACS statistics.

The second source of uncertainty stems from the choice of the wind model. We acknowledge that the Holland (2008) used here has been motivated by and calibrated for North Atlantic hurricanes and might perform less well elsewhere. There is a multitude of other parametric wind models available (Holland et al., 2010; Chavas et al., 2015; Done et al., 2020; Wang et al., 2020), and it would be an interesting avenue for future research to extend the comparison to different wind models. However, such models often do require a substantial amount of input variables that go beyond what most synthetic models can provide.

Furthermore, the different synthetic model types and varying degrees of information provided by the TC track sets is the reason why CHAZ requires the post-processing step of a frequency bias correction (see Methods). The MIT model technique includes a basin-wide calibration to determine the TC frequency: for our analysis, we applied the calibration factor as provided with the event set. This factor is obtained from combining the fraction of initial TC seeds that intensified to become TCs with the actual number of TC tracks in the dataset to match observations. Still, the model is known to exhibit regional biases even after taking this factor into account (Geiger et al., 2021). STORM is designed to follow the IBTrACS TC genesis frequency (Bloemendaal et al., 2020b) and thus requires no further frequency correction.

Besides, we suggest investigating the uncertainty and sensitivity of the TC impact model to the

numerous input variables; including, but not limited to, the different TC track sets. This may be achieved by applying readily available uncertainty and (global) sensitivity analysis software (Pianosi et al., 2016; Saltelli et al., 2019; Kropf et al., 2022). The resulting insights can guide where next improvements of TC impact modelling can be achieved. We propose significant advances may be realized by better constraining the exposure and vulnerability components rather than the hazard part alone.

A suggestion for the future of synthetic TC track modelling is to institute a larger base of TC models of all types, from fully statistical to fully dynamical. Our study has demonstrated that the model choice is largely dependent on the research question and that all model types come with certain limitations. Hence, we advocate for more, and access to more, TC track models of all types to constrain TC risk more reliably in the future.

In addition, while we solely focus on wind-driven impacts in this study, TCs can also cause substantial damage through their storm surges and rainfall-induced freshwater flooding. The synthetic models considered here do not simulate these other hazards. Although, the regionalized impact functions used in this study (Eberenz et al., 2021) implicitly capture the sub-hazards because they were calibrated to total damage values, these functions still underestimate impacts from rain- or storm surge-driven events with low wind speeds (e.g. Hurricane Harvey in 2017). Future model developments, focused around explicitly simulating these sub-hazards, will therefore aid improved risk assessments.

Lastly, while our study only discusses TC risk in the present climate, there is also a growing need for insights into how these TC risks are going to change under future climate conditions. We thus recommend researchers interested in model comparisons for the future-climate to generate synthetic data sets forced by the same climate scenarios. Aside from simulating TC activity under climate change, future-climate risk assessments also require information on how exposure and vulnerability are going to evolve over time.

In summary, we have conducted a global model intercomparison of synthetic TC track sets to evaluate their performance and suitability for TC risk assessments. We used the impact modelling platform CLIMADA to contrast risk views across datasets and provide guidance concerning the suitability of the datasets for various applications and research questions. Different TC risk metrics and the discussion of links to key model characteristics yield an improved understanding of TC impact assessments. We showed that all datasets constitute a valid foundation for impact assessment and that modelled impacts are within one order of magnitude in the North Atlantic/Eastern Pacific where the historical record is considered most reliable. We also showed that the difference between models is largest when studying the long-term risk of rare events, or basins with smaller historical records or small areas. Consequently, modelled losses from rare TCs vary by orders of magnitude across synthetic track sets, which is particularly crucial for risk reduction efforts. Intermodel differences are generally driven by the varying distribution of hazard intensities over land and the inhomogeneously distributed asset values. This variance in the different risk metrics can partly be traced back to the key TC track set and hazard model characteristics and thereby help guide the choice of a TC track set depending on the research question at hand. Our analysis enables better-informed adaptation decisions and mitigation strategies, improves physical risk assessment in climate-related financial disclosure, and

paves the way for impact-based warnings that are tailored to assets and populations at risk. Besides, the guidelines on tropical cyclone track set application can help other researchers determine what datasets are best suited for their research question, and they may also direct researchers in the design of their own datasets and establishing the suitability of their datasets.

2.4 Methods

2.4.1 Study regions

We compare the five different TC track sets over the four main regions shown in Figure 2.4. The regions are chosen to very broadly reflect distinct TC areas. Specifically, we combine the North Atlantic and Eastern Pacific into one region (AP) because TCs originating in both basins may impact the USA, Mexico, and other central American countries with both Atlantic and Pacific coastlines. Yet, we note that most impacts calculated for this combined region stem from TCs with origin in the North Atlantic whereas TCs forming in the Eastern Pacific play a minor role on impacts. Furthermore, we assess TC risk in all of the Southern Hemisphere (SH) combined. The North Indian Ocean (IO) and Western Pacific (WP) complete our regionalization.

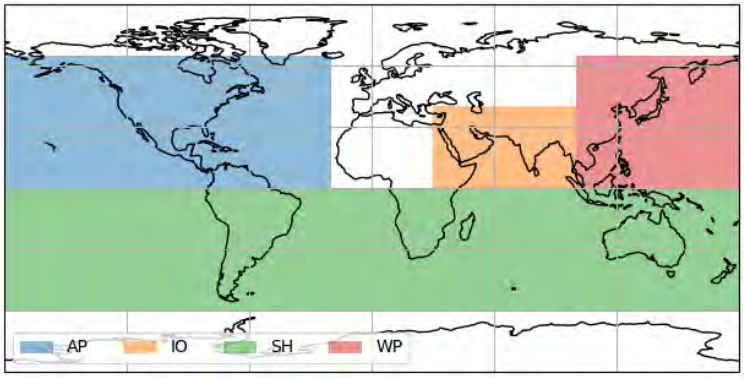

Figure 2.4: Global study regions. North Atlantic/Eastern Pacific (AP, blue), North Indian Ocean (IO, orange), Southern Hemisphere (SH, green), Western Pacific (WP, red).

2.4.2 Tropical cyclone track sets

In this study, we contrast the following sources of TC tracks:

1. observed TCs from the International Best Track Archive for Climate Stewardship (IBTrACS) (Knapp et al., 2010),
2. probabilistic events obtained from historical ones by a direct random-walk process (IBTrACS_p) (Kleppek et al., 2008),
3. synthetic tracks from a fully statistical model, STORM (Bloemendaal et al., 2020b),
4. synthetic tracks from coupled statistical-dynamical models, MIT (Emanuel et al., 2006, 2008), and

5. CHAZ (Lee et al., 2018).

The most important descriptors of the single TC track sets are compiled in Table 2.1. These key characteristics can be used to facilitate the choice of a suiTable track set depending on the research question.

Table 2.1: Key qualitative tropical cyclone track set characteristics.

model	type	years	N of tracks / land-influencing [a]	climate data	open-source code / dataset
IBTrACS	observational	1980-2018	3'068 / 1'858		- / yes
IBTrACS_p	probabilistic	1980-2018 / ×100 tracks	306'100 / 185'944		yes / yes
STORM	fully statistical	10'000 years (1980-2018)	712'800 / 348'670	ERA-5	yes / yes
MIT	statistical-dynamical	1980-2018	82'000 / 80'497	ERA-5	no / no (yes) [b]
CHAZ	statistical-dynamical	1981-2019 / 400 × 39 years	1'395'323 / 960'606	ERA-5	yes / no (yes) [c]

[a] land-influencing is defined as TCs with $> 17.5\,\mathrm{m\,s^{-1}}$ within at most 300 km from land.
[b] The MIT dataset is openly available for research only.
[c] The CHAZ dataset is openly available for research and NGOs.

The different model types underlying the five track sets are described in more detail in the next paragraphs. The length of the dataset is characterized by the number of tracks in each dataset and the time period covered. Further, the climate data used to run the TC track models and their open-source nature are two other important descriptors.

i) Observations from IBTrACS

The IBTrACS dataset is a centralized, global compilation of all TC best track data from the official Tropical Cyclone Warning Centers (TCWCs) and the WMO Regional Specialized Meteorological Centers (RSMCs) (Knapp et al., 2010). The IBTrACS dataset is publicly available and covers records from 1848 to the present, with dataset updates performed annually in August. The official records contain the position, and at least one entry of maximum sustained winds and minimum central pressure at 6-hour intervals in UTC. If provided by the reporting agency, additional variables describing the TC geometry, such as the radius of maximum winds or the radius of the outermost closed isobar, are included, at up to 3-hour intervals.

For this study, we extracted all available TCs in IBTrACS for which at least wind or pressure are reported by some agency. If, for some TCs, there is reported data by the agency that is officially responsible in the region according to WMO, that data is used at the highest available temporal resolution. For TCs that have not been reported about by the officially responsible agency, the data provided by the next-best agency that reported about that TC is used, with a fixed order of preference: 'usa', 'tokyo', 'newdelhi', 'reunion', 'bom', 'nadi', 'wellington', 'cma', and 'hko' (the agency identifiers are according to the IBTrACS data format). The exact IBTrACS reading routine is part of the open-source package CLIMADA (see `TCTracks.from_ibtracs_netcdf` in `climada.hazard.tc_tracks`).

While we only consider this agency selection procedure in this study, we note that the choice of agencies is known to significantly influence the TC statistics. For example, IBTrACS contains data in the Western Pacific (WP) from Japan (JMA), China (CMA), Hong Kong (HKO) and USA (JTWC). The officially responsible agency is Japan (JMA). Still, for almost 20% of the TCs affecting coastal areas

in 1980-2019, there is no reported data from JMA, but only from the other agencies. Furthermore, even though the central pressure measurements are considered to be comparably reliable among agencies, the average pressure reported by JMA in WP is lower by 8 hPa than the CMA average.

The reliability of officially reported TC data has greatly increased in recent years. Still, we note that the IBTrACS-based estimates in this study should not be taken as ground truth, but as another model output. This is due to the comparably short time range over which reliable measurements are available, but also because of the inconsistencies between reporting agencies that can be observed over the whole reporting period.

Furthermore, we acknowledge that the ADT-HURSAT dataset (Kossin et al., 2020) is more homogeneous than the IBTrACS records since it is purely based on a single data source, namely satellite products of the same resolution. However, we chose the IBTrACS as observational reference in this study because IBTrACS combines satellite data with other sources; it is known to be more accurate on a storm-by-storm basis; it includes more meteorological variables; and IBTrACS is based on WMO regional centers official best-track data.

ii) Probabilistic TC tracks from IBTrACS records

The probabilistic TC tracks (IBTrACS_p) obtained from the CLIMADA platform follow a simple interpolation method. In this approach, CLIMADA generates a set of 99 probabilistic tracks for each observed TC obtained by a random-walk process (Kleppek et al., 2008; Gettelman et al., 2018; Aznar-Siguan and Bresch, 2019). The method was designed to infer a probabilistic distribution of tracks from a single track in a physics-, climate-, and basin-agnostic way, and is described in more detail in the supplementary material of Gettelman et al. (2018).

iii) Fully statistical model STORM

STORM (Bloemendaal et al., 2019) is an open-source, global-scale, fully statistical model. STORM takes information on the TC track, characteristics (intensity, radius of maximum winds, and genesis month) from IBTrACS, and environmental variables (monthly averaged mean sea-level pressure and sea-surface temperature) from the European Centre for Medium-Range Weather Forecasting (ECMWF)'s fifth generation climate reanalysis dataset (ERA-5) (Hersbach et al., 2019) as input variables. A new, synthetic TC is then assigned a genesis month and location weighted by the statistics from the input dataset. Consecutive changes in the TC's position (longitude/latitude), intensity (maximum wind speed and minimum pressure) and radius of maximum winds are then calculated through a series of autoregressive formulas. STORM was validated against observations, and results showed that STORM preserves the TC statistics as were found in the original IBTrACS input dataset. The average number of genesis and landfalling events in the STORM dataset, as well as landfall intensity was shown to lie within one standard deviation of those values found in IBTrACS. Similarly, the largest deviations in basin-wide averages of maximum wind speed along a TC track were shown to be $2\,\mathrm{m\,s^{-1}}$ compared to IBTrACS.

iv) Statistical-dynamical model MIT

The MIT model is based on a statistical-dynamical downscaling method developed by Emanuel et al. (2006, 2008) (Emanuel et al., 2006, 2008). In short, this method initiates TCs using a random seeding technique, propagates the TCs via synthetic local winds from a beta-and-advection model, and simulates the TC intensity along each track by a dynamical intensity model (CHIPS, Coupled Hurricane Intensity Prediction System) (Emanuel et al., 2004). In more detail, key statistical properties are drawn from global reanalyses or climate models to generate a global, time-evolving, large-scale atmosphere-ocean environment. TC tracks are then created by randomly seeding warm-core vortices in space and time where the vast majority of seeds fail to amplify to tropical TC strength. Only the disturbances in favorable environments for TC formation survive, making the random seeding a so-called natural selection algorithm (Emanuel et al., 2008). Note that the survivors compose the TC climatology of the respective global reanalyses or climate models and that the simulated genesis rate thus needs to be calibrated to match the global or basin-wide number of genesis events in the historical period. Next, TC tracks are directed by a beta-and-advection displacement model, which is driven by large-scale winds in the synthetic environment. Finally, a simple coupled ocean-atmosphere TC intensity model (CHIPS) is driven along the TC tracks. The intensity model has very high radial resolution of the TC core and can resolve high-intensity TCs. The statistical-dynamical MIT model is computationally efficient, making it possible to generate very large numbers of TCs at a low computational cost and has been shown to accurately simulate all important TC features of the current climatology when applied to global reanalysis data (Emanuel et al., 2008).

v) Statistical-dynamical model CHAZ

The Columbia HAZard model (CHAZ) encodes physical relationships between TCs and their large-scale environmental variables to simulate TCs with low computational requirements (Lee et al., 2018). In CHAZ, synthetic TCs are randomly seeded with a distribution given by the Tropical Cyclone Genesis Index (TCGI) of Camargo et al. (2014); Tippett et al. (2011). Following genesis, the track of each synthetic TC is advanced in time with a beta-and-advection model (Xiaofan Li and Bin Wang, 1994), using monthly-averaged environmental winds, and a statistical parameterization of the sub-monthly variability, same as what is used in the MIT model (Emanuel et al., 2008). Along the synthetic TC track, the intensity is calculated using an autoregressive linear statistical model (Lee et al., 2016), with the monthly-averaged potential intensity, vertical wind shear, and mid-level relative humidity as environmental predictors, and with an additional variable to account for stochasticity. In this study, CHAZ is downscaled from 39 years (1981-2019) of ERA5 data with 10 different realizations of the genesis and subsequent tracks. For each realization, 40 ensemble members are generated using the intensity model, totalling 400 ensemble members of the 1981-2019 period.

2.4.3 Impact model CLIMADA

The impact model CLIMADA is developed and maintained as a community project, and the Python 3 source code is openly available under the terms of the GNU General Public License Version 3

(Aznar-Siguan and Bresch, 2019; Bresch and Aznar-Siguan, 2021). It was designed to simulate the interaction of climate and weather-related hazards, the exposure of assets or populations to this hazard, and the specific vulnerability of exposed infrastructure and people in a globally consistent fashion (Aznar-Siguan and Bresch, 2019; Bresch and Aznar-Siguan, 2021). Here, CLIMADA is used for the spatially explicit computation of direct economic damage from the five different sources of TC track sets on a global grid at 300 arc-seconds (∼10 km) resolution.

i) Tropical cyclone hazard

The TC hazard model in CLIMADA consists of two components: i) the TC track sets, which are coupled with ii) a parametric wind model to yield a 2D wind field (Holland, 2008).

CLIMADA's parametric wind model component computes the gridded 1-minute sustained winds at 10 meters above ground as the sum of a circular wind field (Holland, 2008) and the translational wind speed that arises from the TC movement. We incorporate the decline of the translational component from the cyclone centre by multiplying it by an attenuation factor as further described in Geiger et al. (2018). Apart from the TC location and central pressure, the wind model requires values for the radius of maximum winds. Where either pressure or radius are missing from the data (as is the case for the whole CHAZ dataset), we estimate the missing values from the provided variables, using simple linear relationships inferred statistically from observational data (IBTrACS). Note that the absolute wind speeds over land tend to be overestimated by this model since it does not consider any surface roughness on its own. Still, this effect is included at least in part in the track data since the overall TC intensity decays over land. We calculate the wind fields at a resolution of 300 arc-seconds (∼10 km) for this study. The hazard variable used in CLIMADA is lifetime maximum wind speed at each spatial location; 1-minute sustained wind speeds below 34 kn (17.5 $\mathrm{m\,s^{-1}}$) are discarded.

ii) Asset exposure

Exposure data for direct economic risk assessment contains information of asset value exposed to hazards. The dataset for gridded asset exposure value is spatially explicit and based on the LitPop method, which distributes national estimates of total asset value to the grid-level proportional to the product of nightlight intensity (Lit) and population count (Pop) (Eberenz et al., 2020). We use asset exposure value at a resolution of 300 arc-seconds (∼10 km) and the 2014 value in USD for GDP. Figure 2.5 shows a global map of the LitPop exposure dataset, limited to a distance of 1000 km inland. Additionally, we calculate the results on a normalized exposure layer (removing the spatial heterogeneity of asset values on land) and report impacts as fraction of affected assets to remove the potentially confounding signal of inhomogeneously distributed asset values and show the sole effect of the hazard component on the impact (see Supplementary Figure A.2, Supplementary Tables A.3 and A.4).

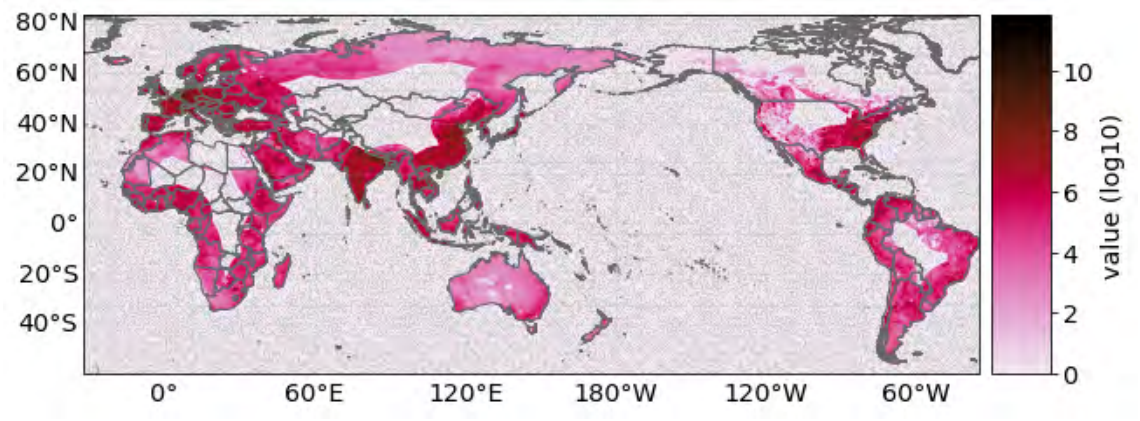

Figure 2.5: Global distribution of asset exposure value. Data is given in log10 USD based on the LitPop (Eberenz et al., 2020) method with an inland distance to coast of 1000 km.

iii) Impact function

In the CLIMADA terminology, vulnerability is described with impact functions. An impact function is a relationship between hazard intensity and the relative amount of destroyed assets, and can be used to calculate absolute direct damages for TC events at exposed locations. We use a set of calibrated regional TC impact functions following Eberenz et al. (2021), building on the idealized sigmoidal impact function as proposed by Emanuel (2011). Eberenz et al. (2021) fitted regional impact functions to reported damage data to account for the heterogeneous picture of TC risk in different regions. They grouped a varying number of TC-prone countries with similar vulnerability into nine distinct regions to obtain a globally consistent set of regionally calibrated impact functions. We use their root-mean-squared fraction (RMSF) optimized set of impact functions which is designed to minimize the spread of damage ratios of single events in contrast to the other, complementary approach that was optimized for aggregated damage.

2.4.4 Methods for TC model intercomparsion

We compare the maximum TC wind speeds over land of the synthetic datasets with the historical IBTrACS records. Specifically, we contrast events whose wind fields reach wind speeds of at least tropical storm strength (17.5 $\mathrm{m\,s^{-1}}$) over land. For this comparison we apply a subsampling method and draw 100 to 1000 samples of the synthetic hazard sets (IBTrACS_p, STORM, MIT, CHAZ) at the length of the historical IBTrACS records. A detailed description of the subsampling method applied can be found in the Supplementary Methods A. We then categorize the wind speeds according to the the Saffir-Simpson Hurricane Wind Scale (SSHWS) (Simpson and Saffir, 1974) and calculate the mean and standard deviation over all the subsamples in each category. The results are shown in Figure 2.1 as probability densities for each dataset in each intensity bin.

We repeat the analysis for the maximum wind speed variable provided with the track data as opposed to the wind field intensities in Supplementary Figure A.1. For that, we take the maximum wind speed associated with a track position within at most 300 km from land to account for tracks that pass near the coast but whose tracks do not make landfall in the strict sense.

The EAD over all exposures follows equation 5 in Aznar-Siguan and Bresch (2019). For the synthetic datasets, we again use the subsampling routine (see Supplementary Methods A) to compute the EAD for 100 to 1000 samples and report the mean and standard deviation thereof. Impact RP curves following the formalism of Cardona et al. (2012) are shown up to a RP of ∼1000 years. For this, we first concatenate random selections of 26 of the subsamples (see Supplementary Methods A) to a longer sample; yielding N=1000 samples, each covering 1014 years of TC activity. We calculate the median and 5th and 95th percentile of each subsample to obtain the 90% CI of each impact. Besides, we show the impact RP curve of the historical IBTrACS records up to its maximum RP of 39 years (Fig. 2.2).

Lastly, we assess the long-term risk of extreme TCs (Fig. 2.3) by analyzing the most damaging events exceeding the 100 billion USD threshold in each of the synthetic datasets; again, applied to all subsamples generated from the bootstrapping approach (Supplementary Methods A).

Note, the CHAZ hazard set is frequency bias-corrected throughout all impact calculations because it is known to have a bias in its genesis frequency (Lee et al., 2018; Sobel et al., 2019). To remove the influence of this bias, we adjust the sample period based on the observed frequencies in each basin and as described in Sobel et al. (2019).

Furthermore, we calculate the EAD and impact RPs curves on a normalized exposure layer in order to remove the potentially confounding signal of spatially inhomogeneously distributed asset values on land. Specifically, we report impacts as damaged fraction of the total asset value of the area of interest; or in other words, as "affected area" according to the regional damage functions (Eberenz et al., 2021) applied to perfectly uniformly distributed exposure (Supplementary Figure A.2, Supplementary Tables A.3 and A.4).

Data Availability

The observed TCs from IBTrACS (Knapp et al., 2010) are distributed under the permissive WMO open data license through the IBTrACS website (`https://www.ncdc.noaa.gov/ibtracs/index.php?name=ib-v4-access`) and can be directly retrieved through the CLIMADA platform (Aznar-Siguan and Bresch, 2019). The probabilistic IBTrACS are obtained from the random-walk process directly executed in CLIMADA (Kleppek et al., 2008; Gettelman et al., 2018; Aznar-Siguan and Bresch, 2019). The statistical model STORM is fully open: the model code can be obtained from GitHub (`https://github.com/NBloemendaal`) under the terms of the GNU General Public License Version 3 and datasets are available from the 4TU.ResearchData data repository (Bloemendaal et al., 2020b), licensed as public domain (CC0). CHAZ is an open-source model and can be downloaded at (`https://github.com/cl3225/CHAZ`). The CHAZ data are available to scientific reseachers upon request to the CHAZ development team at Columbia University. The synthetic TC data from the MIT model are property of WindRiskTech L.L.C., which is a company that provides hurricane risk assessments to clients worldwide. Upon request, the company provides datasets free of charge to scientific researchers, subject to a non-redistribution agreement. All of the TC track sets can be fed into CLIMADA to calculate TC impacts, independent from their respective licenses. For this study we used the Python (3.8+) version of CLIMADA release v3.1.2.

Code Availability

Code to reproduce the results of this paper is available at a GitHub repository with the identifier https://doi.org/10.5281/zenodo.6782091(Meiler and Vogt, 2022).

Acknowledgements

T.V. received funding from the German Federal Ministry of Education and Research (BMBF) under the research project QUIDIC (01LP1907A), and through the CHIPS project, part of AXIS, an ERA-NET initiated by JPI Climate, and funded by FORMAS (SE), DLR/BMBF (DE, Grant No. 01LS1904A), AEI (ES) and ANR (FR) with co-funding by the European Union (Grant No. 776608). N.B. is funded by a VICI grant from the Netherlands Organization for Scientific Research (NWO) (Grant Number 453-13-006) and the ERC Advanced Grant COASTMOVE #884442. C.Y.L. and S.J.C. thank the support from Vetlesen foundation to Lamont-Doherty Earth Observatory of Columbia University, they also acknowledge funding from the National Science Foundation (Grant AGS 20-43142), and the SwissRe Foundation. A.C. was funded by the EU Horizon 2020 REmote Climate Effects and their Impact on European sustainability, Policy and Trade (RECEIPT) project, grant agreement No 820712.

Author contributions statement

S.M. and T.V. conceived and designed the research and analysed the results and A.C. contributed to it. S.M. conducted the impact simulations. K.E., D.N.B. and A.C. supervised the analysis and the interpretation of the results. N.B., C.Y.L, S.J.C., K.E. provided synthetic TC tracks used as input for this study. S.M., T.V., N.B. contributed to the writing of the manuscript. All authors (S.M., T.V., N.B., A.C., C.Y.L., S.J.C., K.E., D.N.B.) reviewed and edited the manuscript.

CHAPTER 3

Uncertainties and sensitivities in the quantification of future tropical cyclone risk

Tropical cyclone risks are expected to increase with climate change and socio-economic development and are subject to substantial uncertainties. We thus assess future global tropical cyclone risk drivers and perform a systematic uncertainty and sensitivity analysis. We combine synthetic tropical cyclones downscaled from CMIP6 global climate models for several emission scenarios with economic growth factors derived from the Shared Socioeconomic Pathways and a wide range of vulnerability functions. We highlight non-trivial effects between climate change and socio-economic development that drive future tropical cyclone risk. Furthermore, we show that the choice of climate model affects the output uncertainty most among all varied model input factors. Finally, we discover a positive correlation between climate sensitivity and tropical cyclone risk increase. We assert that quantitative estimates of uncertainty and sensitivity to model parameters greatly enhance the value of climate risk assessments, enabling more robust decision-making and offering a richer context for model improvement.

3.1 Introduction

Tropical cyclones (TCs) are among the most devastating natural hazards putting populations (Geiger et al., 2018) and assets (Berlemann and Wenzel, 2018) at risk. TC risks (or impacts) are a function of TC hazard, exposure of people or assets to this hazard, and the respective vulnerability of the exposed people or the (built) environment (IPCC, 2012). Over the last 50 years, TCs worldwide caused, on average, 28 billion USD in economic losses every year (WMO, 2021). In the future, TC impacts are expected to increase even further with climate change and socio-economic development (Mendelsohn et al., 2012; Gettelman et al., 2018; Geiger et al., 2018). Climate change is projected to drive an increase in TCs of the highest category, enhance precipitation rates and amplify the destructive power of TC-induced flooding by rising sea levels (Knutson et al., 2020). Concurrently, socio-economic development yields an expansion of population (Geiger et al., 2021) and assets

This chapter is published as Meiler et al. (2023c)

(Noy, 2016) exposed to TCs. Hence, it is crucial to support at-risk communities with transparent information of future TC risk changes.

Quantifying future TC risks is particularly challenging because it requires dealing with the absence of robust verification data (Pianosi et al., 2016; Wagener et al., 2022) and large, possibly cascading uncertainties in the model input components and model structure (Kropf et al., 2022). To date, studies have focused on changes in the physical properties of TCs (for example, changes in intensity (Elsner et al., 2008) and frequency (Kang and Elsner, 2015)) or future TC exposure (Geiger et al., 2021). No study has performed a systematic and thorough uncertainty and sensitivity analysis of future, global TC risk. We thus assess the drivers and uncertainties of direct economic damages from TCs in the future, considering wind as the driving physical hazard. Importantly, we refrain from making a priori choices regarding emission scenarios, particular global climate models (GCMs), preferable narratives developed for the Shared Socioeconomic Pathways (SSPs) (Riahi et al., 2017) or optimized representations of vulnerability. Instead, we include all available future TC hazard simulations and socio-economic development scenarios and represent vulnerabilities across a wide range to explore an extensive future TC risk space. Therefore, the results presented here go beyond the standard climate risk analyses, which often only provide a comparably basic uncertainty estimation but hardly ever include a thorough and systematic treatment of uncertainty and sensitivity (Beven et al., 2018; Saltelli et al., 2019).

To study uncertainties and sensitivities in future TC risk estimates, we select from a list of scientifically justified inputs based on alternative representations of the future climate and socio-economic systems rather than defining a set of additive or multiplicative perturbation factors for each input factor whenever possible. This approach has several advantages. First, it is inherently difficult to precisely define all input uncertainties through a set of perturbation factors. Often, such information is unavailable because it is missing from future climate and socio-economic model output documentation. Second, employing a limited yet plausible range of input choices establishes a direct correlation between our output and the specific combinations of inputs employed to produce it. Lastly, we avoid assuming the likelihood of specific input combinations and instead describe the results based on the uncertainty and sensitivity observed across the explored discrete settings. Consequently, we do not investigate all uncertainties of the diverse models used to simulate such future climate and socio-economic states (e.g., the TC downscaling model or the GDP model for SSP projections). Instead, we focus on the uncertainties of the three main physical climate risk model components by sampling from a list of state-of-the-art future representations of hazard, exposure and vulnerability.

For the hazard, we use large sets of synthetic TCs (Emanuel et al., 2006, 2008; Emanuel, 2021) downscaled from nine different GCMs and three warming scenarios of the CMIP6 generation (SSP245, SSP370, SSP585), simulating TC activity of the historical period (1995-2014) and in the middle (2041-2060) and end of this century (2081-2100). This statistical-dynamical technique requires daily wind output in addition to monthly mean thermodynamic quantities and was applied for all GCMs of the newest generation, which provide this data for all ensemble members. The technique is well-established (Emanuel, 2013, 2021) and has been shown to replicate key features of the observed historical TC climatology (Emanuel et al., 2008). Furthermore, we use two different parametric

wind models to derive 2D wind fields along each TC track (Holland, 2008; Emanuel and Rotunno, 2011). Note that we do not explore uncertainties of the TC downscaling model itself; this is beyond the scope of this study and was addressed elsewhere (Meiler et al., 2022b). However, we review the implications of this TC model choice in the discussion section in more detail. For exposure, we use economic growth factors from different SSPs (Riahi et al., 2017) to approximate socio-economic development and analyze exposure uncertainties. We include all five SSPs, each describing a different possible future scenario for society; ranging from a world of low economic growth, low population growth, and limited technological innovation (SSP1) to a world of high economic growth, high population growth, and rapid technological innovation (SSP5). For vulnerability, we test uncertainties by varying the vulnerability function's slope parameter of regionally-calibrated vulnerability functions (Eberenz et al., 2021) across a wide range. We combine these representations of hazard, exposure, and vulnerability to estimate future TC risk increase and quantify the uncertainties and sensitivities thereof using an open-source probabilistic risk model (CLIMADA) (Aznar-Siguan and Bresch, 2019). We repeat the risk calculations many times (>40,000), relying on a numerical Monte Carlo scheme (Lemieux, 2009) to cover all possible combinations of input factor variations.

Our results highlight the full uncertainty distribution of model outputs and how these variations can be attributed to variations in input factors. This additional information is incredibly valuable to identify the most important and uncertain drivers of TC risk increase in a changing climate and evolving society. It can help model developers focus research efforts on model inputs that matter most for reducing uncertainty in the output. It may provide decision-makers with a much more representative range of plausible future outcomes and thus a more transparent and valuable information basis. Ultimately, our approach of analyzing different types of uncertainties enables better-informed adaptation decisions and mitigation strategies.

3.2 Results

3.2.1 Drivers of future tropical cyclone risk

We first assess the two main drivers of future TC risk increase - climate change and socio-economic development - independently and contrast them with the total risk increase later. For the independent assessment of the two TC risk drivers, we fix exposure at the reference state (year 2005, see Methods) to quantify the contribution from climate change and, analogously, evaluate socio-economically-driven risk change on historical hazard data. We express TC risk by the standard metrics of expected annual damages (EAD) and 100-year damage event (100-yr event in short). The former is the integrated value of impacts across all probabilities and is thus commonly used as a proxy for risk-based insurance premiums (Unterberger et al., 2019). The latter is an extreme event that is expected to occur once every 100 years, on average. In other words, it is an event with a 1% chance of occurring in any given year. In this study, we focus on four distinct global regions (Fig. 3.1 a) and Methods) and evaluate the future TC risk increase relative to the respective, present-day baseline reporting results as relative changes in percent.

We find that the median climate change-driven TC risk increase is smaller than the contribution

from socio-economic development in all regions, both periods and risk metrics (Fig. 3.1). For example, climate change yields a median TC risk increase ranging from 0.3% (Southern Hemisphere) to 2.5% (Western Pacific) for EAD in 2050 and 0.6% (Southern Hemisphere) to 1.8% (North Indian Ocean) in 2090. On the other hand, socio-economic development causes EAD to increase by 0.8% (North Atlantic/Eastern Pacific) to 2.5% (North Indian Ocean) in 2050 and 2.0% (North Atlantic/Eastern Pacific) to 7.1% (Southern Hemisphere) in 2090 (Fig. 3.1 b)-e)). We note that 100-yr event values are comparable (Fig. 3.1 f)-i)), and the complete results overview can be found in Supplementary Tables B.1 and B.2. Climate change is, in most cases, the driver with the higher uncertainty, which can be deduced from the width of the inter-quartile range (IQR). Exceptions are results in the Southern Hemisphere for both metrics in 2090 (Fig. 3.1 d), h)) and 100-yr event values in the North Indian Ocean and Western Pacific in 2090 (Fig. 3.1 g), i)). Accordingly, extremes on both ends of the distribution are more pronounced for climate change in these cases too. Besides, climate change produces a risk decrease (-0.1% to -0.7%), whereas socio-economic development nearly always amounts to a risk increase (Supplementary Tables B.1 and B.2), implying that climate change may offset part of the socio-economically-driven TC risk increase in these cases.

Next, we evaluate the total risk increase, including both climate change and socio-economic development in the risk calculation. Most notably, the total TC risk increase (Fig. 3.1, total; right-most column) includes non-trivial effects between the two key drivers and it is not the mere sum of its parts nor simple, a posteriori multiplication of hazard and exposure (Fig. 3.1, sum; inner right column). In contrast, the total TC risk increase from the full risk calculation, including climate change applied to the hazard and socio-economic development in the exposure from the beginning, contains excess non-linearity that cannot be accounted for by the simple multiplication of hazard and exposure. Median values of total TC risk increase shown in Figure 3.1 range from 2.4% (5.3%) in the North Atlantic/Eastern Pacific to 5.3% (21.7%) in the North Indian Ocean in 2050 (2090). The last value (21.7%), for example, results from the interplay of the individual contributions of climate change (1.8%) and socio-economic development (6.8%) and is notably larger than the product of the two drivers (10.1%), thus illustrating the excess non-linear effects. This non-linearity also influences the uncertainty of total TC risk increase (Fig. 3.1), which spans wider ranges of possible EAD and 100-yr event values than for the two single drivers and their product). It likewise affects the most extreme values. For instance, the maximum TC risk increase surpasses 400% (422% 100-yr event; 467% EAD) in the North Indian Ocean by the end of the century (Supplementary Tables B.1 and B.2). Note that we focus on total risk increase for the remainder of the study.

3.2.2 Sensitivity analysis of future tropical cyclone risk

The sensitivity analysis helps to determine how uncertainties in total TC risk change described in the last section can be attributed to variations in model input factors (Pianosi et al., 2016) (Table 3.1). These model input factors encompass various representations of future TC hazard, exposure and vulnerability components and uncertainties therein. Here, we present first- and total-order Sobol sensitivity indices (Sobol, 2001; Saltelli et al., 2010) of our total TC risk change estimations. First-order sensitivity indices measure the effect of variations in a single input factor, and total-order sensitivity indices the combined effect of changes in multiple input factors on the model output

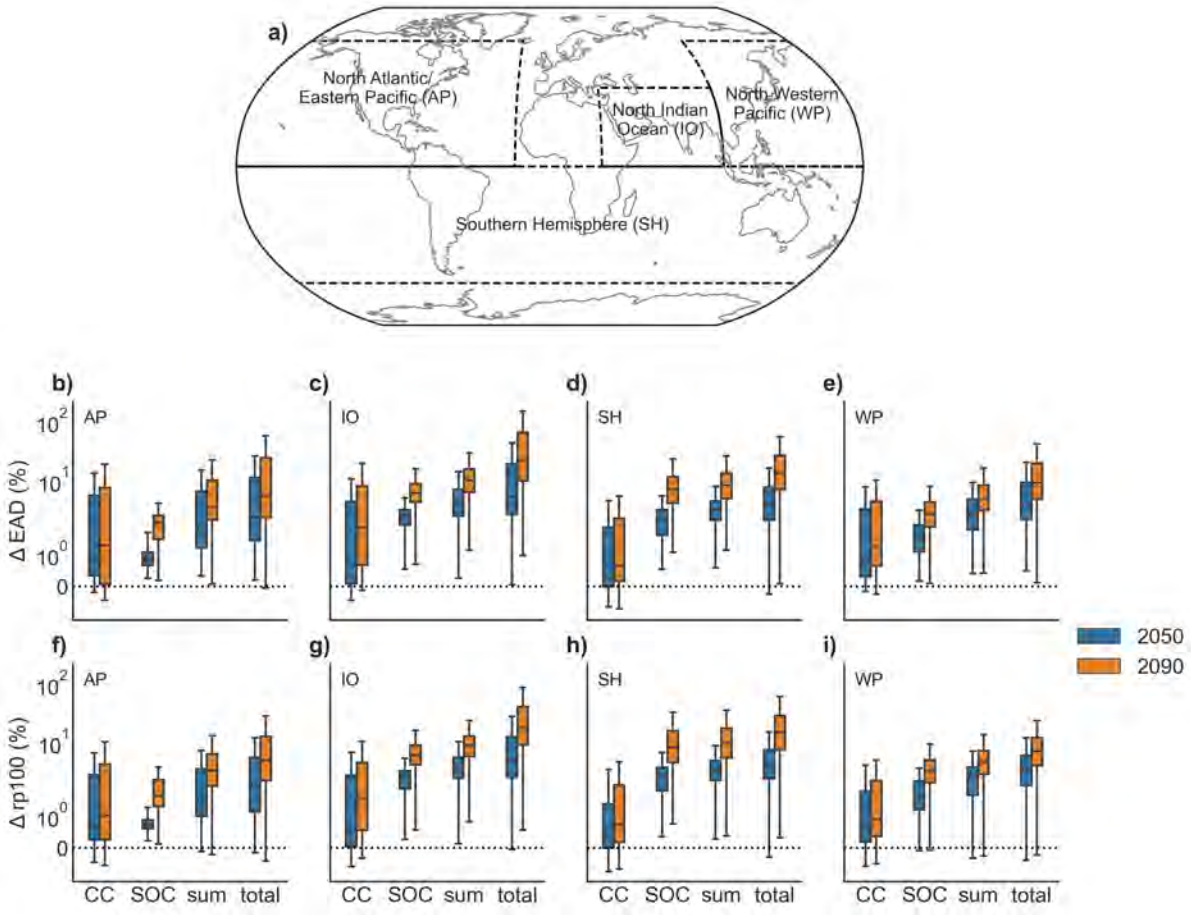

Figure 3.1: Drivers of future tropical cyclone risk change. Relative change in tropical cyclone risk by 2050 (blue) and 2090 (orange) due to climate change (CC), socio-economic development (SOC), the product of CC and SOC calculated from the sum of their log values (sum) and both drivers interacting (total) with respect to the historical baseline. The relative change in expected annual damage (EAD) (b, c, d, e) and 100-yr event (rp100) values (f, g, h, i) are reported for the four study regions (a) North Atlantic/Eastern Pacific (AP), North Indian Ocean (IO), Southern Hemisphere (SH), and North Western Pacific (WP). Boxplots show the interquartile range (IQR) for the uncertainty over all input factors (see Methods), while the whiskers extend to 1.5 times the IQR. More extreme points (outliers) are not shown. Statistical summary metrics of all boxplots are provided in Supplementary Tables B.1 and B.2

(Saltelli, 2002).

The input factor with the highest first-order sensitivity over almost all regions, periods, and metrics is the choice of GCM underlying the hazard model (*GCM*) (Fig. 3.2 a)). One exception is found in the Southern Hemisphere for 100-yr event values at the end of the century, where the SSP-informed GDP scaling of exposure points (*SSP exposure*) exhibits the largest sensitivity. This finding is also mirrored by the results in Figure 3.1 d) and h) for the Southern Hemisphere, where socio-economic development is the notably more uncertain TC risk driver than climate change. Moreover, *SSP exposure* has the second-highest sensitivity index in other regions. In contrast, all other input factors have little influence on the model output.

In essence, total-order sensitivity indices broadly mirror the ranking and distribution of first-order indices (Fig. 3.2 b)). Generally, total-order sensitivity indices are higher than first-order

indices, which implies interactions between input factors. However, all increases we find here are relatively small, meaning most interactions between input factors are weak. We report that the GCM model choice (*GCM*) still ranks as the most important factor, and the SSP-based scaling of the exposure layer (*SSP exposure*) is the second most important. Furthermore, we discover very small sensitivities for the wind model choice (*Wind model*), the two hazard sub-sampling variables (*Event subsampling base/future*), and the Lit (m) and Pop (n) exponent variations (Eberenz et al., 2020) (*Exposure urban/rural weighting*). Note, the latter allows emphasizing densely populated and rural areas differently (see Methods). Finally, the input factor describing the slope parameter of impact functions (*Vulnerability function midpoint*) has a small to moderate effect on risk output. However, we emphasize that this importance changes if we report TC risk in absolute values (Supplementary Figure B.1), in which case this input factor (*Vulnerability function midpoint*) controls a substantial share of the output uncertainty. Still, the GCM choice (*GCM*) retains a notable effect but is no longer the single key driver of the output uncertainty.

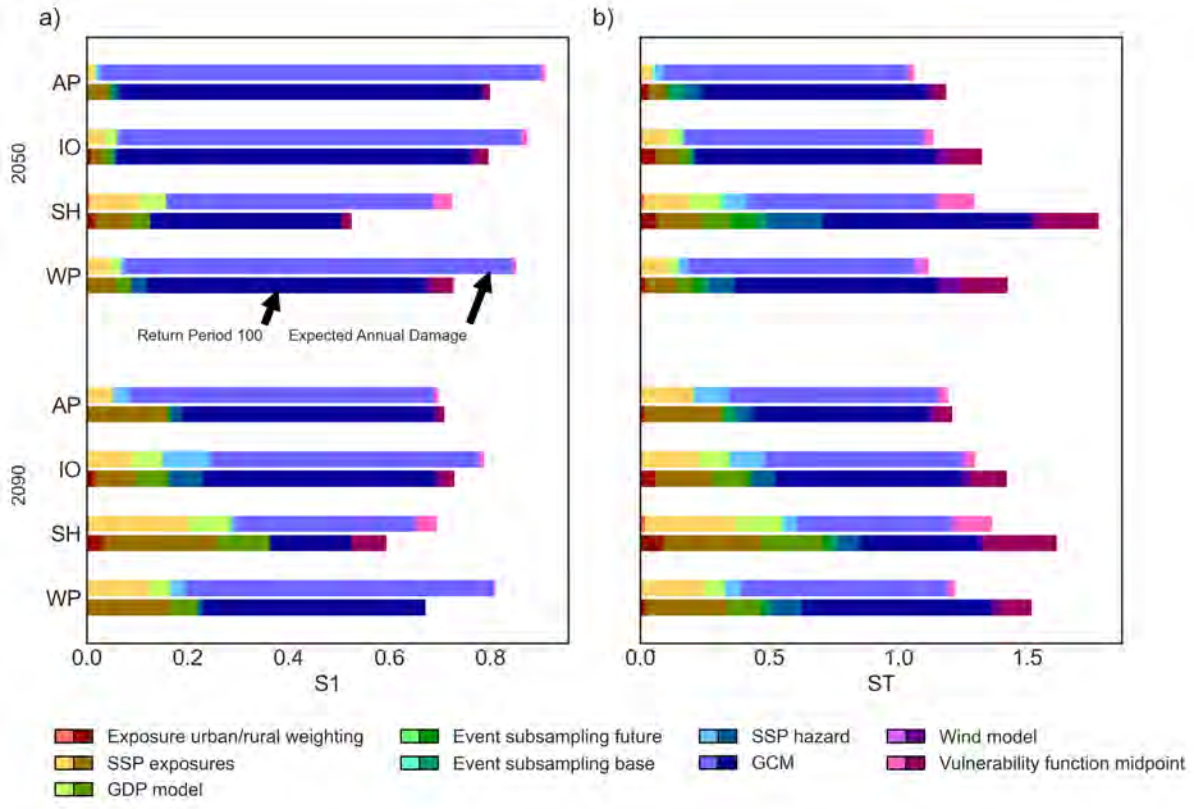

Figure 3.2: First- (S1) and total-order (ST) sensitivity indices. First- (a)) and total-order (b)) Sobol sensitivity indices for future (2050, 2090) TC risk change expressed as %-change in expected annual damage (EAD; upper bar) and 100-yr event values (rp100; lower bar) over the four study regions (cf. Fig 3.1 a) North Atlantic/Eastern Pacific (AP), North Indian Ocean (IO), Southern Hemisphere (SH), and North Western Pacific (WP) and all input factors (see Methods and Table 3.1 therein). Results are grouped by input factors (different colors); *Vulnerability function midpoint* describes the impact function; *Wind model*; *GCM*, *SSP hazard*, *Event subsampling base*, *Event subsampling future* pertain to the hazard component; *GDP model*; *SSP exposure*, *Exposure urban/rural weighting* relate to the exposure.

3.2.3 Uncertainty of future tropical cyclone risk apportioned to GCMs

We disentangle key input factors of the TC risk model to evaluate uncertainty in TC risk increase in more detail. In the last section, we showed that the GCM model choice (*GCM*) affects the output uncertainty of the relative change in TC risk most among all varied input factors. Here, we further investigate the role of this important modeling choice by exploiting the advantages of uncertainty analyses. We evaluate the entire distribution of output values, including all sources of uncertainties from different input factors (Table 3.1), split up by the nine GCMs (*GCM*), ordered by their transient climate response (TCR; Supplementary Table B.6) and grouped by emission scenario (*SSP hazard*) (Fig. 3.3). The corresponding results for the 100-yr event (Supplementary Figure B.2) are comparable, and we thus limit the results' description here to the EAD.

We discover two broad GCM clusters. TC event sets downscaled from one model cluster (FGOALS, MIROC6, MPI6, MRI6, UKMO6) yield a low TC risk increase ($\leq$ 10%), event sets based on the remaining models (CESM2, CNRM6, ECEARTH, and IPSL6) a medium to high risk increase ($\geq$ 10%). Particularly, simulations from the IPSL6 model stand out with the most substantial growth of TC risk (Fig. 3.3). Moreover, TC risk change estimates from the first GCM cluster (low risk change) are more narrowly constrained. In contrast, models from the second cluster produce results with a much wider delta EAD range.

The selection of emission scenarios for future TC projections (SSP245, SSP370, SSP585) shapes the distribution of TC risk change estimates much less than the GCM choice (Fig. 3.3), which is also mirrored by the low sensitivity indices for the respective input factor (*SSP hazard*) described in the last section (Fig. 3.2). Notably, results for the GCM cluster of low TC risk increase are similar for all three hazard emission scenarios (Fig. 3.3). Generally, model simulations for the SSP370 hazard/SSP3 exposure combination (green colored) form the low end of the results and the SSP585 hazard/SSP5 exposure combination (blue colored) the high end (Fig. 3.3). Furthermore, differences between emission scenarios are more pronounced by the end of the century (Fig. 3.3 b), d), f), h)) in contrast to the middle of the century (Fig. 3.3 a), c), e), g)), which again reflects the interplay of diverging hazard and exposure projections further out into the future. Consequently, end-of-century TC risk changes are more uncertain and of greater magnitude than mid-century simulations. Lastly, the Southern Hemisphere results (Fig. 3.3 e), f)) broadly reflect outcomes described for the other regions. However, it is the region where GCM differences are smallest. There, other input factors (co-)shape the output uncertainty more strongly. Again, this finding aligns with the sensitivity indices reported in the last section.

3.2.4 Tropical cyclone risk change relationship to climate sensitivity

Here we link the TC risk change values resulting from TC events sets downscaled from different GCMs with the climate sensitivity of the respective model. We suggest that the intermodel differences we found and described in the last section (3.2.3) may be related to climate sensitivity. It is known that some CMIP6-generation GCMs run hotter than others (Hausfather et al., 2022; He et al., 2022). Specifically, some models of the newest generation exhibit a higher climate sensitivity than in previous generations, which lies outside the range of "likely" (or "very likely") values as defined by authors of

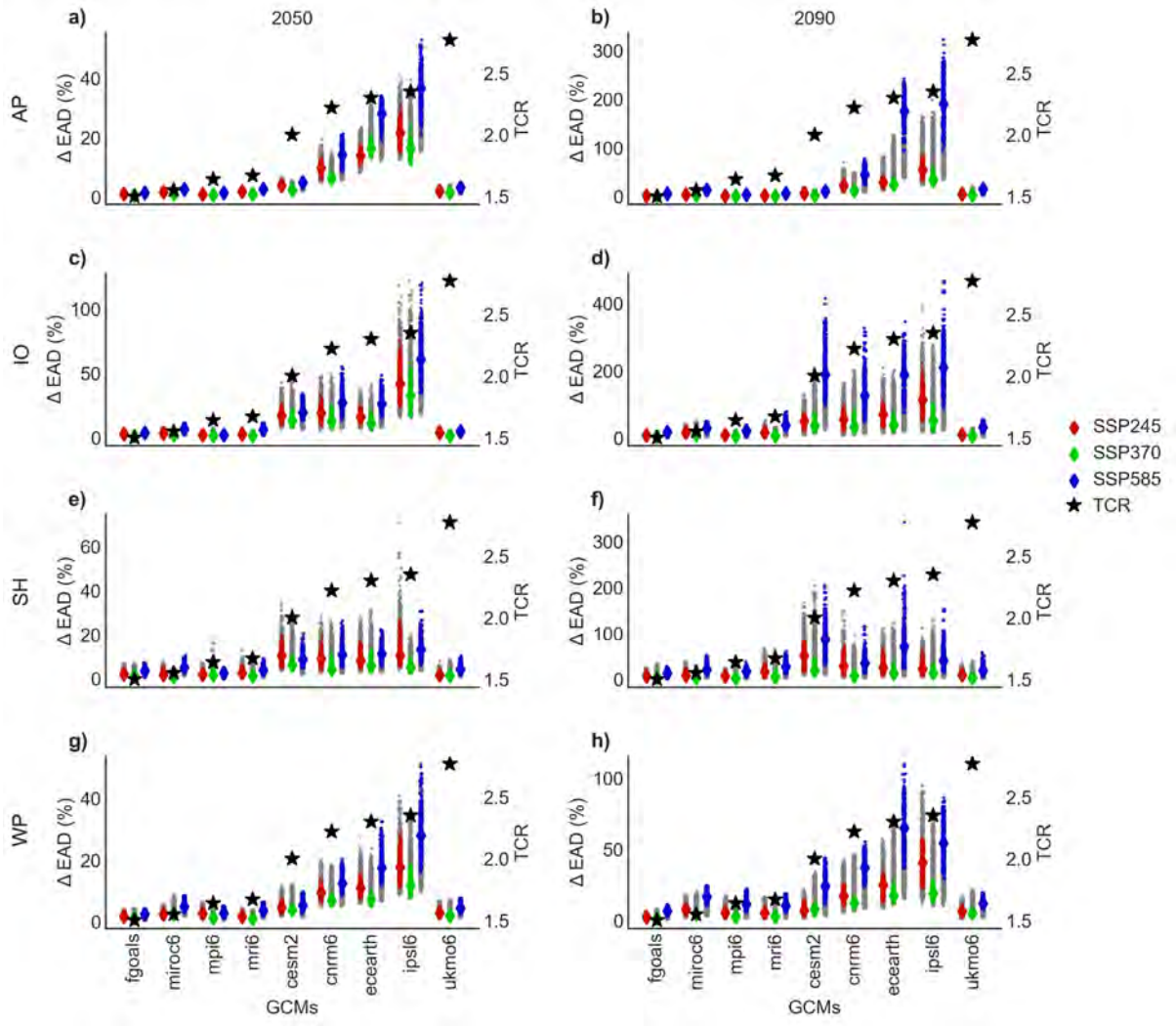

Figure 3.3: TC risk change from different global climate models (GCMs) and emission scenarios. Model simulations of the expected annual damage (EAD) change by 2050 (a, c, e, g) and 2090 (b, d, f, h) attributed to the nine GCMs and three emission scenarios underlying the TC hazard sets (see Methods). GCMs are ordered by increasing transient climate response (TCR) values (Supplementary Table B.6), which are shown as black stars on a secondary y-axis. Model realization of matching hazard and exposure scenarios are marked in color (SSP245 in red, SSP370 in green, SSP585 in blue) with diamond-shaped markers delineating the median of their distribution. Results are shown over the four study regions North Atlantic/Eastern Pacific (AP), North Indian Ocean (IO), Southern Hemisphere (SH), and North Western Pacific (WP) (cf. Fig. 3.1 a)).

the Sixth Assessment Report (AR6) of the Intergovernmental Panel on Climate Change (IPCC).

We present a striking relationship between climate sensitivity and TC risk values. TCR and equilibrium climate sensitivity (ECS) values for the nine GCMs, including a screen if the models fall into the likely range of projected TCR or ECS (Supplementary Table B.6), are compared to the two distinct model clusters identified in the last section. TC event sets downscaled from GCMs with climate sensitivity values in the likely range generally belong to the cluster of models we identified to produce low TC risk increases (Supplementary Table B.6). The UKMO6 model constitutes the sole exception. It has a high climate sensitivity but generates low TC risk increases (Fig. 3.3). This qualitative assessment is supported by positive correlation coefficients calculated for TCR and TC

risk values (Supplementary Table B.7). The highest correlation is found between TCR values and EAD changes in the North Atlantic/Eastern Pacific in the middle of the century (0.71), the lowest correlation is between TCR and 100-yr event changes in the Southern Hemisphere at the end of the century. Besides, we calculated correlations between TCR and global TC risk changes because climate sensitivity is a global measure. The correlation coefficients are 0.39, 0.46, 0.48 and 0.54 for change in 100-yr event in 2090, 100-yr event in 2050, EAD in 2090 and EAD in 2050 respectively. Hence, on a global scale, the correlation is highest for changes in EAD in the mid-century and decreases with time and for the change in 100-yr damage values.

3.3 Discussion

Our results confirm that considering the effect of climate change alone yields an incomplete picture of future TC risk (Fig. 3.1). Consequently, it is important to include socio-economic development because climate impacts manifest as non-linear interactions between the two components. Hence, we find that also the uncertainty associated with future TC risk projections increases non-linearly when considering the two drivers together.

The average contribution of climate change and socio-economic development to the total future TC risk increase is of the same order of magnitude in all Northern Hemisphere regions (Fig. 3.1 and Supplementary Tables B.1 and B.2). But climate change is the notably more uncertain risk driver for most regions, both future periods and risk metrics, than socio-economic development (Fig. 3.1). We attribute the reason for this uncertainty to variations in GCMs used to downscale TCs from (Fig. 3.2 and Fig. 3.3) and found the varying climate sensitivity of these GCMs as an important contributor to the dissimilar TC event sets (Section 3.2.4).

The case where climate change is not the more uncertain risk driver is for Southern Hemisphere end-of-century risk changes. In contrast, socio-economic development is the substantially more uncertain driver there (Fig. 3.1d), h), Supplementary Tables B.1 and B.2). From our study, we learn that the magnitude of socio-economically-driven risk change in the Southern Hemisphere at the end of the century is substantially larger (more than an order of magnitude) than the one of climate change. We furthermore see that the input factor for the SSP-based exposure scaling is the most important driver for the output uncertainty in this case (Fig. 3.2). We thus hypothesize that the SSPs describing the socio-economic growth factors by the end of the century diverge more strongly between scenarios in the Southern Hemisphere than in the other regions - explaining the uncertainty. Additionally, Southern Hemisphere SSPs may include narratives for stronger growing economies than in the North - explaining the magnitude. Furthermore, in the Southern Hemisphere, there are island states (like Indonesia) where the entire country's GDP is exposed to TCs in contrast to large countries in the Northern Hemisphere (e.g., USA, China) whose coastal areas are exposed to TCs but areas further inland are not affected. Accordingly, the Southern Hemisphere is also the region where inter-GCM differences are lowest (Fig. 3.3) and the correlation to climate sensitivity is weakest (Supplementary Table B.7).

Next, we discuss the findings and implications of the GCM choice (*GCM*) as a major determinant of output uncertainty in TC risk assessment (Fig. 3.2). By investigating the uncertainty space

of event sets downscaled from the nine different GCMs in more detail, we found two distinct model clusters: One producing low TC risk increases, the other medium to high TC risk increases (Fig. 3.3). We suggest that these intermodel differences can partly be explained by climate sensitivity (Section 3.2.4). This correlation may not be surprising as TC potential intensity generally scales linearly with global warming (Emanuel, 2007). Furthermore, TC potential intensity is a strong predictor for TC genesis potential indices (Emanuel and Nolan, 2004; Emanuel, 2010; Rappin et al., 2010). Climate sensitivity thus helps drive TC hazard frequencies and intensities, the two critical hazard characteristics for TC risk. We are therefore not surprised to see that GCMs with frequencies and intensities below the multimodel mean broadly constitute the model cluster yielding low TC risk increases (FGOALS, MIROC6, MPI6, MRI6, UKMO6), whereas the GCMs with above-average frequencies and intensities form the second cluster (CESM2, CNRM6, ECEARTH, and IPSL6) with medium-high TC risk increases (Supplementary Table B.3, B.4 , and B.5). Yet, it remains to be investigated if this finding is generalizable beyond the particular statistical-dynamical TC model used in this study. We acknowledge the presence of epistemic uncertainty regarding the response of TC frequency to global warming. The TC downscaling method (Emanuel et al., 2008) used in this study indicates increased genesis rates with global warming, especially in the northern hemisphere (Emanuel, 2021), in contrast to the majority of GCMs that show decreases (Knutson et al., 2020). However, caution is needed when comparing the downscaling TC model to a consensus greatly influenced by GCMs with horizontal grid spacings too coarse for tropical cyclone resolution (Davis, 2018). Notably, one NOAA Geophysical Fluid Dynamics Laboratory (GFDL) model demonstrates decreasing TC frequencies under global warming at a 50 km grid spacing, while reducing the grid spacing to 25 km alone leads to increasing genesis rates (Vecchi et al., 2019). Similarly, the TC downscaling model by Lee et al. (2020) indicates varying frequency changes depending on the version of Genesis Potential Indices employed.

Besides, TC risk also depends on the track TCs take, which is not clearly related to climate sensitivity. Additionally, we did not know before our study if future TC risk change was mainly driven by climate change, socio-economic development, or the two drivers more or less equally. If the total risk were dominated by socio-economic development, we might not have found such a clear connection between TC risk increase and climate sensitivity. Indeed, our discussion of the magnitude of socio-economically-driven risk change at the end of the century Southern Hemisphere supports this statement.

In conclusion, the relationship between TC risk increase and climate sensitivity is an important discovery: we may use the climate sensitivity of GCMs as a first indicator for TC risk increase. Yet, some inter-GCM variations may arise from natural climate variability rather than only in response to increased greenhouse gas concentrations. Specifically, we used single ensemble members from each GCM and hence, any inter-GCM comparison of climate change signals will be affected by different phases of natural variability too. Moreover, it remains to be investigated if this finding is generalizable beyond the particular statistical-dynamical TC model used in this study.

These findings certainly prompt further research opportunities for TC hazard modellers. However, they are also a representation of the maturity of TC hazard modelling as a field, which is important from a risk modelling perspective. In contrast to the other key components of risk modelling -

exposure and vulnerability - hazard simulations are substantially more advanced. We have many skillful models and approaches available to simulate future TCs (Emanuel et al., 2008; Lee et al., 2020; Bloemendaal et al., 2022). But this availability is unmatched on the side of exposure and vulnerability. Hence, we should not confuse low sensitivity indices for exposure- and vulnerability-related input factors (Fig. 3.2) with low importance for TC risk assessment in general. The comparably low sensitivity indices for exposure and vulnerability may simply result from a limited capability to simulate socio-economic development and changing vulnerabilities. Specifically, in this study, we neglect possible changes in vulnerability in the future because such competencies are largely nonexistent. Moreover, our choice to report the relative TC risk change and not a change in absolute terms masks the importance of the impact function-related input factor for the output uncertainty further (compare Fig. 3.2 and Supplementary Figure B.1). For exposure, we used SSP-based GDP growth factors to approximate socio-economic development. However, the SSPs were not designed to be used in a spatially explicit fashion (Riahi et al., 2017), which is required for our type of risk assessment. Also, the GDP scaling ignores spatial patterns in socio-economic growth like urbanization.

These limitations consequently restrict our possibilities to inform the input factors central to the uncertainty and sensitivity analysis. In this study, we limit the input factors to all available, plausible representations of the future climate and socio-economic system. Hence, as long as such models for future exposure and vulnerability are missing, they remain blind spots in our assessment of future TC risk changes. The results from our sensitivity analysis suggest that hazard uncertainty needs to be reduced, and there is no question that more research is needed in this direction. However, our interpretation is that model maturity and complexity are not even across the three components, and therefore we recommend focusing future research efforts on better understanding and representing socio-economic development in a spatio-temporally explicit way. In parallel, improved vulnerability representations, including changing aspects of vulnerability in the future, would advance TC risk assessment further. Nonetheless, we note that TC risk estimates vary based on the chosen TC hazard model (Meiler et al., 2022b). Similar to the epistemic uncertainty discussed for changing TC frequency in a warming climate, uncertainties exist among TC hazard models. For example, future TC risk calculations based on a fully statistical TC model (Bloemendaal et al., 2022) yield comparable findings for assessing future TC risk drivers but differ in the results of the sensitivity analysis due to the differences in the underlying modelling approach and model structure (Meiler et al., 2023b). More generally speaking, in the context of uncertainty and sensitivity analysis, the choice of model and its meta-parameters represent normative uncertainty (Knüsel et al., 2020; Kropf et al., 2022). This includes, for instance, using a risk model based on hazard, exposures, and impact functions; selecting output metrics of interest; focusing on specific large-scale regions. While most of these uncertainties are not per se quantifiable and thus not reported as results, they can be identified and discussed systematically (Knüsel et al., 2020), particularly regarding the fitness for purpose. The here chosen model setup is designed to study uncertainties in societal TC risk at a national scale, rather than focusing on TC climatology. This justifies the choice of basin boundaries based on countries' borders which encompass TCs originating in different basins with distinct characteristics of TC formation, intensification, and movement, and the choice of relative change in EAD and 100-y events as risk metrics. The results presented here are only meaningful within the context of this

study design choice, and extrapolation to other purposes should be treated with restraint.

Ultimately, we caution against deriving strong policy statements given that the uncertainty parametrization is subject to the abovementioned limitations and biases, and only those input factors included in the study design can be analyzed for their sensitivity. However, we can still draw important, potentially policy-relevant conclusions from our analysis. We suggest using a variety of GCMs to tailor future TC risk assessments for different levels of risk aversion. For instance, to study TC risk at the very hot tail of the global model temperature change distribution, we can pick a TC event set downscaled from a GCM with high climate sensitivity. The probability of ECS exceeding 5° C is higher than 5% after all (Sherwood et al., 2020). Considering such scenarios is important for conservative risk assessment and may be combined with a storyline approach to analyze and communicate high-impact TC in the climate change context (Shepherd et al., 2018; Ciullo et al., 2021).

In conclusion, our study setup allows analyzing different types and sources of uncertainty in the same quantitative framework. Our results increase the information value of future TC risk assessment and thus provide a more transparent basis for decision-making than conventional analyses.

3.4 Methods

3.4.1 Study regions

We compare the increase of future TC risk over four main global regions shown in Figure 3.1 a) and previously defined by Meiler et al. (2022b) and also used in a study of analogous setup but different TC hazard model (Meiler et al., 2023b). The regions broadly reflect distinct TC areas with a focus on the landmasses affected by the respective TC activity in contrast to regionalizations focused on the ocean basins of TC origin. Because we focus on the socio-economic impacts of TCs on nations as a whole, we include TCs originating in two basins for the USA, Mexico and other Central American countries with both Atlantic and Pacific coastlines. Yet, we note that TC frequencies and other shifts in TC climatology are basin-specific. Landfalling TCs originating in the North Atlantic are much more frequent and thus play a major role for the region in contrast to TCs forming in the Eastern Pacific. The diverse shifts in TC climatology in a warming climate for both basins are encompassed by the TC event set we employ. Whether changes arise from shifts in TC climatology in either basin is of secondary importance, as we quantify effects on the country's overall GDP. While we capture these variations, we do not separate them. Hence, we combine the North Atlantic and Eastern Pacific into one region (AP) and evaluate TC risk in all of the Southern Hemisphere (SH) combined, applying the same logic as in the AP region. The North Indian Ocean (IO) and Western Pacific (WP) complete our geographical split.

3.4.2 Synthetic tropical cyclone tracks

Synthetic TC tracks are generated using a statistical-dynamical downscaling method developed by Emanuel et al. (2006, 2008)). This method builds on three components to simulate TCs: initialization

using a random seeding technique, propagation of the TCs via synthetic local winds from a beta-and-advection model, and TC intensity simulation along each track by a dynamical intensity model (CHIPS, Coupled Hurricane Intensity Prediction System) (Emanuel et al., 2004). We note that a detailed model description and evaluation can be found in Emanuel et al. (2008). For this study, the TC model is driven by climate input data from nine different GCMs (Supplementary Table B.8) and three emission scenarios (SSP245, SSP370, SSP585) from the CMIP6 generation. Climate models include a range of scenarios for future greenhouse gas emissions and atmospheric concentrations based on the socio-economic development described in the SSPs (Section 3.4.3. In previous climate model generations, they were defined under the Representative Concentration Pathways (RCPs); in the newest generation, they follow the notation of the socio-economic projections. Together, the SSPs and resulting scenarios simulated in the GCMs provide a framework for exploring the potential impacts of different socio-economic and environmental futures on the global climate system. The model is run for a present climate reference state (1995-2014) and two future periods in the middle (2041-2060) and the end of this century (2081-2100). For each simulated year, 500 TCs are generated by the three steps described above. Driven by the boundary conditions of the different GCMs (e.g., sea surface temperatures and wind shear), a changing number of the initial seeds survive to become TCs. The TC frequency for each simulated year is then determined by the fraction of initial seeds and the final generated count of 500 events per year after calibrating with a constant as provided with the event set.

3.4.3 Socio-economic growth data

We derive economic growth factors from different SSPs to approximate socio-economic development. These factors are acquired from the SSP database, which aims to document the quantitative projections of SSPs and related Integrated Assessment scenarios (for an overview see Riahi et al. (2017)). SSPs comprise five trajectories that examine how global population, economic growth, technological development, governance and social norms might change over the next century. A range of different SSP elements have been quantified (e.g., population growth, urbanization, economic development) considering the main characteristics of the SSP future development pathways. Here, we focus on economic development only, reported as GDP projections. For GDP, three alternative interpretations of the SSPs have been developed by different teams (the Organization for Economic Co-operation and Development (OECD) (Dellink et al., 2017), the International Institute for Applied Systems Analysis (IIASA) (Crespo Cuaresma, 2017) and the Potsdam Institute for Climate Impact Research (PIK) (Leimbach et al., 2017)). All resulting GDP projections were built on the same guiding assumptions for interpreting the SSPs regarding the key determinants of economic growth; however, they differ in the employed methods and outcomes. For this study, we query the SSP database for GDP growth factors for the years 2050 and 2090 for each country and all five SSPs from the three models (Riahi et al., 2017). Note, the years 2050 and 2090 constitute the central time points of the respective future TC simulations for the middle and end of this century (see previous section).

3.4.4 Risk model CLIMADA

CLIMADA is an open-source risk model, which was created to simulate the interaction of climate and weather-related hazards, the exposure of assets or populations to this hazard, and the specific vulnerability of exposed infrastructure and people in a globally consistent fashion (Aznar-Siguan and Bresch, 2019; Bresch and Aznar-Siguan, 2021). The model is developed and maintained as a community project, and the Python 3 source code is openly and freely available under the terms of the GNU General Public License Version 3 (Aznar-Siguan and Bresch, 2019; Bresch and Aznar-Siguan, 2021). In this study, we use CLIMADA v3.2 (gabrielaznar et al., 2022) to calculate the increase in direct economic damage from TCs in the middle and end of this century compared to a present-day baseline. We compute spatially explicit damage values on a global grid at 300 arc-seconds (~10 km) resolution.

3.4.5 Tropical cyclone hazard data

The TC hazard layer in CLIMADA is described by a 2D-wind field obtained from coupling TC track sets with a parametric wind model. Here, we apply two different wind models based on parameterizations following Holland (2008) and Emanuel and Rotunno (2011) to all TC track sets described above. Both parametric wind models compute the gridded 1-minute sustained winds at 10 meters above the ground as the sum of a circular wind field and the translational wind speed that arises from the TC movement. The wind models differ in their derivation of the (absolute) angular velocity from the parametric wind profile. For both wind models, the decline of the translational component from the cyclone center is incorporated by multiplying it by an attenuation factor (Geiger et al., 2018).

We calculate the wind fields at a resolution of 300 arc seconds ($\sim$ 10 km) for this study. The hazard variable used in CLIMADA is lifetime maximum wind speed at each spatial location; values below 34 kn (17.5 $\mathrm{m\,s^{-1}}$) are discarded.

3.4.6 Asset exposure data

Exposure data for direct economic risk assessment contains information on asset value exposed to hazards. We create a dataset of spatially explicit, gridded asset exposure value using the LitPop method. LitPop distributes national estimates of total asset value to the grid-level, proportional to the product of nightlight intensity (Lit) and population count (Pop) (Eberenz et al., 2020). The present-day, reference exposure layer is computed at a resolution of 300 arc-seconds ($\sim$ 10 km) and the 2005 Gross Domestic Product (GDP) value (in USD). Note, the present-day TC track sets (1995-2004) are centered around the exposure reference year 2005. Future projections of exposed asset values are constructed by scaling these reference asset values at every grid point with the growth factors derived for the two future time periods, five SSPs and three models described above (Section 3.4.3). The distribution of assets is thus static and is independent of future changes to the climate, the environment and the socio-economic factors.

3.4.7 Impact functions

In the field of risk assessment, we use impact functions to describe vulnerability; in other words, the relationship between hazard intensity and the amount of damage it causes to assets. Impact functions are thus the critical link between hazard and exposure to calculate absolute direct damages for TC events at exposed locations. Here, we use sets of regionally calibrated impact functions (Eberenz et al., 2021), which build on the idealized sigmoidal impact function suggested by Emanuel (2011). Eberenz et al. (2021) grouped countries of similar vulnerability into nine distinct regions and fitted impact functions to reported damage data in these regions to account for the heterogeneous picture of TC risk across the globe. In this study, we use impact functions that were calibrated on historical records (Eberenz et al., 2021) and not synthetic TC tracks. We furthermore note that we focus on wind-driven risks in this study and neglect the explicit representation of TC risks from storm surge or TC rainfall-driven flooding. However, these sub-hazards are implicitly captured by the impact functions because they were calibrated to total damage values.

3.4.8 Uncertainty and sensitivity analysis

We use the uncertainty and sensitivity quantification (unsequa) module of CLIMADA (Kropf et al., 2022) to compute the model uncertainties and sensitivity indices reported in this study. This module seamlessly integrates the *SALib – Sensitivity Analysis Library in Python* package (Herman and Usher, 2017) into the CLIMADA risk model, hence supporting all sampling and sensitivity index algorithms implemented therein. In general, the workflow of this module follows the steps of common uncertainty and sensitivity quantification schemes (Pianosi et al., 2016; Saltelli et al., 2019). Here we describe the key steps in more detail.

Table 3.1: Input factors and their variability space.

Input factor	Variable name	Type	Range
Hazard: GCM	*GCM*	discrete	1-9
Hazard: Emission scenario	*SSP hazard*	discrete	1-3
Hazard: Wind model	*Wind model*	discrete	1-2
Hazard: Bootstrapping	*Event subsampling base/future*	continuous	80% of every year
Exposure: SSP-based GDP scaling	*SSP exposure*	discrete	1-5
Exposure: GDP model	*GDP model*	discrete	1-3
Exposure: m, n scaling LitPop	*Exposure urban/rural weighting*	discrete	1-9; m=[0.5, 1.0, 1.5], n=[0.5, 1.0, 1.5]
Impact functions	*Vulnerability function midpoint*	continuous	within IQR of regional TC calibration[a]

[a] (Eberenz et al., 2021)

First, we define the input factors and their variability space. Table 3.1 lists all input factors and the corresponding input parameter ranges, which describe the probability distributions of these random variables. Specifically, we define four input factors characterizing the hazard component of our risk model. We draw from a discrete distribution of i) GCMs driving the TC model boundary conditions (*GCM*); ii) emission scenarios (*SSP hazard*); iii) wind models to calculate the 2D wind field (*Wind model*); and iv) sub-sample 80% of the events in every year of the synthetic TC event set to represent natural variability (*Event subsampling base*, Event subsampling future). The exposure

variable consists of three input factors. We sample from a discrete list of i) GDP growth factors derived from five different SSPs (*SSP exposure*); ii) three models used to translate the SSPs into economic growth factors (*GDP model*); and iii) we generate exposure layers after nine different formulations of the Lit (m) and Pop (n) components to explore the uncertainty of the LitPop method. In more detail, varying the two exponents allows us to weight densely populated and rural areas differently. A higher value of n (Pop component) emphasizes highly populated areas, and a lower value the sparsely populated areas (*Exposure urban/rural weighting*). Note, the total asset value remains constant. Finally, we vary the slope parameter (*Vulnerability function midpoint*) of the impact function, which describes the wind speed at which the function's slope is steepest and a damage ratio of 50 % is reached. We inform the range of this parameter by the IQR of the regionally calibrated impact functions in Eberenz et al. (2021, cf. Fig. 5).

The next step is to draw samples of the input parameter values according to their respective uncertainty probability distribution. In this study, we use the Sobol sampling algorithm (Sobol, 2001; Saltelli et al., 2010) to draw 2^{11} samples, which translates into 40,960 input factor combinations. The TC risk calculation is then executed for each combination, yielding a distribution of model outputs, which can then be analyzed and visualized. In this study, we evaluate the uncertainty in TC risk increase of the EAD and the 100-yr event. Finally, the quantification of the relative influence of the input factors on output variability is achieved by calculating sensitivity indices. We apply a variance-based method, the Sobol quasi-Monte Carlo sequence (Sobol, 2001). Sobol indices describe the ratio of the marginal variances to the total variance of the output metric. In this study, we evaluate first- and total-order indices. The former measure the direct contribution from each input parameter to the output variance, and the latter the overall contribution from an input parameter considering its direct effect and its interactions with all the other input parameters.

Data Availability

The synthetic TC data are property of WindRiskTech L.L.C., which is a company that provides hurricane risk assessments to clients worldwide. Upon request (info@windrisktech.com), the company provides datasets free of charge to scientific researchers, subject to a non-redistribution agreement. For this study we used the Python (3.8+) version of CLIMADA release v3.2.0 (gabrielaznar et al., 2022). Source code is openly and freely available under the terms of the GNU General Public License Version 3 (Aznar-Siguan and Bresch, 2019; Bresch and Aznar-Siguan, 2021).

Code Availability

Code to reproduce the results of this paper is available at a GitHub repository with the identifier https://doi.org/10.5281/zenodo.8073353 (Meiler, 2023).

Acknowledgements

Kerry Emanuel acknowledges support from the MIT Climate Grand Challenge on Weather and Climate Extremes. This project has received funding from the European Union's Horizon 2020 research and innovation program (grant agreement No 820712)

Author contributions statement

S.M. conceived and designed the study, analyzed the results and wrote the manuscript. C.M.K., A.C., K.E., and D.N.B. contributed to it and supervised the analysis and interpretation of the results. K.E. provided synthetic TC tracks used as input for this study. C.M.K. wrote the unsequa module of CLIMADA, which is central to this study. All authors (S.M., A.C., C.M.K., K.E., D.N.B.) reviewed and edited the manuscript.

CHAPTER 4

Uncertainty and sensitivity analysis for probabilistic, global modelling of future tropical cyclone risk

Modelling the risk of natural hazards for society, ecosystems, and the economy is subject to strong uncertainties, even more so in the context of a changing climate, growing economies, evolving societies, and declining ecosystems. Here we apply a new feature of the CLIMADA climate risk modelling platform, which allows carrying out global uncertainty and sensitivity analysis. We showcase the comprehensive treatment of uncertainty and sensitivity of CLIMADA's outputs for the assessment of future global tropical cyclone (TC) risk. Our results show that socio-economic development contributes more strongly to TC risk increase in the future and is a more uncertain risk driver than climate change. Besides, we find that exposure scaling based on the Shared Socioeconomic Pathways (SSPs) is the input variable with the most significant impact on TC risk change calculations. In conclusion, we argue that a thorough and systematic assessment of future global TC risk will help focus forthcoming research efforts and enable better-informed adaptation decisions and mitigation strategies.

4.1 Introduction

Natural hazards pose risks to society, ecosystems, and the economy, and modelling these risks is subject to notoriously high uncertainties, especially in the face of a changing climate and developing societies and economies (Kropf et al., 2022). In the present study, we utilize and showcase a new feature of the open-source, probabilistic climate risk modeling platform CLIMADA (Aznar-Siguan and Bresch, 2019), which allows conducting global uncertainty and sensitivity analysis of weather and climate risk assessments (Kropf et al., 2022). This approach exceeds conventional climate risk analyses by examining the entire uncertainty space of the model output uncertainty analysis) and investigating how this uncertainty can be attributed to variations of the model input actors (sensitivity analysis). Both uncertainty and sensitivity analyses use numerical techniques, such as Monte Carlo or quasi-Monte Carlo schemes (Lemieux, 2009; Leobacher and Pillichshammer, 2014), to repeat the

This chapter is published as Meiler et al. (2023b)

model runs multiple times with varying input parameters. The input parameter ranges should be (physically) plausible and ideally be informed by background knowledge concerning these parameters (Beven et al., 2018). We argue that this thorough and systematic application of uncertainty and sensitivity analyses will enhance the information value of risk modeling efforts and generate more transparent and comprehensive outcomes for decision-making.

One of the most devastating natural hazards are tropical cyclones (TCs), which have caused over 1400 billion USD in economic losses in the US alone over the past 50 years (WMO, 2021) and threaten tropical and subtropical regions worldwide. In the future, TC impacts (and risks) will aggravate further due to climate change and socio-economic development (Peduzzi et al., 2012; Noy, 2016; Geiger et al., 2021). Therefore, it is essential to support risk reduction efforts and improve societal resilience towards TCs through the provision of reliable risk assessments. A common practice in TC risk modelling is integrating probabilistic sets of synthetic TC data with information on exposure and vulnerability. In this study, we use a large set of synthetic, global TC data from a fully-statistical TC model, the Synthetic tropical cyclOne geneRation Model (STORM), for historical (Bloemendaal et al., 2020b) and future climate conditions (Bloemendaal et al., 2022). Moreover, we approximate socioeconomic development in line with different Shared Socioeconomic Pathways (SSPs) and scale Gross Domestic Product (GDP) projections accordingly (Riahi et al., 2017). Finally, we complement these future representations of hazard and exposure data with regionally calibrated vulnerability functions (Eberenz et al., 2021) to estimate the TC risk change in the future, expressed by the standard metrics of expected annual damages (EAD) and the 1-in-100 year damage event (100-yr event in short). On this basis, we assess the drivers and uncertainties of global TC risk change in the future and quantify how these uncertainties can be attributed to variations in input factors.

In this paper, we describe the data and methods used for probabilistic, global modelling of future tropical cyclone risk and the uncertainty and sensitivity analysis (Section 4.2), we then report results (Section 4.3) and finish with a brief discussion (Section 4.4) and overall conclusion (Section 4.5).

4.2 Methods

4.2.1 Impact model CLIMADA

The impact model CLIMADA (CLIMate ADAptation) is an open-source framework to simulate the interaction of weather and climate-related hazards, the exposure of assets or populations to this hazard, and the specific vulnerability of exposed infrastructure and people in a globally consistent way (Aznar-Siguan and Bresch, 2019; Bresch and Aznar-Siguan, 2021). Here, we use CLIMADA to calculate the change in direct economic damage from TCs in the middle of this century compared to a historical baseline. Specifically, we calculate spatially explicit damage values for thousands of events on a global grid at 300 arc-seconds ($\sim$ 10 km) resolution. Moreover, we use the uncertainty and sensitivity quantification (unsequa) module of CLIMADA (Kropf et al., 2022) to perform the uncertainty and sensitivity analysis central to this study. Via the unsequa module, CLIMADA users have direct access to the *SALib – Sensitivity Analysis Library in Python* package (Herman and Usher, 2017), including all sampling and sensitivity index algorithms implemented therein.

i) Tropical cyclone hazard

The TC hazard layer in CLIMADA consists of a 2D-wind field obtained from coupling TC track sets with a parametric wind model. Here, we use synthetic TC tracks from a fully statistical model developed by Bloemendaal et al. (2020b, 2022). For this study, we use 10,000 years of synthetic, global TC data for historical (1980–2017) and future climate conditions (SSP585; 2015–2050) from an ensemble of four high-resolution climate models of the CMIP6 generation. We then apply two wind models based on parameterizations following Holland (2008) and Emanuel and Rotunno (2011) to all TC track sets. The hazard variable used for risk and impact calculations in CLIMADA is the lifetime maximum wind speed at each spatial location; 1-minute sustained wind speeds below 34 kn (17.5 $\mathrm{m\,s^{-1}}$) are discarded.

ii) Asset exposure data

In CLIMADA, we create datasets of spatially explicit, gridded asset exposure values using the LitPop method (Eberenz et al., 2020) to obtain information on asset value exposed to hazards for direct economic risk estimates. First, the historical reference exposure layer is calculated based on the year 2000 GDP value (in USD). Then, future exposure projections are constructed by scaling these reference asset values at every grid point with the growth factors derived in line with the SSPs for 2050. Specifically, we retrieve GDP growth factors for each country from the SSP database (Riahi et al., 2017) for all five SSP narratives from three alternative model interpretations by teams from the Organization for Economic Co-operation and Development (OECD; Dellink et al., 2017), the International Institute for Applied Systems Analysis (IIASA; Crespo Cuaresma, 2017) and the Potsdam Institute for Climate Impact Research (PIK; Leimbach et al., 2017)).

iii) Impact functions

Impact functions link hazard intensity with the relative degree of damage, which is needed to calculate absolute damages for events at exposed locations. Here, we use sets of regionally calibrated TC impact functions (Eberenz et al., 2021).

4.2.2 Uncertainty and sensitivity analysis

The workflow of CLIMADA's unsequa module follows the steps of consolidated uncertainty and sensitivity quantification schemes (e.g., Pianosi et al., 2016; Saltelli et al., 2019). Here we describe the critical steps of this workflow in more detail. First, we define the input factors (random variables) and their variability space in terms of their distributions and parametrization (Table 4.1). In this study, we define both discrete sets of scientifically justified inputs based on alternative representations of the future and one continuous parameter range. In detail, we define three input factors characterizing the hazard component, three for the exposure and one for the impact function. To perturb the hazard, we sample from a discrete distribution of

1. climate models used to generate the future TC datasets (gc_model),
2. wind models (wind_model), and

3. sub-samples of the total TC hazard set, each containing 1000 years of TC activity (ensemble_pres, ensemble_fut).

For the exposure, we draw samples from a discrete list of

1. five different SSPs (ssp_exp),

2. three models used to translate the SSPs into GDP growth factors (gdp_model), and

3. we generate exposure layers after nine different compositions of the Lit (m) and Pop (n) exponents with values for m and n of [0.5, 1.0, 1.5] (Kropf et al., 2022, cf. Appendix B).

Finally, we vary the parameter of the impact function, which describes the steepest point of the vulnerability curve (v_half), and define its variability space by the respective interquartile range (IQR) as presented in Eberenz et al. (2021, cf. Fig. 5).

Table 4.1: Input factors and their variability space.

Input factor	**Type**	**Range**
Hazard: GCM model	discrete	1-4
Hazard: Wind model	discrete	1-2
Hazard: Sub-sample	discrete	1-10
Exposure: SSP-based GDP scaling	discrete	1-5
Exposure: GDP model	discrete	1-3
Exposure: m, n scaling LitPop	discrete	1-9
Impact functions: v_half	continuous	within IQR of TC calibration

We then generate a set of $N=2^{11}$ samples of the input parameters yielding 36,864 input factor combinations for sampling by applying the Sobol' sampling algorithm (Sobol, 2001; Saltelli et al., 2010) using the *SALib* Python package (Herman and Usher, 2017) as seamlessly integrated into CLIMADA (Kropf et al., 2022). For each sample, the TC risk change is computed, which yields a distribution for both risk metrics analyzed in this study (change in EAD and 100-yr event). This resulting distribution of model output forms the basis for the uncertainty analysis. Besides, it is the starting point for the sensitivity analysis. Namely, we perform a variance-based analysis using the Sobol' quasi-Monte Carlo sequence (Sobol, 2001). We report first- and total-order indices as measures of each input factor to the output variance considering their direct effect (first order) and interactions with all the other input parameters (total order).

4.2.3 Metrics for tropical cyclone risk assessment

The risk metrics of interest are the EAD and the 100-yr event, and we calculate the future TC risk change relative to the historical baseline. Hence, we report results as relative changes of the EAD and 100-yr event in percent. We first quantify the contributions of climate change and socio-economic development to future TC risk change. To do so, we run our study setup on a) the historical exposure layer and future climate hazard data to assess the contribution of climate change, and b) on the historical hazard data and future exposure layers to evaluate the magnitude of socio-economic

development to the risk change. We compare these two drivers to the total change in TC risk, including contributions and interactions from climate change and socio-economic development. In the second part, we evaluate the first and total order sensitivities of the total TC risk change in more detail.

4.2.4 Study regions

We compare the change of future TC risk over four distinct global regions (Meiler et al., 2022b, cf. Fig. 4) with a focus on the landmasses affected by the respective TC activity; namely, the North Atlantic/Eastern Pacific (AP), North Indian Ocean (IO), Southern Hemisphere (SH), and North Western Pacific (WP).

4.3 Results

4.3.1 Drivers and uncertainties of future TC risk change

The future change in TC risk can be driven by climate change (CC), socio-economic development (SOC) and both factors interacting (total). Here we assess the main drivers and their uncertainty across the four study regions and two risk metrics (Fig. 4.1).

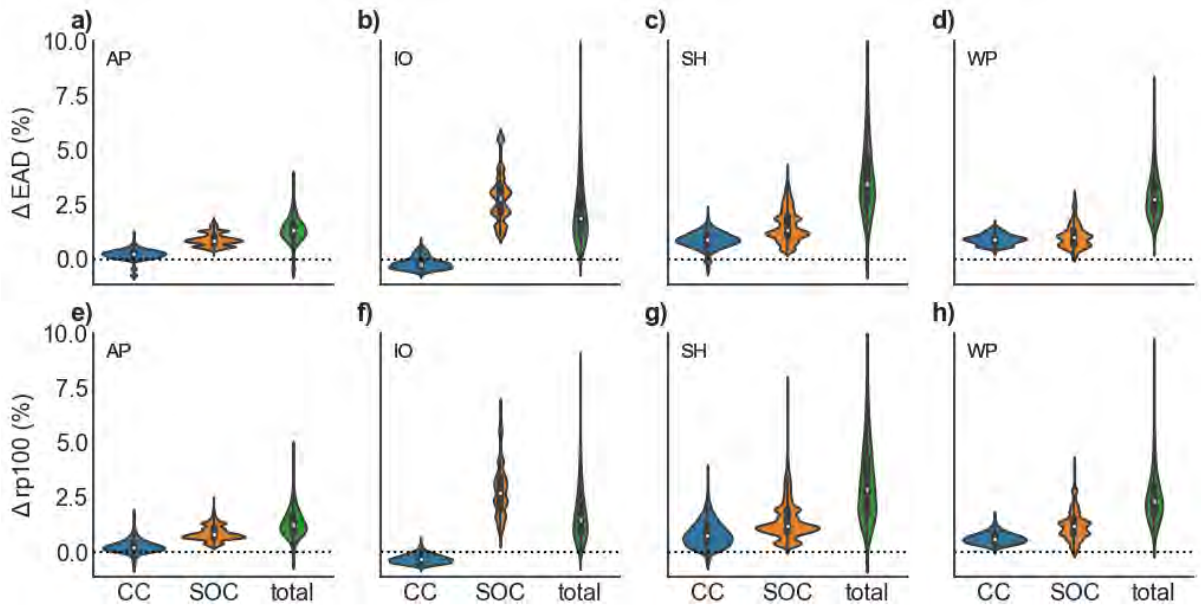

Figure 4.1: Tropical cyclone risk change due to climate change (CC), socio-economic development (SOC), and both drivers interacting (total) with respect to the historical baseline. The change (%) in expected annual damage (EAD) (panels a, b, c, d) and 100-yr event (rp100) values (panels e, f, g, h) are reported for the four study regions North Atlantic/Eastern Pacific (AP), North Indian Ocean (IO), Southern Hemisphere (SH), and North Western Pacific (WP).

Socio-economic development yields a larger TC risk increase than climate change in all regions. For example, the median risk change in EAD from climate change alone ranges from -0.2 % (IO) to +0.9% (SH, WP), and the change in the 100-yr event from -0.3% (IO) to +0.7% (SH). Socio-economic development, in contrast, yields a TC risk increase from +0.9% (+0.8%) in the AP to +2.8% (2.7%)

in the IO region for the EAD (100-yr event). The total TC risk increase is higher than the contributions of the single drivers (CC, SOC) in all regions except for the North Indian Ocean. There, climate change offsets part of the TC risk increase from socio-economic development. The total TC risk increase amounts to +1.3% (1.2%), +1.9% (1.5%), +3.4% (2.9%), and +2.8% (2.8%) in the AP, IO, SH, and WP, for the EAD (100-yr event) respectively.

The total TC risk change includes non-linear effects between the two key drivers (CC, SOC) and it is not the mere result of their sum. These interactions increase the output uncertainty in contrast to the distribution of EAD and 100-yr event values for the single drivers, which can be inferred from the shapes of the violin plots (Fig. 4.1). The climate change-driven EAD and 100-yr event values exhibit a uniform distribution and the smallest uncertainties (Fig. 4.1, left violin plots) compared to changes from SOC and total TC risk change. The distributions of the socio-economically-driven, future TC risk change values (Fig. 4.1, middle violin plots) carry the imprint to the five SSPs, which can be recognized from the kernel density of the violin plots.

4.3.2 Sensitivity indices

This sensitivity analysis helps to determine how the uncertainties in TC risk change described in the last section can be attributed to variations in model input factors. Here, we present the first- and total-order sensitivity indices of our TC risk calculations.

The input variable describing the SSP-scaling of the exposure layer (ssp_exp; see Methods) exhibits the highest first-order sensitivity index in all regions and for both risk metrics (Fig. 4.2). The sole exception is the 100-yr event results in the North Indian Ocean, where the GCM underlying the TC hazard set (gc_model) dominates (Fig. 4.2 c)). In contrast, input factors with little influence on the output are generally the wind model selection (wind_model), Lit (m) and Pop (n) exponent variations (mn_scaling), and both hazard ensemble choices (ensemble_pres, ensemble_fut). Besides, the input factor describing the impact functions (v_half) has a moderate impact on the output in the SH and WP regions but a small effect in the other two regions. Note that this relative importance changes if we report TC risk in absolute values (not shown here), in which case v_half controls the output uncertainty over all regions and metrics. Finally, the sensitivity indices of the gc_model and gdp_model variables vary over small to moderate values depending on regions and metrics with the abovementioned exception.

In essence, the total-order sensitivity indices broadly mirror the ranking and distribution of the first-order indices (Fig. 4.2). The ssp_exp still ranks as the most or second most important factor. One notable exception is the AP region (Fig. 4.2 b)), where gc_model, ensemble_fut (both metrics), and ensemble_pres, wind_model, mn_exp, v_half for the 100-yr event stand out with notably higher total- than first-order sensitivity indices. This increase implies that these input factors interact considerably with other factors. Besides, the gc_model input variable has a significant impact on the EAD but a much smaller effect on the 100-yr event in the AP and IO.

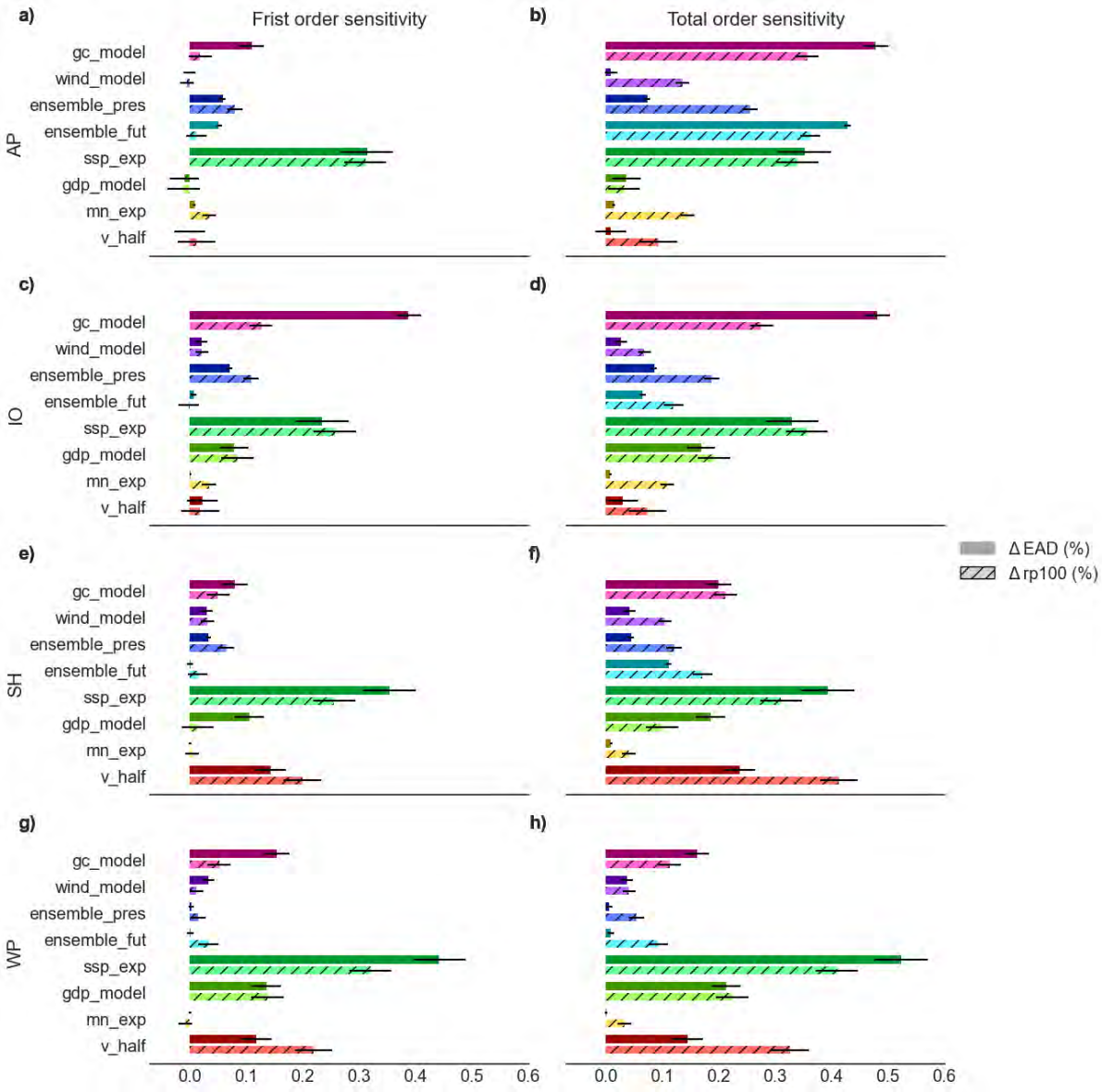

Figure 4.2: First- (panels a, c, e, f) and total-order (panels b, d, f, h) sensitivity indices for future TC risk change expressed as %-change in EAD (solid bars) and 100-yr event values (rp100; bars with hatching) over the four study regions North Atlantic/Eastern Pacific (AP), North Indian Ocean (IO), Southern Hemisphere (SH), and North Western Pacific (WP) and all input variables (see Section 4.2.2 and Table 4.1 therein).

4.4 Discussion

Our results show that non-linear interactions between climate change and socio-economic development drive TC risk change in the future. Disentangling the contributions of both key drivers yields a smaller TC risk increase from climate change than socio-economic development in all study regions. Climate change even reduces TC risk in the North Indian Ocean by a few permille and thus compensates for a part of the risk increase induced by socio-economic development. This finding may seem surprising as the literature generally documents a TC intensity increase in all ocean basins with climate change (Knutson et al., 2020). However, (Bloemendaal et al., 2022) - which generated the TC data we use in this paper - report a decrease in wind speeds for their future TC projections in

the Bay of Bengal, which elucidates our results.

Furthermore, we report a median TC risk change in the future on the order of 2-3%. This may seem like a minor change. However, if we evaluate the entire distribution of possible TC risk changes, we obtain values that exceed a 10% increase. In absolute terms, the future 100-yr event can exceed 2300 bn, 2400 bn, 3500 bn, and 3700 bn USD in the SH, IO, AP, and WP, respectively. This wide distribution of possible outputs comes with implications for TC risk assessments. Depending on the specific aim and application, one may want to consider the risk estimate with the highest probability density, hence median or mean values. However, if a conservative risk assessment is the central focus of a study, the risk analyst should consider the worst-case output values at the high end of the uncertainty distribution.

The sensitivity indices are used to quantify the relative importance of different input factors and can be used to identify which variables have the most significant impact on the output. We show that the SSP-informed exposure scaling is a major determinant of output uncertainty. In our approach, the GDP scaling ignores spatial patterns in socio-economic growth. Therefore, we recommend focusing future research efforts on better understanding and representing socio-economic development. In parallel, improved impact functions would advance TC risk assessment further. We use impact functions that were calibrated on historical records and not synthetic TC tracks. Besides, in this study, the relative importance of the parameter describing the impact functions is partially masked by our choice to report the relative TC risk change and not a change in absolute terms. Moreover, we neglect possible changes in vulnerability in the future. More accurate impact functions would ultimately benefit TC risk assessments in relative and absolute terms. Additionally, we recommend a careful selection of the GCM underlying the hazard set. This input factor is a key driver for the uncertainty in some regions, and depending on the application, users may apply the multi-model mean or select the GCM producing the worst-case results. Finally, while our results will help guide future research efforts, we caution against deriving strong policy statements given that the uncertainty parametrization is subject to limitations and biases, and only those input factors included in the study design can be analyzed for their sensitivity.

4.5 Conclusion

In conclusion, this study shows that exploiting the full range of output values and assessing their probability increases the information density for TC risk assessment. Besides, sensitivity indices are a powerful tool to deepen model understanding and to focus future research efforts.

CHAPTER 5

A cross-model exploration of uncertainty and sensitivity analysis for future tropical cyclone risk

Future tropical cyclone risks will evolve depending on climate change and socio-economic development, entailing significant uncertainties. A comprehensive uncertainty and sensitivity analysis of future tropical cyclone risk changes is thus vital for robust decision-making and model improvement. However, the outcomes of such uncertainty and sensitivity analyses are closely tied to the chosen model setup, warranting caution in interpretation and extrapolation. Our study investigates how four distinct tropical cyclone hazard models as well as alternate representations of socio-economic development influence future tropical cyclone risk. We find that socio-economic factors consistently drive increased risk across all models, while the uncertainty in these risk drivers is hazard model-specific. For instance, the MIT model-based results are sensitive to the choice of global climate model, while estimates from CHAZ, STORM, and climate-conditioned IBTrACS are mainly influenced by exposure scaling based on Shared Socio-economic Pathways. Finally, we differentiate between aleatory, epistemic, and normative uncertainties, offering guidance to reduce these uncertainties and provide better-informed decision-making.

5.1 Introduction

Providing reliable tropical cyclone (TC) risk assessment is challenging due to severe uncertainties in the model input components and model structure (Kropf et al., 2022). Uncertainties can be classified into distinct categories; here we distinguish aleatory, epistemic and normative uncertainty. This classification provides a structured approach to understanding and analyzing uncertainty. It helps in devising appropriate risk management and decision-making strategies and focusing research efforts for model improvements. Aleatory uncertainty, rooted in inherent randomness within natural processes, encompasses the variability of factors like atmospheric conditions and ocean temperatures affecting tropical cyclone behavior (Walker et al., 2003). Epistemic uncertainty, arising from our limited understanding of the modelled system, relates to uncertainties in synthetic tropical cyclone models, historical data quality, and comprehension gaps in environmental interactions (Walker et al.,

2003). Climate-related studies furthermore distinguish two kinds of epistemic uncertainty: scenario uncertainty, reflecting diverse potential emissions scenarios, and projection uncertainty (also called model or representational uncertainty), arising from the inherent limitations of climate models in representing real-world systems (Hawkins and Sutton, 2009; Parker, 2010; Knutti, 2018). Normative uncertainty, on the other hand, emerges from subjective decisions and ethical considerations, influencing choices like valuation units and risk metrics for tropical cyclone risk assessment (Bradley and Drechsler, 2014; Bradley and Steele, 2015; Mayer et al., 2017). These types of uncertainties are interrelated and often co-occur in risk assessment, reflecting the complexity and challenges of understanding and managing tropical cyclone risks.

Efforts can be made to quantify and reduce some aspects of uncertainty in tropical cyclone risk assessment. Aleatory uncertainty is quantifiable using statistical methods, such as Monte Carlo simulations, to determine the probability distribution of potential outcomes. However, it cannot be entirely reduced due to its inherent nature in natural processes (Henrion and Morgan, 1990). Epistemic uncertainty can be quantified in some cases, for example, by employing multiple tropical cyclone hazard models (Chapter 2); their spread of results provides some indication of the epistemic uncertainty, though as with climate models, it is well accepted that the range of model outputs does not fully describe epistemic uncertainties. While model improvements, data acquisition, and research can reduce this uncertainty, complete eradication remains improbable (Walker et al., 2003; Curry and Webster, 2011; Bradley and Steele, 2015; Knutti, 2018). Scenario uncertainty, a form of epistemic uncertainty, is not directly quantifiable as it relies on future human actions, but it can be represented using diverse scenarios outlining possible futures (Moss et al., 2010; Knutti, 2018). Lastly, normative uncertainty relates to value judgments and thus is often not quantifiable in the same way as aleatory and epistemic uncertainty. For example, whether adaptation decisions should be based only on expected annual damage (USD), on numbers of people expected to be affected, or both combined, relates to normative uncertainty. However, efforts can be made to reduce it by promoting transparency and inclusiveness in decision-making, engaging stakeholders with diverse viewpoints, and integrating ethical perspectives in risk assessment (Hansson, 2016). Understanding the quantifiability and potential reduction of these uncertainty types is relevant for informed decision-making and guiding future research.

Uncertainties in tropical cyclone risk model input components and model structure are numerous, complex and dependent on the scope of analysis. In Chapter 2, we demonstrate the importance of tropical cyclone hazard set choice on the modelled, present-day loss estimates. This illustrates both the epistemic uncertainty inherent to TC hazard modelling and the normative uncertainty of the hazard model choice for TC risk assessment.

Assessing future tropical cyclone risks requires additional layers of modelling, each introducing its own set of uncertainties and is further confounded by the lack of verification data (Pianosi et al., 2016; Wagener et al., 2022). Future TC event sets are generated for various emission scenarios (scenario uncertainty), based on different climate models (projection uncertainty), and cover diverse future periods (normative uncertainty). These differences compound with varying TC hazard modelling approaches (epistemic uncertainty) and interact with uncertainties in the future exposure and vulnerability representation. Hence, in Chapters 3 and 4, we systematically assess the uncertainties

and sensitivities in the quantification of future tropical cyclone risks, encompassing uncertainties in all risk model components. These studies show that the results of such an uncertainty and sensitivity analysis are highly dependent on the scope of the study setup; a form of normative uncertainty. For example, the chosen risk metric affects the contribution of the vulnerability function to model results. For future tropical cyclone risks expressed as changes relative to today's baseline, its role is minor. However, when risk is expressed in absolute terms without baseline, its significance rises (see Section 3.3, Fig. 3.2 and Supplementary Figure B.1). Additionally, the choice of hazard model influences the results (see Chapters 3 and 4). Notably, uncertainties using TC event sets from the MIT model are dominated by the choice of global climate model (GCM) used to downscale tropical cyclone tracks from (Chapter 3), whereas the output uncertainty for simulations using the STORM model is most strongly influenced by future representations of the exposure layer according to the Shared Socioeconomic Pathways (SSPs) (Chapter 4). From a risk modelling perspective, such dissimilarities constitute a form of epistemic uncertainty of the TC hazard model. Hence, in this thesis chapter, I further investigate the uncertainty in estimated future TC risk that arises from the choice hazard models, alongside choices of alternative representations of socio-economic development. I use the same four synthetic TC models as featured in the model intercomparison of present-day loss estimates presented in Chapter 2. These models differ in structure and approach, thereby leaving their imprint on the resulting future TC event sets.

While we cannot meaningfully investigate future TC risk estimates from different TC hazard models in the same model setup akin to Chapter 2, we can compare the single uncertainty and sensitivity analysis of future global tropical cyclone risk changes using the different hazard models in an otherwise unchanged setup for exposure and vulnerability. This allows us to determine which findings are generalizable beyond the single studies and which are inherently linked to their hazard model components and study setup. Furthermore, it helps us reflect on structural differences between the tropical cyclone hazard models and the level of maturity and complexity of how the hazard component is represented in risk models, in contrast to how exposure and vulnerability are represented in the same risk models. I synthesize these aspects of model choice, model complexity, and their implication for uncertainty and sensitivity analysis of future tropical cyclone risk models. Finally, I reflect on the different types of uncertainty and their significance for risk modelling and decision-making.

5.2 Methods

In this section, I limit data and methods description to elements that are different from other chapters of this thesis and that are central to this study. For all other model and data features, I refer readers to the respective sections in the thesis. Specifically, consult Sections 2.4.3, 3.4.4, and 4.2.1 for a description of the impact model CLIMADA; Section 3.4.6 for details on asset exposure representation; Section 3.4.3 for the representation of socio-economic development; Section 3.4.7 for impact functions; Sections 2.4.3 i) for a general tropical cyclone hazard and wind model description. Details of the MIT event sets are provided in Section 3.4.2 and 3.4.5; and the STORM tracks in Section 4.2.1 i). Metrics for tropical cyclone risk change are introduced in Section 4.2.3 and the

study regions in Sections 2.4.1 and 3.4.1. The uncertainty quantification module is introduced in (Kropf et al., 2022) and highlighted in Sections 1.2.2, 3.4.8 and 4.2.2.

Next, I briefly summarize the different TC models (Section 5.2.1) and describe the future TC hazard sets from the CHAZ model and the probabilistic, climate-conditioned IBTrACS obtained from the CLIMADA platform (Section 5.2.2). I provide an overview of the representation of future exposure and uncertainty in vulnerability (Section 5.2.3). Finally, I introduce the definition of input factors and their variability space central to uncertainty and sensitivity analysis of this study (Section 5.2.4).

5.2.1 Tropical cyclone models

Different synthetic TC models exist, each with its unique modeling approach that influences the resulting TC event sets. Prominent methods are either purely statistical (e.g., Bloemendaal et al., 2020b, 2022) or coupled statistical-dynamical (Emanuel et al., 2006, 2008; Lee et al., 2018, 2020). I briefly review the key similarities and differences of the approaches used in the TC models of this study.

Statistical-dynamical TC models like the MIT (Emanuel et al., 2006, 2008) and Columbia HAZard model (CHAZ) (Lee et al., 2018, 2020) both use dynamical downscaling of TC tracks from climate model output (beta-and-advection model, Marks, 1992). The main genesis mechanism of the MIT model is random seeding and natural selection (Emanuel et al., 2006, 2008) while CHAZ uses a tropical cyclone genesis index (TCGI) (Lee et al., 2018, 2020), which statistically links the occurrence of TCs to large-scale environmental conditions favorable for TC development. Intensity changes along the tracks are simulated using a dynamical model (MIT, Emanuel et al., 2006, 2008) or an autoregressive model using physics-based drivers (CHAZ, Lee et al., 2018, 2020).

In contrast, the fully statistical model STORM (Bloemendaal et al., 2020b, 2022) uses autoregressive formulas to simulate both track and intensity of a TC. For future climate simulations, Bloemendaal et al. (2022) derived changes in key TC variables from four high-resolution GCM simulations (1979-2014 vs. 2015-2050) and applied these to TC variables from historical data. On this basis, they ran STORM to simulate future TC activity under climate change.

Similarly, the probabilistic IBTrACS obtained from the CLIMADA platform as described in the supplementary material of (Gettelman et al., 2018) can be climate-conditioned by changing their frequency and intensity according to scaling factors derived by Knutson et al. (2015) for the CMIP5 generation of climate models. This approach is simpler than the STORM model. Instead of rerunning a TC model based on several scaled key TC variables, it just applies scaling factors to both hazard intensity and frequency. We note that, to date, climate-conditioned IBTrACS are not available for the newest generation of climate models (CMIP6). Furthermore, the resulting future TC event sets from both the STORM model and probabilistic, climate-conditioned IBTrACS do not contain spatial variations compared to their present-day counterparts. In comparison, future MIT and CHAZ hazard sets are completely new event sets, including spatial variations of the tracks.

5.2.2 Tropical cyclone hazard set from CHAZ and IBTrACS_p

The statistical-dynamical TC model CHAZ (Lee et al., 2018, 2020) is described in more detail in Section 2.4.2 v) of this thesis. CHAZ was used to generate TC event sets for three emission scenarios (SSP245, SSP370, SSP585) drawing from six (CESM2, CNRM-CM6-1, EC-Earth3, IPSL-CM6A-LR, MIROC6, UKESM1-0-LL) of the nine CMIP6 GCMs also utilized by the MIT model (cf. Supplementary Table B.8) and two distinctly different choices of moisture variable used in the TCGI component of CHAZ (Lee et al., 2020). CHAZ is downscaled for every combination of emission scenario, GCM, and TCGI with 10 different realizations of the genesis model and resulting tracks. For each genesis realization, 40 ensembles of the intensity model are produced. In this study, we use all 10 genesis ensembles but select only 8 out of the 40 intensity ensembles. This results in a total of 80 ensemble members, reducing computational costs while maintaining a crucial sample size.

Analogous to the MIT hazard sets, we contrast TC event sets for a present climate reference state (1995-2014) with two future periods: mid-century (2041-2060) and end of the century (2081-2100). Additionally, CHAZ hazard sets require a frequency bias correction (Lee et al., 2018; Sobel et al., 2019). As with the frequency correction applied to CHAZ hazard sets in Chapter 2, we adjust the hazard frequency of all reference state hazard sets using the observed frequencies in each basin. Numbers for the observed IBTrACS genesis events are derived from Bloemendaal et al. (2020b, Table 3) and are combined to values relevant to the study regions of this thesis (Section 2.4.1). Each TC in the baseline hazard set is adjusted to ensure the overall frequency aligns with the observed average. This adjusted frequency is then applied to the TCs in the future climate hazard sets. While each future TC maintains the same frequency as a present-day counterpart, the entire event set's frequency shifts due to variations in the total storm count, thereby reflecting the hazard set's frequency changes in the future.

The generation of probabilistic TC tracks from the CLIMADA platform follows a simple interpolation method using a random-walk process (Kleppek et al., 2008; Gettelman et al., 2018). The method was formulated to deduce a probabilistic track distribution from a single storm, neglecting any particular physics, climate, or basin characteristics. A more detailed description can be found in the supplementary material of Gettelman et al. (2018), and the handling of observations from the IBTrACS record (Knapp et al., 2010) is detailed in Section 2.4.2 i).

For this study, we generate a set of 24 probabilistic tracks for each observed TC between the years 1990 and 2010. Upon generating wind fields from these tracks using two different parametric wind models (Holland, 2008; Emanuel and Rotunno, 2011), the hazard sets are climate-conditioned by applying constant, basin-specific factors to the tracks' intensity and frequency. These factors were derived from the meta-analysis by Knutson et al. (2015) summarizing the effects of climate change on tropical cyclones by CMIP5 climate models under RCP4.5 projections for the late 21st century. A linear scaling approach is used to estimate parameters for different future periods and the other three RCP scenarios (2.6, 6.0, 8.5) according to the RCP database (IIASA, 2009). Note that we did not generate climate-conditioned hazard sets for the RCP8.5 scenario at end-of-the-century as the current implementation of the respective module on the CLIMADA platform produces erroneous results. In the remainder of this study, we refer to hazard sets generated via this approach as *IBTrACS_p*

analogous to the naming in Chapter 2.

5.2.3 Exposure and vulnerability representations

In addition to uncertainties related to future tropical cyclone hazard simulations, we represent changes in socio-economic systems and vulnerability contributing to risk changes. However, in contrast to hazard modelling, the options for globally consistent, future exposure representations are more constrained, and simulations for changing vulnerabilities are not available at all. Instead - and identical to Chapters 3 and 4 - we use economic growth factors from all five SSPs (Riahi et al., 2017) derived by three different models (Dellink et al., 2017; Crespo Cuaresma, 2017; Leimbach et al., 2017) to approximate socio-economic development and analyze exposure uncertainties. For vulnerability, we test uncertainties by varying the vulnerability function's slope parameter of regionally-calibrated vulnerability functions (Eberenz et al., 2021) across a wide range but do not hypothesize about changes to the vulnerability function in the future.

5.2.4 Uncertainty and sensitivity analysis

A central aspect of uncertainty and sensitivity analysis is determining input factors and characterizing their variability space (Pianosi et al., 2016; Saltelli et al., 2019; Kropf et al., 2022). This section delineates our approach to address uncertainties in inputs related to (future) TC hazards, exposure, and vulnerability within the context of our study.

We choose from a discrete list of scientifically justified alternative versions of future climate and socio-economic systems. We prioritize this approach over simply defining additive or multiplicative perturbations for each input factor because it avoids the challenges of defining perturbations in the absence of relevant information, directly relates the output to chosen input combinations, and circumvents assumptions about the likelihood of specific input scenarios. Specifically, we define five input factors characterizing the hazard components, three for the exposure and one for the impact function (see Table 5.1). For event subsampling, targeting the aleatory uncertainty of the hazard set, we favor continuous sampling to better represent its inherent variability. For the parameters describing the impact function, continuous sampling is employed due to the absence of a scientifically supported discrete alternative.

Table 5.1: Input factors and their variability space. The first column lists all input factors of the uncertainty and sensitivity analysis, indicating which risk model component they relate to. Variable names, as referred to in the text and figures of this study, are listed in the second column; short names thereof in the third; the type of the parameter range in the fourth; and the actual parameter ranges for each hazard model in the last four columns.

Input factor	Variable name	Short name	Type	Range			
				MIT	STORM	CHAZ	IBTrACS[a]
Hazard: GCM	GCM	gc_model	discrete	1 - 9	N/A	1 - 6	N/A
Hazard: Emission scenario	SSP hazard	ssp_haz	discrete	1 - 3	1 - 4	1 - 3	1 - 4 (3 for 2100)
Hazard: Wind Model	Wind model	wind_model	discrete	1 - 2	1 - 2	1 - 2	1 - 2
Hazard: Moisture variable TCGI	Moisture variable TCGI	tcgi_var	discrete	N/A	N/A	1 - 2	N/A
Hazard: Bootstrapping	Event subsampling base/future	HE_base/HE_fut	continuous	80 % of every year	1/10 ensembles	80 % of event set	80 % of event set
Exposure: SSP-based GDP scaling	SSP exposure	ssp_exp	discrete	1 - 5			
Exposure: GDP model	GDP model	gdp_model	discrete	1 - 3			
Exposure: m,n scaling LitPop	Exposure urban/rural weighting	mn_scaling	discrete	1 - 9			
Impact functions	Vulnerability function midpoint	v_half	continuous	within IQR of regional TC calibration[b]			

[a] CMIP5

[b] (Eberenz et al., 2021)

We then generate a set of N=2^9 (CHAZ and MIT), N=2^{10} (IBTrACS_p), and N=2^{11} (STORM) samples of the input parameters. We note that for all hazard sets, the sample size is large enough for the uncertainty analysis to converge. This means that the analysis has reached a state where additional samples do not significantly change the results. Analogous to Chapters 3 and 4, the Sobol' sampling algorithm (Sobol, 2001; Saltelli et al., 2010) as implemented in the *SALib* Python package (Herman and Usher, 2017) and seamlessly integrated into CLIMADA (Kropf et al., 2022) is applied to the resulting 10,240 (MIT) to 36,864 (STORM) input factor combinations. For each sample, we calculate the TC risk change, resulting in distributions for both analyzed risk metrics (change in EAD and 100-yr event). This output distribution underpins the uncertainty analysis and initiates the sensitivity analysis. Utilizing the Sobol' quasi-Monte Carlo sequence (Sobol, 2001), we present first- and total-order sensitivity indices to estimate each input factor's contribution to output variance. Specifically, the first-order sensitivity index measures the direct impact of a single input factor on the output uncertainty, independent of other factors. The total-order sensitivity index, on the other hand, captures both the direct effects and any potential interactions with other input parameters. Together, these indices provide a comprehensive view of how changes in input variables influence the uncertainty in our results.

5.3 Results

5.3.1 Drivers of future TC risk change: comparison across hazard models

Risk change serves as a useful metric for both risk modelling and effective communication with stakeholders, offering a comparative perspective between present-day and future scenarios. Future tropical cyclone risks change in a warming climate and with socio-economic development, which together shape the total TC risk change. Here, we evaluate the contributions and role of these two key drivers to future TC risk estimates across hazard models. To consider the influence of climate change on risk, we hold exposure constant at a reference state while using varying future climate hazard representations. Conversely, to assess the impact of socio-economic factors, we keep the hazard data fixed at the present-day baseline, allowing socio-economic conditions to vary. TC risks are expressed by the common metric of expected annual damage (EAD) and 100-yr damage event (100-yr event in short), reported as relative changes (in %) compared to present-day baselines. We present results for four study regions as introduced in this thesis (Sections 2.4.1, 3.4.1, 4.2.4). The study approach aligns with the setup used in Sections 3.2.1 and 4.3.1. While those sections focus on individual hazard models (MIT in 3.2.1 and STORM in 4.3.1), our current evaluation spans all four synthetic TC hazard models featured in this thesis (Fig. 5.1). Note that we limit the results' description to the EAD in this section because the corresponding key findings for the 100-yr event are comparable (cf. Supplementary Figure C.1).

Climate change, in general, affects the median TC risk changes comparably across hazard models, study regions and periods (Fig. 5.1, left most boxplots in all panels). Specifically, the median change in EAD is on the order of 1% in most cases. However, the uncertainty in TC risk change estimates is notably higher for all MIT hazard results than the other hazard model outputs, as can be derived from

the width of the interquartile range of the boxplots shown in Figure 5.1. Furthermore, maximum values for climate change-driven EAD increase from the MIT hazard reach 20% (45%), 16% (23%), 6% (8%), and 13% (15%) in the North Atlantic/Eastern Pacific, North Indian Ocean, Southern Hemisphere, and Western Pacific in the middle (at the end) of the century. In contrast, maximum risk increases from the other hazard models do not exceed the 5%-mark except in the North Indian Ocean. There, climate change raises EAD values from CHAZ by 7.5% (6%) and IBTrACS_p by 21% (21%) in 2050 (2090), respectively. Only the results from STORM remain low due to known high-intensity biases in the reference period hazard set as discussed in Sections 2.3 and 4.4. The North Indian Ocean is furthermore the region where uncertainties in the climate-driven risk change are highest across all hazard models. Additionally, median TC risk changes are lowest in the Southern Hemisphere over all regions, including negative values for CHAZ and IBTrACS_p. In other words, climate-driven TC risk decreases in these cases. Indeed, we find negative minima (ca. 0 % to −1 % for all hazard models and regions except for STORM in the Western Pacific (Fig. 5.1 g)).

Socio-economic development emerges as the predominant driver for TC risk increase, consistent across all hazard models (refer to Fig. 5.1). This consistent pattern across models is due to the fact that we utilized the same future socio-economic representation for each. Notably, any difference between the hazard models stems primarily from their distinct present-day baseline. Specifically, the median EAD changes driven by socio-economics are around 1 % to 2 % by 2050. In regions like the North Atlantic/Eastern Pacific and Western Pacific, this is roughly double the changes attributed to climate change. However, in the North Indian Ocean, median values are higher: 2.5 % to 3 % (and 6 % to 7 % by 2050 (2090), which is about four times the climate change contributions. Furthermore, the uncertainty tied to socio-economic development is most pronounced in the Southern Hemisphere across regions (with potential reasons discussed in Section 3.3). Finally, when considering the hazard sets CHAZ, STORM, and IBTrACS_p, socio-economic development presents more uncertainty than climate change. In contrast, for MIT-based calculations, climate change is the more uncertain risk driver.

Next, we assess the total TC risk increase, factoring in both climate change and socio-economic development. Notably, the total TC risk increase, as depicted in Figure 5.1 (total; right-most column), reveals intricate interdependencies between these drivers, which exceeds a simple arithmetic sum or the product of hazard and exposure as illustrated in Figure 5.1 (sum; inner right column) and also discussed in Section 3.2.1. Contrarily, an excess non-linearity emerges when including climate change applied to the hazard and socio-economic development in the exposure from the beginning, defying the basic summation or multiplication of hazard and exposure components in isolation.

Median EAD raises by 0.9% (CHAZ) to 2.3% (MIT), 1.9% (STORM) to 5.2% (MIT), 1.2% (CHAZ, IBTrACS_p) to 3.8% (MIT), and 1.4% (CHAZ, IBTrACS_p) to 3.8% (MIT) in the North Atlantic/Eastern Pacific, North Indian Ocean, Southern Hemisphere, and Western Pacific by 2050. In all regions, the median risk increase is highest for the MIT hazard, while the other three models tend to cluster around similar values, with STORM producing slightly higher results in the Southern Hemisphere and Western Pacific than CHAZ and IBTrACS_p. By the end of the century, the median risk increases further, reaching levels that are approximately two to three times the increase in EAD estimated for 2050. Furthermore, maximum total EAD increases by 2090 span from 11% (CHAZ) to 263% (MIT),

90% (CHAZ) to 393% (MIT), 23% (IBTrACS_p) to 148% (MIT), and 14% (CHAZ) to 103% (MIT) in the North Atlantic/Eastern Pacific, North Indian Ocean, Southern Hemisphere, and Western Pacific respectively, highlighting the significant uncertainty in these results. Note that we focus on total risk increases as described in this last paragraph for the remainder of the study.

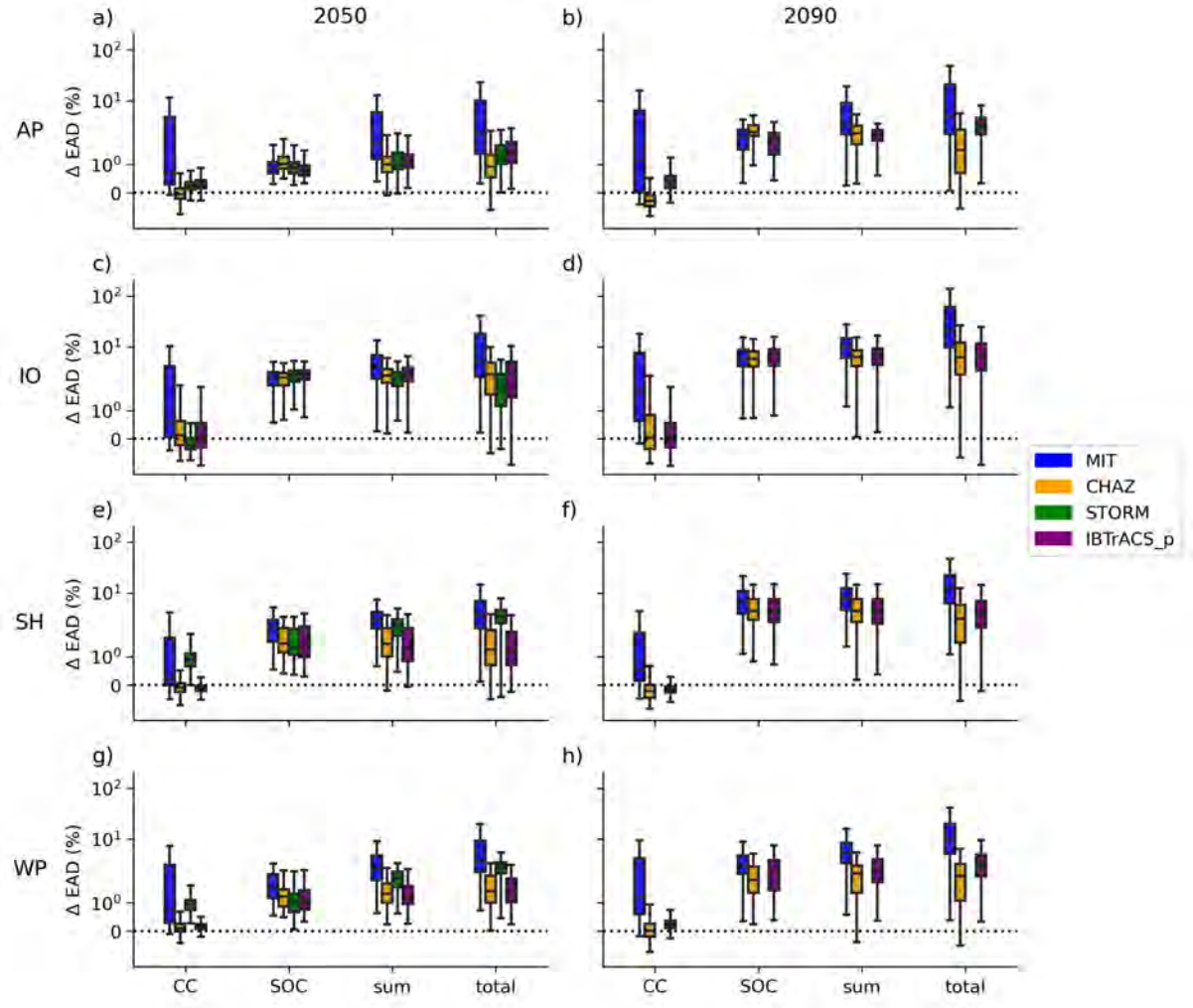

Figure 5.1: Drivers of future tropical cyclone risk change: comparison across hazard models. Relative change in expected annual damage (EAD) by 2050 (left panels) and 2090 (right panels) due to climate change (CC), socio-economic development (SOC), the product of CC and SOC calculated from the sum of their log values (sum) and both drivers interacting (total) with respect to the historical baseline. The relative change EAD is reported for the four study regions (North Atlantic/Eastern Pacific (AP), North Indian Ocean (IO), Southern Hemisphere (SH), and North Western Pacific (WP)). Boxplots are shown for the four models MIT (blue), CHAZ (orange), STORM (green), IBTrACS_p (purple) and display the interquartile range (IQR) for the uncertainty over all input factors (see Methods), while the whiskers extend to 1.5 times the IQR. More extreme points (outliers) are not shown. Note that STORM results are only available for 2050.

5.3.2 Uncertainty of future TC risk change: comparison across hazard models

To quantify uncertainty, we compute a probability distribution of results for each input factor combination. Here, we analyze this output distribution of risk change estimates across the four hazard models (Fig. 5.2). We present the main findings for uncertainties of future TC risk change,

focusing on changes in EAD, consistent with the preceding section. For results of the 100-yr event, which are comparable, readers are directed to Supplementary Figure C.2.

In essence, Figure 5.2 presents the probability density distributions of the total TC risk change, derived from the same data as the boxplots (total) in Figure 5.1. We identify density peaks of EAD change for CHAZ, STORM, and IBTrACS_p hazard sets in each region and both future periods around 1 % to 3 %. The density distributions from the MIT model, however, peak at higher values, consistent with the assessment of median total TC risk change from the previous section. Interestingly, when considering both risk metrics - EAD (Fig. 5.2) and the 100-yr event (Fig. C.2) - we observe that their density distributions peak at very similar values for each combination of region, year, and hazard model (Supplementary Table C.1). This consistency suggests that socio-economic development is the predominant driver for total TC risk change, influencing the magnitude and peak of the density distribution. Consequently, the choice between the two risk metrics does not significantly affect this outcome. Any differences between these metrics are predominantly shaped by the hazard, making them secondary in this context.

Conversely, when examining the entire probability density distribution, the MIT results display a notably broader distribution compared to the other three hazard sets, a finding consistent with results from Figure 5.1. The width of a distribution can serve as an indication of its associated uncertainty. Drawing from insights in the previous section, the width of the MIT-based distribution can be interpreted as an imprint of the uncertainties associated with climate change as a more uncertain risk driver. In contrast, the similar shapes of distributions from CHAZ, STORM, and IBTrACS_p models indicate socio-economic development as their main source of uncertainty, as corroborated by Figure 5.1. Furthermore, we observe wider distributions for results in 2090 compared to 2050 for all hazard models, related to increasing uncertainty in time. While this analysis provides insights into the overarching uncertainty, a more detailed examination of individual input factors is essential. In the following section, we explore these factors through a sensitivity analysis in detail. Finally, it is worth noting that the shape of the distribution also bears the influence of the sample size used in the uncertainty and sensitivity analysis, which is not identical across the hazard models in the current setup. Typically, a more extensive sample size can amplify the peak density, reflecting a more concentrated consensus among the data points.

5.3.3 Sensitivity of future TC risk change: comparison across hazard models

Sensitivity analysis helps identify and quantify the relative importance of individual input factors for the output uncertainty of future tropical cyclone risk change estimates as described in the last section. The model input factors and their parameter ranges are defined to capture the inherent uncertainties in the different components related to the future TC hazard, exposure and vulnerability representation. Here, we present first-order and total-order Sobol sensitivity indices (Sobol, 2001; Saltelli et al., 2010), analogous to the sensitivity analyses of individual hazard models (MIT in Section 3.2.2 and STORM in Section 4.3.2), to assess the impact of these factors on our TC risk change calculations across the four hazard models. We note that not all hazard models encompass all input factors, as described in Section 5.2.4. First-order sensitivity indices measure the effect of variations in a single input factor, while total-order indices evaluate the cumulative effect, considering

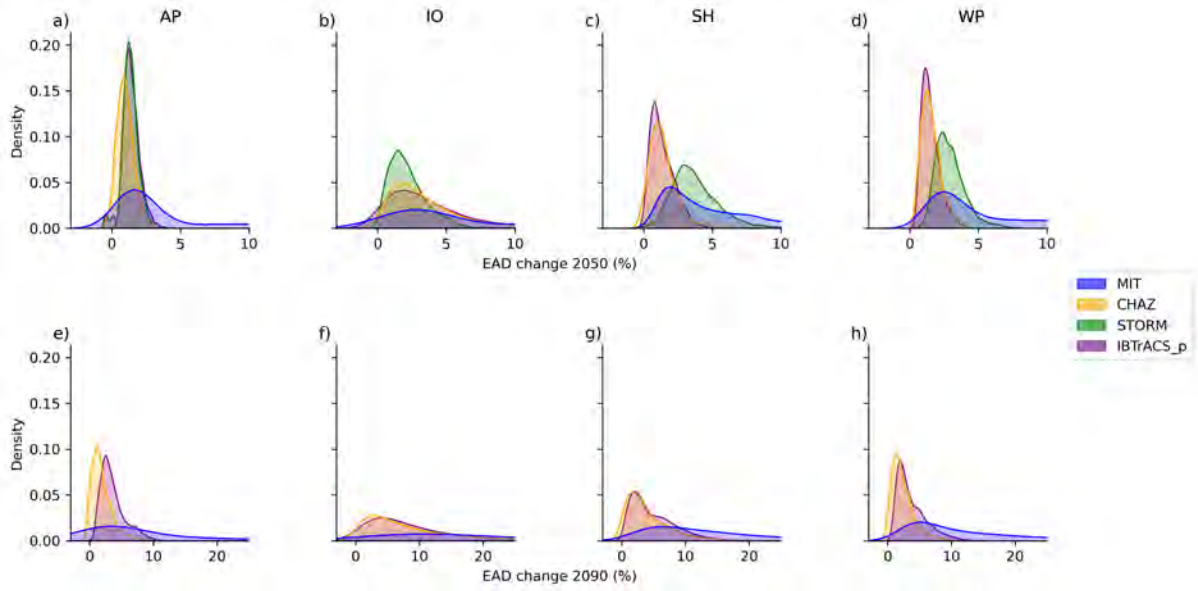

Figure 5.2: Uncertainty distribution of TC risk change: comparison across hazard models. Kernel density estimation plots showcasing the uncertainty distribution of estimated relative change in expected annual damage (EAD) across study regions (North Atlantic/Eastern Pacific (AP), North Indian Ocean (IO), Southern Hemisphere (SH), and North Western Pacific (WP)) for the years 2050 and 2090. Each subplot represents a specific region and year combination, with different models (MIT, CHAZ, STORM, IBTrACS_p) depicted in distinct colors. Note, the model STORM only provides data for 2050. Each plot shows a normalized probability distribution with an integral sum of 1. The x-axis is truncated in some figures, potentially influencing the interpretation of distribution tails, particularly for the MIT hazard-based results.

all factors and their potential interactions (Saltelli et al., 2008).

The dominant source of uncertainty for future TC risk changes varies when different hazard models are used to calculate risk. In the MIT model-based analyses, the primary source of uncertainty stems from the choice of GCM used in downscaling TC events sets (*GCM*) (Fig. 5.3 a), e) and Section 3.2.2). Conversely, for all other hazard models, the SSP-based scaling of the exposure points (*SSP exposure*) generally exhibits the largest sensitivity. Specifically, this holds for most results in the Southern Hemisphere and Western Pacific for the CHAZ, STORM and IBTrACS_p and both future periods. In the North Indian Ocean, sensitivity indices are highest for input factors related to the hazard component and results in the North Atlantic/Eastern Pacific follow no consistent trend beyond the primary observations mentioned. A detailed compilation of the most significant sensitivity indices for future TC risk estimates can be found in Supplementary Table C.2.

The sensitivity analysis reveals several distinctive patterns. First, the GCM choice (*GCM*) is more important in the North Atlantic/Eastern Pacific, North Indian Ocean, and Western Pacific than in the Southern Hemisphere for the three hazard models (MIT, CHAZ, STORM), which encompass this input factor. This pattern largely aligns with regions where uncertainties in climate change as a risk driver exceed those from socio-economic development (see Fig. 5.1). Furthermore, the GCM choice is more important for changes in EAD than in the 100-yr event. Second, for CHAZ model-based sensitivity analyses, the moisture variable within the TCGI (*TCGI*) is mostly of equal importance for the TC risk change uncertainty as the GCM choice (*GCM*) (Fig. 5.3 b), f)). Third, the variability in event subsampling for baseline and future hazard sets (*Event subsampling base, future*) is most

pronounced in the IBTrACS_p-related result (Fig. 5.3 b), g)), in contrast to the other hazard models.

Next, we evaluate the total-order sensitivity indices (total effects) across the four hazard models. Namely, total effects are notably increased for CHAZ hazard-based results in comparison to their first-order indices, meaning that this model setup encompasses many interactions between input factors (Supplementary Figure C.3). In contrast, total-order sensitivity indices broadly mirror the ranking and distribution of the first-order indices for MIT- and STORM-related results as described in Sections 3.2.2 and 4.3.2. Moreover, in the IBTrACS_p-based sensitivity analysis, total effects include influences from the wind model choice (*wind model*), a factor that is nearly irrelevant in all other hazard sets. Note that both the largest first- and total-order sensitivity indices are compiled in Supplementary Table C.2.

Finally, we emphasize that sensitivity analysis is specific to the model setup; thus, sensitivity indices are influenced by the choice of risk metric. To illustrate this, we show the implications of assessing TC risk in absolute terms versus changes relative to a baseline. For absolute TC risk estimates, the primary source of uncertainty across all hazard models is the input factor associated with the vulnerability function (*Vulnerability function midpoint*), as depicted in Supplementary Figures C.4 and C.5 and first mentioned in Section 3.2.2.

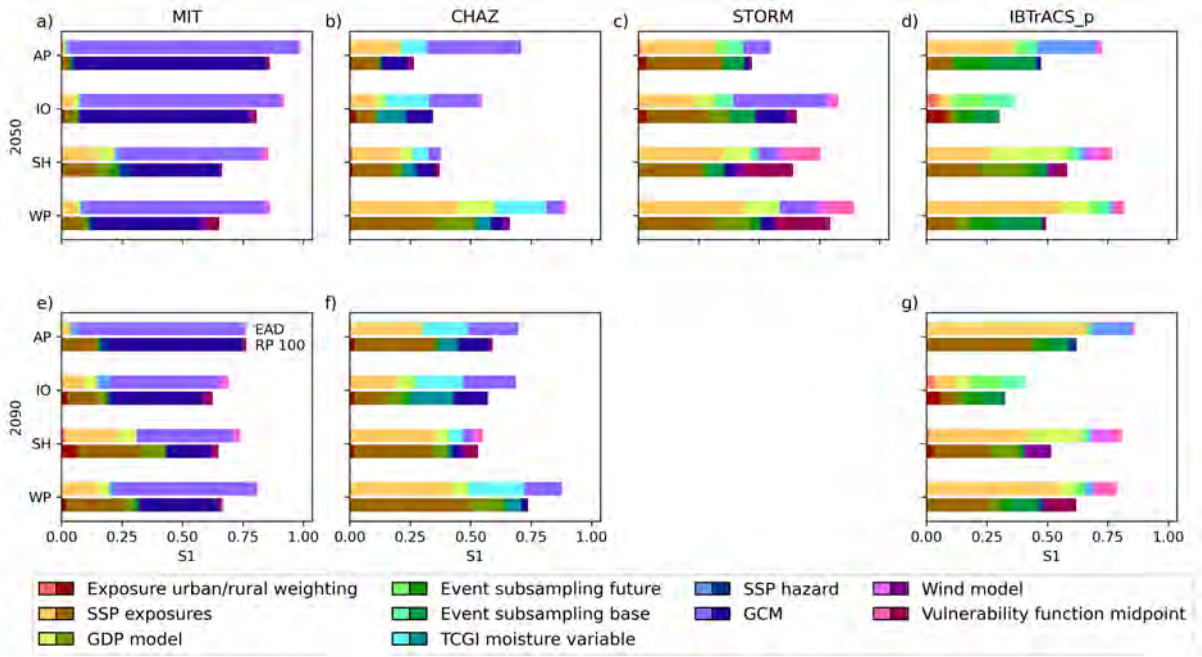

Figure 5.3: Sensitivity indices of future TC risk change: comparison across hazard models. First-order Sobol sensitivity indices for future (2050, 2090) TC risk change calculated with the four models (MIT, CHAZ, STORM, IBTrACS_p), expressed as %-change in expected annual damage (EAD; upper bar, lighter colors) and 100-yr event values (RP 100; lower bar, darker colors) over the four study regions (North Atlantic/Eastern Pacific (AP), North Indian Ocean (IO), Southern Hemisphere (SH), and North Western Pacific (WP)) and all input factors (different colors); *Vulnerability function midpoint* describes the impact function; *Wind model*; *GCM*, *SSP hazard*, *TCGI moisture variable*, *Event subsampling base*, *Event subsampling future* pertain to the hazard component; *GDP model*; *SSP exposure*, *Exposure urban/rural weighting* relate to the exposure. Note that STORM results are only available for 2050.

5.4 Discussion

Our results show that while both climate change and socio-economic development influence TC risk changes, socio-economic factors are the predominant drivers of increased risk across all hazard models. While studying these drivers in isolation provided distinct insights, their combined effects are intricate, revealing non-trivial interactions. This suggests that merely summing or multiplying their individual effects might not capture the full complexity of their combined impact on TC risk. It underscores the importance of integrating both drivers from the onset in risk assessments to ensure a comprehensive understanding. Moreover, the sensitivity analysis reveals varying sources of uncertainty in TC risk assessments depending on the hazard model choice. In the MIT hazard-based analysis, the choice of GCM dominates uncertainty, while results using the other hazard models (CHAZ, STORM, IBTrACS_p) highlight the significance of SSP-based exposure scaling. Generally, for high uncertainty surrounding climate change as a risk driver, input factors tied to the hazard component become more influential. Conversely, in cases where socio-economic development uncertainties prevail, input factors related to exposure take priority.

Beyond these general aspects, we delve into findings that are intrinsically linked to single hazard models, examining subtleties in modelling approaches and their influence on risk assessment in the following sections. Furthermore, we reflect on the structural nuances and development levels of all three risk model components. Concluding this discussion, we relate our findings to the different categories of uncertainty and reflect on their broader implications for risk modelling and decision-making.

Hazard model-specific findings

In Chapter 3, we show that the choice of climate model dominates the output uncertainty for TC risk estimates based on the MIT model (Emanuel et al., 2006, 2008). Moreover, we find a positive relationship between the climate sensitivity of GCMs used to downscale TCs and the corresponding increase in tropical cyclone risk (see Section 3.2.4). This increase is directly related to the scaling of TC potential intensity with global warming (Emanuel, 2007). Additionally, this scaling serves as a strong predictor for TC genesis potential indices (Emanuel and Nolan, 2004; Emanuel, 2010; Rappin et al., 2010). These indices, in turn, influence TC hazard frequencies and intensities, which are critical characteristics for assessing TC risk. However, from Chapter 3 alone, we lack the basis to assess if this finding is generalizable beyond the MIT TC model.

The present study helps address this gap by investigating the role of climate sensitivity in CHAZ, which is another statistical-dynamical model (Lee et al., 2018, 2020). Namely, we found no striking relationship between transient climate response (TCR) as a measure of climate sensitivity and changes in CHAZ-based TC risk estimates (Supplementary Figures C.6 and C.7) and CHAZ frequency (Supplementary Figure C.8) and intensity changes (Supplementary Figure C.9). Therefore, we conclude that the direct relationship between climate sensitivity and resulting hazard frequency and intensity is a unique feature of the MIT model and not generalizable for all statistical-dynamical models; at least not for statistical-dynamical models with a different genesis component. The MIT

model applies a coupled ocean-atmosphere TC intensity model (CHIPS; Emanuel and Nolan, 2004) driven along the TC tracks. The intensity model has a very high radial resolution of the TC core and can resolve high-intensity TCs. Conversely, CHAZ employs an autoregressive linear statistical model (Lee et al., 2016), incorporating monthly-averaged potential intensity, vertical wind shear, and mid-level relative humidity as environmental predictors, along with a stochastic component for added variability. Nonetheless, the linear methodology of CHAZ, applied to GCM output with a typical resolution of around 50 km, is constrained by the limited representation of high-intensity TCs in these climate models. This resolution, while sufficient for representing TCs, falls short in accurately resolving their intensity (Davis, 2018). Consequently, using this GCM output in a linear regression model like CHAZ leads to an underrepresentation of high-intensity TCs. Similarly, the STORM model, despite utilizing *high-resolution* GCMs (up to 25 km resolution), encounters the same limitation, as this resolution is still inadequate for accurately capturing the intensity of high-end TCs (Bloemendaal et al., 2022). Hence, we suggest that the difference in the intensity models helps explain the dissimilar importance of climate sensitivity for TC risk increases between the MIT and CHAZ models. However, to fully comprehend the role of GCM's climate sensitivity in TC hazard modeling, further research is essential.

Moreover, we investigate the role of the two distinctly different moisture variables used in the TCGI component of CHAZ, which modulate the resulting CHAZ hazard frequency (Lee et al., 2020). Specifically, event sets generated using column-integral relative humidity (CRH, Tippett et al., 2011) as a moisture variable show an increase in TC frequencies in a warming climate, whereas those based on saturation deficit (SD, Camargo et al., 2014) indicate a decrease (Supplementary Figure C.8). Despite this distinct divergence in TC frequencies, similar variations are not observed in the TC risk changes when using CHAZ (Supplementary Figures C.6 and C.7). Furthermore, the sensitivity indices for the TCGI variable are not the highest (Fig. 5.3). On the other hand, events generated using both CRH and SD as moisture variables offer comparable TC risk change estimates, although CRH-TCGI-based hazard sets generally exhibit higher maxima (Supplementary Figures C.6 and C.7).

This smaller impact of TCGI on risk estimates, in contrast to its evident role in hazard frequency, can be attributed to CHAZ hazard intensity. In this aspect, the choice of GCM exerts a more substantial influence than the TCGI moisture variable (Supplementary Figure C.9). Given these insights, we argue that TCGI selection may be of secondary importance in a decision-critical context, especially when socio-economic and exposure-related uncertainties are more pronounced. Nonetheless, the use of both TCGI versions is advisable to avert possible blind spots in representing future TC risks. In terms of model refinement, both the choice of TCGI and GCM remain critical aspects of epistemic uncertainty that warrant further investigation.

Development levels of risk model components

We named the key influence of hazard-related input factors a representation of the maturity of TC hazard modelling as a field in Chapter 3. Specifically, we interpreted the importance of the GCM choice for MIT-based TC risk change estimates (Fig. 3.2) as the consequence of using a complex TC hazard model with a wealth of model parameters informing future TC simulations. Here, we contrast

this statement with results from the other hazard models of differing model structure and complexity. Comparing results from both statistical-dynamical TC models (MIT and CHAZ) shows that the results from the CHAZ model spread a notably narrower range of outputs than MIT-based values. This seems particularly surprising given that CHAZ includes an additional input factor related to the hazard component - the TCGI moisture variable - as described in the previous paragraph. This additional factor is not present in the MIT model. Given the inclusion of this additional factor, one might expect a corresponding increase in the model's uncertainty. Conversely, for CHAZ-based simulation, the SSP-based exposure scaling is often the most influential input factor (Fig. 5.3, Supplementary Table C.2). Furthermore, socio-economic development is the stronger and more uncertain risk driver than climate change in the CHAZ world (Fig. 5.1). Thus, we propose that uncertainty is not solely determined by model complexity but also by how the uncertainty of hazard-related factors compares to that of exposure-related variables. In essence, the complexity of the hazard model becomes secondary if uncertainties stemming from socio-economic development outweigh those from hazard-related inputs.

Furthermore, in Chapter 3, we reflect on the state of TC hazard modelling in contrast to exposure and vulnerability. Here, we re-examine this aspect, including the newest insights from this study. We reaffirm that the availability of TC hazard models in risk assessment surpasses that of models for exposure and vulnerability. Moreover, in Chapter 3, we initially hypothesized that comparably low sensitivity indices for exposure and vulnerability (Fig. 3.2) may simply result from a limited capability to simulate socio-economic development and changing vulnerabilities. However, the present study reveals that the results from the two statistical-dynamical hazard models of comparable complexity and structure, MIT and CHAZ, lead to different sensitivity analysis results in an unchanged setup for exposure and vulnerability (Fig. 5.3). This finding undermines the initial hypothesis proposed solely on sensitivity analysis for MIT-based results. As previously discussed, we propose that the relative magnitude of uncertainty associated with each input component of the risk model is also relevant for the interpretation of sensitivity analysis results.

Classification of uncertainties and their implications

Most of the input factors defined for the uncertainty and sensitivity analysis of our study represent a form of epistemic uncertainty, which can further be split up into scenario and projection uncertainty (Hawkins and Sutton, 2009; Parker, 2010; Knutti, 2018). Scenario uncertainty in the hazard component described by the varying hazard emission scenarios (*SSP hazard*) exhibits a minor influence on the output uncertainty of TC risk change estimates across all models. In contrast, scenario uncertainty of the exposure described by the SSP-based scaling factors for GDP growth (*SSP exposure*) is the key source of uncertainty across a wide range of outputs (Section 5.3.3). Projection uncertainty can be evaluated on two levels. First, across TC hazard models, in which case the difference between model outputs from the four models constitutes a form of TC model (or projection) uncertainty. Second, within each hazard model, the projection uncertainty is substantial for hazard-related input factors, particularly the GCM choice (*GCM*) and TCGI formulation (*TCGI moisture variable*). Contrarily, for the exposure component, projection uncertainty related to the GDP

model choice (*GDP model*) is small.

Aleatory uncertainty is only represented in the event subsampling of the hazard sets in this study. In our sensitivity analysis and as described above, we observe divergent responses to subsampling (*Event subsampling base/future*) across different hazard models (Fig. 5.3, Supplementary Table C.2). Specifically, the statistical-dynamical models MIT and CHAZ show no sensitivity to event subsampling, suggesting that they may inherently capture natural variability through their physics-based methodologies and the generation of new event sets for future climates. In contrast, the purely statistical models, IBTrACS and STORM, exhibited sensitivity to subsampling. This indicates that these models, which have the historical track sets at their foundation, may require the inclusion of a subsampling step to adequately represent aleatory uncertainty. However, it is important to note that further validation is needed to strengthen this conclusion.

The different types of uncertainty vary in their reducibility. Our study reveals that projection uncertainty is especially significant in the hazard component and is, theoretically, reducible through model refinement, enhanced data collection, and focused research (Walker et al., 2003; Curry and Webster, 2011; Bradley and Steele, 2015; Knutti, 2018). Given its substantial impact and potential for reduction, we advocate prioritizing research efforts in hazard modelling to minimize this specific form of uncertainty. However, the less available nature of exposure and vulnerability modelling in risk assessments offers immediate opportunities for impactful research, as these areas have a pronounced influence on results.

On the other hand, scenario uncertainty is inherently tied to human choices and is therefore not reducible. In the context of this specific study, this form of uncertainty may hold secondary importance in hazard modeling due to its observed low sensitivity. However, it becomes critically relevant from a decision-making standpoint when evaluating exposure-related scenario uncertainty. Although the uncertainty itself is immutable, it can serve as an incentive for directing human decisions toward scenarios of minimal risk. In essence, the prominence of scenario uncertainty in the exposure component may, for instance in a policy context, act as a reference to minimize TC risks by aligning with scenarios that yield the least hazardous outcomes.

Although aleatory uncertainty is by its very nature non-reducible, it is crucial to quantify it, as demonstrated by the event subsampling in this study or the separation of ENSO-modulated patterns from general weather variations, as outlined in Emanuel et al. (2012). Such quantification aids in distinguishing aleatory uncertainty from epistemic uncertainty, thereby guiding research efforts more effectively.

Normative uncertainty emerges from the many choices we make in the course of TC risk assessment and cannot be quantified in the same way as aleatory and epistemic uncertainty (Bradley and Drechsler, 2014; Bradley and Steele, 2015; Mayer et al., 2017). However, considering aspects of normative uncertainty has multi-faceted implications for TC risk assessment.

Regarding scenario uncertainty, it is vital to consider a broad range of possible scenarios to avoid blind spots in risk assessment. Unlike in policy-making, where scenarios often represent a favored developmental path, excluding specific scenarios a priori in a risk setting could result in either under- or overestimation of risk. Furthermore, caution is also advised when weighting these scenarios, as improper weighting could exacerbate the risk of over- or underestimation.

To address projection uncertainty, fitness for purpose is key (Parker, 2010). Different sectors and stakeholders require varied model outputs. Given practical constraints, it is often necessary to select specific TC hazard models early in the risk assessment process. However, this model choice is very important for the resulting output, as shown in this study. To best tailor risk assessments, we recommend a bottom-up approach that incorporates stakeholder needs and helps guide model choices accordingly.

In TC risk assessment, including the setup of this study, numerous choices are made that represent forms of normative uncertainty. These decisions inevitably introduce blind spots. It is crucial to be aware of these limitations when interpreting results. These choices condition our findings, and care must be exercised in extrapolating these context-specific insights to broader, real-world implications.

In conclusion, understanding the different types of uncertainties — aleatory, epistemic, and normative — is vital for both risk modeling and informed decision-making. Linking these types of uncertainty to systematic uncertainty and sensitivity quantification across different TC hazard models, this study offers a nuanced view of TC risk assessment, which can guide future research and provide decision-critical insights. Providing this type of guidance is particularly important for emerging new fields like physical climate risk disclosure (Fiedler et al., 2021; Arribas et al., 2022) or changing traditional sectors like insurance. In both cases, rules by which climate risk science can be used appropriately to inform climate risk assessment have not yet been developed or are changing. As we move forward, it is essential to continually refine our models, choose models according to their application, and be critically aware of the normative assumptions that underlie our assessments. Ultimately, we aim to balance risk assessments that are both accurate and actionable.

CHAPTER 6

Conclusions and outlook

The powerful impact of tropical cyclones disrupts societies in many coastal regions in the tropics and subtropics. In a warming climate and with socio-economic development, tropical cyclone risks will evolve, entailing substantial uncertainties. Consequently, the demand for robust and reliable tropical cyclone risk assessments is increasing, both in emerging and changing traditional sectors. In response, the overarching goal of this thesis is to identify and systematically quantify the crucial sources of uncertainty in global tropical cyclone risk assessments, thereby enhancing the value of these assessments for risk analysis, research, and decision-making. First, it provides an in-depth evaluation of present-day, global tropical cyclone hazard datasets, highlighting the importance of hazard model choice for loss estimation (Aim I). This guides stakeholders in hazard set choice, thereby strengthening risk assessment reliability. Second, it systematically investigates the key drivers and uncertainties in future global tropical cyclone risks, identifying the most influential model inputs (Aim II). This enhances both the transparency and depth of risk assessments. Third, synthesizing uncertainty and sensitivity analyses across multiple hazard models and evaluating these by uncertainty types (Aim III) offers a structured and comprehensive perspective to navigate the implications and reducibility of uncertainties. Collectively, these contributions advance tropical cyclone risk assessment, promoting better-informed decision-making and presenting avenues for model improvement.

In this chapter, I conclude by highlighting the central findings and implications of the thesis and by providing an outlook for future research. The chapter is organized as follows. I first present the central findings emerging from Chapters 2, 3, 4, and 5 in Section 6.1. Section 6.2 presents the implications of the thesis findings for broader scientific and public debates. I then offer suggestions for further research in Section 6.3 before ending with some closing remarks in Section 6.4.

6.1 Central findings

Synthetic TC models are a vital tool for tropical cyclone (TC) risk assessment. They are specifically designed to overcome the spatial and temporal limitations imposed by historical TC observation, which are inadequate for reliable risk assessment. These models have all been evaluated and used in various contexts to study TC climatology or perform risk assessment in specific contexts. Prior to this thesis, they have never been directly compared as input hazard datasets in catastrophe models

for TC risk assessment and loss estimation. Nor have uncertainties and sensitivities throughout the entire TC risk model been assessed and quantified systematically. The central finding of both types of analysis is that the choice of TC model strongly influences risk assessment results. Here, I review key characteristics of the four synthetic TC models and how they shape the results of TC risk assessments.

Probabilistic IBTrACS (IBTrACS_p), obtained from the CLIMADA platform (Aznar-Siguan and Bresch, 2019) by a random-walk process applied to historical observations (Kleppek et al., 2008; Gettelman et al., 2018) is a simple, computationally efficient and open-source TC dataset, making it well-suited for broad, high-level TC risk assessments. However, as discussed in Chapter 2, the dataset is limited by a notable low-intensity bias, which compromises its utility in evaluating the rarer, more severe (tail) risks associated with TC events. Furthermore, its climate-conditioned version used for future TC risk estimates relies exclusively on CMIP5-based data, which is less up-to-date compared to other hazard sets evaluated in this study (Chapter 5).

The openly available STORM datasets use a statistical modelling approach and encompass 10,000 years' worth of TC data for both historical and future time periods (Bloemendaal et al., 2020b, 2022). The hazard sets are thus well-suited for a broad range of global-scale applications but have certain limitations linked to their statistical modelling approach. Specifically, in Chapter 2, we found that the historical STORM hazard set overestimates TC intensity in the Bay of Bengal, a bias not present in its future dataset. This discrepancy in biases between historical and future datasets results in projections of decreasing wind speeds in this basin (Chapter 4), which contradicts prevailing literature forecasting increased future TC wind speeds (Knutson et al., 2020). Moreover, in Chapter 5, we describe that STORM-based future TC risk change estimates are sensitive to subsampling, likely due to the future event sets utilizing the same track set as their historical counterparts. Besides, the future event sets of STORM are limited to a single greenhouse gas emission scenario (SSP585) and extend only up to 2050, making them less comprehensive compared to other datasets in our study.

The MIT model follows a statistical-dynamical approach (Emanuel et al., 2006; Emanuel, 2008), effectively balancing physics-based modelling with computational efficiency and versatile applications. Although not fully open source, its datasets are openly available for research. Risk estimates using the MIT hazard sets stand out as the most uncertain compared across hazard sets and studies. Specifically, in Chapter 2, we reported the highest uncertainties for EAD and 1000-yr event estimates from the MIT model, and in Chapter 5, we highlighted TC risk increases from MIT-based simulations spanning the widest range of outputs. Unlike the other models, which depend on historical tracks and statistics to varying degrees, the MIT model employs a distinct statistical-dynamical approach. The result is a broad range of future TC risk estimates, which are notably influenced by the global climate models (GCMs) used for downscaling. Significantly, we discovered a striking relationship between the climate sensitivity of these GCMs and projected TC risk increases (Chapter 3). This relationship is unique to the MIT model (Chapter 5). As a result, in MIT-based estimates only, climate change introduces higher uncertainty for future risk estimates than socio-economic variables (Chapter 5).

CHAZ, another statistical-dynamical model, downscales TC tracks from climate model outputs and reanalyses (Lee et al., 2018, 2020), yielding an extensive TC track catalog akin to the other models, suitable for many applications. Like the MIT model, CHAZ is not fully open, with an openly accessible source code and datasets available for research. However, it diverges from the MIT model

in its genesis and intensity modelling approach, necessitating a frequency bias correction based on historical IBTrACS records (Knapp et al., 2010). CHAZ also outputs fewer variables, demanding estimations for parameters like the radius of maximum wind or central pressure. Consequently, CHAZ requires more post-processing than other models. In Chapter 2, we found that CHAZ consistently estimates higher losses from frequent events than other hazard sets. Yet, in other risk metrics, its performance aligns with the other models. Interestingly, the uncertainty analysis of CHAZ more closely aligns with STORM or IBTrACS_p results than with MIT estimates (Chapter 5), likely due to its distinct intensity model. The sensitivity analysis underscores the significance of GCM choice and CHAZ-specific tropical cyclone genesis index (TCGI) moisture variables alongside socio-economic factors. Interestingly, even though the TCGI moisture variable is a strong modulator for hazard frequency (Lee et al., 2020), it does not affect risk estimates to the same extent.

The synthetic track sets discussed in the preceding paragraphs serve as input hazard datasets in risk models. Translating this hazard into risk also requires information on social and economic variables (Box 1.1). Throughout this thesis, we thus highlight the importance of exposure and vulnerability for TC risk estimates.

In Chapter 2, we demonstrate the sensitivity of loss estimates to exposure by calculating results on a normalized exposure layer without the spatial heterogeneity of asset values on land. These results generally yield smaller intermodel differences than the ones computed on a spatially explicit representation of asset exposure values (Eberenz et al., 2020). This underscores the important role that the exposure component plays in risk assessments, a significance further highlighted in our subsequent analysis of future TC risk drivers. Socio-economic development, which pertains to exposure, consistently emerges as a stronger driver for future TC risk increase than climate change, as shown in Chapters 3, 4, and 5. It is, furthermore, the more uncertain risk driver compared to climate change for estimates based on three out of four hazard sets (Chapters 4 and 5). Consequently, a significant portion of the output uncertainty in future TC risk change estimates is attributable to the exposure scaling based on the Shared Socioeconomic Pathways (SSPs). Ultimately, this uncertainty is best characterized as scenario uncertainty, as discussed in Chapter 5. This means it is intrinsically linked to human decisions and, as such, cannot be reduced. Therefore, for risk assessments, it is crucial to encompass a broad range of socio-economic development scenarios to eliminate potential blind spots. Importantly, while working with diverse TC hazard sets can be challenging, incorporating a varied set of future representations is not computationally demanding.

Compared to exposure and especially hazard modelling, vulnerability modelling is less advanced in risk assessment. Within the scope of this thesis, potential future changes in vulnerability were not considered due to the current lack of readily accessible, geospatially explicit data for calibration and validation, which in turn limits the current modeling competencies in the field. Instead, we assessed uncertainties pertaining to regionally-calibrated impact functions (Eberenz et al., 2021) by varying their slope parameter. The extent of this variation was informed by the interquartile range of calibration results, which was quite extensive. Despite the substantial uncertainty and limited capabilities in vulnerability modelling, our findings in Chapters 3, 4, and 5 revealed less uncertainty associated with the impact functions than initially anticipated. This can be explained by our choice of risk metric: By representing TC risk change relative to a present-day baseline as

opposed to absolute values, the impact function primarily serves as a key to translate hazard intensity into corresponding damage (Chapters 3, 4, and 5). In this setting, it should not be interpreted as an accurate representation of vulnerability.

This thesis demonstrates that quantitative estimates of uncertainty and sensitivity to model parameters significantly enhance the value of TC risk assessments, providing a more comprehensive representation of possible future outputs. Examining the distribution of outputs provides a valuable starting point to inform decision-making and model development. In this thesis, we analyzed climate change and socio-economic development as key drivers of future TC risk (Chapters 3.2.1, 4.3.1, and 5.3.1), primarily studying the *magnitude* of the risk change. We also quantified the *uncertainties* of the total risk change of both drivers combined (Chapters 3.2.3 and 5.3.2). Discerning these roles of *magnitude* and *uncertainty* in TC risk change provides valuable insights, aiding in interpreting the implications of subsequent uncertainty and sensitivity analyses. While the mathematical concepts are straightforward - where *magnitude* often corresponds to the mode (peak) of probability density distributions and *uncertainty* affects the distribution's width (spread or variance) (Saltelli et al., 2008; Pianosi et al., 2016; Kropf et al., 2022) - grasping their practical implications is important for areas such as model refinement and decision-making. When prioritizing best estimates and central distribution values, the dominant driver takes priority, while uncertainties become secondary. Conversely, in analyzing extremes or in efforts to understand and reduce uncertainties, the significance of the central peak diminishes relative to uncertainty. This nuanced understanding is essential for stakeholders to make informed decisions based on model outputs and for model developers to prioritize research efforts.

Furthermore, the use of uncertainty and sensitivity analysis in this thesis establishes a necessary foundation for comparing future TC risk estimates across different hazard sets (Chapter 5). Without this framing, a meaningful comparison would be unfeasible due to the absence of a shared baseline among the various hazard models under consideration. Still, the outcomes of such uncertainty and sensitivity analyses are closely tied to the respective model setup and warrant caution in interpretation and extrapolation beyond the model boundaries. In Chapter 5, I thus illustrated how relating the outcomes of uncertainty and sensitivity quantification to aleatory, epistemic and normative types of uncertainty can help translate results into actionable information beyond the model setup. For example, this structured approach may help identify reducible sources of uncertainty and thereby guide research efforts.

In conclusion, all these aspects of uncertainty and sensitivity analysis enable better-informed decision-making and offer a rich context for future research efforts.

6.2 Implications

Tropical cyclones are a classical example of a natural hazard. They are complex, large-scale, extreme weather events with some level of predictability but notable uncertainties. Their potentially devastating impacts constitute a form of tail risk and thus pose a particular modelling challenge. Nevertheless, there is a robust body of scientific knowledge and understanding of TCs, with multiple hazard models available for their representation. These models can be employed within event-based, probabilistic

risk modeling frameworks like CLIMADA (Aznar-Siguan and Bresch, 2019). In this thesis, I have addressed issues of uncertainties in TC risk assessment with a particular emphasis on hazard model choice. Furthermore, I have made an effort to translate the results of my studies, which are inherently bound to the scope of the study setup, into more tangible and actionable findings. Specifically, I conclude Chapter 2 with guidance on TC track set choice depending on the application. Chapters 3 and 4 illustrate the enhanced value of climate risk assessments when uncertainty and sensitivity to model parameters are quantitatively estimated. Finally, Chapter 5 provides a structured approach to navigate the quantitative uncertainty and sensitivity output from the perspective of different classes of uncertainty, helping to assess the reducibility of these uncertainties. These contributions collectively enable better-informed decision-making and offer a rich context for future research efforts. While this thesis focuses on TC risk assessments, such findings have implications for the supply and demand of reliable weather and climate risk information more generally.

In recent years, catastrophe modelling has expanded beyond its traditional realm in the (re-)insurance industry to serve the broader global financial market. An increasing number of consultancies, financial technology firms, data providers, and investment advisory groups now offer information about localized physical climate risks, entering a technology arms race among climate services providers (Keenan, 2019; Condon, 2023). However, as these companies claim to employ methods, models, and data that are superior and more extensive than those of their competitors, the proprietary nature of their products introduces significant challenges, including a lack of transparency and accessibility, for comparison and evaluation (Keenan, 2019; Arribas et al., 2022; Condon, 2023).

Chapter 2 in this thesis presents an intercomparison of the most influential, academically available global tropical cyclone track sets at the impact level, serving as a valuable benchmark for the analysis of other TC models. The insights and methods of this chapter may act as a template for intercomparison studies across diverse hazard models in the impact domain. Moreover, the chapter casts a critical lens on traditional hazard models prevalent in the (re-)insurance industry, which predominantly depend on historical data. Such data is a poor guide for today's TC risk due to its temporal and spatial limitations and varying quality. In addition, assuming stationary statistics is problematic for weather-related hazards like TCs, already affected by climate change, especially concerning rare, high-impact tail events (Knutson et al., 2019). Therefore, the findings and approach outlined in Chapter 2 not only contribute to the enhancement of model comparison and evaluation but also provide a critical perspective on the limitations and challenges associated with traditional modeling approaches in the industry.

Given these considerations, Chapter 2 provides a transparent and accessible framework that counters the proprietary nature of private models, addressing the significant challenges of comparison and evaluation faced by the increasing number of companies entering the climate services sector.

While the private sector is experiencing a surge in demand for dependable climate risk assessments, driven by increasing pressures from investors, underwriters, and policy initiatives, there is a noticeable lack of capacity within the sector to critically evaluate the quality and reliability of available climate service products. This need for dependable assessments is further intensified by the growing push towards transparency and responsibility regarding climate-related risks from global networks and regulatory bodies like the Network for Greening the Financial System (NGFS), European Commission,

and the Financial Stability Board's Task Force on Climate-Related Financial Disclosures (TCFD). These entities are crafting systems and guidelines for measuring and reporting climate risks (Keenan, 2019).

Despite these advancements, the private sector often finds itself ill-equipped to adequately assess and utilize these climate service products. Notably, assessing the suitability of climate projections as used by many climate analytics firms for applications in financial risk analysis, management and disclosure, requires training and knowledge most of these companies lack. Consequently, such companies may overstate the capabilities and suitability of climate model output for projections at fine geographic scales and in short-term forecasts, both crucial for informed business decision-making (Fiedler et al., 2021). Moreover, the efforts of regulatory bodies to establish standards for measuring and reporting are still developing (Fiedler et al., 2021). The physical-risk scores produced by various commercial providers, each developing their own firm-level indicators of physical climate risk, diverge substantially (Hain et al., 2022).

This thesis exemplifies what is needed to build the capacity to critically evaluate the quality and reliability of climate service products; a role that Fiedler et al. (2021) termed 'climate translators'. In Chapter 2, we translate differences in loss estimates derived from various TC hazard models into guidance for hazard model choice, thereby assisting risk analysts who may lack an in-depth understanding of each model's intricate workings. In Chapters 3, 4, and 5, we communicate the effect of climate change and socio-economic development on future risk increase, including a systematic assessment of uncertainties along the entire modelling chain. This open and structured approach is crucial to limit over- or underestimation of risks. It helps navigate a broad space of future outcomes and provides a more transparent basis to evaluate climate risk assessments. For example, it could serve as a starting point in the design of robust physical risk scores, guiding financial decision-making.

The value chain of emerging climate service providers extends from public institutions - responsible for collecting weather data and operating climate models on supercomputers - to private consultancies that assess and communicate localized risk (Condon, 2023). These risk assessments significantly influence the economy, affecting equity capital allocation, insurance premiums, housing prices, and thus, leading to demographic changes (Elliott, 2021). They further impact municipal bond ratings, influencing the prioritization of infrastructure projects in specific neighborhoods (Cox, 2022). Given this influence, Condon (2023) urges increased investment in public climate risk assessment resources to minimize reliance on private-party risk assessment for public-relevant decisions. Importantly, risk assessments that lack a solid scientific basis can lead to maladaptation across the economy (Nissan et al., 2019; Keenan, 2019; Fiedler et al., 2021; Condon, 2023), underscoring the critical need for rigorous, scientifically validated assessments. Unreliable assessments not only misguide investments and policy planning but can also inadvertently exacerbate vulnerabilities and economic disparities in regions prone to tropical cyclones and other hazards (Schipper, 2020).

This thesis, while not originally designed to address this specific issue, makes timely contributions to enhance public sector capabilities in climate risk assessment. By employing an open scientific framework for tropical cyclone risk assessment and using data that often transitions from academia to the private sector, the thesis supports capacity-building for public climate services. It advances

open-source risk modeling and identifies crucial knowledge gaps. Furthermore, by incorporating systematic uncertainty quantification, the thesis strengthens the reliability and robustness of public climate risk assessments. It provides recommendations for research prioritization and uncertainty reduction and underlines the urgent need for increased public resources for climate risk assessment, aligning with the advocacy of Condon (2023).

This thesis, positioned in the scientific community but with points of contact to public and private stakeholders, offers insights with implications for the field of weather and climate risk science itself. In this thesis, I often motivate my work by highlighting its implications for stakeholders in decision-making positions. At the same time, I caution risk analysts to follow principles of fitness for purpose (Parker, 2010) when selecting TC hazard models or designing study setups. While my thesis can make valuable contributions to large-scale, big-picture type of questions, it is not apt to answer questions at the very local scale. But the impacts of global climate change manifest at the local scale and differ according to the particularities of this localness (Shepherd and Sobel, 2020). There is thus a growing consensus in the scientific community to include 'bottom-up' approaches and storylines for robust, localized, actionable science (e.g., Shepherd and Sobel, 2020; Ciullo et al., 2021; Pitman et al., 2022; Ranger et al., 2022; Sobel, 2021). For such approaches to be successful, a strong and direct exchange with stakeholders is needed.

Additionally, untapped collaborative opportunities exist between weather and climate risk science and the (re-)insurance industry. Such partnerships are important for understanding the (re-)insurance sector's specific needs, thus helping build models and generate scientific contributions that meet the stakeholders' needs. On the other hand, accessing data on exposure and vulnerability currently proprietary to the industry and limited in scientific literature would allow for refining models and hypotheses to align with real-world scenarios, enhancing their accuracy and relevance. While this application is outlined for collaboration with the (re-)insurance industry, stronger interaction with any stakeholder would likely yield comparable improvements in climate risk assessments for respective applications. Ultimately, fostering these collaborative efforts can significantly enhance the precision and utility of climate risk assessments, paving the way for fruitful future research and collaboration.

The preceding outline of implications is non-exhaustive, and the insights derived from this thesis may find applications in various other fields too. For example, enhanced reliability and precision of tropical cyclone risk assessments bear implications for public policy, disaster response strategies, and community engagement initiatives. Policymakers may leverage these refined assessments to devise informed, resilient urban planning and infrastructure investment strategies in cyclone-prone areas. Similarly, agencies responsible for disaster preparedness and response can utilize this data for efficient resource allocation, improved readiness, and the development of impact-based warnings, ultimately safeguarding communities and economies from the devastating impacts of tropical cyclones. The findings also serve as a valuable resource for international development and humanitarian organizations, facilitating strategic planning and resource allocation for climate monitoring and disaster management. Lastly, the thesis opens new avenues for academic exploration and research, some of which I detail in the next section.

6.3 Future research and outlook

Understanding limitations in current TC risk assessment methodologies and the study setup of this thesis is essential, as it paves the way for future research endeavors. In this section, I discuss themes emerging from this thesis that need further investigation. These encompass the need for explicit representation of TC sub-hazards and adoption of a multi-hazard approach, providing a holistic understanding of the intertwined risks posed by TC and other hazards. Exploration of alternative exposure representations is also important, as traditional metrics may fall short in capturing the diverse vulnerabilities across various communities and settings. Additionally, incorporating philosophy of science and decision theory can enhance decision-making processes under uncertainty, offering a more informed and rational framework for TC risk management.

A prevalent limitation in most global-scale TC risk assessments - including this thesis - is the sole consideration of wind as the primary driver of impacts, whereas actual damages arise from a combination of rainfall-driven floods, storm surges, and direct wind effects. Therefore, traditional risk assessment methods are likely to underestimate the possible impact. For example, Hurricane Katrina (2005) was classified as a Category 3 at landfall with wind speeds of around $55\,\mathrm{m\,s^{-1}}$ but its 8.6 m storm surge caused widespread levee failure around New Orleans (LA), resulting in over 1800 casualties and 125 billion USD in damage, making it the costliest U.S. TC to date (NOAA, 2021).

Recent research efforts have focused on a more detailed hurricane hazard risk communication (Bloemendaal et al., 2021) and include advances in the explicit representation of sub-hazards (e.g., Frieler et al., 2023). Particularly, TC sub-hazard risk assessment has seen much progress in the field of compound flooding (e.g., Gori et al., 2020, 2022). Recent studies in this field primarily aim to either characterize the occurrence of compound flooding events or quantify their impact on flood hazards. Techniques like Bayesian networks, application of copulas, and bivariate extreme value distributions have been employed to analyze the statistical dependence between storm surge occurrences, high river discharge, and precipitation (Zheng et al., 2014; Sebastian et al., 2017; Couasnon et al., 2018; Wu et al., 2018; Moftakhari et al., 2019). The impact of correlated extremes on flood depth or extent has been assessed through various methods, including storm event reconstruction, synthetic scenarios, and compound return period estimation (Ray et al., 2011; Torres et al., 2015; Kumbier et al., 2018; Silva-Araya et al., 2018; Bilskie and Hagen, 2018; Herdman et al., 2018; Khanal et al., 2018; Moftakhari et al., 2019; Orton et al., 2020). Notably, a study by Bates et al. (2020) introduced a comprehensive multi-peril flood risk analysis for the conterminous US, considering pluvial, fluvial, and coastal flooding. For the first time, flood risks from all major sources are considered within the same framework on the national scale for both current and future climate conditions.

Currently, there is a gap in comprehensive, global-scale studies integrating torrential rain, storm surges, and wind to quantify cumulative sub-hazard impacts. The absence of such research is likely due to exhaustive computational costs and a lack of detailed data, with reported damages often not delineated by sub-hazard, as seen in sources like (e.g., EM-DAT Guha-Sapir, 2023). To address this challenge, I propose two novel approaches.

First, a physics-based, local-scale approach for advancing TC sub-hazard risk assessment, which is feasible and meaningful at the local scale despite the computational intensity of probabilistic analyses.

This approach utilizes synthetic TC tracks simulated for current and future climates (Emanuel et al., 2006; Emanuel, 2008) to derive wind hazard footprints (Emanuel and Rotunno, 2011), generate TC rainfall data (TCR, Feldmann et al., 2019) and drive a storm surge model (Geoclaw, Mandli et al., 2016). Precipitation fields and storm surge heights can be translated into inundation levels using a hydrodynamic model (LISFLOOD-FP, Bates et al., 2013). A key open question is determining the optimal method for integrating TC wind and flood hazard components to accurately assess total impacts. We may combine them before the impact calculation using a hazard index approach; during the impact calculation through multidimensional, multivariate impact functions, for example, using a Bayesian framework for univariate and multivariate non-stationary risk analyses; or after the impact calculation in an actuarial approach.

Second, a more simplified representation at the global scale enables the calibration of TC impact functions for sub-hazard risk assessment, using historical TC records and a damage database. Windfields and rainfall data for each TC are extracted from IBTrACS records (Knapp et al., 2010) and ERA-5 rainfall reanalysis respectively, providing two hazard intensity values: maximum sustained wind speed and precipitation per location and time step. This data allows the calibration of idealized impact functions against reported damages (analogous to Eberenz et al., 2021), with the calibration process optimized for combined rain- and wind-driven TC impacts. This methodology can also be expanded to include surge heights for a refined TC sub-hazard risk assessment.

The high-resolution, local-scale approach helps assess joint impacts of TC rainfall, storm surges, and wind impacts, aiding urban planners, emergency officials, and policymakers in disaster risk reduction and climate adaptation. Meanwhile, the simplified global-scale approximation of TC sub-hazard risk supports organizations engaged in global disaster risk reduction and international development. Collectively, these approaches may inform decision-making, promote resilience in vulnerable areas, and contribute to the establishment of global risk management standards and policies.

As with most high-impact events, TC damages emerge from multiple drivers and factors acting together on various temporal and spatial scales (Zscheischler et al., 2018). This is not limited to TC sub-hazards as described above but includes interactions with other hazards, leading to multi-hazard and compound risks.

In recent years, we have seen a few powerful examples illustrating the challenge of TC risk assessment in a multi-risk and compound event setting. Tropical Cyclone Amphan (2020) struck amidst the global COVID-19 pandemic, amplifying existing evacuation and relief challenges due to obligatory health protocols (Meng et al., 2023). It concurrently affected regions already vulnerable due to pre-existing issues like poverty and limited infrastructure, while also inducing significant storm surges and rainfall, thereby exacerbating flooding in low-lying areas (Mitchell et al., 2022). Similarly, Tropical Cyclone Hagibis (2019), characterized by rapid intensification and a vast size, impacted regions previously affected by Typhoon Faxai, thereby compounding existing damages and recovery challenges while also inflicting broad economic and infrastructural damage (Li and Otto, 2022). Meanwhile, Tropical Cyclone Idai (2019) unleashed a devastating combination of strong winds, storm surges, and flooding, intensified by major river overflows in regions with dense populations

in low-lying areas, leading to profound immediate and long-term impacts on local economies and livelihoods. (Eilander et al., 2023; Williamson et al., 2023).

Various concepts have been developed to address this multifaceted nature of risk. For instance, multi-layer single-hazard risk assessment combines risks from different hazards assumed to be independent (Fleming et al., 2016; Zschau, 2017). Another approach involves evaluating interactions between distinct hazards, a practice known as multi-hazard risk assessment (Gill and Malamud, 2014, 2016; de Ruiter et al., 2020; Ward et al., 2022). Additionally, the concept of compound events and risks has been introduced to encompass multiple drivers and hazards that jointly contribute to societal or environmental risk, (Zscheischler et al., 2018; Hillier et al., 2020). These concepts collectively offer a broader framework for understanding and managing the intricate risks associated with tropical cyclones and other high-impact events.

Researchers can utilize the aforementioned concepts to analyze past events, such as Tropical Cyclones Amphan (2020), Hagibis (2019), and Idai (2019), studying the dynamics and interactions of multiple hazards and risks associated with each. An alternative methodology is storylines, where researchers design bottom-up narratives of specific, physically plausible events (Shepherd et al., 2018). This strategy elucidates the numerous factors and sequential progression of compound events, providing a clearer and more tangible understanding of their unfolding and impacts. Furthermore, by adopting a forward-looking multi-hazard perspective (e.g., as suggested in Stalhandske et al., 2023), researchers can better anticipate the likelihood of future compound events and identify regions that are particularly susceptible. This proactive approach facilitates informed planning and risk mitigation efforts in areas most prone to these complex and multifaceted events.

In this thesis, impacts and risks are quantified as direct economic damages to the built environment expressed as expected annual damage (EAD) and 100-year damage events (100-yr event) (see Section 2.4.3 ii)). While these metrics serve as a suitable approximation for understanding large-scale, macroeconomic effects, they capture risk in an aggregated way, which can mask local variations in risk and vulnerabilities. I therefore suggest considering more granular, spatially resolved risk metrics to capture these nuances in future research. Moreover, solely focusing on direct economic damages overlooks the broader spectrum of impacts, which can encompass indirect economic effects (e.g., Otto et al., 2023), as well as more comprehensive and intricate forms of impacts. This is especially noteworthy given the challenges in future exposure modelling, its substantial uncertainties, and the key role exposure plays as a driver of future risk, as elaborated in Chapters 3, 4, and 5. Importantly, each alternative exposure representation that is adopted brings specific facets of vulnerability into focus. The diversity in exposure representations inherently discloses a range of vulnerabilities, each of which requires tailored impact functions for accurate risk assessment.

For instance, assessing excess mortality linked to tropical cyclones offers a human-centric dimension of exposure that brings vulnerabilities related to public health and emergency management into focus (Parks et al., 2023). Similarly, evaluating the social cost of tropical cyclones provides an economic perspective that highlights vulnerabilities in socio-economic structures and long-term development (Krichene et al., 2023). Assessing risk to critical infrastructure and networks underscores vulnerabilities in essential services and societal functions (Mühlhofer et al., 2023). Additionally, incorporating social vulnerability indices as exposure representations can shed light on the socio-

demographic factors that exacerbate vulnerability during tropical cyclones, offering insights into the distribution of risk among different social groups (Baldwin et al., 2023). Integrating human mobility and population dynamics in exposure models can reveal the transient nature of vulnerability, capturing how population movements before, during, and after cyclones may alter the risk landscape and affect response and recovery efforts (Mester et al., 2023).

Furthermore, alternative damage and disaster loss databases that offer globally consistent information such as DesInventar (DesInventar, n.d.), a Disaster Information Management System developed by UNDRR, can help bridge current data gaps, given the limited disaster data available from traditional sources (EM-DAT Guha-Sapir, 2023) for model calibration and validation. Additionally, technological advances, particularly the integration of satellite imagery and machine learning, present promising opportunities for refining exposure representations (Rolf et al., 2021). These innovative techniques can remotely sense socio-economic data at a global scale, providing valuable updates to existing tools like LitPop (Eberenz et al., 2020). Novel datasets, which include representations of poverty (Aiken et al., 2023) and national development (Sherman et al., 2023), facilitate a more nuanced understanding of exposure and vulnerability. I suggest the application of such advanced technologies to track socio-economic development over historical periods, providing a quantitative foundation for trends and trajectories. With careful extrapolation, these insights may be projected into the future, aligning with various Shared Socio-economic Pathways, thereby offering a dynamic and forward-looking approach in contrast to the constant scaling factors we applied in our studies to represent socio-economic development (see Section 3.4.3 and 3.4.6). Each of these alternative representations of exposure and associated vulnerabilities provides a starting point for future research exploration.

In Chapters 3, 4, and 5, we focused on uncertainties and sensitivities of future tropical cyclone risk changes. Our results highlight the full uncertainty distribution of model outputs and how these variations can be attributed to variations in input factors. This information guides model developers in focusing research efforts to minimize output uncertainty. For decision-makers, it provides a much more representative range of plausible future outcomes and thus a more transparent and valuable information basis. The question then is: How can decisions made in the face of uncertainty be both confident and robust? And how should these decisions reflect the scientific uncertainty embedded in the utilized models?

Decision theory provides various methods to address these questions. Options include Bayesian decision theory (Smith, 2010), robust control (Lempert et al., 2006; Hansen and Sargent, 2008), real options (Dixit and Pindyck, 1994; Gollier and Treich, 2003) and ambiguity theory (Ghirardato et al., 2004; Klibanoff et al., 2005; Heal and Millner, 2014; Gilboa and Marinacci, 2016). In climate risk and adaptation decisions, these approaches offer valuable applications. Bayesian decision theory is a framework that combines probability theory and decision theory to make rational decisions under uncertainty. It involves using Bayesian inference to update beliefs and make decisions based on available evidence. Bayesian decision theory involves assigning prior probabilities to different possible outcomes, updating these probabilities based on new information, and selecting the decision that maximizes the expected utility or value. It provides a systematic approach to decision-making by incorporating both subjective beliefs and objective data (Smith, 2010). Robust control theory

focuses on making decisions that are resilient to uncertainties and disturbances. It aims to find a control policy that performs well across a range of possible scenarios. Instead of optimizing for the best outcome in a specific scenario, robust control seeks to minimize the worst-case outcome. It is commonly applied in engineering and systems control, where there are uncertainties in the system dynamics or external disturbances (Lempert et al., 2006; Hansen and Sargent, 2008). Real options theory is primarily used in the field of finance and investment. It extends traditional financial option pricing models to value investment opportunities that have flexibility and can be delayed, expanded, or abandoned based on future conditions. Real options recognize that investments often involve the ability to make decisions and take actions in response to changing market conditions, rather than being fixed and irreversible. This theory helps decision-makers evaluate the value of flexibility and the potential benefits of waiting for more information before committing to a course of action (Dixit and Pindyck, 1994; Gollier and Treich, 2003). Ambiguity theory deals with decision-making in situations where there is a lack of information or imprecise knowledge. It recognizes that decision-makers may have incomplete or contradictory beliefs about the probabilities of different outcomes. Ambiguity aversion refers to a preference for known risks over unknown risks. Ambiguity theory incorporates decision criteria that consider both probabilities and the degree of ambiguity associated with those probabilities (Ghirardato et al., 2004; Klibanoff et al., 2005; Heal and Millner, 2014; Gilboa and Marinacci, 2016).

Different decision rules have been formulated for situations in which decision-makers face ambiguity. One such method to tackle inputs from model ensembles (multi- or single-model ensembles) and address ambiguity is the confidence approach (Hill, 2013; Bradley, 2017; Roussos et al., 2021). Key strengths of the confidence approach are that it transparently reflects the outputs of all ensembles used for probabilistic climate risk assessment and includes the decision-makers' levels of stakes and cautiousness. As a result, the confidence approach provides a framework to efficiently navigate the output range from the ensembles and provide decision-makers with a defensible level of information based on their risk tolerance.

Demand for probabilistic tropical cyclone risk information is rising in many sectors. Yet, decision models are still widely unused in combination with tropical cyclone and other probabilistic weather and climate risk applications, and there is no standardized way to support climate-related decisions under uncertainty. Thus, I suggest introducing robust decision-making methods under uncertainty for probabilistic climate risk-related adaptation decisions.

6.4 Final remarks

This thesis identifies and systematically quantifies the crucial sources of uncertainty in global tropical cyclone risk assessments, thereby enhancing the value of these assessments for risk analysis, research, and decision-making. The challenges associated with leveraging model uncertainties to generate actionable outputs are not unique to this domain; similar issues are observed and debated in other fields. A recent discussion highlighted the influence of the uncertainty in gene copy conversion to biomass and the need for further investigation of how to best take advantage of gene copy data for global diazotroph biogeography modelling purposes (Meiler et al., 2022a; Zehr and Riemann,

2023). Despite these uncertainties, there is a consensus on the value of gene count quantification as a powerful tool for analyzing marine diazotroph distributions (Meiler et al., 2023a; Zehr and Riemann, 2023). Meiler et al. (2023a) have outlined various areas for future investigation in this field. Similarly, this thesis offers guidance on navigating through the uncertainties inherent in tropical cyclone risk assessment and provides insights to inform model selection, application and improvement.

APPENDIX A

Supplement to Chapter 2

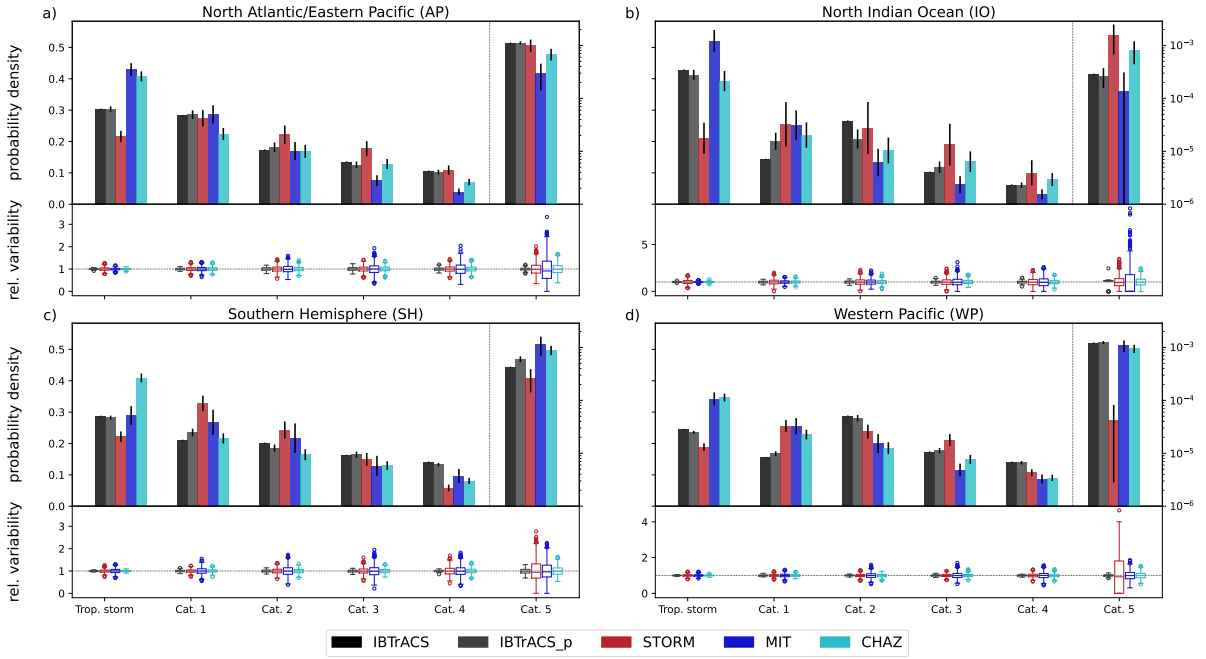

Supplementary Figure A.1: Regional distribution of track intensities for the five datasets. Panels a)-d) compare the relative frequency of tropical cyclones belonging to each category of the Saffir-Simpson Hurricane Wind Scale across the five track sets (IBTrACS, IBTrACS_p, STORM, MIT, CHAZ), separately for the four regions a) North Atlantic/Eastern Pacific, b) North Indian Ocean, c) Southern Hemisphere, and d) Western Pacific. The mean and standard deviation (black error bars) of the frequencies are shown in the upper part of the plots while the lower part displays the relative variability in each intensity bin (as box plots with a line at the median, a box denoting the inter-quartile range (IQR) and whiskers extending 1.5-times IQR; points are outliers). Note that the frequencies of Cat. 5 TCs are shown on a secondary y-axis in log scale. For this figure, the maximum wind speed included in the track data at positions that are within 300 km from land are considered. The same plot with wind speeds taken directly from the wind fields over land is provided in Fig. 1.

Supplementary Table A.1: Calculated direct economic damages in billion USD for the Expected Annual Damage (EAD). Mean and standard deviation (absolute, relative) for all synthetic tropical cyclone track sets (IBTrACS_p, STORM, MIT, CHAZ) and the EAD for the historical IBTrACS in the four regions are shown.

	North Atlantic/Eastern Pacific			North Indian Ocean			Southern Hemisphere			Western Pacific		
IBTrACS	50.86			2.32			5.41			43.05		
IBTrACS_p	31.50	±1.07	(3.4%)	2.08	±0.16	(3.4%)	6.61	±0.33	(5.0%)	36.68	±1.01	(2.8%)
STORM	55.61	±2.46	(4.4%)	13.25	±1.38	(4.4%)	14.17	±1.23	(8.7%)	169.43	±5.30	(3.1%)
MIT	25.65	±1.34	(5.2%)	8.32	±0.66	(5.2%)	9.36	±0.99	(10.6%)	49.70	±2.89	(5.8%)
CHAZ	82.47	±2.86	(3.5%)	11.51	±0.82	(3.5%)	31.32	±1.72	(5.5%)	115.49	±3.25	(2.8%)

Supplementary Table A.2: Calculated direct economic damages in billion USD for the 100-yr and 1000-yr events. Results are shown for all synthetic tropical cyclone track sets (IBTrACS_p, STORM, MIT, CHAZ) in the four regions. The values in brackets indicate the 90% confidence interval expressed as percent of the mean 100-yr and 1000-yr damage values.

	North Atlantic/Eastern Pacific				North Indian Ocean				Southern Hemisphere				Western Pacific			
	100-yr		*1000-yr*		*100-yr*		*1000-yr*		*100-yr*		*1000-yr*		*100-yr*		*1000-yr*	
IBTrACS_p	231	(39%)	589	(68%)	40	(39%)	86	(94%)	60	(33%)	111	(37%)	165	(55%)	439	(37%)
STORM	344	(31%)	603	(51%)	246	(54%)	517	(78%)	193	(60%)	529	(143%)	664	(33%)	1213	(66%)
MIT	169	(58%)	379	(185%)	106	(46%)	251	(48%)	109	(54%)	400	(231%)	430	(60%)	1191	(38%)
CHAZ	359	(43%)	813	(98%)	109	(31%)	227	(60%)	295	(52%)	678	(87%)	445	(29%)	814	(70%)

Supplementary Table A.3: Calculated normalized impact given as fraction of the area affected for the Expected Annual Damage (EAD). Mean and standard deviation (absolute, relative) for all synthetic tropical cyclone track sets (IBTrACS_p, STORM, MIT, CHAZ) and the EAD for the historical IBTrACS in the four regions are shown.

	North Atlantic/Eastern Pacific			North Indian Ocean			Southern Hemisphere			Western Pacific		
IBTrACS	3.2E-04			7.4E-05			1.1E-03			3.2E-04		
IBTrACS_p	2.4E-04	±4.2E-06	(1.8%)	8.1E-05	±2.5E-06	(3.0%)	7.9E-04	±9.7E-06	(1.2%)	2.6E-04	±2.9E-06	(1.1%)
STORM	4.9E-04	±1.6E-05	(3.3%)	4.0E-04	±2.7E-05	(6.6%)	7.2E-04	±2.0E-05	(2.8%)	9.7E-04	±1.9E-05	(2.0%)
MIT	3.5E-04	±1.1E-05	(3.3%)	2.3E-04	±9.9E-06	(4.3%)	6.8E-04	±2.6E-05	(3.8%)	4.9E-04	±1.8E-05	(3.6%)
CHAZ	9.9E-04	±1.9E-05	(1.9%)	5.9E-04	±2.1E-05	(3.5%)	1.9E-03	±3.0E-05	(1.6%)	1.1E-03	±2.3E-05	(2.1%)

Supplementary Table A.4: Calculated normalized impact given as percentage of the area affected for the 100-yr and 1000-yr events. Results are shown for all synthetic tropical cyclone track sets (IBTrACS_p, STORM, MIT, CHAZ) in the four regions. The values in brackets indicate the 90% confidence interval expressed as percent of the median 100-yr and 1000-yr damage values.

	North Atlantic/Eastern Pacific				North Indian Ocean				Southern Hemisphere				Western Pacific			
	100-yr		*1000-yr*		*100-yr*		*1000-yr*		*100-yr*		*1000-yr*		*100-yr*		*1000-yr*	
IBTrACS_p	0.088%	(14%)	0.146%	(101%)	0.087%	(14%)	0.150%	(60%)	0.202%	(29%)	0.355%	(42%)	0.056%	(18%)	0.083%	(16%)
STORM	0.185%	(25%)	0.340%	(117%)	0.380%	(37%)	1.062%	(75%)	0.209%	(24%)	0.433%	(98%)	0.196%	(26%)	0.386%	(87%)
MIT	0.129%	(37%)	0.231%	(46%)	0.119%	(22%)	0.212%	(49%)	0.315%	(33%)	0.488%	(33%)	0.224%	(25%)	0.397%	(28%)
CHAZ	0.169%	(21%)	0.262%	(66%)	0.210%	(17%)	0.300%	(39%)	0.251%	(13%)	0.349%	(135%)	0.272%	(19%)	0.400%	(43%)

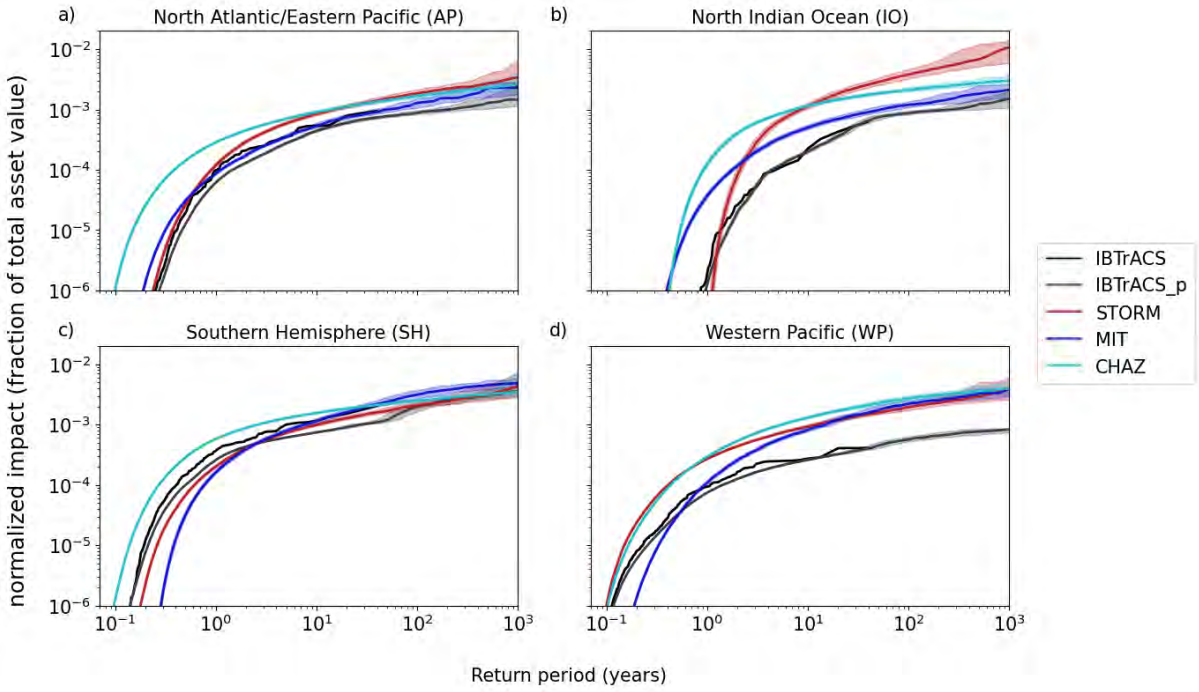

Supplementary Figure A.2: Normalized impact return period curves for the five tropical cyclone track sets. Return periods up to 1000 years for the synthetic track sets (IBTrACS_p, STORM, MIT, CHAZ) and 39 years for the IBTrACS record (black solid curve) in the four regions (a) North Atlantic/Eastern Pacific, b) North Indian Ocean, c) Southern Hemisphere, d) Western Pacific). We use a sub-sampling approach on the synthetic track sets to calculate the median (colored solid curves), the 90% confidence intervals of the impact distribution over 1000 years. Note, impacts are given as normalized results as fraction of the area affected.

Supplementary Methods

When analyzing the synthetic datasets, we apply a bootstrapping method in which we draw 100 to 1000 subsamples of the synthetic datasets at a chosen length. This allows us to calculate statistics over the subsamples like the mean and standard deviation for the TC track (Supplementary Figure A.1) and hazard intensities (Figure 2.1), EAD estimates (Supplementary Table A.1) and the median and 5th and 95th percentile of each subsample to obtain the 90 % confidence interval (CI) of impacts (Figure 2.2 and Supplementary Figure A.2).

Depending on the synthetic track set, varying approaches in the subsampling routine are taken to account for the different ways in which each synthetic dataset integrates probabilistic variability. The only dataset that does not associate a specific year in the historic period to each synthetic track is STORM. In STORM, each of the 10000 years is a representation of the whole observational 1980 to 2018 climatology. Accordingly, we randomly subsampled N=1000 year sets, each at the length of the years covered by IBTrACS (Figure 2.1 and Supplementary Figure A.1) or 1014 years for the impact analyses (Figure 2.2 and Supplementary Figure A.2). For the remaining track sets, we draw subsamples in a way that retains the intrinsic association with historic years. The probabilistic IBTrACS is a dataset that consists of the original historical IBTrACS record plus 99 probabilistic tracks for each observed TC (see Methods); we thus evaluate the desired statistics over the total of 100 probabilistic IBTrACS ensembles. The CHAZ hazard set comes as an ensemble of 10 full model runs, each containing 40 intensity ensembles per track; hence a total of 400 ensembles of 39 years of TC activity. We take these 400 ensembles to generate the CIs and the median value. For each year, the MIT dataset contains a fixed number of 500 synthetic tracks that, together with an information of average number of events to occur, represent the probabilistic variability of that year's TC climatology. For our analysis, we draw N=1000 random subsamples from each year set in such a way that the size of the subsamples is distributed according to a Poisson distribution with mean given by the provided expected number of events for that year.

Supplementary Discussion

First, in STORM the regression coefficients for TC intensity are generally derived in $5° \times 5°$-boxes (Bloemendaal et al., 2020a). However, in the North Indian Ocean, the sample size is too small to adequately fit STORM's regression formulas, and as such these formulas were derived over larger areas (N. Bloemendaal, personal communication, October 2021), thereby omitting spatial heterogeneity within the basin. Furthermore, and perhaps most importantly, TC intensity in STORM is modelled through a strong dependency on the Maximum Potential Intensity (MPI), which, in turn, depends on sea-surface temperatures (SST). In the North Indian Ocean and particularly the Bay of Bengal, there is little variation in SST, which means that obtaining spatially varying MPI values becomes challenging (Bloemendaal et al., 2019). Without varying MPI values, initiating TC decay is virtually impossible. As a consequence, the entire region is supportive of very intense TCs (<900 hPa). This combined with the regression formula problem allows for TCs to intensify all the way up to category 4 and 5 events in the Bay of Bengal as simulated by STORM. According to Figure

2.1 in our study, STORM largely underestimates the lowest category events in the North Indian Ocean and overestimates higher category events. However, Bloemendaal et al. (2020a) report that the high intensities in the North Indian Ocean are well in line with IBTrACS observations. In contrast to our analysis, Bloemendaal et al. (2020a) only analyzed the average max. wind speeds over all events in a basin (not differentiating between TC categories). Presumably, this the reason that Bloemendaal et al. (2020a) concluded that STORM is well in line with IBTrACS observations in the North Indian Ocean while our study indicates that STORM overestimates intensities in this basin.

APPENDIX B

Supplement to Chapter 3

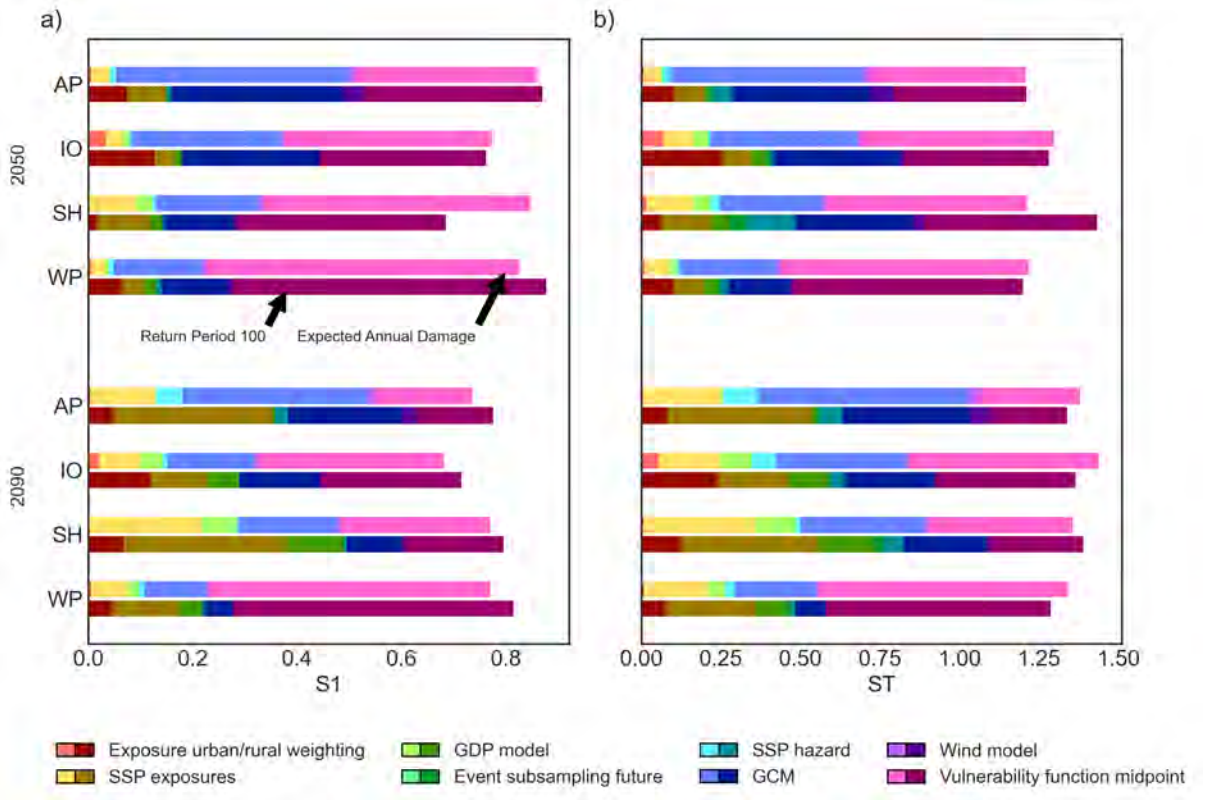

Supplementary Figure B.1: First- (S1) and total-order (ST) sensitivity indices. First- (a) and total-order (b) sensitivity indices for absolute (calculated in USD) future (2050, 2090) TC risk expressed as expected annual damage (EAD; upper bar) and 100-yr event values (rp100; lower bar) over the four study regions (see Fig. 3.1 a) North Atlantic/Eastern Pacific (AP), North Indian Ocean (IO), Southern Hemisphere (SH), and North Western Pacific (WP) and all input factors (see Methods and Table 3.1 therein). Results are grouped by input factors (different colors); *Vulnerability function midpoint* describes the impact function; *Wind model*; *GCM*, *SSP hazard*, *Event subsampling base*, *Event subsampling future* pertain to the hazard component; *GDP model*; *SSP exposure*, *Exposure urban/rural weighting* relate to the exposure.

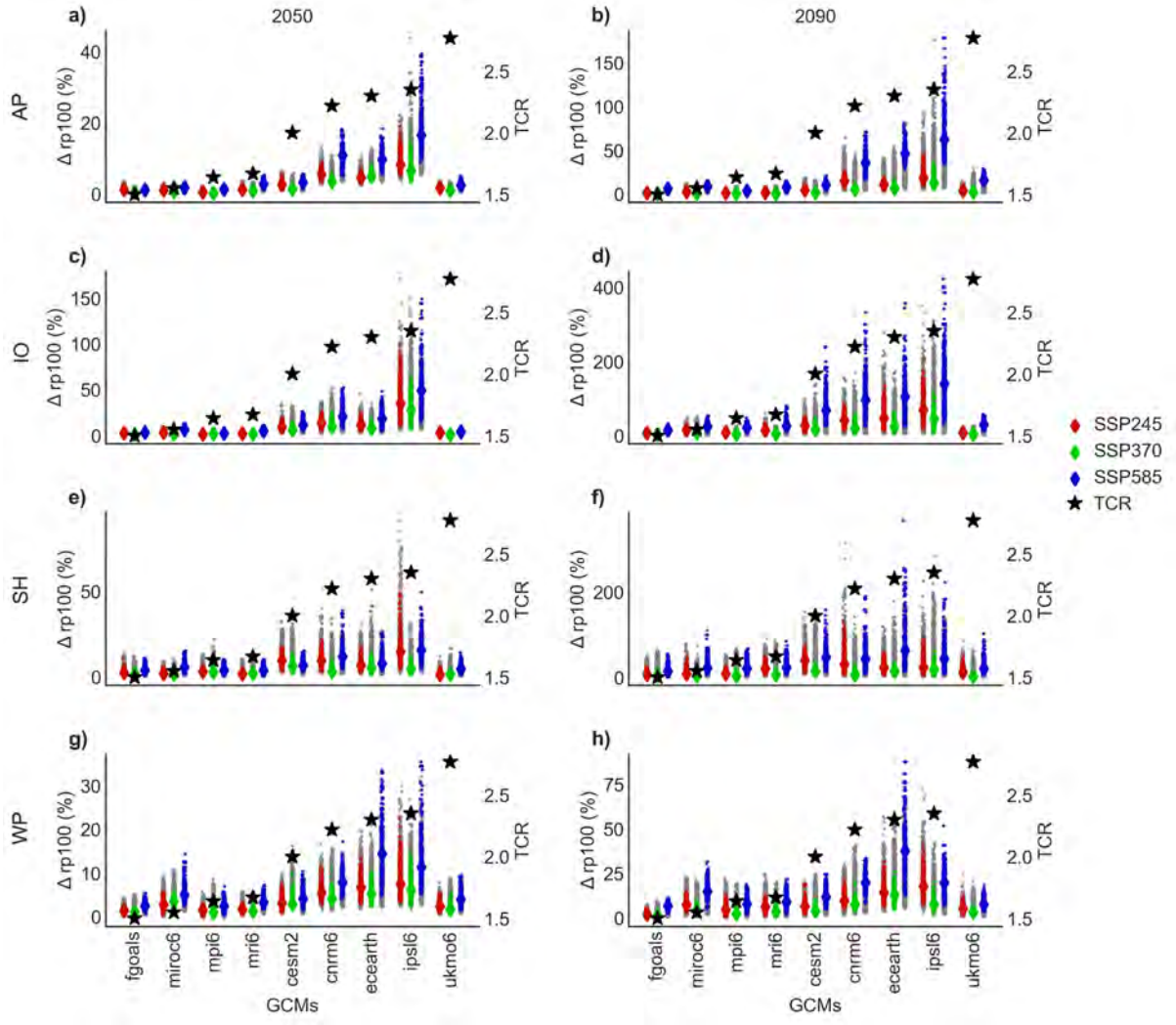

Supplementary Figure B.2: TC risk change from different global climate models (GCMs) and emission scenarios. Model simulations of the expected 100-yr event (rp100) change by 2050 (a, c, e, g) and 2090 (b, d, f, h) attributed to the nine GCMs and three emission scenarios underlying the TC hazard sets (see Methods). GCMs are ordered by increasing transient climate response (TCR) values (Supplementary Table B.6), which are shown as black stars on a secondary y-axis. Model realization of matching hazard and exposure scenarios are marked in color (SSP245 in red, SSP370 in green, SSP585 in blue) with diamond-shaped markers delineating the median of their distribution. Results are shown over the four study regions North Atlantic/Eastern Pacific (AP), North Indian Ocean (IO), Southern Hemisphere (SH), and North Western Pacific (WP) (see Fig. 3.1 a)).

Supplementary Table B.1: Statistical summary metrics of expected annual damage (EAD) change values by 2050 and 2090 in the four regions North Atlantic/Eastern Pacific (AP), North Indian Ocean (IO), Southern Hemisphere (SH), and North Western Pacific (WP), reported for climate change (CC), socio-economic development (SOC), the product of CC and SOC calculated from the sum of their log values (sum) and total TC risk change (total).

AP	delta	year	mean	std	min	25%	50%	75%	max
	CC	2050	3.5	4.7	-0.2	0.3	0.8	5.5	23.7
	CC	2090	6.0	9.8	-0.4	0.1	1.3	7.5	57.4
	SOC	2050	0.9	0.3	0.3	0.6	0.8	1.1	1.8
	SOC	2090	2.3	1.3	0.2	1.4	2.0	2.5	5.6
	sum	2050	4.3	4.7	0.3	1.2	1.8	6.5	24.8
	sum	2090	8.3	10.0	0.1	2.1	3.6	10.0	59.7
	total	2050	7.1	8.6	0.2	1.4	2.4	11.1	52.9
	total	2090	20.5	33.6	0.0	2.3	5.4	23.7	321.6

IO	delta	year	mean	std	min	25%	50%	75%	max
	CC	2050	2.8	3.7	-0.4	0.1	0.7	4.3	19.5
	CC	2090	4.9	5.4	-0.1	0.7	1.8	8.1	31.0
	SOC	2050	2.6	1.1	0.5	1.9	2.5	3.1	5.7
	SOC	2090	6.7	3.7	0.7	4.2	6.1	8.8	17.6
	sum	2050	5.4	4.0	0.3	2.5	4.2	7.0	24.2
	sum	2090	11.6	6.9	1.1	6.3	10.1	15.3	46.3
	total	2050	13.0	15.5	0.1	2.6	5.3	18.6	121.5
	total	2090	44.8	51.6	1.0	10.0	21.7	64.9	466.6

SH	delta	year	mean	std	min	25%	50%	75%	max
	CC	2050	0.9	1.2	-0.6	0.0	0.3	1.8	13.3
	CC	2090	1.3	1.6	-0.7	0.2	0.6	2.2	12.6
	SOC	2050	2.5	1.2	0.5	1.6	2.2	3.1	9.6
	SOC	2090	8.8	6.7	1.1	4.1	7.1	11.6	57.5
	sum	2050	3.4	1.7	0.6	2.1	3.2	4.4	16.4
	sum	2090	10.1	7.2	1.1	4.9	8.3	13.2	61.0
	total	2050	5.5	4.7	-0.2	2.1	4.0	7.6	70.8
	total	2090	20.8	22.2	0.1	6.9	13.3	25.7	341.2

WP	delta	year	mean	std	min	25%	50%	75%	max
	CC	2050	2.0	2.4	-0.2	0.3	0.8	3.3	15.7
	CC	2090	2.8	3.1	-0.2	0.6	1.2	4.4	16.1
	SOC	2050	1.6	0.7	0.2	1.1	1.5	1.9	4.1
	SOC	2090	3.3	2.0	0.1	1.8	2.7	4.3	13.2
	sum	2050	3.6	2.6	0.4	1.7	2.6	4.8	18.3
	sum	2090	6.1	3.9	0.4	3.1	4.9	8.2	20.7
	total	2050	6.5	6.3	0.5	2.2	3.7	9.3	51.2
	total	2090	14.3	13.7	0.1	4.8	9.2	19.1	110.1

Supplementary Table B.2: Statistical summary metrics of 100-yr event change values by 2050 and 2090 in the four regions North Atlantic/Eastern Pacific (AP), North Indian Ocean (IO), Southern Hemisphere (SH), and North Western Pacific (WP), reported for climate change (CC), socio-economic development (SOC), the product of CC and SOC calculated from the sum of their log values (sum) and total TC risk change (total).

AP	delta	year	mean	std	min	25%	50%	75%	max
	CC	2050	1.7	2.1	-0.4	0.3	0.7	2.8	18.8
	CC	2090	2.6	3.5	-0.5	0.3	1.0	4.2	33.2
	SOC	2050	0.8	0.3	0.2	0.6	0.7	0.9	2.3
	SOC	2090	2.1	1.4	0.1	1.3	1.6	2.3	8.2
	sum	2050	2.4	2.2	-0.1	1.0	1.5	3.5	20.1
	sum	2090	4.7	3.9	-0.2	1.9	3.2	6.2	37.5
	total	2050	3.6	3.8	-0.1	1.1	1.9	5.4	43.9
	total	2090	9.7	12.7	-0.4	2.2	4.8	12.4	178.6

IO	delta	year	mean	std	min	25%	50%	75%	max
	CC	2050	2.0	3.3	-0.6	0.0	0.5	2.7	25.3
	CC	2090	3.1	3.7	-0.3	0.5	1.5	4.4	24.5
	SOC	2050	2.6	1.1	0.3	1.8	2.5	3.2	6.5
	SOC	2090	6.7	3.7	0.5	4.1	6.0	8.8	21.2
	sum	2050	4.6	3.6	0.1	2.4	3.6	5.5	29.5
	sum	2090	9.8	5.5	0.8	5.6	8.7	12.6	42.1
	total	2050	10.3	14.1	0.0	2.5	4.7	12.4	170.9
	total	2090	31.1	36.2	0.6	9.0	17.2	39.6	422.4

SH	delta	year	mean	std	min	25%	50%	75%	max
	CC	2050	0.9	1.4	-0.7	0.0	0.4	1.3	20.4
	CC	2090	1.3	1.5	-0.6	0.2	0.7	1.9	10.5
	SOC	2050	2.9	1.7	0.3	1.8	2.5	3.7	10.9
	SOC	2090	11.7	10.4	0.7	4.4	8.1	15.4	67.9
	sum	2050	3.8	2.2	0.3	2.2	3.3	4.8	25.1
	sum	2090	13.0	10.8	0.4	5.3	9.5	17.1	72.0
	total	2050	5.9	5.7	-0.3	2.4	4.1	7.4	91.5
	total	2090	22.1	23.3	0.3	7.4	14.4	28.3	367.6

WP	delta	year	mean	std	min	25%	50%	75%	max
	CC	2050	1.2	1.4	-0.6	0.2	0.7	1.7	11.8
	CC	2090	1.5	1.8	-0.5	0.4	0.9	2.2	18.8
	SOC	2050	1.7	0.8	-0.1	1.2	1.6	2.1	4.6
	SOC	2090	3.9	2.7	-0.1	2.0	3.2	4.9	18.0
	sum	2050	2.9	1.7	-0.3	1.6	2.5	3.7	13.7
	sum	2090	5.4	3.4	-0.2	2.8	4.6	7.1	26.2
	total	2050	4.5	3.7	-0.4	1.9	3.4	5.9	35.5
	total	2090	9.1	7.6	-0.2	4.0	7.0	11.7	87.7

Supplementary Table B.3: TC hazard frequency values for event sets of the nine different GCMs and three emission scenarios in the two future time periods (2050, 2090) and four study regions North Atlantic/Eastern Pacific (AP), North Indian Ocean (IO), Southern Hemisphere (SH), and North Western Pacific (WP). Frequency values above the multimode average (last row) are highlighted in red.

		AP		IO		SH		WP	
GCM	**emission scenario**	**2050**	**2100**	**2050**	**2100**	**2050**	**2100**	**2050**	**2100**
CESM2	SSP245	13.47	11.99	7.52	7.47	15.97	19.67	19.53	16.88
CESM2	SSP370	12.53	10.64	7.31	8.15	15.82	20.36	20.22	20.99
CESM2	SSP585	12.70	9.71	7.09	10.74	16.15	22.79	18.37	19.22
CNRM6	SSP245	15.16	15.63	5.53	5.85	10.94	11.19	21.61	22.05
CNRM6	SSP370	14.83	15.69	5.40	6.24	11.44	11.76	21.61	23.42
CNRM6	SSP585	15.93	15.96	5.51	6.21	11.53	10.94	22.13	25.32
ECEARTH	SSP245	19.57	19.76	6.17	7.79	13.42	13.53	25.35	24.79
ECEARTH	SSP370	22.65	23.71	5.81	7.84	13.25	12.89	25.25	26.58
ECEARTH	SSP585	21.81	28.38	6.89	9.12	13.85	13.72	26.33	27.64
FGOALS	SSP245	9.32	8.56	2.92	2.99	8.95	8.66	14.76	13.93
FGOALS	SSP370	9.04	7.73	2.80	2.99	8.87	8.61	14.77	13.99
FGOALS	SSP585	8.97	7.81	2.97	3.17	9.06	8.93	14.29	14.60
IPSL6	SSP245	19.42	20.44	7.78	7.89	12.88	11.38	23.29	24.56
IPSL6	SSP370	18.83	20.51	7.49	7.45	12.50	11.38	22.26	26.52
IPSL6	SSP585	20.06	23.76	8.29	8.91	12.01	11.35	25.04	29.61
MIROC6	SSP245	10.74	11.06	3.20	3.73	9.15	9.05	17.54	18.78
MIROC6	SSP370	10.76	11.72	3.09	4.14	8.87	9.79	18.50	18.47
MIROC6	SSP585	11.24	12.42	3.86	4.42	9.68	9.39	18.28	21.37
MPI6	SSP245	9.73	8.78	2.86	3.54	9.68	9.32	17.62	17.50
MPI6	SSP370	9.91	7.73	2.29	3.21	9.16	9.31	16.34	14.91
MPI6	SSP585	9.66	8.34	2.69	3.60	9.45	9.08	16.88	16.27
MRI6	SSP245	11.27	9.86	3.07	3.80	8.27	9.12	17.08	15.88
MRI6	SSP370	10.09	7.93	2.72	3.59	8.52	9.13	15.03	14.83
MRI6	SSP585	10.81	9.12	3.62	4.87	8.21	8.98	15.84	15.74
UKMO6	SSP245	11.51	12.42	3.59	3.55	8.91	8.55	17.58	17.72
UKMO6	SSP370	11.58	12.03	3.04	3.84	8.78	8.81	15.93	16.81
UKMO6	SSP585	11.51	12.91	3.52	4.32	8.96	8.71	18.38	16.11
average		13.45	13.50	4.70	5.53	10.90	11.35	19.25	19.80

Supplementary Table B.4: TC hazard intensity change values for event sets of the nine different GCMs and three emission scenarios in the two future time periods (2050, 2090) and four study regions North Atlantic/Eastern Pacific (AP), North Indian Ocean (IO), Southern Hemisphere (SH), and North Western Pacific (WP). Intensity values above the multimode average (last row) are highlighted in red. Note, the intensity change is calculated relative to the historical period (1995-2014) and we used the Holland (2008) wind model for the hazard generation.

		AP		IO		SH		WP	
GCM	**emission scenario**	**2050**	**2100**	**2050**	**2100**	**2050**	**2100**	**2050**	**2100**
CESM2	SSP245	4.22	4.53	3.97	5.50	3.90	4.28	5.26	5.26
CESM2	SSP370	4.19	3.77	4.27	6.19	3.51	5.36	4.96	7.49
CESM2	SSP585	4.47	3.93	4.25	8.15	3.36	5.80	4.91	9.58
CNRM6	SSP245	7.11	7.97	3.17	4.00	4.71	4.14	7.06	7.65
CNRM6	SSP370	6.84	8.09	3.31	4.20	4.69	4.32	7.64	8.37
CNRM6	SSP585	7.58	9.18	3.63	4.46	4.62	3.86	6.87	8.76
ECEARTH	SSP245	5.25	6.09	2.82	3.83	4.61	4.15	5.23	6.39
ECEARTH	SSP370	6.45	7.30	2.72	3.82	3.83	4.65	5.04	6.64
ECEARTH	SSP585	6.32	8.74	3.04	4.57	3.78	5.98	5.86	8.71
FGOALS	SSP245	0.16	-0.31	0.66	0.91	0.78	1.02	1.31	1.05
FGOALS	SSP370	-0.07	-0.80	0.44	0.97	1.19	2.07	1.45	1.13
FGOALS	SSP585	0.08	-0.26	0.67	2.47	1.17	1.85	1.10	2.91
IPSL6	SSP245	6.38	7.71	5.18	5.85	5.90	6.11	8.12	9.07
IPSL6	SSP370	6.22	8.17	4.73	5.49	5.72	5.12	7.50	7.44
IPSL6	SSP585	7.31	8.74	5.32	6.79	5.61	5.74	8.03	7.75
MIROC6	SSP245	0.98	1.57	0.55	1.61	-0.66	0.42	0.41	1.57
MIROC6	SSP370	1.23	1.57	0.70	1.63	-0.62	1.34	1.09	2.55
MIROC6	SSP585	1.42	2.92	1.17	2.49	0.01	0.78	2.45	3.63
MPI6	SSP245	0.27	0.04	-0.70	0.14	-0.58	-0.80	1.30	0.83
MPI6	SSP370	0.70	-0.04	-0.52	-0.12	-0.49	-0.78	0.76	1.28
MPI6	SSP585	0.41	0.56	-0.16	0.39	-0.79	-0.36	0.61	2.25
MRI6	SSP245	1.69	1.69	0.28	1.68	-0.03	0.86	0.43	0.35
MRI6	SSP370	0.88	1.97	0.64	1.51	0.10	0.43	-0.51	0.36
MRI6	SSP585	1.96	2.75	1.23	2.17	-0.10	2.00	0.42	2.61
UKMO6	SSP245	1.48	2.10	0.60	1.28	-0.08	0.17	1.17	0.94
UKMO6	SSP370	1.94	3.17	0.43	1.17	0.13	1.19	0.10	1.47
UKMO6	SSP585	1.93	4.16	0.58	1.97	-0.17	1.06	1.23	1.76
average		3.24	3.90	1.96	3.08	2.00	2.62	3.33	4.36

Supplementary Table B.5: TC hazard intensity change values for event sets of the nine different GCMs and three emission scenarios in the two future time periods (2050, 2090) and four study regions North Atlantic/Eastern Pacific (AP), North Indian Ocean (IO), Southern Hemisphere (SH), and North Western Pacific (WP). Intensity values above the multimode average (last row) are highlighted in red. Note, the intensity change is calculated relative to the historical period (1995-2014) and we used the Emanuel and Rotunno (2011) wind model for the hazard generation.

		AP		IO		SH		WP	
GCM	**emission scenario**	**2050**	**2100**	**2050**	**2100**	**2050**	**2100**	**2050**	**2100**
CESM2	SSP245	5.09	5.72	4.47	6.39	4.75	5.58	5.82	5.85
CESM2	SSP370	5.13	5.22	4.97	7.94	4.23	7.18	5.69	9.44
CESM2	SSP585	5.51	6.04	5.02	10.35	4.36	8.10	5.53	11.79
CNRM6	SSP245	8.61	9.91	4.17	5.06	6.31	5.81	8.86	9.56
CNRM6	SSP370	8.33	10.19	4.37	5.53	6.25	6.24	9.46	10.45
CNRM6	SSP585	9.31	11.61	4.64	5.96	6.38	5.84	8.59	11.15
ECEARTH	SSP245	6.12	7.09	3.13	4.29	5.29	4.92	6.12	7.29
ECEARTH	SSP370	7.23	8.63	3.05	4.60	4.52	5.87	5.88	8.41
ECEARTH	SSP585	7.37	10.73	3.34	5.83	4.51	7.75	6.90	11.17
FGOALS	SSP245	0.79	0.31	1.07	1.31	1.04	1.31	1.78	1.40
FGOALS	SSP370	0.70	0.28	0.76	1.49	1.44	2.49	1.90	1.59
FGOALS	SSP585	0.84	1.10	1.04	3.27	1.42	2.36	1.42	3.63
IPSL6	SSP245	7.37	9.19	5.89	6.81	7.18	7.49	9.64	10.70
IPSL6	SSP370	7.36	9.85	5.56	6.56	7.07	6.54	9.03	9.08
IPSL6	SSP585	8.61	11.09	6.24	8.43	6.89	7.28	9.78	9.71
MIROC6	SSP245	1.24	2.04	0.53	1.59	-0.69	0.58	0.53	2.05
MIROC6	SSP370	1.64	2.26	0.74	1.74	-0.61	1.81	1.33	3.17
MIROC6	SSP585	1.74	3.78	1.19	2.86	0.10	1.20	2.91	4.61
MPI6	SSP245	0.47	0.26	-0.62	0.26	-0.46	-0.70	1.60	1.06
MPI6	SSP370	0.92	0.31	-0.38	0.46	-0.38	-0.29	1.02	2.24
MPI6	SSP585	0.65	1.24	-0.15	1.28	-0.67	0.45	0.85	3.50
MRI6	SSP245	1.92	1.85	0.28	1.81	0.00	1.16	0.70	0.73
MRI6	SSP370	1.17	2.47	0.60	1.80	0.23	1.09	-0.29	1.27
MRI6	SSP585	2.26	3.72	1.29	2.99	0.12	3.31	0.71	4.02
UKMO6	SSP245	2.22	2.86	0.72	1.56	0.04	0.52	1.37	1.59
UKMO6	SSP370	2.67	4.66	0.54	1.87	0.24	2.24	0.26	2.87
UKMO6	SSP585	2.72	5.98	0.76	3.22	0.02	2.64	1.69	3.50
average		4.00	5.13	2.34	3.90	2.58	3.66	4.04	5.62

Supplementary Table B.6: Transient climate response (TCR) and equilibrium climate sensitivity (ECS) values for the nine GCMs, including a screen if the models fall into the likely range of projected TCR or ECS. Values are obtained from Hausfather et al. (2022) supplementary data. The last column groups GCMs into two clusters of low and medium-high TC risk change according to the results of Section 2.3 in the main text.

Model	TCR	TCR screen (likely)	ECS150	ECS130	ECS screen (likely)	TC risk increase
CESM2	2.00	yes	5.15	6.43	no	med-high
CNRM-CM6-1	2.22	no	4.90	4.76	no	med-high
EC-Earth3	2.30	no	4.26	N/A	no	med-high
FGOALS-g3	1.50	yes	2.87	3.10	yes	low
IPSL-CM6A-LR	2.35	no	4.70	5.18	no	med-high
MIROC6	1.55	yes	2.60	2.59	yes	low
MPI-ESM1-2-HR	1.64	yes	2.98	3.34	yes	low
MRI6-ESM2-0	1.67	yes	3.13	3.42	yes	low
UKESM1-0-LL	2.77	no	5.36	5.49	no	low

Supplementary Table B.7: Spearman's rank correlation coefficients (rho) between the TCR values (B.6) and the calculated TC risk metrics (change in expected annual damage (EAD) and 100-yr event (rp100)) in the future (2050, 2090) in the four study regions North Atlantic/Eastern Pacific (AP), North Indian Ocean (IO), Southern Hemisphere (SH), and North Western Pacific (WP) and for the entire globe (regions combined). Correlation coefficients between TCR and global hazard frequency and intensity are reported as well.

risk metric	year	region	rho	pval
EAD	2050	AP	0.71	0.0
		IO	0.52	0.0
		SH	0.44	0.0
		WP	0.60	0.0
		global	0.54	0.0
EAD	2090	AP	0.66	0.0
		IO	0.48	0.0
		SH	0.33	0.0
		WP	0.57	0.0
		global	0.48	0.0
rp100	2050	AP	0.65	0.0
		IO	0.48	0.0
		SH	0.34	0.0
		WP	0.50	0.0
		global	0.46	0.0
rp100	2090	AP	0.66	0.0
		IO	0.45	0.0
		SH	0.27	0.0
		WP	0.41	0.0
		global	0.39	0.0
hazard metric	**year**	**region**	**rho**	**pval**
frequency	2050	global	0.65	0.00
	2090	global	0.63	0.00
intensity	2050	global	0.59	0.00
	2090	global	0.57	0.00

Supplementary Table B.8: List of CMIP6 models used in the downscaling of tropical cyclone event sets.

Institution	Model	Short name	Source
National Center for Atmospheric Research	CESM2	CESM2	Danabasoglu et al. (2020)
Centre National de Recherches Météorologiques	CNRM-CM6-1	CNRM6	Voldoire et al. (2019)
EC-Earth consortium	EC-Earth3	ECEARTH	EC Earth Consortium (2019)
Institute of Atmospheric Physics, Chinese Academy of Sciences	FGOALS-g3	FGOALS	Li (2019)
Institut Pierre Simon Laplace	IPSL-CM6A-LR	IPSL6	Hourdin et al. (2020)
Japan Agency for Marine-Earth Science and Technology	MIROC6	MIROC6	Tatebe et al. (2019)
Max Planck Institute	MPI-ESM1-2-HR	MPI2	Müller et al. (2018)
Meteorological Research Institute, Tsukuba, Japan	MRI6-ESM2-0	MRI6	Yukimoto et al. (2019)
United Kingdom Met Office	UKESM1-0-LL	UKMO6	Sellar et al. (2020)

APPENDIX C

Supplement to Chapter 5

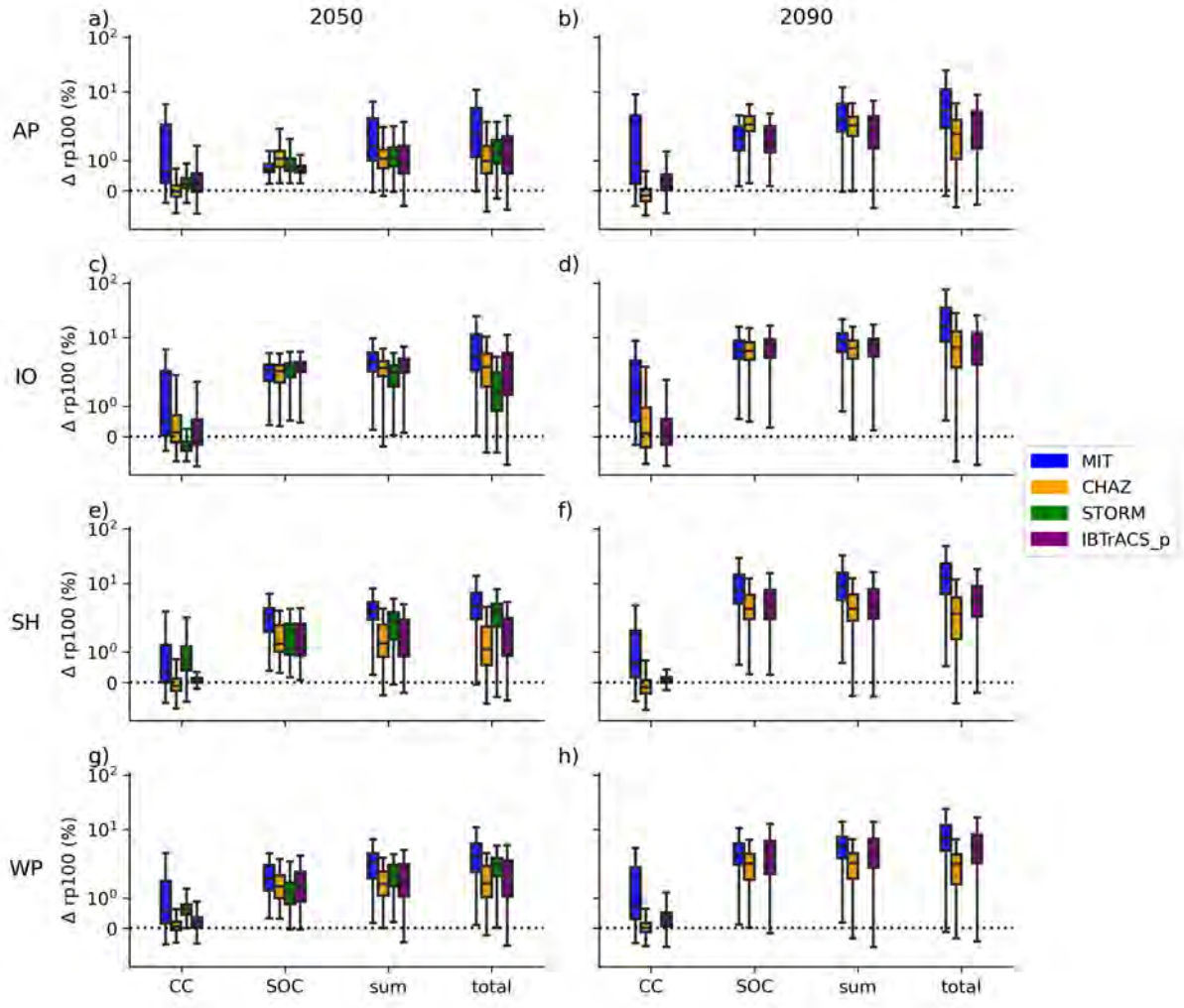

Supplementary Figure C.1: Drivers of future tropical cyclone risk change: comparison across hazard models. Relative change in 100-yr event (rp100) by 2050 (left panels) and 2090 (right panels) due to climate change (CC), socio-economic development (SOC), the product of CC and SOC calculated from the sum of their log values (sum) and both drivers interacting (total) with respect to the historical baseline. The relative change EAD is reported for the four study regions (North Atlantic/Eastern Pacific (AP), North Indian Ocean (IO), Southern Hemisphere (SH), and North Western Pacific (WP)). Boxplots are shown for the four models MIT (blue), CHAZ (orange), STORM (green), IBTrACS_p (purple) and display the interquartile range (IQR) for the uncertainty over all input factors (see Methods), while the whiskers extend to 1.5 times the IQR. More extreme points (outliers) are not shown. Note that STORM results are only available for 2050.

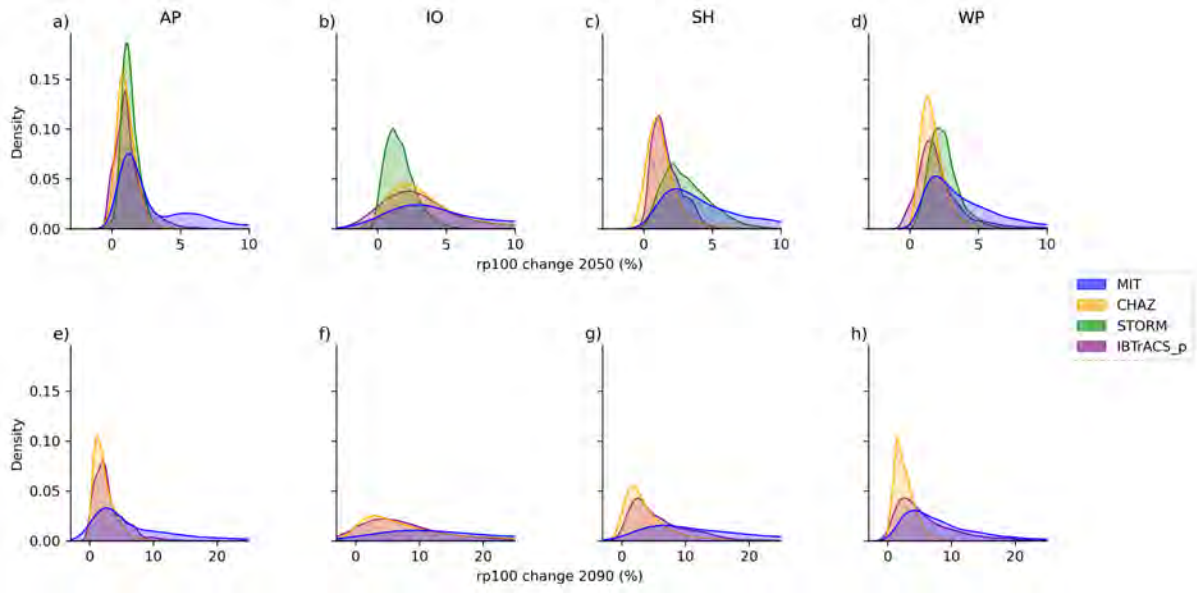

Supplementary Figure C.2: Uncertainty distribution of TC risk change: comparison across hazard models. Kernel density estimation plots showcasing the uncertainty distribution of estimated relative change in 100-yr event (rp100) across study regions (North Atlantic/Eastern Pacific (AP), North Indian Ocean (IO), Southern Hemisphere (SH), and North Western Pacific (WP)) for the years 2050 and 2090. Each subplot represents a specific region and year combination, with different models (MIT, CHAZ, STORM, IBTrACS_p) depicted in distinct colors. Note, the model STORM only provides data for 2050. Each plot shows a normalized probability distribution with an integral sum of 1. The x-axis is truncated in some figures, potentially influencing the interpretation of distribution tails, particularly for the MIT hazard-based results.

Supplementary Table C.1: Maximum kernel density of TC risk change uncertainty distribution: comparison across hazard models. Maximum kernel density estimation of TC risk change uncertainty distribution for estimated change in expected annual damage (EAD) and 100-yr event (rp100) across study regions (North Atlantic/Eastern Pacific (AP), North Indian Ocean (IO), Southern Hemisphere (SH), and North Western Pacific (WP)) for the years 2050 and 2090 and the four models (MIT, CHAZ, STORM, IBTrACS_p). The full uncertainty distribution is shown in Figure 5.2 and Supplementary Figure C.2.

region	year	model	Δ EAD (%)	Δ rp100 (%)
AP	2050	MIT	1.66	1.24
		CHAZ	0.88	0.80
		STORM	1.24	1.10
		IBTrACS_p	1.22	0.97
	2090	MIT	3.52	2.61
		CHAZ	1.22	1.14
		STORM	N/A	N/A
		IBTrACS_p	2.50	2.09
IO	2050	MIT	2.82	2.83
		CHAZ	1.75	1.98
		STORM	1.48	1.10
		IBTrACS_p	1.85	2.21
	2090	MIT	10.00	9.41
		CHAZ	2.79	2.86
		STORM	N/A	N/A
		IBTrACS_p	4.05	4.35
SH	2050	MIT	1.89	2.34
		CHAZ	1.05	0.93
		STORM	2.95	2.09
		IBTrACS_p	0.79	1.10
	2090	MIT	6.42	6.58
		CHAZ	1.67	1.75
		STORM	N/A	N/A
		IBTrACS_p	2.09	2.50
WP	2050	MIT	2.47	1.85
		CHAZ	1.26	1.33
		STORM	2.39	2.01
		IBTrACS_p	1.11	1.49
	2090	MIT	5.12	4.16
		CHAZ	1.31	1.57
		STORM	N/A	N/A
		IBTrACS_p	1.94	2.61

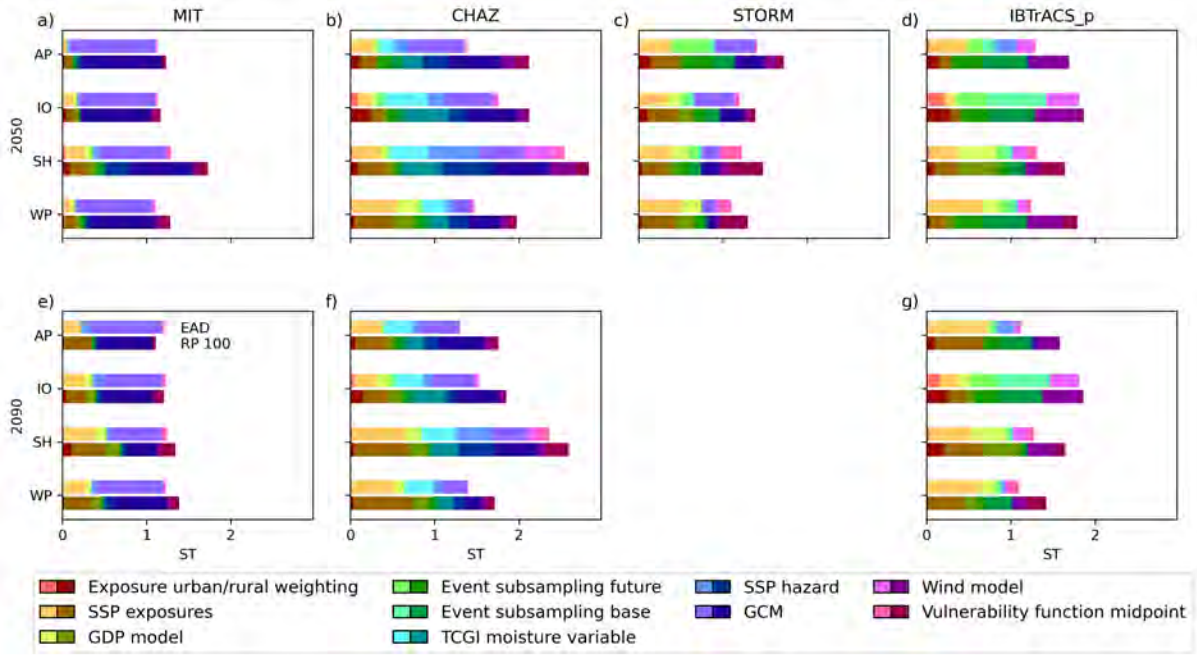

Supplementary Figure C.3: Sensitivity indices of future TC risk change: comparison across hazard models. Total-order Sobol sensitivity indices for future (2050, 2090) TC risk change calculated with the four models (MIT, CHAZ, STORM, IBTrACS_p), expressed as %-change in expected annual damage (EAD; upper bar, lighter colors) and 100-yr event values (RP 100; lower bar, darker colors) over the four study regions (North Atlantic/Eastern Pacific (AP), North Indian Ocean (IO), Southern Hemisphere (SH), and North Western Pacific (WP)) and all input factors (different colors); *Vulnerability function midpoint* describes the impact function; *Wind model*; *GCM*, *SSP hazard*, *TCGI moisture variable*, *Event subsampling base*, *Event subsampling future* pertain to the hazard component; *GDP model*; *SSP exposure*, *Exposure urban/rural weighting* relate to the exposure. Note that STORM results are only available for 2050.

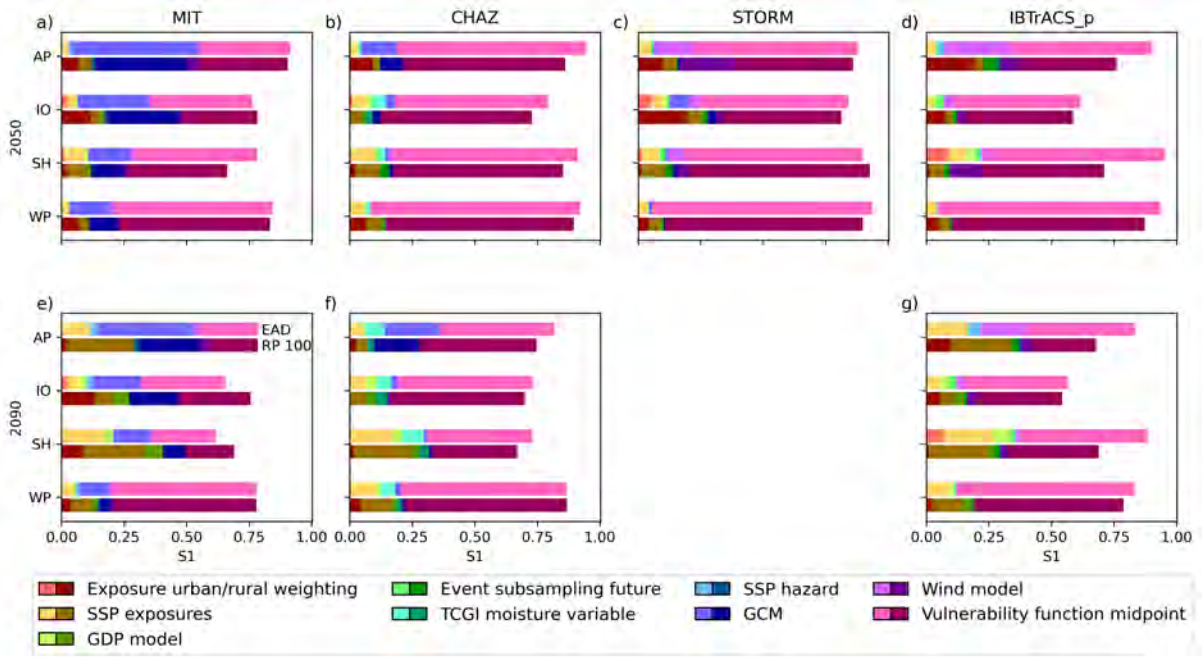

Supplementary Figure C.4: First-order sensitivity indices of future TC risk across hazard models. First-order Sobol sensitivity indices for future (2050, 2090) TC risk calculated with the four models (MIT, CHAZ, STORM, IBTrACS_p), expressed as absolute (calculated in USD) expected annual damage (EAD; upper bar) and 100-yr event values (RP 100; lower bar) over the four study regions (North Atlantic/Eastern Pacific (AP), North Indian Ocean (IO), Southern Hemisphere (SH), and North Western Pacific (WP) and all input factors (different colors); *Vulnerability function midpoint* describes the impact function; *Wind model*; *GCM*, *SSP hazard*, *TCGI moisture variable*, *Event subsampling base*, *Event subsampling future* pertain to the hazard component; *GDP model*; *SSP exposure*, *Exposure urban/rural weighting* relate to the exposure. Note that STORM results are only available for 2050.

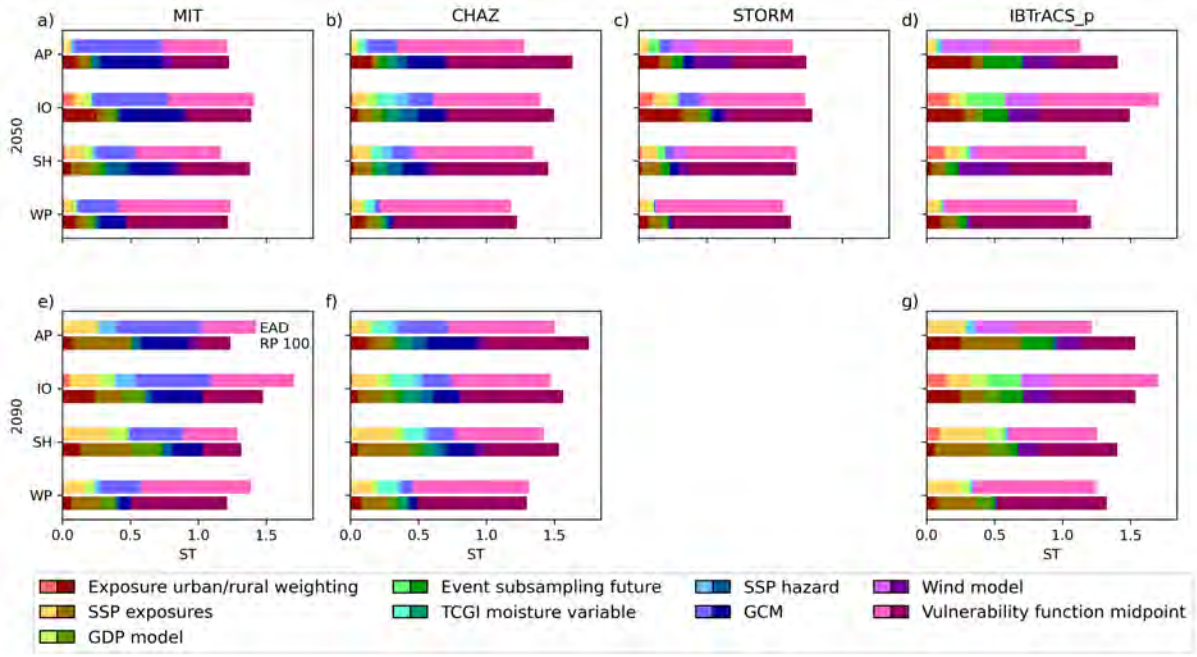

Supplementary Figure C.5: Total-order sensitivity indices of future TC risk across hazard models. Total-order Sobol sensitivity indices for future (2050, 2090) TC risk calculated with the four models (MIT, CHAZ, STORM, IBTrACS_p), expressed as absolute (calculated in USD) expected annual damage (EAD; upper bar) and 100-yr event values (RP 100; lower bar) over the four study regions (North Atlantic/Eastern Pacific (AP), North Indian Ocean (IO), Southern Hemisphere (SH), and North Western Pacific (WP) and all input factors (different colors); *Vulnerability function midpoint* describes the impact function; *Wind model*; *GCM*, *SSP hazard*, *TCGI moisture variable*, *Event subsampling base*, *Event subsampling future* pertain to the hazard component; *GDP model*; *SSP exposure*, *Exposure urban/rural weighting* relate to the exposure. Note that STORM results are only available for 2050.

Supplementary Table C.2: Largest sensitivity indices for future TC risk change estimates. Highest first- (S1) and total-order (ST) Sobol sensitivity indices for both risk change metrics (expected annual damage (EAD) and 100-yr event (rp100)), expressed as %-change in the four study regions (North Atlantic/Eastern Pacific (AP), North Indian Ocean (IO), Southern Hemisphere (SH), and North Western Pacific (WP) for both future periods (2050, 2090) and all four models (MIT, CHAZ, STORM, IBTrACS_p. Indices colored blue pertain to the hazard component, green to the exposure and red to the impact function. Plots showing all sensitivity indices can be found in Figure 5.3 and Supplementary Figure C.3.

region	year	model	S1 EAD	S1 rp100	ST EAD	ST rp100
AP	2050	MIT	gc_model	gc_model	gc_model	gc_model
		CHAZ	gc_model	ssp_exp	gc_model	gc_model
		STORM	ssp_exp	ssp_exp	gc_model	HE_fut
		IBTrACS_p	ssp_exp	HE_base	ssp_exp	HE_base
	2090	MIT	gc_model	gc_model	gc_model	gc_model
		CHAZ	ssp_exp	ssp_exp	gc_model	gc_model
		STORM	N/A	N/A	N/A	N/A
		IBTrACS_p	ssp_exp	ssp_exp	ssp_exp	ssp_exp
IO	2050	MIT	gc_model	gc_model	gc_model	gc_model
		CHAZ	gc_model	tcgi_var	gc_model	gc_model
		STORM	gc_model	ssp_exp	gc_model	ssp_exp
		IBTrACS_p	HE_fut	HE_base	HE_base	HE_base
	2090	MIT	gc_model	gc_model	gc_model	gc_model
		CHAZ	gc_model	tcgi_var	gc_model	gc_model
		STORM	N/A	N/A	N/A	N/A
		IBTrACS_p	HE_fut	HE_base	HE_base	HE_base
SH	2050	MIT	gc_model	gc_model	gc_model	gc_model
		CHAZ	ssp_exp	ssp_exp	ssp_haz	gc_model
		STORM	ssp_exp	ssp_exp	ssp_exp	v_half
		IBTrACS_p	gdp_model	ssp_exp	gdp_model	gdp_model
	2090	MIT	gc_model	ssp_exp	gc_model	ssp_exp
		CHAZ	ssp_exp	ssp_exp	ssp_exp	ssp_exp
		STORM	N/A	N/A	N/A	N/A
		IBTrACS_p	ssp_exp	ssp_exp	ssp_exp	ssp_exp
WP	2050	MIT	gc_model	gc_model	gc_model	gc_model
		CHAZ	ssp_exp	ssp_exp	ssp_exp	ssp_exp
		STORM	ssp_exp	ssp_exp	ssp_exp	ssp_exp
		IBTrACS_p	ssp_exp	HE_base	ssp_exp	HE_base
	2090	MIT	gc_model	gc_model	gc_model	gc_model
		CHAZ	ssp_exp	ssp_exp	ssp_exp	ssp_exp
		STORM	N/A	N/A	N/A	N/A
		IBTrACS_p	ssp_exp	ssp_exp	ssp_exp	ssp_exp

Supplementary Table C.3: Largest sensitivity indices for future TC risk estimates. Highest first- (S1) and total-order (ST) Sobol sensitivity indices for both risk metrics (expected annual damage (EAD) and 100-yr event (rp100)), expressed in absolute values (USD) in the four study regions (North Atlantic/Eastern Pacific (AP), North Indian Ocean (IO), Southern Hemisphere (SH), and North Western Pacific (WP) for both future periods (2050, 2090) and all four models (MIT, CHAZ, STORM, IBTrACS_p. Indices colored blue pertain to the hazard component, green to the exposure and red to the impact function. Plots showing all sensitivity indices can be found in Supplementary Figure C.3 and C.5.

region	year	model	S1 EAD	S1 rp100	ST EAD	ST rp100
AP	2050	MIT	gc_model	gc_model	gc_model	gc_model
		CHAZ	v_half	v_half	v_half	v_half
		STORM	v_half	v_half	v_half	v_half
		IBTrACS_p	v_half	v_half	v_half	v_half
	2090	MIT	gc_model	ssp_exp	gc_model	ssp_exp
		CHAZ	v_half	v_half	v_half	v_half
		STORM	v_half	v_half	v_half	v_half
		IBTrACS_p	N/A	N/A	N/A	N/A
IO	2050	MIT	v_half	v_half	v_half	v_half
		CHAZ	v_half	v_half	v_half	v_half
		STORM	v_half	v_half	v_half	v_half
		IBTrACS_p	v_half	v_half	v_half	v_half
	2090	MIT	v_half	v_half	v_half	v_half
		CHAZ	v_half	v_half	v_half	v_half
		STORM	N/A	N/A	N/A	N/A
		IBTrACS_p	v_half	v_half	v_half	v_half
SH	2050	MIT	v_half	v_half	v_half	v_half
		CHAZ	v_half	v_half	v_half	v_half
		STORM	v_half	v_half	v_half	v_half
		IBTrACS_p	v_half	v_half	v_half	v_half
	2090	MIT	v_half	ssp_exp	v_half	ssp_exp
		CHAZ	v_half	v_half	v_half	v_half
		STORM	N/A	N/A	N/A	N/A
		IBTrACS_p	v_half	v_half	v_half	v_half
WP	2050	MIT	v_half	v_half	v_half	v_half
		CHAZ	v_half	v_half	v_half	v_half
		STORM	v_half	v_half	v_half	v_half
		IBTrACS_p	v_half	v_half	v_half	v_half
	2090	MIT	v_half	v_half	v_half	v_half
		CHAZ	v_half	v_half	v_half	v_half
		STORM	N/A	N/A	N/A	N/A
		IBTrACS_p	v_half	v_half	v_half	v_half

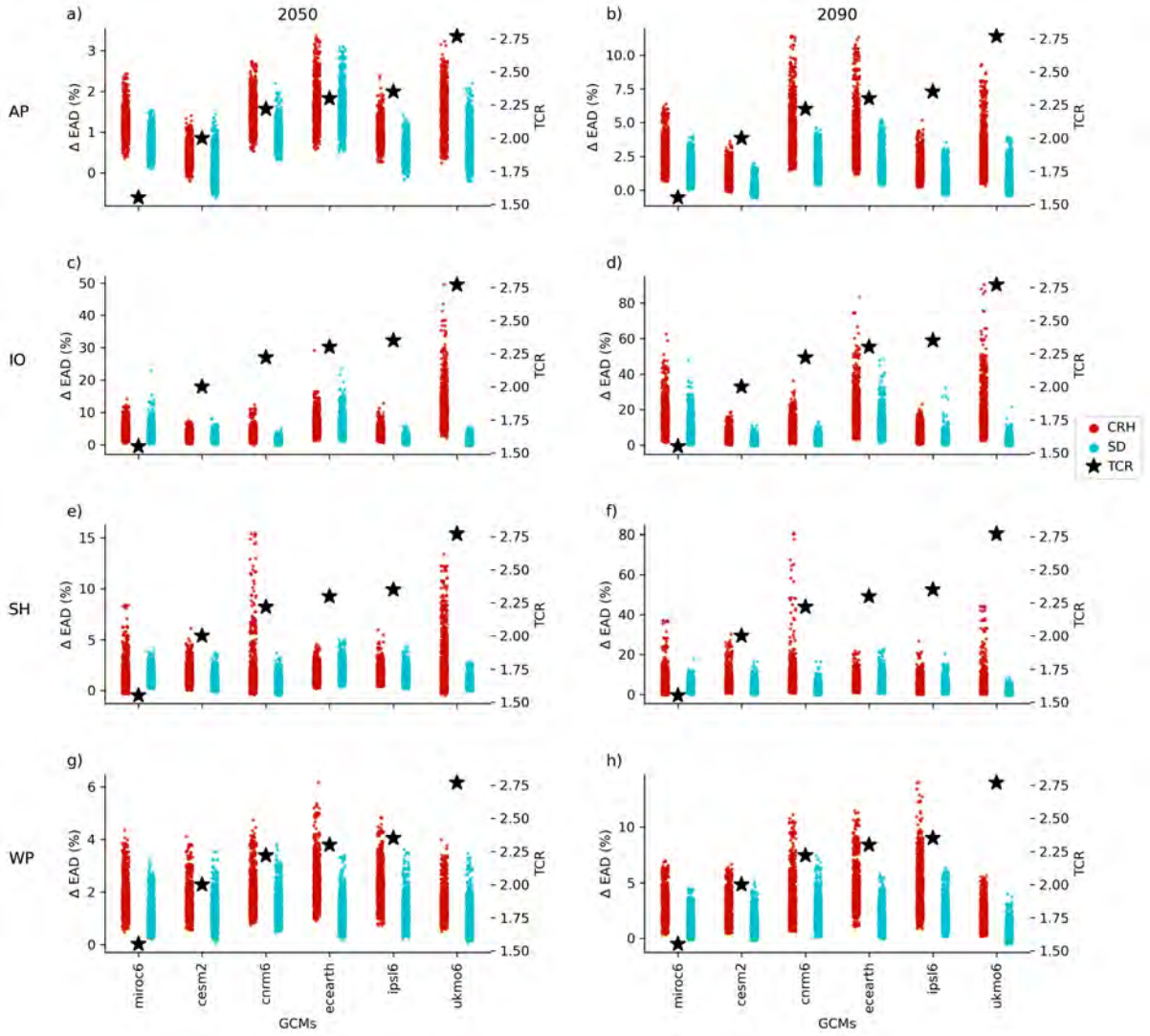

Supplementary Figure C.6: EAD change in CHAZ apportioned to GCMs and TCGI variables. Model simulations of the expected annual damage (EAD) change by 2050 (a, c, e, g) and 2090 (b, d, f, h) attributed to the six GCMs and two moisture variables used in the TCGI underlying the CHAZ TC hazard sets. GCMs are ordered by increasing transient climate response (TCR) values (Supplementary Table B.6), which are shown as black stars on a secondary y-axis. Results are shown over the four study regions North Atlantic/Eastern Pacific (AP), North Indian Ocean (IO), Southern Hemisphere (SH), and North Western Pacific (WP).

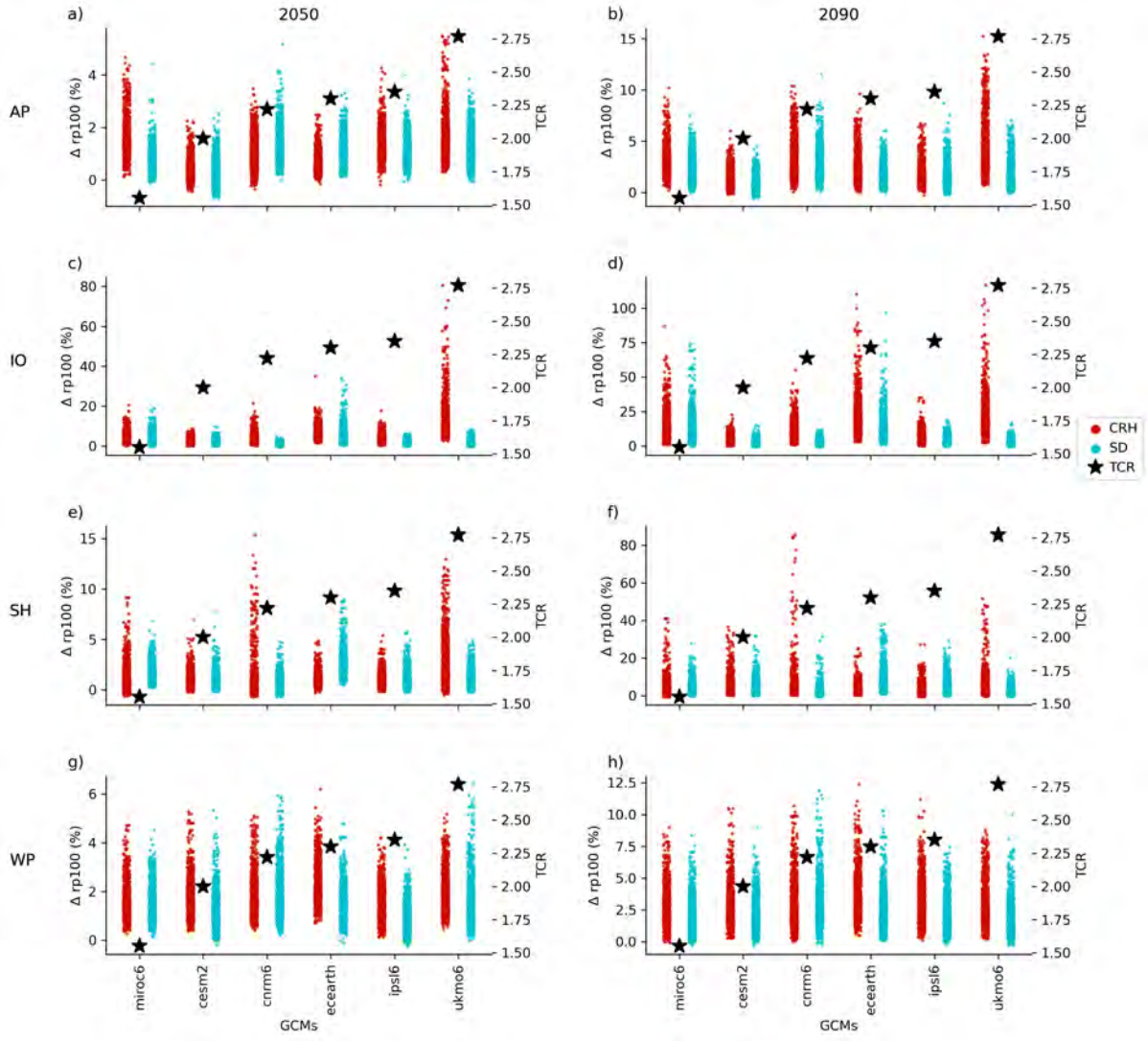

Supplementary Figure C.7: RP100 change in CHAZ apportioned to GCMs and TCGI variables. Model simulations of the 100-yr event (rp100) change by 2050 (a, c, e, g) and 2090 (b, d, f, h) attributed to the six GCMs and two moisture variables used in the TCGI underlying the CHAZ TC hazard sets. GCMs are ordered by increasing transient climate response (TCR) values (Supplementary Table B.6), which are shown as black stars on a secondary y-axis. Results are shown over the four study regions North Atlantic/Eastern Pacific (AP), North Indian Ocean (IO), Southern Hemisphere (SH), and North Western Pacific (WP).

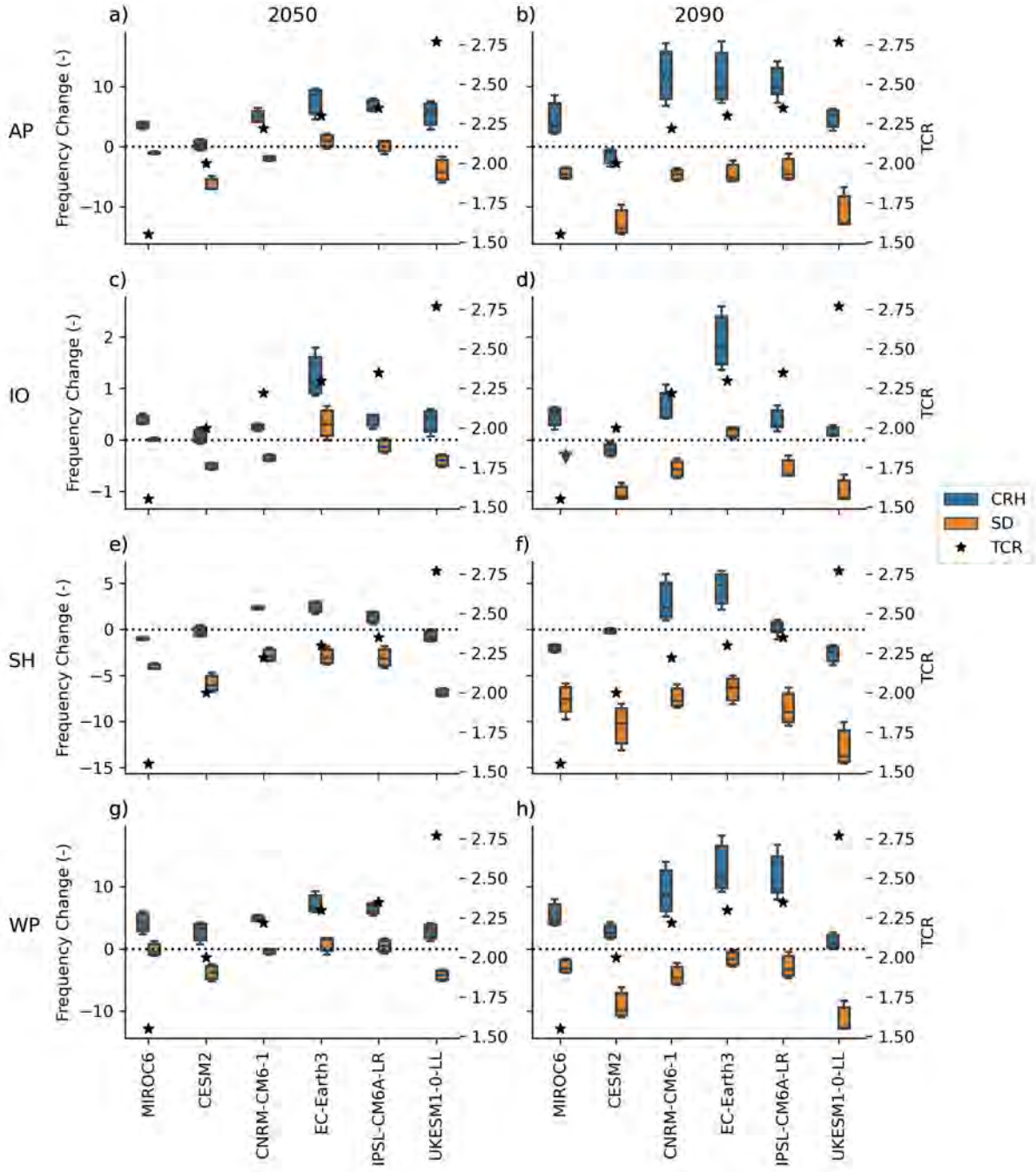

Supplementary Figure C.8: Frequency changes in CHAZ hazard sets. CHAZ hazard frequency change values for event sets of the six different GCMs, separated by the two TCGI moisture variables (CRH, SD) and shown for two future time periods (2050, 2090) and four study regions North Atlantic/Eastern Pacific (AP), North Indian Ocean (IO), Southern Hemisphere (SH), and North Western Pacific (WP). Frequency change values were calculated relative to the historical period and analyzed for the full event set, hence not limited to land-influencing storms. Additionally, transient climate response (TCR) values for the six GCMs are shown on a secondary y-axis (see Supplementary Table B.6).

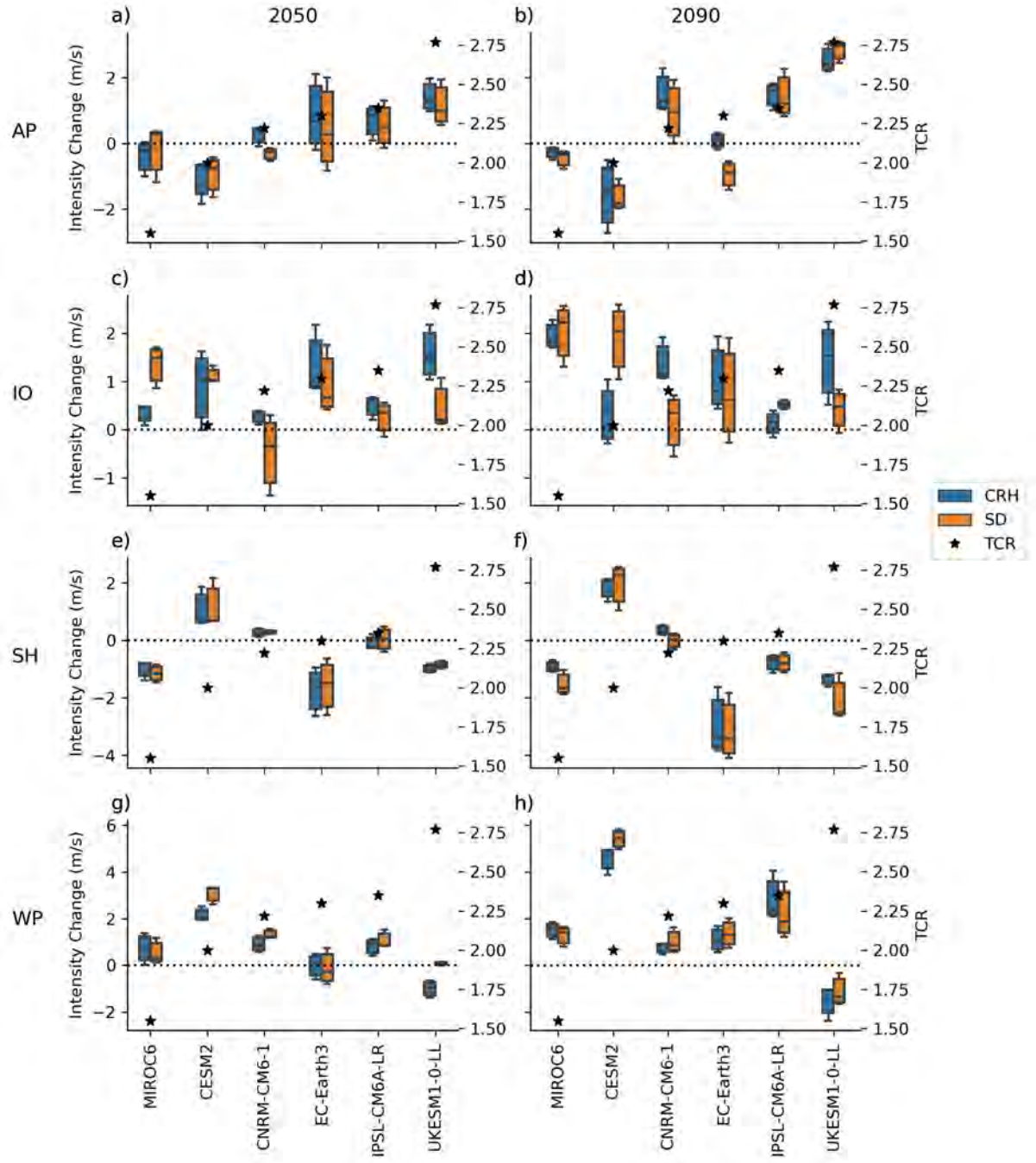

Supplementary Figure C.9: Intensity changes in CHAZ hazard sets. CHAZ hazard intensity change values for event sets of the six different GCMs, separated by the two TCGI moisture variables (CRH, SD) and shown for two future time periods (2050, 2090) and four study regions North Atlantic/Eastern Pacific (AP), North Indian Ocean (IO), Southern Hemisphere (SH), and North Western Pacific (WP). Intensity change values were derived for both wind models used in the hazard generation (Holland, 2008; Emanuel, 2021). Intensity changes are calculated as the mean over the maximum sustained wind speeds of all TCs in the future event sets minus the equivalent of the historical period. Note, we analyze the full event set and do not limit the analysis to land-influencing storms. Additionally, transient climate response (TCR) values for the six GCMs are shown on a secondary y-axis (see Supplementary Table B.6).

References

Aiken, E., E. Rolf, and J. Blumenstock, 2023: Fairness and representation in satellite-based poverty maps: Evidence of urban-rural disparities and their impacts on downstream policy. preprint. doi:10.48550/arXiv.2305.01783, url http://arxiv.org/abs/2305.01783.

Altman, J., and Coauthors, 2018: Poleward migration of the destructive effects of tropical cyclones during the 20th century. *Proceedings of the National Academy of Sciences of the United States of America*, **115 (45)**, 11 543–11 548, doi:10.1073/pnas.1808979115.

Arribas, A., R. Fairgrieve, T. Dhu, J. Bell, R. Cornforth, G. Gooley, C. J. Hilson, A. Luers, T. G. Shepherd, R. Street, and N. Wood, 2022: Climate risk assessment needs urgent improvement. *Nature Communications*, **13 (1)**, 4326, doi:10.1038/s41467-022-31979-w.

Aznar-Siguan, G., and D. N. Bresch, 2019: CLIMADA v1: A global weather and climate risk assessment platform. *Geoscientific Model Development*, **12 (7)**, 3085–3097, doi:10.5194/gmd-12-3085-2019.

Bacmeister, J. T., K. A. Reed, C. Hannay, P. Lawrence, S. Bates, J. E. Truesdale, N. Rosenbloom, and M. Levy, 2018: Projected changes in tropical cyclone activity under future warming scenarios using a high-resolution climate model. *Climatic Change*, **146 (3-4)**, 547–560, doi:10.1007/s10584-016-1750-x.

Baldwin, J. W., C.-Y. Lee, B. J. Walsh, S. J. Camargo, and A. H. Sobel, 2023: Vulnerability in a Tropical Cyclone Risk Model: Philippines Case Study. *Weather, Climate, and Society*, **15 (3)**, 503–523, doi:10.1175/WCAS-D-22-0049.1.

Bates, P., M. Trigg, J. Neal, and A. Dabrowa, 2013: LISFLOOD-FP User manual. Tech. rep. url https://svn.ggy.bris.ac.uk/subversion/lisflood/.

Bates, P. D., and Coauthors, 2020: Combined modelling of US fluvial, pluvial and coastal flood hazard under current and future climates. *Water Resources Research*, 1–29, doi:10.1029/2020wr028673.

Berlemann, M., and D. Wenzel, 2018: Hurricanes, economic growth and transmission channels: Empirical evidence for countries on differing levels of development. *World Development*, **105**, 231–247, doi:10.1016/j.worlddev.2017.12.020.

Beven, K. J., W. P. Aspinall, P. D. Bates, E. Borgomeo, K. Goda, J. W. Hall, T. Page, J. C. Phillips, M. Simpson, P. J. Smith, T. Wagener, and M. Watson, 2018: Epistemic uncertainties and natural hazard risk assessment – Part 2: What should constitute good practice? *Natural Hazards and Earth System Sciences*, **18 (10)**, 2769–2783, doi:10.5194/nhess-18-2769-2018.

Bhatia, K., G. Vecchi, H. Murakami, S. Underwood, and J. Kossin, 2018: Projected response of tropical cyclone intensity and intensification in a global climate model. *Journal of Climate*, **31 (20)**, 8281–8303, doi:10.1175/JCLI-D-17-0898.1.

Bilskie, M. V., and S. C. Hagen, 2018: Defining Flood Zone Transitions in Low-Gradient Coastal Regions. *Geophysical Research Letters*, **45 (6)**, 2761–2770, doi:10.1002/2018GL077524.

Bloemendaal, N., H. de Moel, J. M. Mol, P. R. M. Bosma, A. N. Polen, and J. M. Collins, 2021: Adequately reflecting the severity of tropical cyclones using the new Tropical Cyclone Severity Scale. *Environmental Research Letters*, **16 (1)**, 014 048, doi:10.1088/1748-9326/abd131.

Bloemendaal, N., H. de Moel, S. Muis, I. D. Haigh, and J. C. J. H. Aerts, 2020a: Estimation of global tropical cyclone wind speed probabilities using the STORM dataset. *Scientific Data*, **7 (1)**, 377, doi:10.1038/s41597-020-00720-x.

Bloemendaal, N., I. D. Haigh, H. de Moel, S. Muis, R. J. Haarsma, and J. C. J. H. Aerts, 2020b: Generation of a global synthetic tropical cyclone hazard dataset using STORM. *Scientific Data*, **7 (1)**, 40, doi:10.1038/s41597-020-0381-2.

Bloemendaal, N., and E. E. Koks, 2022: Current and Future Tropical Cyclone Wind Risk in the Small Island Developing States. *Hurricane Risk in a Changing Climate*, J. M. Collins, and J. M. Done, Eds., Springer International Publishing, Cham, 121–142, doi:10.1007/978-3-031-08568-0_6.

Bloemendaal, N., S. Muis, R. J. Haarsma, M. Verlaan, M. Irazoqui Apecechea, H. de Moel, P. J. Ward, and J. C. J. H. Aerts, 2019: Global modeling of tropical cyclone storm surges using high-resolution forecasts. *Climate Dynamics*, **52 (7-8)**, 5031–5044, doi:10.1007/s00382-018-4430-x.

Bloemendaal, N., H. de Moel, A. B. Martinez, S. Muis, I. D. Haigh, K. van der Wiel, R. J. Haarsma, P. J. Ward, M. J. Roberts, J. C. M. Dullaart, and J. C. J. H. Aerts, 2022: A globally consistent local-scale assessment of future tropical cyclone risk. *Science Advances*, **8 (17)**, eabm8438, doi:10.1126/sciadv.abm8438.

Bradley, R., 2017: *Decision Theory with a Human Face*. Cambridge University Press, Cambridge, doi:10.1017/9780511760105.

Bradley, R., and M. Drechsler, 2014: Types of Uncertainty. *Erkenntnis*, **79 (6)**, 1225–1248, doi:10.1007/s10670-013-9518-4.

Bradley, R., and K. Steele, 2015: Making Climate Decisions. *Philosophy Compass*, **10 (11)**, 799–810, doi:10.1111/phc3.12259.

Bresch, D. N., 2016: Shaping climate resilient development: Economics of climate Adaptation. *Climate Change Adaptation Strategies - An Upstream-downstream Perspective*, Springer International Publishing, 241–254, doi:10.1007/978-3-319-40773-9_13.

Bresch, D. N., and G. Aznar-Siguan, 2021: CLIMADA v1.4.1: Towards a globally consistent adaptation options appraisal tool. *Geoscientific Model Development*, **14 (1)**, 351–363, doi:10.5194/gmd-14-351-2021.

Camargo, S. J., M. K. Tippett, A. H. Sobel, G. A. Vecchi, and M. Zhao, 2014: Testing the performance of tropical cyclone genesis indices in future climates using the HiRAM model. *Journal of Climate*, **27 (24)**, 9171–9196, doi:10.1175/JCLI-D-13-00505.1.

Camargo, S. J., and A. A. Wing, 2016: Tropical cyclones in climate models. *Wiley Interdisciplinary Reviews: Climate Change*, **7 (2)**, 211–237, doi:10.1002/wcc.373.

Cardona, O.-D., and Coauthors, 2012: Determinants of Risk: Exposure and Vulnerability. *Managing the Risks of Extreme Events and Disasters to Advance Climate Change Adaptation*, C. B. Field, V. Barros, T. F. Stocker, and Q. Dahe, Eds., Vol. 9781107025, Cambridge University Press, Cambridge, 65–108, doi:10.1017/CBO9781139177245.005.

Cardona, O.-D., M. G. Ordaz, M. G. Mora, M. A. Salgado-Gálvez, G. A. Bernal, D. Zuloaga-Romero, M. C. Marulanda Fraume, L. Yamín, and D. González, 2014: Global risk assessment: A fully probabilistic seismic and tropical cyclone wind risk assessment. *International Journal of Disaster Risk Reduction*, **10**, 461–476, doi:10.1016/j.ijdrr.2014.05.006.

Chavas, D. R., and N. Lin, 2016: A Model for the Complete Radial Structure of the Tropical Cyclone Wind Field. Part II: Wind Field Variability. *Journal of the Atmospheric Sciences*, **73 (8)**, 3093–3113, doi:10.1175/JAS-D-15-0185.1.

Chavas, D. R., N. Lin, and K. Emanuel, 2015: A model for the complete radial structure of the tropical cyclone wind field. Part I: Comparison with observed structure. *Journal of the Atmospheric Sciences*, **72 (9)**, 3647–3662, doi:10.1175/JAS-D-15-0014.1.

Ciullo, A., O. Martius, E. Strobl, and D. N. Bresch, 2021: A framework for building climate storylines based on downward counterfactuals: The case of the European Union Solidarity fund. *Climate Risk Management*, **33**, 100 349, doi:10.1016/j.crm.2021.100349.

Ciullo, A., E. Strobl, S. Meiler, O. Martius, and D. Bresch, 2023: Increasing countries' financial resilience through global catastrophe risk pooling. *Nature Communications*, **14**, doi:10.1038/s41467-023-36539-4.

Cologna, V., S. Meiler, N. Mede, C. M. Kropf, S. Lüthi, C. M. Kropf, J. Besley, S. Berger, C. Brick, M. Joubert, E. W. Maibach, S. Miheli, N. Oreskes, M. S. Schäfer, and S. van der Linden, 2023: Historical and projected prevalence of extreme weather events and attitudes towards climate change, to be submitted to *Nature Climate Change*.

Condon, M., 2023: Climate Services: The Business of Physical Risk. preprint. doi:10.2139/ssrn.4396826, url https://papers.ssrn.com/abstract=4396826.

Couasnon, A., A. Sebastian, and O. Morales-Nápoles, 2018: A Copula-based bayesian network for modeling compound flood hazard from riverine and coastal interactions at the catchment scale: An application to the houston ship channel, Texas. *Water (Switzerland)*, **10 (9)**, 1190, doi:10.3390/w10091190.

Cox, S., 2022: Inscriptions of resilience: Bond ratings and the government of climate risk in Greater Miami, Florida. *Environment and Planning A: Economy and Space*, **54 (2)**, 295–310, doi:10.1177/0308518X211054162.

Crespo Cuaresma, J., 2017: Income projections for climate change research: A framework based on human capital dynamics. *Global Environmental Change*, **42**, 226–236, doi:10.1016/j.gloenvcha.2015.02.012.

Cummins, J. D., and O. Mahul, 2009: *Catastrophe Risk Financing in Developing Countries : Principles for Public Intervention*. Washington, DC: World Bank, doi:10.1596/978-0-8213-7736-9.

Curry, J. A., and P. J. Webster, 2011: Climate Science and the Uncertainty Monster. *Bulletin of the American Meteorological Society*, **92 (12)**, 1667–1682, doi:10.1175/2011BAMS3139.1.

Danabasoglu, G., and Coauthors, 2020: The Community Earth System Model Version 2 (CESM2). *Journal of Advances in Modeling Earth Systems*, **12 (2)**, e2019MS001 916, doi:10.1029/2019MS001916.

Davis, C. A., 2018: Resolving Tropical Cyclone Intensity in Models. *Geophysical Research Letters*, **45 (4)**, 2082–2087, doi:10.1002/2017GL076966.

Dawkins, L., D. Bernie, J. Lowe, T. Economou, and F. Pianosi, 2023: Quantifying Uncertainty and Sensitivity in Climate Risk Assessments: Varying Hazard, Exposure and Vulnerability Modelling Choices. preprint. doi:10.2139/ssrn.4353832, url https://papers.ssrn.com/abstract=4353832.

de Ruiter, M. C., A. Couasnon, M. J. van den Homberg, J. E. Daniell, J. C. Gill, and P. J. Ward, 2020: Why We Can No Longer Ignore Consecutive Disasters. *Earth's Future*, **8 (3)**, doi:10.1029/2019EF001425.

Dellink, R., J. Chateau, E. Lanzi, and B. Magné, 2017: Long-term economic growth projections in the Shared Socioeconomic Pathways. *Global Environmental Change*, **42**, 200–214, doi:10.1016/j.gloenvcha.2015.06.004.

DesInventar, n.d.: United Nations DesInventar Open Source Initiative - Official Website. url https://www.desinventar.net/, Accessed on 2023-10-13.

Dixit, A. K., and R. S. Pindyck, 1994: *Investment under Uncertainty*. 1st ed., Princeton University Press.

Done, J. M., M. Ge, G. J. Holland, I. Dima-West, S. Phibbs, G. R. Saville, and Y. Wang, 2020: Modelling global tropical cyclone wind footprints. *Natural Hazards and Earth System Sciences*, **20 (2)**, 567–580, doi:10.5194/nhess-20-567-2020.

Eberenz, S., S. Lüthi, and D. N. Bresch, 2021: Regional tropical cyclone impact functions for globally consistent risk assessments. *Natural Hazards and Earth System Sciences*, **21 (1)**, 393–415, doi:10.5194/nhess-21-393-2021.

Eberenz, S., D. Stocker, T. Röösli, and D. N. Bresch, 2020: Asset exposure data for global physical risk assessment. *Earth System Science Data*, **12 (2)**, 817–833, doi:10.5194/essd-12-817-2020.

EC Earth Consortium, 2019: EC-Earth-Consortium EC-Earth3 model output prepared for CMIP6 ScenarioMIP ssp245. url https://doi.org/10.22033/ESGF/CMIP6.4880, publisher: Earth System Grid Federation, Accessed on 2023-02-16, doi:10.22033/ESGF/CMIP6.4880.

ECMWF, 2022: Integrated Forecasting System. url https://www.ecmwf.int/en/forecasts/documentation-and-support/changes-ecmwf-model, Accessed on 2023-08-14.

Eilander, D., A. Couasnon, T. Leijnse, H. Ikeuchi, D. Yamazaki, S. Muis, J. Dullaart, A. Haag, H. C. Winsemius, and P. J. Ward, 2023: A globally applicable framework for compound flood hazard modeling. *Natural Hazards and Earth System Sciences*, **23 (2)**, 823–846, doi:10.5194/nhess-23-823-2023.

Elliott, R., 2021: *Underwater: Loss, Flood Insurance, and the Moral Economy of Climate Change in the United States*. Society and the Environment, Columbia University Press.

Elsner, J. B., J. P. Kossin, and T. H. Jagger, 2008: The increasing intensity of the strongest tropical cyclones. *Nature*, **455 (7209)**, 92–95, doi:10.1038/nature07234.

Emanuel, K., 2007: Environmental Factors Affecting Tropical Cyclone Power Dissipation. *Journal of Climate*, **20 (22)**, 5497–5509, doi:10.1175/2007JCLI1571.1.

Emanuel, K., 2010: Tropical cyclone activity downscaled from NOAA-CIRES Reanalysis, 1908–1958. *Journal of Advances in Modeling Earth Systems*, **2**, 1, doi:10.3894/JAMES.2010.2.1.

Emanuel, K., 2021: Response of Global Tropical Cyclone Activity to Increasing CO2: Results from Downscaling CMIP6 Models. *Journal of Climate*, **34 (1)**, 57–70, doi:10.1175/JCLI-D-20-0367.1.

Emanuel, K., C. DesAutels, C. Holloway, and R. Korty, 2004: Environmental control of tropical cyclone intensity. *Journal of the Atmospheric Sciences*, **61 (7)**, 843–858, doi:10.1175/1520-0469(2004)061<0843:ECOTCI>2.0.CO;2.

Emanuel, K., F. Fondriest, and J. Kossin, 2012: Potential Economic Value of Seasonal Hurricane Forecasts. *Weather, Climate, and Society*, **4 (2)**, 110–117, doi:10.1175/WCAS-D-11-00017.1.

Emanuel, K., S. Ravela, E. Vivant, and C. Risi, 2006: A Statistical Deterministic Approach to Hurricane Risk Assessment. *Bulletin of the American Meteorological Society*, **87 (3)**, S1–S5, doi:10.1175/bams-87-3-emanuel.

Emanuel, K., and R. Rotunno, 2011: Self-stratification of tropical cyclone outflow. Part I: Implications for storm structure. *Journal of the Atmospheric Sciences*, **68 (10)**, 2236–2249, doi:10.1175/JAS-D-10-05024.1.

Emanuel, K., R. Sundararajan, and J. Williams, 2008: Hurricanes and global warming: Results from downscaling IPCC AR4 simulations. *Bulletin of the American Meteorological Society*, **89 (3)**, 347–367, doi:10.1175/BAMS-89-3-347.

Emanuel, K. A., 1986: An air-sea interaction theory for tropical cyclones. Part I: Steady-state maintenance. *Journal of Atmospheric Sciences*, **43 (6)**, 585–605.

Emanuel, K. A., 1987: The dependence of hurricane intensity on climate. *Nature*, **326 (6112)**, 483–485, doi:10.1038/326483a0.

Emanuel, K. A., 2008: The Hurricane - Climate Connection. *Bulletin of the American Meteorological Society*, **89 (5)**, ES10–ES20, doi:10.1175/BAMS-89-5-Emanuel.

Emanuel, K. A., 2011: Global warming effects on U.S. hurricane damage. *Weather, Climate, and Society*, **3 (4)**, 261–268, doi:10.1175/WCAS-D-11-00007.1.

Emanuel, K. A., 2013: Downscaling CMIP5 climate models shows increased tropical cyclone activity over the 21st century. *Proceedings of the National Academy of Sciences of the United States of America*, **110 (30)**, 12 219–12 224, doi:10.1073/pnas.1301293110.

Emanuel, K. A., 2017: Assessing the present and future probability of Hurricane Harvey's rainfall. *Proceedings of the National Academy of Sciences of the United States of America*, **114 (48)**, 12 681–12 684, doi:10.1073/pnas.1716222114.

Emanuel, K. A., and D. S. Nolan, 2004: Tropical cyclone activity and global climate. Publication Title: Preprints, 26th Conf. on Hurricanes and Tropical Meteorology, Miami, FL, Amer. Meteor. Soc., 240–241.

Evans, C., and Coauthors, 2017: The Extratropical Transition of Tropical Cyclones. Part I: Cyclone Evolution and Direct Impacts. *Monthly Weather Review*, **145 (11)**, 4317–4344, doi:10.1175/MWR-D-17-0027.1.

Feldmann, M., K. Emanuel, L. Zhu, and U. Lohmann, 2019: Estimation of atlantic tropical cyclone rainfall frequency in the United States. *Journal of Applied Meteorology and Climatology*, **58 (8)**, 1853–1866, doi:10.1175/JAMC-D-19-0011.1.

Fiedler, T., A. J. Pitman, K. Mackenzie, N. Wood, C. Jakob, and S. E. Perkins-Kirkpatrick, 2021: Business risk and the emergence of climate analytics. *Nature Climate Change*, **11 (2)**, 87–94, doi:10.1038/s41558-020-00984-6.

Flavelle, C., 2022: Why Ian May Push Florida Real Estate Out of Reach for All but the Super Rich. *The New York Times*.

Fleming, K., S. Parolai, A. Garcia-Aristizabal, S. Tyagunov, S. Vorogushyn, H. Kreibich, and H. Mahlke, 2016: Harmonizing and comparing single-type natural hazard risk estimations. *Annals of Geophysics*, **59 (2)**, S0216–S0216, doi:10.4401/ag-6987.

Frieler, K., and Coauthors, 2023: Scenario set-up and forcing data for impact model evaluation and impact attribution within the third round of the Inter-Sectoral Model Intercomparison Project (ISIMIP3a). preprint. doi:10.5194/egusphere-2023-281, url https://egusphere.copernicus.org/preprints/2023/egusphere-2023-281/.

Füssel, H.-M., 2007: Vulnerability: A generally applicable conceptual framework for climate change research. *Global Environmental Change*, **17 (2)**, 155–167, doi:10.1016/j.gloenvcha.2006.05.002.

gabrielaznar, and Coauthors, 2022: CLIMADA-project/climada_python: v3.2.0. Zenodo, url https://zenodo.org/record/6807463, doi:10.5281/zenodo.6807463.

Garner, A. J., M. E. Mann, K. A. Emanuel, R. E. Kopp, N. Lin, R. B. Alley, B. P. Horton, R. M. DeConto, J. P. Donnelly, and D. Pollard, 2017: Impact of climate change on New York City's coastal flood hazard: Increasing flood heights from the preindustrial to 2300 CE. *Proceedings of the National Academy of Sciences of the United States of America*, **114 (45)**, 11 861–11 866, doi:10.1073/pnas.1703568114.

Geiger, T., K. Frieler, and D. N. Bresch, 2018: A global historical data set of tropical cyclone exposure (TCE-DAT). *Earth System Science Data*, **10 (1)**, 185–194, doi:10.5194/essd-10-185-2018.

Geiger, T., J. Gütschow, D. N. Bresch, and K. Emanuel, 2021: Double benefit of limiting global warming for tropical cyclone exposure. *Nature Climate Change 2021*, **11**, 861–866, doi:10.1038/s41558-021-01157-9.

Gettelman, A., D. N. Bresch, C. C. Chen, J. E. Truesdale, and J. T. Bacmeister, 2018: Projections of future tropical cyclone damage with a high-resolution global climate model. *Climatic Change*, **146 (3-4)**, 575–585, doi:10.1007/s10584-017-1902-7.

Ghirardato, P., F. Maccheroni, and M. Marinacci, 2004: Differentiating ambiguity and ambiguity attitude. *Journal of Economic Theory*, **118 (2)**, 133–173, doi:10.1016/j.jet.2003.12.004.

Gilboa, I., and M. Marinacci, 2016: Ambiguity and the Bayesian Paradigm. *Readings in Formal Epistemology: Sourcebook*, H. Arló-Costa, V. F. Hendricks, and J. van Benthem, Eds., Springer Graduate Texts in Philosophy, Springer International Publishing, Cham, 385–439, doi:10.1007/978-3-319-20451-2_21.

Gill, J. C., and B. D. Malamud, 2014: Reviewing and visualizing the interactions of natural hazards: Interactions of Natural Hazards. *Reviews of Geophysics*, **52 (4)**, 680–722, doi:10.1002/2013RG000445.

Gill, J. C., and B. D. Malamud, 2016: Hazard interactions and interaction networks (cascades) within multi-hazard methodologies. *Earth System Dynamics*, **7 (3)**, 659–679, doi:10.5194/esd-7-659-2016.

Gollier, C., and N. Treich, 2003: Decision-Making Under Scientific Uncertainty: The Economics of the Precautionary Principle. *Journal of Risk and Uncertainty*, **27 (1)**, 77–103.

Gori, A., N. Lin, and J. Smith, 2020: Assessing Compound Flooding From Landfalling Tropical Cyclones on the North Carolina Coast. *Water Resources Research*, **56 (4)**, doi:10.1029/2019WR026788.

Gori, A., N. Lin, D. Xi, and K. Emanuel, 2022: Tropical cyclone climatology change greatly exacerbates US extreme rainfall–surge hazard. *Nature Climate Change 2022 12:2*, **12 (2)**, 171–178, doi:10.1038/s41558-021-01272-7.

Gray, I., 2021: Hazardous simulations: Pricing climate risk in US coastal insurance markets. *Economy and Society*, **50 (2)**, 196–223, doi:10.1080/03085147.2020.1853358.

Guha-Sapir, D., 2023: EM-DAT disaster risk database. url https://www.emdat.be/, place: Brussels, Belgium Publisher: CRED/UCLouvain.

Gutmann, E. D., R. M. Rasmussen, C. Liu, K. Ikeda, C. L. Bruyere, J. M. Done, L. Garrè, P. Friis-Hansen, and V. Veldore, 2018: Changes in Hurricanes from a 13-Yr Convection-Permitting Pseudo–Global Warming Simulation. *Journal of Climate*, **31 (9)**, 3643–3657, doi:10.1175/JCLI-D-17-0391.1.

Ha, Y.-C., 2018: Proposal of Return Period and Basic Wind Speed Map to Estimate Wind Loads for Strength Design in Korea. *Journal of the Architectural Institute of Korea Structure & Construction*, **34 (2)**, 29–40, doi:10.5659/JAIK_SC.2018.34.2.29.

Hain, L. I., J. F. Kölbel, and M. Leippold, 2022: Let's get physical: Comparing metrics of physical climate risk. *Finance Research Letters*, **46**, 102 406, doi:10.1016/j.frl.2021.102406.

Hallegatte, S., A. Vogt-Schilb, M. Bangalore, and J. Rozenberg, 2017: *Unbreakable: Building the Resilience of the Poor in the Face of Natural Disasters*. Washington, DC: World Bank, doi:10.1596/978-1-4648-1003-9.

Hansen, L. P., and T. J. Sargent, 2008: *Robustness*. Princeton University Press.

Hansson, S. O., 2016: Evaluating the Uncertainties. *The Argumentative Turn in Policy Analysis: Reasoning about Uncertainty*, S. O. Hansson, and G. Hirsch Hadorn, Eds., Logic, Argumentation & Reasoning, Springer International Publishing, Cham, 79–104, doi:10.1007/978-3-319-30549-3_4.

Hausfather, Z., K. Marvel, G. A. Schmidt, J. W. Nielsen-Gammon, and M. Zelinka, 2022: Climate simulations: recognize the 'hot model' problem. *Nature*, **605 (7908)**, 26–29, doi:10.1038/d41586-022-01192-2.

Hawkins, E., and R. Sutton, 2009: The Potential to Narrow Uncertainty in Regional Climate Predictions. *Bulletin of the American Meteorological Society*, **90 (8)**, 1095–1108, doi:10.1175/2009BAMS2607.1.

He, H., B. Soden, and R. J. Kramer, 2022: On the Prevalence of High Climate Sensitivity Models. preprint, Climatology (Global Change). doi:10.1002/essoar.10512532.1, url https://essopenarchive.org/doi/full/10.1002/essoar.10512532.1.

Heal, G., and A. Millner, 2014: Reflections Uncertainty and Decision Making in Climate Change Economics. *Review of Environmental Economics and Policy*, **8 (1)**, 120–137, doi:10.1093/reep/ret023.

Henrion, M., and M. G. Morgan, 1990: The Nature and Sources of Uncertainty. *Uncertainty: A Guide to Dealing with Uncertainty in Quantitative Risk and Policy Analysis*, Cambridge University Press, Cambridge, 47–72, doi:10.1017/CBO9780511840609.005.

Herdman, L., L. Erikson, and P. Barnard, 2018: Storm surge propagation and flooding in small tidal rivers during events of mixed coastal and fluvial influence. *Journal of Marine Science and Engineering*, **6 (4)**, 158, doi:10.3390/JMSE6040158.

Herman, J., and W. Usher, 2017: SALib: An open-source Python library for Sensitivity Analysis. *Journal of Open Source Software*, **2 (9)**, 97, doi:10.21105/joss.00097.

Hersbach, H., B. Bell, P. Berrisford, A. Horányi, J. M. Sabater, J. Nicolas, R. Radu, D. Schepers, A. Simmons, C. Soci, and D. Dee, 2019: Global reanalysis: goodbye ERA-Interim, hello ERA5. *ECMWF Newsletter*, **(159)**, 17–24, doi:10.21957/vf291hehd7.

Hewitt, C., S. Mason, and D. Walland, 2012: The Global Framework for Climate Services. *Nature Climate Change*, **2 (12)**, 831–832, doi:10.1038/nclimate1745.

Hill, B., 2013: Confidence and decision. *Games and Economic Behavior*, **82**, 675–692, doi:10.1016/j.geb.2013.09.009.

Hillier, J. K., T. Matthews, R. L. Wilby, and C. Murphy, 2020: Multi-hazard dependencies can increase or decrease risk. *Nature Climate Change*, **10 (7)**, 595–598, doi:10.1038/s41558-020-0804-2.

Hinkel, J., 2011: "Indicators of vulnerability and adaptive capacity": Towards a clarification of the science–policy interface. *Global Environmental Change*, **21 (1)**, 198–208, doi:10.1016/j.gloenvcha.2010.08.002.

Holland, G., 2008: A revised hurricane pressure-wind model. *Monthly Weather Review*, **136 (9)**, 3432–3445, doi:10.1175/2008MWR2395.1.

Holland, G. J., J. I. Belanger, and A. Fritz, 2010: A Revised Model for Radial Profiles of Hurricane Winds. *Monthly Weather Review*, **138 (12)**, 4393–4401, doi:10.1175/2010MWR3317.1.

Hourdin, F., and Coauthors, 2020: LMDZ6A: The Atmospheric Component of the IPSL Climate Model With Improved and Better Tuned Physics. *Journal of Advances in Modeling Earth Systems*, **12 (7)**, e2019MS001 892, doi:10.1029/2019MS001892.

Hsiang, S., and A. Jina, 2014: The Causal Effect of Environmental Catastrophe on Long-Run Economic Growth: Evidence From 6,700 Cyclones. Tech. Rep. w20352, National Bureau of Economic Research, Cambridge, MA, w20352 pp. doi:10.3386/w20352, url http://www.nber.org/papers/w20352.pdf.

IIASA, 2009: RCP Database (Version 2.0.5). url https://tntcat.iiasa.ac.at/RcpDb/, Accessed on 2023-09-18.

IMF, 2021: Dominica: Disaster Resilience Strategy. *IMF Staff Country Reports*, **2021 (182)**, 1, doi:10.5089/9781513588469.002.

IPCC, 2012: *Managing the Risks of Extreme Events and Disasters to Advance Climate Change Adaptation. A Special Report of Working Groups I and II of the Intergovernmental Panel on Climate Change [Field, C.B., V. Barros, T.F. Stocker, D. Qin, D.J. Dokken, K.L. Ebi, M.D.* Cambridge University Press, doi:10.1017/CBO9781139177245.

ISO, 2009: ISO 31000:2009(en), Risk management - Principles and guidelines. manual.

ISO, 2018: ISO 31000:2018(en), Risk management - Guidelines. manual.

Jarzabkowski, P., K. Chalkias, E. Cacciatori, and R. Bednarek, 2023: *Disaster Insurance Reimagined: Protection in a Time of Increasing Risk*. 1st ed., Oxford University PressOxford, doi:10.1093/oso/9780192865168.001.0001.

Jing, R., N. Lin, K. Emanuel, G. Vecchi, and T. R. Knutson, 2021: A Comparison of Tropical Cyclone Projections in a High-resolution Global Climate Model and from Downscaling by Statistical and Statistical-deterministic Methods. *Journal of Climate*, **34 (23)**, 9349–9364, doi:10.1175/jcli-d-21-0071.1.

Jones, S. C., P. A. Harr, J. Abraham, L. F. Bosart, P. J. Bowyer, J. L. Evans, D. E. Hanley, B. N. Hanstrum, R. E. Hart, F. Lalaurette, M. R. Sinclair, R. K. Smith, and C. Thorncroft, 2003: The Extratropical Transition of Tropical Cyclones: Forecast Challenges, Current Understanding, and Future Directions. *Weather and Forecasting*, **18 (6)**, 1052–1092, doi:10.1175/1520-0434(2003)018<1052:TETOTC>2.0.CO;2.

Joyette, A. R., L. A. Nurse, and R. S. Pulwarty, 2015: Disaster risk insurance and catastrophe models in risk-prone small Caribbean islands. *Disasters*, **39 (3)**, 467–492, doi:10.1111/disa.12118.

Kang, N.-Y., and J. B. Elsner, 2015: Trade-off between intensity and frequency of global tropical cyclones. *Nature Climate Change*, **5 (7)**, 661–664, doi:10.1038/nclimate2646.

Keenan, J. M., 2019: A climate intelligence arms race in financial markets. *Science*, **365 (6459)**, 1240–1243, doi:10.1126/science.aay8442.

Khanal, S., N. Ridder, H. de Vries, W. Terink, and B. van den Hurk, 2018: Storm surge and extreme river discharge: a compound event analysis using ensemble impact modelling. *Hydrology and Earth System Sciences Discussions*, 1–25, doi:10.5194/hess-2018-103.

Kim, H.-S., G. A. Vecchi, T. R. Knutson, W. G. Anderson, T. L. Delworth, A. Rosati, F. Zeng, and M. Zhao, 2014: Tropical Cyclone Simulation and Response to CO2 Doubling in the GFDL CM2.5 High-Resolution Coupled Climate Model. *Journal of Climate*, **27 (21)**, 8034–8054, doi:10.1175/JCLI-D-13-00475.1.

Kleppek, S., V. Muccione, C. C. Raible, D. N. Bresch, P. Koellner-Heck, and T. F. Stocker, 2008: Tropical cyclones in ERA-40: A detection and tracking method. *Geophysical Research Letters*, **35 (10)**, doi:10.1029/2008GL033880.

Klibanoff, P., M. Marinacci, and S. Mukerji, 2005: A Smooth Model of Decision Making under Ambiguity. *Econometrica*, **73 (6)**, 1849–1892.

Klotzbach, P. J., C. J. Schreck, J. M. Collins, M. M. Bell, E. S. Blake, and D. Roache, 2018: The extremely active 2017 North Atlantic hurricane season. *Monthly Weather Review*, **146 (10)**, 3425–3443, doi:10.1175/MWR-D-18-0078.1.

Knabb, R. D., J. R. Rhome, and D. P. Brown, 2005: Hurricane Katrina: August 23–30, 2005. Tropical Cyclone Report, United States National Oceanic and Atmospheric Administration's National Weather Service. url https://www.nhc.noaa.gov/pdf/TCR-AL122005_Katrina.pdf.

Knapp, k. R., J. A. Knaff, C. R. Sampson, G. M. Riggio, and A. D. Schnapp, 2013: A pressure-based analysis of the historical Western North pacific tropical cyclone intensity record. *Monthly Weather Review*, **141 (8)**, 2611–2631, doi:10.1175/MWR-D-12-00323.1.

Knapp, K. R., M. C. Kruk, D. H. Levinson, H. J. Diamond, and C. J. Neumann, 2010: The International Best Track Archive for Climate Stewardship (IBTrACS). *Bulletin of the American Meteorological Society*, **91 (3)**, 363–376, doi:10.1175/2009BAMS2755.1.

Knutson, T., S. J. Camargo, J. C. L. Chan, K. Emanuel, C.-H. Ho, J. Kossin, M. Mohapatra, M. Satoh, M. Sugi, K. Walsh, and L. Wu, 2019: Tropical Cyclones and Climate Change Assessment: Part I: Detection and Attribution. *Bulletin of the American Meteorological Society*, **100 (10)**, 1987–2007, doi:10.1175/BAMS-D-18-0189.1.

Knutson, T., S. J. Camargo, J. C. Chan, K. Emanuel, C. H. Ho, J. Kossin, M. Mohapatra, M. Satoh, M. Sugi, K. Walsh, and L. Wu, 2020: Tropical cyclones and climate change assessment part II: Projected response to anthropogenic warming. *Bulletin of the American Meteorological Society*, **101 (3)**, E303–E322, doi:10.1175/BAMS-D-18-0194.1.

Knutson, T. R., J. J. Sirutis, M. Zhao, R. E. Tuleya, M. Bender, G. A. Vecchi, G. Villarini, and D. Chavas, 2015: Global projections of intense tropical cyclone activity for the late twenty-first century from dynamical downscaling of CMIP5/RCP4.5 scenarios. *Journal of Climate*, **28 (18)**, 7203–7224, doi:10.1175/JCLI-D-15-0129.1.

Knutson, T. R., J. J. Sirutis, G. A. Vecchi, S. Garner, M. Zhao, H.-S. Kim, M. Bender, R. E. Tuleya, I. M. Held, and G. Villarini, 2013: Dynamical Downscaling Projections of Twenty-First-Century Atlantic Hurricane Activity: CMIP3 and CMIP5 Model-Based Scenarios. *Journal of Climate*, **26 (17)**, 6591–6617, doi:10.1175/JCLI-D-12-00539.1.

Knutti, R., 2018: Climate Model Confirmation: From Philosophy to Predicting Climate in the Real World. *Climate Modelling: Philosophical and Conceptual Issues*, E. A. Lloyd, and E. Winsberg, Eds., Springer International Publishing, Cham, 325–359, doi:10.1007/978-3-319-65058-6_11.

Knüsel, B., C. Baumberger, M. Zumwald, D. N. Bresch, and R. Knutti, 2020: Argument-based assessment of predictive uncertainty of data-driven environmental models. *Environmental Modelling & Software*, **134**, 104 754, doi:10.1016/j.envsoft.2020.104754.

Kossin, J. P., 2018: A global slowdown of tropical-cyclone translation speed. *Nature*, **558 (7708)**, 104–107, doi:10.1038/s41586-018-0158-3.

Kossin, J. P., K. A. Emanuel, and S. J. Camargo, 2016: Past and Projected Changes in Western North Pacific Tropical Cyclone Exposure. *Journal of Climate*, **29 (16)**, 5725–5739, doi:10.1175/JCLI-D-16-0076.1.

Kossin, J. P., K. A. Emanuel, and G. A. Vecchi, 2014: The poleward migration of the location of tropical cyclone maximum intensity. *Nature*, **509 (7500)**, 349–352, doi:10.1038/nature13278.

Kossin, J. P., K. R. Knapp, T. L. Olander, and C. S. Velden, 2020: Global increase in major tropical cyclone exceedance probability over the past four decades. *Proceedings of the National Academy of Sciences of the United States of America*, **117 (22)**, doi:10.1073/pnas.1920849117.

Kossin, J. P., T. L. Olander, and K. R. Knapp, 2013: Trend analysis with a new global record of tropical cyclone intensity. *Journal of Climate*, **26 (24)**, 9960–9976, doi:10.1175/JCLI-D-13-00262.1.

Krichene, H., T. Vogt, F. Piontek, T. Geiger, C. Schötz, and C. Otto, 2023: The social costs of tropical cyclones. *Nature Communications*, **14 (1)**, 7294, doi:10.1038/s41467-023-43114-4.

Kropf, C. M., A. Ciullo, L. Otth, S. Meiler, A. Rana, E. Schmid, J. W. McCaughey, and D. N. Bresch, 2022: Uncertainty and sensitivity analysis for probabilistic weather and climate-risk modelling: an implementation in CLIMADA v.3.1.0. *Geoscientific Model Development*, **15 (18)**, 7177–7201, doi:10.5194/gmd-15-7177-2022.

Kumbier, K., R. C. Carvalho, A. T. Vafeidis, and C. D. Woodroffe, 2018: Investigating compound flooding in an estuary using hydrodynamic modelling: A case study from the Shoalhaven River, Australia. *Natural Hazards and Earth System Sciences*, **18 (2)**, 463–477, doi:10.5194/nhess-18-463-2018.

Kunreuther, H., 2000: Insurance as Cornerstone for Public-Private Sector Partnerships. *Natural Hazards Review*, **1 (2)**, 126–136, doi:10.1061/(ASCE)1527-6988(2000)1:2(126).

Lanzante, J. R., 2019: A global slowdown of tropical-cyclone translation speed. *Nature*, **570 (7759)**, E6–E15, doi:10.1038/s41586-019-1223-2.

Lark, J., 2015: *ISO 31000 risk management: A practical guide for SMEs*. ISO.

Lee, C. Y., S. J. Camargo, A. H. Sobel, and M. K. Tippett, 2020: Statistical–Dynamical Downscaling Projections of Tropical Cyclone Activity in a Warming Climate: Two Diverging Genesis Scenarios. *Journal of Climate*, **33 (11)**, 4815–4834, doi:10.1175/jcli-d-19-0452.1.

Lee, C. Y., M. K. Tippett, A. H. Sobel, and S. J. Camargo, 2016: Autoregressive modeling for tropical cyclone intensity climatology. *Journal of Climate*, **29 (21)**, 7815–7830, doi:10.1175/JCLI-D-15-0909.1.

Lee, C. Y., M. K. Tippett, A. H. Sobel, and S. J. Camargo, 2018: An environmentally forced tropical cyclone hazard model. *Journal of Advances in Modeling Earth Systems*, **10 (1)**, 223–241, doi:10.1002/2017MS001186.

Leimbach, M., E. Kriegler, N. Roming, and J. Schwanitz, 2017: Future growth patterns of world regions – A GDP scenario approach. *Global Environmental Change*, **42**, 215–225, doi:10.1016/j.gloenvcha.2015.02.005.

Lemieux, C., 2009: *Monte Carlo and Quasi-Monte Carlo Sampling*. Springer Science & Business Media.

Lempert, R. J., D. G. Groves, S. W. Popper, and S. C. Bankes, 2006: A General, Analytic Method for Generating Robust Strategies and Narrative Scenarios. *Management Science*, **52 (4)**, 514–528, doi:10.1287/mnsc.1050.0472.

Leobacher, G., and F. Pillichshammer, 2014: *Introduction to Quasi-Monte Carlo Integration and Applications*. Compact Textbooks in Mathematics, Springer International Publishing, Cham, doi:10.1007/978-3-319-03425-6.

Li, L., 2019: CAS FGOALS-g3 model output prepared for CMIP6 ScenarioMIP ssp245. url https://doi.org/10.22033/ESGF/CMIP6.3469, publisher: Earth System Grid Federation, Accessed on 2023-02-16, doi:10.22033/ESGF/CMIP6.3469.

Li, S., and F. E. L. Otto, 2022: The role of human-induced climate change in heavy rainfall events such as the one associated with Typhoon Hagibis. *Climatic Change*, **172 (1)**, 7, doi:10.1007/s10584-022-03344-9.

Lin, N., K. Emanuel, M. Oppenheimer, and E. Vanmarcke, 2012: Physically based assessment of hurricane surge threat under climate change. *Nature Climate Change*, **2 (6)**, 462–467, doi:10.1038/nclimate1389.

Linnerooth-Bayer, J., and S. Hochrainer-Stigler, 2015: Financial instruments for disaster risk management and climate change adaptation. *Climatic Change*, **133 (1)**, 85–100, doi:10.1007/s10584-013-1035-6.

Little, C. M., R. M. Horton, R. E. Kopp, M. Oppenheimer, G. A. Vecchi, and G. Villarini, 2015: Joint projections of US East Coast sea level and storm surge. *Nature Climate Change*, **5 (12)**, 1114–1120, doi:10.1038/nclimate2801.

Liu, I. C., S. J. Camargo, and A. H. Sobel, 2021: Understanding differences in tropical cyclone activity over the arabian sea and bay of bengal. *Mausam*, **72 (1)**, 187–198, doi:10.54302/mausam.v72i1.3591.

Liu, J., Z. Chen, and J. Li, 2020: The Comparison of the Tropical Cyclone Number Over the Western North Pacific Between Summer and Autumn. *Frontiers in Earth Science*, **8**, 533, doi:10.3389/feart.2020.597912.

Liu, M., G. A. Vecchi, J. A. Smith, and H. Murakami, 2018: Projection of Landfalling–Tropical Cyclone Rainfall in the Eastern United States under Anthropogenic Warming. *Journal of Climate*, **31 (18)**, 7269–7286, doi:10.1175/JCLI-D-17-0747.1.

Lohmann, U., F. Lüönd, and F. Mahrt, 2016: *An Introduction to Clouds: From the Microscale to Climate*. 1st ed., Cambridge University Press, doi:10.1017/CBO9781139087513.

Mandli, K. T., A. J. Ahmadia, M. Berger, D. Calhoun, D. L. George, Y. Hadjimichael, D. I. Ketcheson, G. I. Lemoine, and R. J. LeVeque, 2016: Clawpack: Building an open source ecosystem for solving hyperbolic PDEs. *PeerJ Computer Science*, **2016 (8)**, e68, doi:10.7717/peerj-cs.68.

Marks, D. G., 1992: The Beta and advection model for hurricane track forecasting. url https://repository.library.noaa.gov/view/noaa/7184, series Title: NOAA technical memorandum NWS NMC ; 70.

Mayer, L., K. Loaa, B. Cwik, N. Tuana, K. Keller, C. Gonnerman, A. Parker, and R. Lempert, 2017: Understanding Scientists' Computational Modeling Decisions About Climate Risk Management Strategies Using Values-Informed Mental Models. *Global Environmental Change*, **42**, 107–116, doi:10.1016/j.gloenvcha.2016.12.007.

McInnes, K. L., K. J. E. Walsh, R. K. Hoeke, J. G. O'Grady, F. Colberg, and G. D. Hubbert, 2014: Quantifying storm tide risk in Fiji due to climate variability and change. *Global and Planetary Change*, **116**, 115–129, doi:10.1016/j.gloplacha.2014.02.004.

Mcinnes, K. L., K. J. E. Walsh, G. D. Hubbert, and T. Beer, 2003: Impact of Sea-level Rise and Storm Surges on a Coastal Community. *Natural Hazards*, **30 (2)**, 187–207, doi:10.1023/A:1026118417752.

Meiler, S., 2023: simonameiler/TC_future_mit: v1.0.0. Zenodo, url https://zenodo.org/record/8073353, doi:10.5281/zenodo.8073353.

Meiler, S., G. L. Britten, S. Dutkiewicz, M. R. Gradoville, P. H. Moisander, O. Jahn, and M. J. Follows, 2022a: Constraining uncertainties of diazotroph biogeography from nifH gene abundance. *Limnology and Oceanography*, **67 (4)**, 816–829, doi:10.1002/lno.12036.

Meiler, S., G. L. Britten, S. Dutkiewicz, P. H. Moisander, and M. J. Follows, 2023a: Challenges and opportunities in connecting gene count observations with ocean biogeochemical models: Reply to Zehr and Riemann (2023). *Limnology and Oceanography*, **68 (6)**, 1413–1416, doi:10.1002/lno.12363.

Meiler, S., A. Ciullo, D. N. Bresch, and C. M. Kropf, 2023b: Uncertainty and sensitivity analysis for probabilistic, global modelling of future tropical cyclone risk. *14th International Conference on Applications of Statistics and Probability in Civil Engineering, ICASP14*, Dublin, Ireland, 8, doi:https://doi.org/10.25546/103244, url http://hdl.handle.net/2262/103244.

Meiler, S., A. Ciullo, C. M. Kropf, K. Emanuel, and D. N. Bresch, 2023c: Uncertainties and sensitivities in the quantification of future tropical cyclone risk. *Communications Earth & Environment*, **4 (1)**, 1–10, doi:10.1038/s43247-023-00998-w.

Meiler, S., and T. Vogt, 2022: simonameiler/TC_model_comparison: v1.0.0. url https://doi.org/10.5281/zenodo.6782091#.Yr1IQObAm3s.mendeley, doi:10.5281/ZENODO.6782091.

Meiler, S., T. Vogt, N. Bloemendaal, A. Ciullo, C.-Y. Lee, S. J. Camargo, K. Emanuel, and D. N. Bresch, 2022b: Intercomparison of regional loss estimates from global synthetic tropical cyclone models. *Nature Communications*, **13 (1)**, 6156, doi:10.1038/s41467-022-33918-1.

Mendelsohn, R., K. Emanuel, S. Chonabayashi, and L. Bakkensen, 2012: The impact of climate change on global tropical cyclone damage. *Nature Climate Change*, **2 (3)**, 205–209, doi:10.1038/nclimate1357.

Meng, W., K. Zhang, H. Liu, and M. A. Hussain, 2023: Dynamical characteristics of Amphan and its impact on COVID-19 cases in Bangladesh. *Meteorology and Atmospheric Physics*, **135 (2)**, 13, doi:10.1007/s00703-023-00950-9.

Merz, B., and Coauthors, 2020: Impact Forecasting to Support Emergency Management of Natural Hazards. *Reviews of Geophysics*, **58 (4)**, 1–52, doi:10.1029/2020rg000704.

Mester, B., T. Vogt, S. Bryant, C. Otto, K. Frieler, and J. Schewe, 2023: Human displacements from tropical cyclone Idai attributable to climate change. preprint, Sea, Ocean and Coastal Hazards. doi:10.5194/egusphere-2022-1308, url https://egusphere.copernicus.org/preprints/2023/egusphere-2022-1308/.

Mitchell, D., and Coauthors, 2022: Increased population exposure to Amphan-scale cyclones under future climates. *Climate Resilience and Sustainability*, **1 (2)**, e36, doi:10.1002/cli2.36.

Moftakhari, H., J. E. Schubert, A. AghaKouchak, R. A. Matthew, and B. F. Sanders, 2019: Linking statistical and hydrodynamic modeling for compound flood hazard assessment in tidal channels and estuaries. *Advances in Water Resources*, **128**, 28–38, doi:10.1016/j.advwatres.2019.04.009.

Montgomery, M., and R. Smith, 2014: Paradigms for tropical cyclone intensification. *Australian Meteorological and Oceanographic Journal*, **64 (1)**, 37–66, doi:10.22499/2.6401.005.

Montgomery, M. T., and R. K. Smith, 2017: Recent Developments in the Fluid Dynamics of Tropical Cyclones. *Annual Review of Fluid Mechanics*, **49 (1)**, 541–574, doi:10.1146/annurev-fluid-010816-060022.

Moon, I. J., S. H. Kim, and J. C. Chan, 2019: Climate change and tropical cyclone trend. *Nature*, **570 (7759)**, E3–E5, doi:10.1038/s41586-019-1222-3.

Moss, R. H., and Coauthors, 2010: The next generation of scenarios for climate change research and assessment. *Nature*, **463 (7282)**, 747–756, doi:10.1038/nature08823.

Murakami, H., and M. Sugi, 2010: Effect of Model Resolution on Tropical Cyclone Climate Projections. *Sola*, **6**, 73–76, doi:10.2151/sola.2010-019.

Murakami, H., G. A. Vecchi, S. Underwood, T. L. Delworth, A. T. Wittenberg, W. G. Anderson, J.-H. Chen, R. G. Gudgel, L. M. Harris, S.-J. Lin, and F. Zeng, 2015: Simulation and Prediction of Category 4 and 5 Hurricanes in the High-Resolution GFDL HiFLOR Coupled Climate Model. *Journal of Climate*, **28 (23)**, 9058–9079, doi:10.1175/JCLI-D-15-0216.1.

Mühlhofer, E., E. E. Koks, C. M. Kropf, G. Sansavini, and D. N. Bresch, 2023: A generalized natural hazard risk modelling framework for infrastructure failure cascades. *Reliability Engineering & System Safety*, **234**, 109 194, doi:10.1016/j.ress.2023.109194.

Müller, W. A., and Coauthors, 2018: A Higher-resolution Version of the Max Planck Institute Earth System Model (MPI-ESM1.2-HR). *Journal of Advances in Modeling Earth Systems*, **10 (7)**, 1383–1413, doi:10.1029/2017MS001217.

NDRRMC, 2014: FINAL REPORT re EFFECTS of Typhoon "YOLANDA" (HAIYAN). url https://web.archive.org/web/20201105102044/http://ndrrmc.gov.ph/attachments/article/1329/FINAL_REPORT_re_Effects_of_Typhoon_YOLANDA_HAIYAN_06-09NOV2013.pdf, Accessed on 2023-10-16.

Nissan, H., L. Goddard, E. C. de Perez, J. Furlow, W. Baethgen, M. C. Thomson, and S. J. Mason, 2019: On the use and misuse of climate change projections in international development. *WIREs Climate Change*, **10 (3)**, e579, doi:10.1002/wcc.579.

NOAA, 2021: Costliest US tropical cyclones. url www.ncdc.noaa.gov/billions/dcmi.pdf, Accessed on 2021-03-05.

NOAA National Centers for Environmental Information (NCEI), 2023: U.S. Billion-Dollar Weather and Climate Disasters. url https://www.ncdc.noaa.gov/billions, Accessed on 2022-10-15, doi:10.25921/stkw-7w73.

Noy, I., 2016: The socio-economics of cyclones. *Nature Climate Change*, **6 (4)**, 343–345, doi:10.1038/nclimate2975.

Oppenheimer, M., M. Campos, R. Warren, J. Birkmann, G. Luber, B. O'Neill, K. Takahashi, M. Brklacich, S. Semenov, R. Licker, and S. Hsiang, 2014: Emergent risks and key vulnerabilities. *Climate Change 2014 Impacts, Adaptation and Vulnerability: Part A: Global and Sectoral Aspects*, Cambridge University Press, 1039–1100, doi:10.1017/CBO9781107415379.024.

Orton, P. M., F. R. Conticello, F. Cioffi, T. M. Hall, N. Georgas, U. Lall, A. F. Blumberg, and K. MacManus, 2020: Flood hazard assessment from storm tides, rain and sea level rise for a tidal river estuary. *Natural Hazards*, **102 (2)**, 729–757, doi:10.1007/s11069-018-3251-x.

Otto, C., K. Kuhla, T. Geiger, J. Schewe, and K. Frieler, 2023: Better insurance could effectively mitigate the increase in economic growth losses from U.S. hurricanes under global warming. *Science Advances*, **9 (1)**, eadd6616, doi:10.1126/sciadv.add6616.

Parker, W. S., 2010: Predicting weather and climate: Uncertainty, ensembles and probability. *Studies in History and Philosophy of Science Part B: Studies in History and Philosophy of Modern Physics*, **41 (3)**, 263–272, doi:10.1016/j.shpsb.2010.07.006.

Parks, R. M., V. Kontis, G. B. Anderson, J. W. Baldwin, G. Danaei, R. Toumi, F. Dominici, M. Ezzati, and M.-A. Kioumourtzoglou, 2023: Short-term excess mortality following tropical cyclones in the United States. *Science Advances*, **9 (33)**, eadg6633, doi:10.1126/sciadv.adg6633.

Pasch, R. J., A. B. Penny, and R. Berg, 2017: Hurricane Maria. *National Hurricane Center*, **5 (April)**, 16–30.

Paulik, R., N. Horspool, R. Woods, N. Griffiths, T. Beale, C. Magill, A. Wild, B. Popovich, G. Walbran, and R. Garlick, 2022: RiskScape: a flexible multi-hazard risk modelling engine. *Natural Hazards*, doi:10.1007/s11069-022-05593-4.

Peduzzi, P., B. Chatenoux, H. Dao, A. De Bono, C. Herold, J. Kossin, F. Mouton, and O. Nordbeck, 2012: Global trends in tropical cyclone risk. *Nature Climate Change*, **2 (4)**, 289–294, doi:10.1038/nclimate1410.

Pianosi, F., K. Beven, J. Freer, J. W. Hall, J. Rougier, D. B. Stephenson, and T. Wagener, 2016: Sensitivity analysis of environmental models: A systematic review with practical workflow. *Environmental Modelling & Software*, **79**, 214–232, doi:10.1016/j.envsoft.2016.02.008.

Pielke, R. A., J. Gratz, C. W. Landsea, D. Collins, M. A. Saunders, and R. Musulin, 2008: Normalized Hurricane Damage in the United States: 1900–2005. *Natural Hazards Review*, **9 (1)**, 29–42, doi:10.1061/(ASCE)1527-6988(2008)9:1(29).

Pitman, A. J., T. Fiedler, N. Ranger, C. Jakob, N. Ridder, S. Perkins-Kirkpatrick, N. Wood, and G. Abramowitz, 2022: Acute climate risks in the financial system: examining the utility of climate model projections. *Environmental Research: Climate*, **1 (2)**, 025 002, doi:10.1088/2752-5295/ac856f.

Pugh, D., and P. Woodworth, 2014: *Sea-Level Science*. Cambridge University Press, Cambridge, doi:10.1017/CBO9781139235778.

Rana, A., Q. Zhu, A. Detken, K. Whalley, and C. Castet, 2022: Strengthening climate-resilient development and transformation in Viet Nam. *Climatic Change*, **170 (1-2)**, 1–23, doi:10.1007/s10584-021-03290-y.

Ranger, N. A., O. Mahul, and I. Monasterolo, 2022: *Assessing Financial Risks from Physical Climate Shocks: A Framework for Scenario Generation*. World Bank, doi:10.1596/37041.

Rappin, E. D., D. S. Nolan, and K. A. Emanuel, 2010: Thermodynamic control of tropical cyclogenesis in environments of radiative-convective equilibrium with shear: Tropical Cyclogenesis in Variable Climates. *Quarterly Journal of the Royal Meteorological Society*, **136 (653)**, 1954–1971, doi:10.1002/qj.706.

Ray, T., E. Stepinski, A. Sebastian, and P. B. Bedient, 2011: Dynamic Modeling of Storm Surge and Inland Flooding in a Texas Coastal Floodplain. *Journal of Hydraulic Engineering*, **137 (10)**, 1103–1110, doi:10.1061/(asce)hy.1943-7900.0000398.

Red Cross 510, 2021: Impact Based Forecasting for typhoons in the Philippines. url https://www.forecast-based-financing.org/wp-content/uploads/2020/09/Impact-based-forecasting-, Accessed on 2022-02-28.

Riahi, K., and Coauthors, 2017: The Shared Socioeconomic Pathways and their energy, land use, and greenhouse gas emissions implications: An overview. *Global Environmental Change*, **42**, 153–168, doi:10.1016/j.gloenvcha.2016.05.009.

Risser, M. D., and M. F. Wehner, 2017: Attributable Human-Induced Changes in the Likelihood and Magnitude of the Observed Extreme Precipitation during Hurricane Harvey. *Geophysical Research Letters*, **44 (24)**, 12,457–12,464, doi:10.1002/2017GL075888.

Roberts, M. J., and Coauthors, 2020a: Impact of model resolution on tropical cyclone simulation using the HighResMIP-PRIMAVERA multimodel ensemble. *Journal of Climate*, **33 (7)**, 2557–2583, doi:10.1175/JCLI-D-19-0639.1.

Roberts, M. J., and Coauthors, 2020b: Projected Future Changes in Tropical Cyclones Using the CMIP6 HighResMIP Multimodel Ensemble. *Geophysical Research Letters*, **47 (14)**, 1–12, doi:10.1029/2020GL088662.

Rolf, E., J. Proctor, T. Carleton, I. Bolliger, V. Shankar, M. Ishihara, B. Recht, and S. Hsiang, 2021: A generalizable and accessible approach to machine learning with global satellite imagery. *Nature Communications*, **12 (1)**, 4392, doi:10.1038/s41467-021-24638-z.

Roussos, J., R. Bradley, and R. Frigg, 2021: Making Confident Decisions with Model Ensembles. *Philosophy of Science*, **88 (3)**, 439–460, doi:10.1086/712818.

Saltelli, A., 2002: Making best use of model evaluations to compute sensitivity indices. *Computer Physics Communications*, **145 (2)**, 280–297, doi:10.1016/S0010-4655(02)00280-1.

Saltelli, A., K. Aleksankina, W. Becker, P. Fennell, F. Ferretti, N. Holst, S. Li, and Q. Wu, 2019: Why so many published sensitivity analyses are false: A systematic review of sensitivity analysis practices. *Environmental Modelling and Software*, **114 (January)**, 29–39, doi:10.1016/j.envsoft.2019.01.012.

Saltelli, A., P. Annoni, I. Azzini, F. Campolongo, M. Ratto, and S. Tarantola, 2010: Variance based sensitivity analysis of model output. Design and estimator for the total sensitivity index. *Computer Physics Communications*, **181 (2)**, 259–270, doi:10.1016/j.cpc.2009.09.018.

Saltelli, A., M. Ratto, T. Andres, F. Campolongo, J. Cariboni, D. Gatelli, M. Saisana, and S. Tarantola, 2008: *Global Sensitivity Analysis: The Primer*. John Wiley & Sons, Ltd.

Schipper, E. L. F., 2020: Maladaptation: When Adaptation to Climate Change Goes Very Wrong. *One Earth*, **3 (4)**, 409–414, doi:10.1016/j.oneear.2020.09.014.

Schneider, P. J., and B. A. Schauer, 2006: HAZUS—Its Development and Its Future. *Natural Hazards Review*, **7 (2)**, 40–44, doi:10.1061/(ASCE)1527-6988(2006)7:2(40).

Schreck, C. J., K. R. Knapp, and J. P. Kossin, 2014: The impact of best track discrepancies on global tropical cyclone climatologies using IBTrACS. *Monthly Weather Review*, **142 (10)**, 3881–3899, doi:10.1175/MWR-D-14-00021.1.

Sebastian, A., E. J. Dupuits, and O. Morales-Nápoles, 2017: Applying a Bayesian network based on Gaussian copulas to model the hydraulic boundary conditions for hurricane flood risk analysis in a coastal watershed. *Coastal Engineering*, **125**, 42–50, doi:10.1016/j.coastaleng.2017.03.008.

Sellar, A. A., and Coauthors, 2020: Implementation of U.K. Earth System Models for CMIP6. *Journal of Advances in Modeling Earth Systems*, **12 (4)**, e2019MS001 946, doi:10.1029/2019MS001946.

Sharmila, S., and K. J. Walsh, 2018: Recent poleward shift of tropical cyclone formation linked to Hadley cell expansion. *Nature Climate Change*, **8 (8)**, 730–736, doi:10.1038/s41558-018-0227-5.

Shepherd, T. G., and A. H. Sobel, 2020: Localness in Climate Change. *Comparative Studies of South Asia, Africa and the Middle East*, **40 (1)**, 7–16, doi:10.1215/1089201X-8185983.

Shepherd, T. G., and Coauthors, 2018: Storylines: an alternative approach to representing uncertainty in physical aspects of climate change. *Climatic Change*, **151 (3-4)**, 555–571, doi:10.1007/s10584-018-2317-9.

Sherman, L., J. Proctor, H. Druckenmiller, H. Tapia, and S. M. Hsiang, 2023: Working Paper Series. Global High-Resolution Estimates of the United Nations Human Development Index Using Satellite Imagery and Machine-learning. National Bureau of Economic Research, url https://www.nber.org/papers/w31044, Accessed on 2023-09-28, doi:10.3386/w31044.

Sherwood, S. C., and Coauthors, 2020: An Assessment of Earth's Climate Sensitivity Using Multiple Lines of Evidence. *Reviews of Geophysics*, **58 (4)**, e2019RG000 678, doi:10.1029/2019RG000678.

Silva-Araya, W. F., F. L. Santiago-Collazo, J. Gonzalez-Lopez, and J. Maldonado-Maldonado, 2018: Dynamic modeling of surface runoff and storm surge during hurricane and tropical storm events. *Hydrology*, **5 (1)**, 13, doi:10.3390/hydrology5010013.

Simpson, R. H., and H. Saffir, 1974: The Hurricane Disaster - Potential Scale. *Weatherwise*, **27 (4)**, 169–186, doi:10.1080/00431672.1974.9931702.

Smith, I., 2023: Insurers need to 'step up' on catastrophe coverage, says risk modelling chief. url https://www.ft.com/content/0591363a-b9aa-4c9b-9ee9-0f4e1e215cb2, Accessed on 2023-10-15.

Smith, J. Q., 2010: *Bayesian Decision Analysis: Principles and Practice*. Cambridge University Press, Cambridge, doi:10.1017/CBO9780511779237.

Sobel, A. H., 2021: Usable climate science is adaptation science. *Climatic Change*, **166 (1)**, 8, doi:10.1007/s10584-021-03108-x.

Sobel, A. H., C. Y. Lee, S. J. Camargo, K. T. Mandli, K. A. Emanuel, P. Mukhopadhyay, and M. Mahakur, 2019: Tropical cyclone hazard to mumbai in the recent historical climate. *Monthly Weather Review*, **147 (7)**, 2355–2366, doi:10.1175/MWR-D-18-0419.1.

Sobel, A. H., and M. K. Tippett, 2018: Extreme Events: Trends and RiskAssessment Methodologies. *Resilience: The Science of Adaptation to Climate Change*, Elsevier, 3–12, doi:10.1016/B978-0-12-811891-7.00001-3.

Sobol, I. M., 2001: Global sensitivity indices for nonlinear mathematical models and their Monte Carlo estimates. *Mathematics and Computers in Simulation*, doi:10.1016/S0378-4754(00)00270-6.

Souvignet, M., F. Wieneke, L. Mueller, and D. N. Bresch, 2016: Economics of Climate Adaptation (ECA) - Guidebook for Practitioners - A Climate Risk Assessment Approach Supporting Climate Adaptation Investments. Tech. rep., 1000 pp. Issue: 6.

Stalhandske, Z., C. B. Steinmann, S. Meiler, I. Sauer, T. Vogt, D. N. Bresch, and C. M. Kropf, 2023: Global multi-hazard risk assessment in a changing climate. preprint. doi:https://doi.org/10.31223/X56W9N, url https://eartharxiv.org/repository/view/5286/.

Steinmann, C. B., B. P. Guillod, C. Fairless, and D. N. Bresch, 2023: A generalized framework for designing open-source natural hazard parametric insurance. *Environment Systems and Decisions*, doi:10.1007/s10669-023-09934-x.

Swiss Re, 2021: Partnership, perspective and patience: How insurers and the public sector must work together to develop greater climate resilience. url https://www.swissre.com/our-business/public-sector-solutions/contributing-to-the-global-debate/partnership-perspective-patience.html, Accessed on 2023-09-27.

Swiss Re, 2023: Natural catastrophes and inflation in 2022: a perfect storm - Swiss Re sigma | Swiss Re. url https://www.swissre.com/institute/research/sigma-research/sigma-2023-01.html, Accessed on 2023-07-04.

Task Force on Climate-related Financial Disclosures, 2017: Final report: Recommendations of the task force on climate-related financial disclosures. Technical report, Financial Stability Board. url https://assets.bbhub.io/company/sites/60/2020/10/FINAL-2017-TCFD-Report-11052018.pdf.

Tatebe, H., and Coauthors, 2019: Description and basic evaluation of simulated mean state, internal variability, and climate sensitivity in MIROC6. *Geoscientific Model Development*, **12 (7)**, 2727–2765, doi:10.5194/gmd-12-2727-2019.

Tippett, M. K., S. J. Camargo, and A. H. Sobel, 2011: A poisson regression index for tropical cyclone genesis and the role of large-scale vorticity in genesis. *Journal of Climate*, **24 (9)**, 2335–2357, doi:10.1175/2010JCLI3811.1.

Torres, J. M., B. Bass, N. Irza, Z. Fang, J. Proft, C. Dawson, M. Kiani, and P. Bedient, 2015: Characterizing the hydraulic interactions of hurricane storm surge and rainfall-runoff for the Houston-Galveston region. *Coastal Engineering*, **106**, 7–19, doi:10.1016/j.coastaleng.2015.09.004.

UN General Assembly, 2015: Transforming our world : the 2030 Agenda for Sustainable Development. Tech. Rep. A/RES/70/1. url https://www.un.org/sustainabledevelopment/sustainable-development-goals/.

UNISDR, 2015: Sendai Framework for Disaster Risk Reduction 2015-2030 | UNDRR. url http://www.undrr.org/publication/sendai-framework-disaster-risk-reduction-2015-2030, Accessed on 2023-08-10.

United Nations Framework Convention on Climate Change (UNFCCC), 2007: Decision 1/CP.13: Bali action plan. url https://unfccc.int/resource/docs/2007/cop13/eng/06a01.pdf#page=3, Accessed on 2023-10-16.

United Nations Framework Convention on Climate Change (UNFCCC), 2015: FCCC/CP/2015/L.9/Rev.1: the Paris Agreement. url https://unfccc.int/process-and-meetings/

the-paris-agreement?gclid=Cj0KCQjwldKmBhCCARIsAP-0rfzAKwjCymXJUJcBciSWP_9s1S2xuH86-eauxkZ_KlfY0HSrwm-iOIgaAod5EALw_wcB, Accessed on 2023-08-10.

United Nations Framework Convention on Climate Change (UNFCCC), 2023: Decision 2/CP.27: Funding arrangements for responding to loss and damage associated with the adverse effects of climate change, including a focus on addressing loss and damage. url https://unfccc.int/sites/default/files/resource/cp2022_10a01_E.pdf, Accessed on 2023-10-16.

Unterberger, C., P. Hudson, W. J. Botzen, K. Schroeer, and K. W. Steininger, 2019: Future Public Sector Flood Risk and Risk Sharing Arrangements: An Assessment for Austria. *Ecological Economics*, **156**, 153–163, doi:10.1016/j.ecolecon.2018.09.019.

Van Oldenborgh, G. J., K. Van Der Wiel, A. Sebastian, R. Singh, J. Arrighi, F. Otto, K. Haustein, S. Li, G. Vecchi, and H. Cullen, 2017: Attribution of extreme rainfall from Hurricane Harvey, August 2017. *Environmental Research Letters*, **12 (12)**, doi:10.1088/1748-9326/aa9ef2.

Vecchi, G. A., and Coauthors, 2019: Tropical cyclone sensitivities to CO2 doubling: roles of atmospheric resolution, synoptic variability and background climate changes. *Climate Dynamics*, **53 (9)**, 5999–6033, doi:10.1007/s00382-019-04913-y.

Vickery, P. J., P. F. Skerlj, and L. A. Twisdale, 2000: Simulation of Hurricane Risk in the U.S. Using Empirical Track Model. *Journal of Structural Engineering*, **126 (10)**, 1222–1237, doi:10.1061/(asce)0733-9445(2000)126:10(1222).

Voldoire, A., and Coauthors, 2019: Evaluation of CMIP6 DECK Experiments With CNRM-CM6-1. *Journal of Advances in Modeling Earth Systems*, **11 (7)**, 2177–2213, doi:10.1029/2019MS001683.

Wagener, T., R. Reinecke, and F. Pianosi, 2022: On the evaluation of climate change impact models. *WIREs Climate Change*, e772, doi:10.1002/wcc.772.

Walker, W., P. Harremoës, J. Rotmans, J. van der Sluijs, M. van Asselt, P. Janssen, and M. Krayer von Krauss, 2003: Defining Uncertainty: A Conceptual Basis for Uncertainty Management in Model-Based Decision Support. *Integrated Assessment*, **4 (1)**, 5–17, doi:10.1076/iaij.4.1.5.16466.

Walsh, K. J., and Coauthors, 2015: Hurricanes and climate: The U.S. Clivar working group on hurricanes. *Bulletin of the American Meteorological Society*, **96 (6)**, 997–1017, doi:10.1175/BAMS-D-13-00242.1.

Walsh, K. J., J. L. Mcbride, P. J. Klotzbach, S. Balachandran, S. J. Camargo, G. Holland, T. R. Knutson, J. P. Kossin, T. c. Lee, A. Sobel, and M. Sugi, 2016: Tropical cyclones and climate change. *Wiley Interdisciplinary Reviews: Climate Change*, **7 (1)**, 65–89, doi:10.1002/wcc.371.

Wang, X., C. Yao, G. Gao, H. Jiang, D. Xu, G. Chen, and Z. Zhang, 2020: Simulating tropical cyclone waves in the East China Sea with an event-based, parametric-adjusted model. *Journal of Oceanography*, **76 (6)**, 439–457, doi:10.1007/s10872-020-00555-5.

Ward, P., and Coauthors, 2020: Review article: Natural hazard risk assessments at the global scale. *Natural Hazards and Earth System Sciences*, 1–46, doi:10.5194/nhess-2019-403.

Ward, P. J., and Coauthors, 2022: Invited perspectives: A research agenda towards disaster risk management pathways in multi-(hazard-)risk assessment. *Natural Hazards and Earth System Sciences*, **22 (4)**, 1487–1497, doi:10.5194/nhess-22-1487-2022.

Weinkle, J., R. Maue, and R. Pielke, 2012: Historical global tropical cyclone landfalls. *Journal of Climate*, **25 (13)**, 4729–4735, doi:10.1175/JCLI-D-11-00719.1.

Williamson, C., C. McCordic, and B. Doberstein, 2023: The compounding impacts of Cyclone Idai and their implications for urban inequality. *International Journal of Disaster Risk Reduction*, **86**, 103 526, doi:10.1016/j.ijdrr.2023.103526.

Wilson, K. M., J. W. Baldwin, and R. M. Young, 2022: Estimating Tropical Cyclone Vulnerability: A Review of Different Open-Source Approaches. *Hurricane Risk in a Changing Climate*, J. M. Collins, and J. M. Done, Eds., Hurricane Risk, Springer International Publishing, Cham, 255–281, doi:10.1007/978-3-031-08568-0_11.

WMO, 2021: Notable Tropical Cyclones. url https://public.wmo.int/en/our-mandate/focus-areas/natural-hazards-and-disaster-risk-reduction/tropical-cyclones/Notable-tcs, Accessed on 2021-11-22.

WMO, 2023: World Meteorological Organization's World Weather & Climate Extremes Archive. url https://wmo.asu.edu/content/world-meteorological-organization-global-weather-climate-extremes-archive, Accessed on 2023-08-16.

Wright, D. B., T. R. Knutson, and J. A. Smith, 2015: Regional climate model projections of rainfall from U.S. landfalling tropical cyclones. *Climate Dynamics*, **45 (11)**, 3365–3379, doi:10.1007/s00382-015-2544-y.

Wu, W., K. McInnes, J. O'Grady, R. Hoeke, M. Leonard, and S. Westra, 2018: Mapping Dependence Between Extreme Rainfall and Storm Surge. *Journal of Geophysical Research: Oceans*, **123 (4)**, 2461–2474, doi:10.1002/2017JC013472.

Xiaofan Li, and Bin Wang, 1994: Barotropic dynamics of the beta gyres and beta drift. *Journal of the Atmospheric Sciences*, **51 (5)**, 746–756, doi:10.1175/1520-0469(1994)051<0746:bdotbg>2.0.co;2.

Yamada, Y., M. Satoh, M. Sugi, C. Kodama, A. T. Noda, M. Nakano, and T. Nasuno, 2017: Response of Tropical Cyclone Activity and Structure to Global Warming in a High-Resolution Global Nonhydrostatic Model. *Journal of Climate*, **30 (23)**, 9703–9724, doi:10.1175/JCLI-D-17-0068.1.

Yukimoto, S., and Coauthors, 2019: MRI MRI-ESM2.0 model output prepared for CMIP6 ScenarioMIP ssp245. url https://doi.org/10.22033/ESGF/CMIP6.6910, publisher: Earth System Grid Federation, Accessed on 2023-02-16, doi:10.22033/ESGF/CMIP6.6910.

Zehr, J. P., and L. Riemann, 2023: Quantification of gene copy numbers is valuable in marine microbial ecology: A comment to Meiler et al. (2022). *Limnology and Oceanography*, **68 (6)**, 1406–1412, doi:10.1002/lno.12364.

Zheng, F., S. Westra, M. Leonard, and S. A. Sisson, 2014: Modeling dependence between extreme rainfall and storm surge to estimate coastal flooding risk. *Water Resources Research*, **50 (3)**, 2050–2071, doi:10.1002/2013WR014616.

Zschau, J., 2017: Where are we with multihazards, multirisks assessment capacities? *Science for disaster risk management 2017 : knowing better and losing less*, European Union, 98–115, doi:10.2788/688605.

Zscheischler, J., S. Westra, B. J. Van Den Hurk, S. I. Seneviratne, P. J. Ward, A. Pitman, A. Aghakouchak, D. N. Bresch, M. Leonard, T. Wahl, and X. Zhang, 2018: Future climate risk from compound events. *Nature Climate Change*, **8 (6)**, 469–477, doi:10.1038/s41558-018-0156-3.